EVALUATION OF MR-TADF COMPOUNDS AS PHOTOCATALYSTS AND THEIR APPLICATION IN NHC/PHOTOREDOX CATALYSIS

Callum Prentice

A Thesis Submitted for the Degree of PhD
at the
University of St Andrews

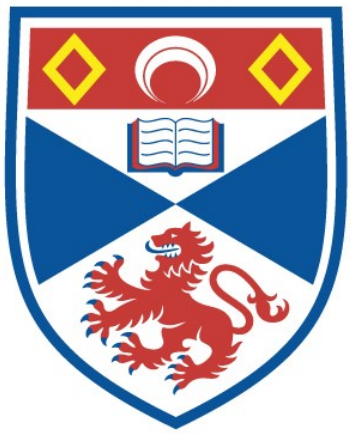

2023

Evaluation of MR-TADF Compounds as Photocatalysts and their Application in NHC/Photoredox Catalysis

Callum Prentice

University of
St Andrews

This thesis is submitted in partial fulfilment for the degree of

Doctor of Philosophy (PhD)

at the University of St Andrews

April 2023

Candidate's declaration

I, Callum Prentice, do hereby certify that this thesis, submitted for the degree of PhD, which is approximately 50,000 words in length, has been written by me, and that it is the record of work carried out by me, or principally by myself in collaboration with others as acknowledged, and that it has not been submitted in any previous application for any degree. I confirm that any appendices included in my thesis contain only material permitted by the 'Assessment of Postgraduate Research Students' policy.

I was admitted as a research student at the University of St Andrews in September 2018.

I received funding from an organisation or institution and have acknowledged the funder(s) in the full text of my thesis.

Date 12/04/2023 Signature of candidate

Supervisor's declaration

I hereby certify that the candidate has fulfilled the conditions of the Resolution and Regulations appropriate for the degree of PhD in the University of St Andrews and that the candidate is qualified to submit this thesis in application for that degree. I confirm that any appendices included in the thesis contain only material permitted by the 'Assessment of Postgraduate Research Students' policy.

Date 12/04/23 Signature of supervisor

Date 12/04/23 Signature of supervisor

Permission for publication

In submitting this thesis to the University of St Andrews we understand that we are giving permission for it to be made available for use in accordance with the regulations of the University Library for the time being in force, subject to any copyright vested in the work not being affected thereby. We also understand, unless exempt by an award of an embargo as requested below, that the title and the abstract will be published, and that a copy of the work may be made and supplied to any bona fide library or research worker, that this thesis will be electronically accessible for personal or research use and that the library has the right to migrate this thesis into new electronic forms as required to ensure continued access to the thesis.

I, Callum Prentice, confirm that my thesis does not contain any third-party material that requires copyright clearance.

The following is an agreed request by candidate and supervisor regarding the publication of this thesis:

Printed copy

No embargo on print copy.

Electronic copy

No embargo on electronic copy.

Date	12/04/23	Signature of candidate
Date	12/04/23	Signature of supervisor
Date	12/04/23	Signature of supervisor

Underpinning Research Data or Digital Outputs

Candidate's declaration

I, Callum Prentice, understand that by declaring that I have original research data or digital outputs, I should make every effort in meeting the University's and research funders' requirements on the deposit and sharing of research data or research digital outputs.

Date 12/04/23 Signature of candidate

Permission for publication of underpinning research data or digital outputs

We understand that for any original research data or digital outputs which are deposited, we are giving permission for them to be made available for use in accordance with the requirements of the University and research funders, for the time being in force.

We also understand that the title and the description will be published, and that the underpinning research data or digital outputs will be electronically accessible for use in accordance with the license specified at the point of deposit, unless exempt by award of an embargo as requested below.

The following is an agreed request by candidate and supervisor regarding the publication of underpinning research data or digital outputs:

No embargo on underpinning research data or digital outputs.

Date 12/04/23 Signature of candidate

Date 12/04/23 Signature of supervisor

Date 12/04/23 Signature of supervisor

Abstract

This thesis concerns the study of TADF and MR-TADF compounds for use as photocatalysts, with a focus on their application in Lewis base/photoredox dual catalysis.

Chapter 1 introduces the important concepts that are key to understanding both TADF photocatalysis and Lewis base catalysis as well as a literature survey of these areas of research.

Chapter 2 describes the synthesis and investigation of a bifunctional material that contains distinct isothiourea (ITU) and TADF moieties. Disappointingly, when incorporated into the same molecule, the two components proved to be incompatible due to oxidation of the Lewis basic ITU. Further investigations into ITU/photoredox dual catalysis using distinct ITU catalysts and photocatalysts also pointed to an issue of incompatibility due to the low oxidation potential of ITU catalysts. However, subsequent investigations by others[1,2] showed that this catalytic system can be utilised effectively if a suitable radical precursor is identified that can be oxidised more easily than the ITU catalyst.

Chapter 3 investigates the benefits of using MR-TADF compounds **DiKTa** and **Mes$_3$DiKTa** as photocatalysts in a series of standard photocatalytic reactions using **4CzIPN** as a benchmark for comparison. These reactions included reductive quenching reactions, oxidative quenching reactions, Dexter energy transfer (DET) reactions and dual catalytic reactions. Further comparisons were made through the analysis of the rates of reaction using the three different catalysts in a standard oxidative quenching reaction using an in-situ NMR technique.

Chapter 4 applies the knowledge gained in chapter 3 to a new NHC/photoredox catalysed synthesis of 1,4-diketones via a three-component radical relay reaction. The optimized conditions combined aroyl fluorides, α-ketoacids and styrenes in the presence of **DiKTa** and an NHC catalyst. Subsequent investigation of the scope was achieved by varying the substituents of each starting material. A mechanism is proposed and supported through Stern-Volmer analysis.

Chapter 5 explores the application of benzophenone as a DET photocatalyst in the key [2+2] photochemical cycloaddition step in the synthesis of dimethyl cubane-1,4-dicarboxylate. This allowed for the use of significantly lower energy light (λ_{exc} = 390 nm) than previously reported (λ_{exc} = 311 nm).[3]

References

1 R. del Río-Rodríguez, M. T. Westwood, M. Sicignano, M. Juhl, J. A. Fernández-Salas, J. Alemán and A. D. Smith, *Chem. Commun.*, 2022, **58**, 7277–7280.
2 W. C. Hartley, F. Schiel, E. Ermini and P. Melchiorre, *Angew. Chem. Int. Ed.*, 2022, **61**, e202204735.
3 D. E. Collin, E. H. Jackman, N. Jouandon, W. Sun, M. E. Light, D. C. Harrowven and B. Linclau, *Synthesis*, 2021, **53**, 1307–1314.

Declaration

I fully acknowledge that the work presented is my own. The research has been carried out in the groups of Prof. Eli Zysman-Colman (University of St Andrews) and Prof. Andrew D. Smith (University of St Andrews). Contributions from others are listed below.

Chapter 1: I am the primary author of this text.

Chapter 2: I am the primary author of this text.

Chapter 3: The synthesis was undertaken by me. UV-vis absorption, electrochemistry, steady-state photophysics and time-resolved photoluminescence decays were measured by me. Stern-Volmer quenching studies were performed with the assistance of Dr Ettore Crovini. Optimization of the synthesis of the water-soluble version of **DiKTa** was done with the assistance of Changfeng Si. Synthesis and elemental analysis of mesoporous silica-based materials was carried out by Montaña Jiménez Garcia from UAM in collaboration with Dr Silvia Cabrera Herranz. I am the primary author of this text. The work in this chapter preceding section 3.2.7 has been published; *Chem. Eur. J.* 2023, **29**, e202202998 (DOI: 10.1002/chem.202202998).

Chapter 4: I am the primary author of this text. The work in this chapter has been published; *Chem. Commun.*, 2022, **58**, 13624-13627.

Chapter 5: The synthesis of starting materials **255** and **256** was carried out by me. Optimization of the photochemical [2+2] cycloaddition was done with the assistance of Alice E. Martin. I am the primary author of this text. The work in this chapter has been published, *Org. Biomol. Chem.*, 2023, Advance Article (DOI: 10.1039/D3OB00231D).

Acknowledgements

Firstly I would like to thank Eli and Andy for their supervision and guidance throughout this PhD. Thanks also goes to AstraZeneca for funding and in particular James for his advice and supervision.

A sincere thank you to all staff at the University of St Andrews, in particular the support staff in the school of chemistry as well as the NMR technicians, Siobhan and Tomas, for their help.

I would also like to thank all collaborators in this work, in particular Silvia and Montaña for their help and advice, it was a pleasure to work with you all.

I would like to thank all members of the ADS group past and present but to name a few in particular I would like to thank Will, Calum, Liz, Mark, Jaci, Jason, and Claire for their help and support at the beginning. Further thanks to Rebecca and Yihong for being there with me throughout. Of course additional thanks to the newer members of the group such as Matt, Duan, Ali, Kevin, Jerson, Justin and Ffion. Also to the CPJ group members, Callum, Reece, Wylan and Nikki.

Next, I would like to thank all members of the EZ-C group who I have had the pleasure of working alongside all these years. A particular thank you to Subeesh, Tomas, Campbell, Chenfei and Dianming for all their help with my many synthetic or photophysical challenges. Of course my time in the EZ-C group would not have been the same without the many wine Friday enjoyers throughout the years from the very old, Dave, to the less old Megan, Ettore, Oil, Moya, Fran, Lea, Tim, Mónica, Sultan, Janine, Tabea, Jasmin, Mahni and Aminata to name a few. I will miss you all dearly.

A penultimate thank you goes to my family. To Dale and Tanya for their understanding of the troubles involved with a PhD and their support throughout. To my parents for their unending love and support throughout my time here in St Andrews and Dundee, without them this whole journey would have been far more difficult and stressful.

Finally, the biggest thank you of all of course goes to Jess, who knows where I would be without you in general let alone during this PhD through the lockdowns and fires etc. Thanks for letting me drag you all the way to Scotland and I can’t wait for what comes next together.

Funding

This work was supported by an AZCASE studentship (SCH0-IUA36).

Research Data Access Statement

Research data underpinning this thesis are available at: https://doi.org/10.17630/b7c334ca-eead-4724-8ef5-4c8f3562f053

List of Abbreviations

Abbreviation	Expansion
µs	Microsecond
Ac	Acyl
Abs	Absorption
acac	Acetyl acetonate
AO	Atomic Orbital
aq.	Aqueous
Ar	Aryl group
ATRA	Atom Transfer Radical Addition
a.u.	Arbitrary Units
BET	Back Electron Transfer
Boc	*tert*-Butyloxycarbonyl
bpy	2,2'-bipyridine
BTM	Benzotetramisole
Bu	Butyl
Bz	Benzoyl
cat.	Catalytic
Cbz	Benzyloxycarbonyl
CFL	Compact Fluorescent Light
conc.	Concentrated
CuAAC	Copper catalysed Azide Alkyne Coupling
CV	Cyclic Voltammetry
CyMe	Methyl Cyclohexane
Cz	Carbazole

D-A	Donor-Acceptor
DBU	1,8-Diazabicyclo[5.4.0]undec-7-ene
DCB	Dichlorobenzene
DCE	1,2-Dichloroethane
DCM	Dichloromethane
DET	Dexter Energy Transfer
DFT	Density Functional Theory
DIPEA	Diisopropyl ethylamine
DMAC	9,9-Dimethyl-9,10-dihydroacridine
DMAP	Dimethyl Amino Pyridine
DME	Dimethyl Ether
DMF	Dimethyl Formamide
DMSO	Dimethyl Sulfoxide
DNB	Dinitrobenzene
DPV	Differential Pulse Voltammetry
dtbbpy	4,4′-Di-tert-butyl-2,2′-dipyridyl
e	Electron charge
e^-	Electron
$E_{0,0}$	Zero-zero excitation energy
EDA	Electron Donor Acceptor
EDC	1-Ethyl-3-(3-dimethylaminopropyl)carbodiimide
ee	Enantiomeric Excess
E_{ox}	Oxidation potential
E_{ox}*	Excited state oxidation potential
E_{PA}	Anodic peak of a redox potential

equiv.	Equivalents
er	Enantiomeric ratio
E_{red}	Reduction potential
E_{red}*	Excited state reduction potential
E_S	Singlet energy
E_T	Triplet energy
Et	Ethyl
et al.	And co-workers
EWG	Electron Withdrawing Group
Ɛ	Molar absorptivity
f	Oscillator strength
fac	Facial isomer
FRET	Förster Resonance Energy Transfer
GCMS	Gas Chromatography Mass Spectrometry
h	Hour
HAT	Hydrogen Atom Transfer
Hex	Hexyl
HOBt	Hydroxybenzotriazole
HOMO	Highest Occupied Molecular Orbital
H_{SOC}	Spin Orbit Coupling constant
hv	Energy of a photon of frequency *v*
I	Intensity
I_0	Intensity in the absence of quencher
IC	Internal Conversion
IPA	*Iso*propanol

i-Pr	*Iso*-propyl
IRF	Instrument Response Function
ISC	Intersystem Crossing
ITU	Isothiourea
J	Exchange integral
k	Rate constant
K_{SV}	Stern-Volmer constant
LA	Lewis Acid
LE	Locally Excited
LED	Light-Emitting Diode
LG	Leaving Group
LRCT	Long Range Charge Transfer
LUMO	Lowest Unoccupied Molecular Orbital
M	Molar, mol dm^{-3}
Me	Methyl
MeCN	Acetonitrile
Mes	Mesityl
MO	Molecular Orbital
mol	Mole
MR-TADF	Multi-Resonance Thermally Activated Delayed Fluorescence
Ms	Mesylate
MS-AP	Mesoporous Silica-Amino Propane
MSN	Mesoporous Silica
NaDT	Sodium Decatatungstate
NHC	N-Heterocyclic Carbene

NIS	*N*-iodosuccinimide
nm	Nanometer
NMR	Nuclear Magnetic Resonance
OLED	Organic Light Emitting Diode
PC	Photocatalyst
PC*	Excited state photocatalyst
$PC^{\bullet-}$	Reduced photocatalyst
$PC^{\bullet+}$	Oxidised photocatalyst
PEnT	Photoinduced Energy Transfer
Ph	Phenyl
PN	Phthalonitrile
PNP	*Para*-nitrophenyl
ppy	2-Phenylpyridine
PS-BEMP	Polymer Supported 2-tert-Butylimino-2-diethylamino-1,3-dimethylperhydro-1,3,2-diazaphosphorine
Q	Quencher
RCA	Radical Conjugate Addition
RISC	Reverse Intersystem Crossing
rt	Room Temperature
S_0	Singlet ground state
S_1	First singlet excited state
S_2	Second singlet excited state
SBA	Mesoporous silica material
SCE	Standard Calomel Electrode
SET	Singlet Electron Transfer

S_n	Any singlet excited state
S_NAr	Nucleophilic aromatic substitution
SRCT	Short Range Charge Transfer
Sub	Substrate
T_1	Lowest triplet state
TADF	Thermally Activated Delayed Fluorescence
TBAB	Tetrabutyl Ammonium Bromide
TBAC	Tertabutyl Ammonium Chloride
TBAF	Tetrabutyl Ammonium Fluoride
t-Bu	Tertiary butyl
THF	Tetrahydrofuran
TIPS	Tri*iso*propyl Silyl
TMS	Trimethyl Silyl
T_n	Any triplet state
Tol	Toluene
Ts	Tosylate
UV	Ultraviolet
V	Voltage
Z	Atomic number
ΔE_{nb}	Energy gap between non-bonding orbitals
ΔE_{ST}	Energy gap between singlet and triplet states
ΔG_{SET}	Gibbs-free energy for single electron transfer
ΔS	Change in spin
λ_{abs}	Wavelength of maximum absorption
λ_{em}	Emission wavelength

λ_{exc}	Excitation wavelength
τ_0	Lifetime in absence of quencher
τ_d	Delayed fluorescence lifetime
τ_p	Prompt fluorescence lifetime
τ_{PL}	Photoluminescence lifetime
Φ	Quantum yield
Φ_{PL}	Photoluminescence quantum yield
ω	Electrostatic work term

Table of Contents

1 Introduction

1.1 Photocatalysis

One of the earliest examples of photochemistry in organic synthesis was published by Giacomo Ciamician over one hundred years ago, where the intramolecular [2+2] cycloaddition of carvone using sunlight as an energy source was undertaken.[1] As Ciamician indicates in this work, the ability to use sunlight to drive chemical reactions is highly desirable as it is so abundant. However, further expansions on sunlight driven photochemistry proved limited in scope, as most relevant organic molecules absorb in the UV region, and a large proportion of the UV radiation emitted by the Sun is absorbed by the atmosphere. While there has been a large number of UV light promoted processes developed, including examples of challenging and interesting transformations,[2] there are significant advantages to using visible light, such as being more tolerant of reactive functional groups and requiring less specialised glassware as standard borosilicate glassware is not transparent to high-energy UV irradiation (λ_{exc} < 300 nm). One way to harness visible light for the use of synthetic organic chemistry is by using a photocatalyst, which can be defined as a substance that absorbs light to promote a chemical transformation without itself being consumed.[3] An early example of this can be seen in Kellogg's work on the photocatalytic reduction of acyl sulfonium salts **1** (Scheme 1.1).[4] While an obscure application, this reaction paved the way for a rapid and recent expansion of the field of photocatalysis 40 years later.

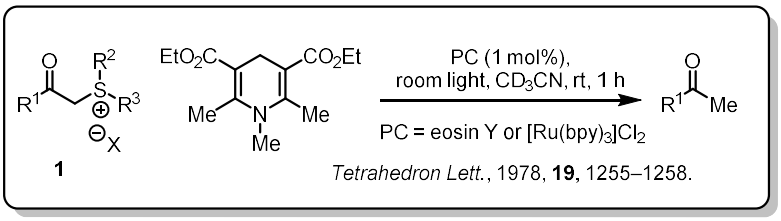

Scheme 1.1 Photocatalytic reduction of acyl sulfonium salts.[4]

1.1.1 Photophysical Processes

The first step of a photocatalysis reaction is the photoexcitation of the photocatalyst from the singlet ground state (S_0) to a singlet excited state (S_n). From this initial excited state there are multiple

processes that can occur, depending on the PC being used and the substrates that are present. Jablonski diagrams are often used to visualise these excited state processes (Figure 1.1). After excitation, the PC could be in any singlet excited state (S_n) and any vibrationally excited state within each electronic excited state depending upon the energy of the photon absorbed. Vibrational relaxation and IC will occur simultaneously. IC is the non-radiative transition from one electronic state to another without changing spin state (e.g. $S_2 \rightarrow S_1$) and is much faster than other processes when $n > 1$, so all further processes will occur from the ground vibrational level of the S_1 state (known as Kasha's rule).[3] The S_1 state can then undergo fluorescence, which is the relaxation back to S_0 accompanied by the emission of light. Alternatively, ISC to a triplet state (T_n) is possible, which again would undergo IC to T_1 and relaxation to the vibrational ground state of the T_1 state. The T_1 state can then emit light and relax to S_0 via phosphorescence. Both ISC and phosphorescence are spin-forbidden processes as $\Delta S \neq 0$, but this rule can be relaxed through mixing of the S and T states.

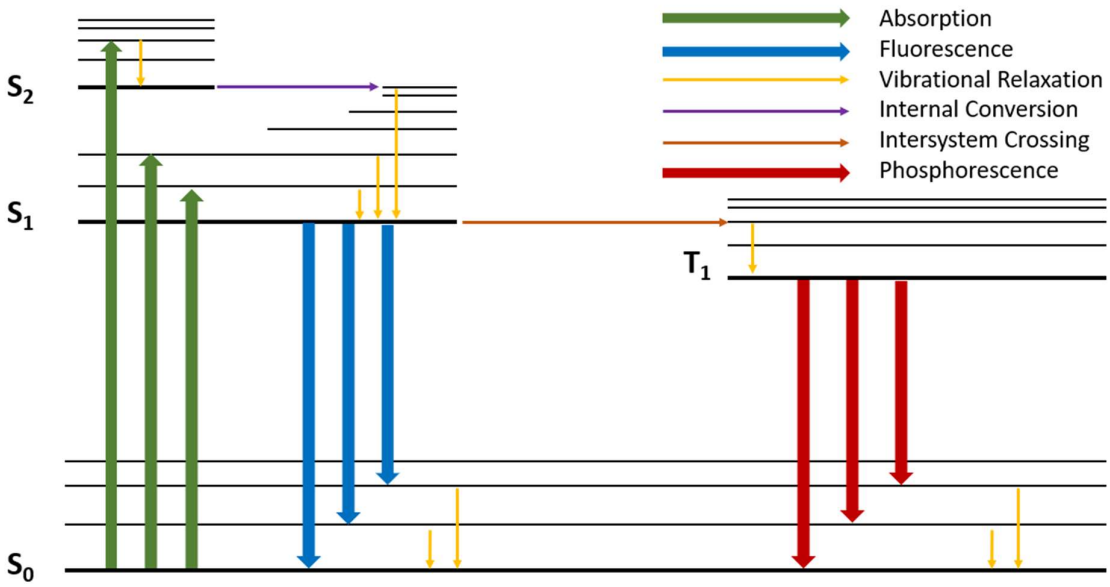

Figure 1.1 Jablonski diagram.

The amount of mixing (λ) is proportional to the degree of spin-orbit coupling (H_{SOC}) and inversely proportional to the energy difference between the S and T states (ΔE_{ST}) (Equation 1.1).[5] H_{SOC} is in turn proportional to the fourth power of the atomic number (Z),[6] therefore heavy atoms are often used to promote formally spin-forbidden processes.

$$\lambda \propto \frac{H_{SOC}}{\Delta E_{ST}} \propto Z^4 \quad (1.1)$$

1.1.2 Excited-State Quenching Mechanisms

Fluorescence and phosphorescence are radiative pathways. Photocatalytic reactions are non-radiative pathways, which typically occur when the excited state is quenched through an interaction with another molecule. In general, a quenching process will involve the absorption of light by the PC and the resulting excitation to PC* (Scheme 1.2). For a reaction to occur with a quencher (Q), PC* and Q will then need to diffuse together and form an encounter complex. Within this encounter complex, the relevant types of quenching that can occur for the work in this thesis are SET or PEnT. Then, for the reaction to progress, PC and Q must diffuse away from each other to avoid a back reaction.

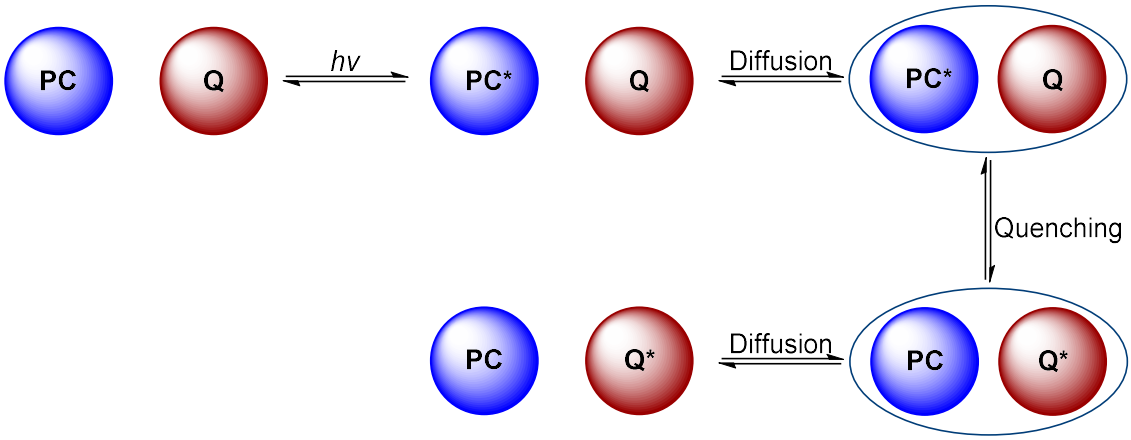

Scheme 1.2 Simplified scheme for a generic quenching process.

1.1.3 Types of Photocatalysis

Quenching through SET can be categorised into oxidative (single electron oxidation of PC*) and reductive (single electron reduction of PC*) quenching reactions between a substrate and a PC that together constitute what is commonly termed photoredox catalysis. The Rehm-Weller equation[7,8] uses the ground state redox potentials of the PC and Q ($E_{red/ox}$), along with the energy of the lowest excited state ($E_{0,0}$) and an electrostatic work term (ω) to describe whether a given SET event is energetically feasible ($\Delta G_{SET} < 0$, exergonic) or not ($\Delta G_{SET} > 0$, endergonic) (Equations 1.2 and 1.3). Ground state redox potentials are easily measured using cyclic voltammetry, ideally in the same solvent in which the reaction is being performed. $E_{0,0}$ for fluorescent compounds is the energy

corresponding to the intersection point of the normalised absorption and emission spectra, but for phosphorescent compounds it is estimated using the onset of the phosphorescence spectrum, as it is frequently not possible to observe the spin-forbidden absorption to the triplet state.

$$\Delta G_{SET} = E_{ox}(PC^+/PC) - E_{red}(Q/Q^-) - E_{0,0} + \omega \quad (1.2)$$

$$\Delta G_{SET} = E_{ox}(Q^+/Q) - E_{red}(PC/PC^-) - E_{0,0} + \omega \quad (1.3)$$

The Rehm-Weller equations can be simplified by introducing terms for the excited state redox potentials of PC and assuming ω is accounted for during the measurement[9] (Equations 1.4 and 1.5). In practice, these excited-state redox potentials are estimated for each PC (Equations 1.6 and 1.7) and used to compare their oxidizing and reducing abilities in the excited state to inform a choice of the optimal PC for the desired transformation based on the substrate's redox potentials.

$$\Delta G_{SET} = E_{ox}(PC^{\bullet+}/PC^*) - E_{red}(Q/Q^-) \quad (1.4)$$

$$\Delta G_{SET} = E_{ox}(Q^+/Q) - E_{red}(PC^*/PC^{\bullet-}) \quad (1.5)$$

$$E^*_{ox}(PC^{\bullet+}/PC^*) = E_{ox}(PC^+/PC) - E_{0,0} \quad (1.6)$$

$$E^*_{red}(PC^*/PC^{\bullet-}) = E_{red}(PC/PC^-) + E_{0,0} \quad (1.7)$$

Oxidative quenching refers to the SET process that results in the oxidation of PC* and is therefore also linked to the single electron reduction of the substrate. As an example, for a PC to be oxidatively quenched (blue) by phenacyl bromide **2** (E_{red}(**2**/**2**$^-$) = – 1.21 V vs SCE) its photooxidation potential would have to be more negative (E_{ox}* < – 1.21 V) for ΔG_{SET} < 0 (Scheme 1.3). Whether PC* is in the singlet or triplet excited state when it is quenched is dependent on how fast ISC and RISC are relative to the quenching rate for the PC being used. The electrophilic radical **3** that is formed can then react with other reagents such as a nucleophilic alkene **4** to form a nucleophilic radical **5**. To close the cycle and recover PC, another SET step is required which is dependent on the redox potentials E_{ox}(PC$^{\bullet+}$/PC) and E_{ox}(+CH/•CH).

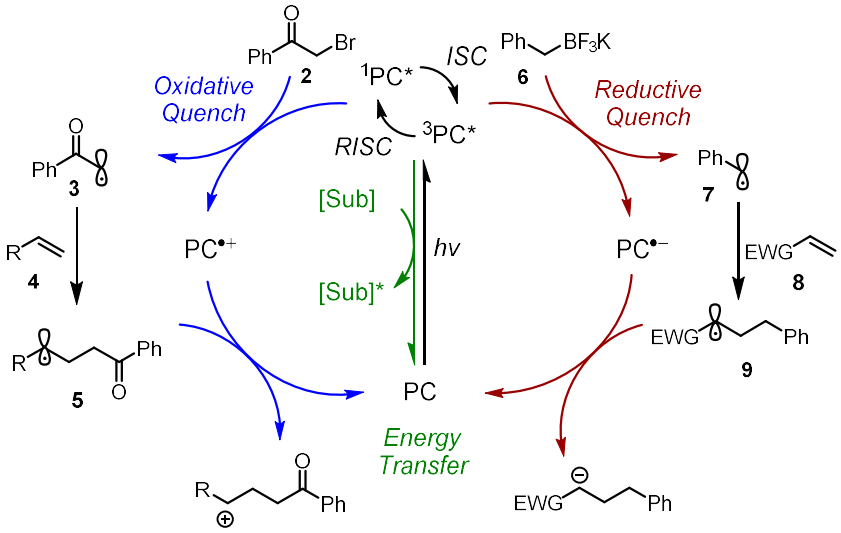

Scheme 1.3 Representative cycles for photocatalysis.

Analogously, a reductive quenching cycle (red) begins with a SET step, this time reducing the PC* and oxidising the substrate. For PC* to be quenched by the benzyl trifluoroborate salt **6** (E_{ox}(**6**$^{+}$/**6**) = + 1.1 V vs SCE),[10] the catalyst would need a photoreduction potential that is more positive (E_{red}* > + 1.1 V) for ΔG_{SET} < 0. This would now form a nucleophilic radical **7** and after reaction with an electrophilic alkene **8** to form an electrophilic radical **9**, the cycle is closed via a SET reduction that will depend upon the redox potentials E_{red}(PC/PC$^{\bullet-}$) and E_{red}(•CH/–CH). PEnT reactions (green) generate the excited state substrate ([Sub]*) rather than going through any redox processes and can occur via two main mechanisms, Förster resonance energy transfer (FRET) and Dexter energy transfer (DET) (Figure 1.2).[11] During FRET, the PC* induces a dipole in the ground state [Sub] through coulombic interactions, which leads to the simultaneous relaxation of PC* and the excitation of [Sub] (Figure 1.2a). The efficiency of the FRET process is dependent on the distance between the two species and also the spectral overlap between the emission spectrum of the donor and the absorption spectrum of the acceptor.[12] However, if the PC* is in a triplet state (as is the case for many PCs) then FRET cannot operate due to spin selection rules and only DET takes place, which is the simultaneous intermolecular exchange of electrons between PC* and [Sub] (Figure 1.2b). A DET reaction is possible if there is spectral overlap between the $S_0 \rightarrow T_1$ absorption spectrum of the substrate and the $T_1 \rightarrow S_0$ emission spectrum of the PC.[11] However, such absorption spectra are not easily obtained, so instead the triplet energies (E_T) of

the substrate and PC are often used as a rough predictive guide. If E_T(PC) > E_T(substrate) then DET is predicted to occur. Given the nature of DET and FRET, if the dominant photoactive state of the PC used is a singlet, then FRET is typically in operation and if it is a triplet then DET is in operation, despite DET being possible from either singlet or triplet excited states. Both DET[13,14] and FRET[15] have been invoked independently, and also in combination,[16] as photophysical processes to activate substrates in photocatalytic transformations.

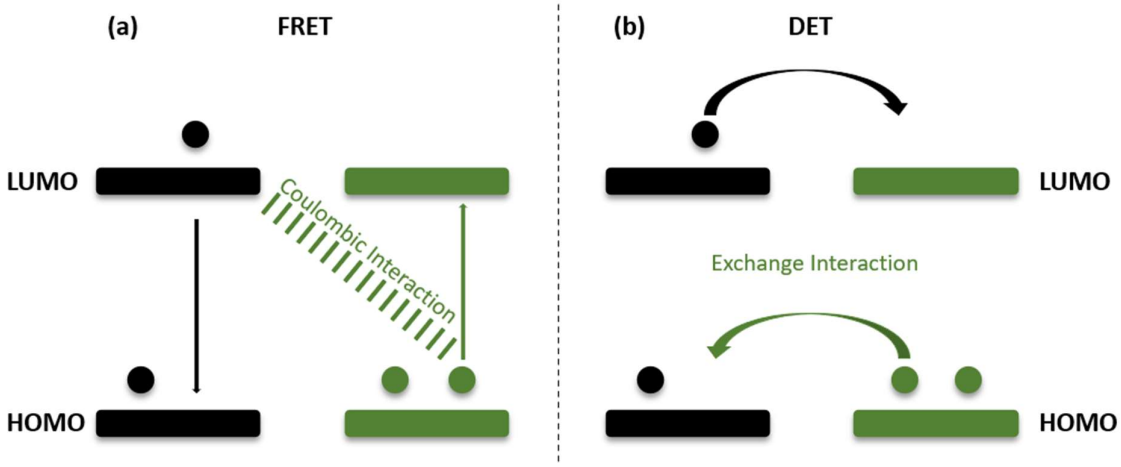

Figure 1.2 (a) FRET mechanism. (b) DET mechanism.

An important value for any photoinduced process is the reaction quantum yield (Φ), which is the ratio of the number of photons used in that process relative to the total number of photons absorbed and is a measure of efficiency for that process (Equation 1.8). The quantum yield for a photochemical reaction can also be useful for mechanistic elucidation because if Φ > 1 then a radical chain reaction is likely in operation, but if Φ ≤ 1 then a closed photocatalytic cycle is expected.[17]

$$\Phi = \frac{Number\ of\ photons\ used\ for\ a\ process}{Total\ number\ of\ photons\ absorbed} \quad (1.8)$$

1.1.4 Photocatalyst Design

Any molecule in its excited state is both a stronger oxidant and reductant than in its ground state, as it simultaneously has a higher energy electron to donate and a lower energy hole to accept an electron. However, there are factors other than redox potentials and triplet energies that are important for a molecule to be considered a good PC:[18]

- Since most organic substrates absorb in the UV region, a good PC will have longer wavelength absorption so it can be excited selectively and a high molar absorptivity (Ɛ) for this wavelength to give faster reaction rates.
- Sufficiently long excited-state lifetimes (on the order of nanoseconds) so that the encounter complex has time to form prior to deexcitation of the PC.
- Reversible redox behaviour suggests stability of the oxidised/reduced PC and would be favourable for high catalyst turnover and therefore low catalyst loadings.
- Inexpensive starting materials, efficient synthesis and tunability of redox properties makes developing PCs specific to a desired transformation simpler and more cost effective.

With these factors and criteria in mind, metal polypyridyl complexes have dominated photocatalysis. Some of the commonly used catalysts are $[Ru(bpy)_3]Cl_2$, *fac*-$Ir(ppy)_3$, $[Ir(ppy)_2(dtbbpy)](PF_6)$, and $[Ir(dF(CF_3)ppy)_2(dtbbpy)](PF_6)$ (Figure 1.3). Variation of the ligands about the metal allows for controlled tuning of the redox properties from the strongly photoreducing ($E_{ox}(PC^{\bullet+}/PC^*) < -1.7$ V) to the highly photooxidising ($E_{red}(PC^*/PC^{\bullet-}) > +1.2$ V). While excited-state redox potentials are significant, ground-state redox potentials are also important in photocatalysis. This is particularly relevant in net reductive and net oxidative transformations that use sacrificial reductants and oxidants to access the strongly reducing and oxidizing intermediates $PC^{\bullet-}$ and $PC^{\bullet+}$, respectively.

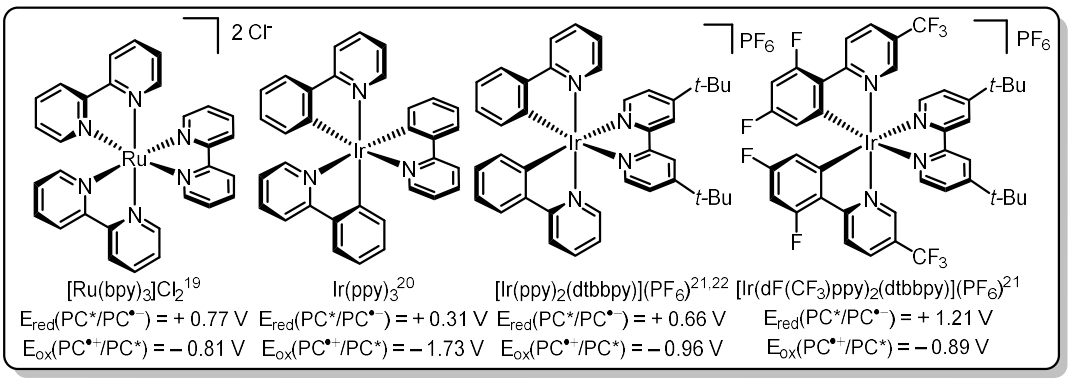

$[Ru(bpy)_3]Cl_2$[19] $Ir(ppy)_3$[20] $[Ir(ppy)_2(dtbbpy)](PF_6)$[21,22] $[Ir(dF(CF_3)ppy)_2(dtbbpy)](PF_6)$[21]

$E_{red}(PC^*/PC^{\bullet-}) = +0.77$ V; $E_{ox}(PC^{\bullet+}/PC^*) = -0.81$ V

$E_{red}(PC^*/PC^{\bullet-}) = +0.31$ V; $E_{ox}(PC^{\bullet+}/PC^*) = -1.73$ V

$E_{red}(PC^*/PC^{\bullet-}) = +0.66$ V; $E_{ox}(PC^{\bullet+}/PC^*) = -0.96$ V

$E_{red}(PC^*/PC^{\bullet-}) = +1.21$ V; $E_{ox}(PC^{\bullet+}/PC^*) = -0.89$ V

Figure 1.3 Examples of organometallic photocatalysts with excited state redox properties reported vs SCE.[19–22]

In recent years, there has been an increasing focus on moving away from PCs that use noble metals due to their intrinsic scarcity, and instead towards the use of organic PCs.[23] Some of the most

commonly used organic PCs are the natural dyes eosin Y, fluorescein, and rose bengal (Figure 1.4). The greater difficulty to tune their redox potentials is viewed as a significant weakness of organic PCs; however, recent examples have demonstrated their tuneability, which will be discussed in the next section.

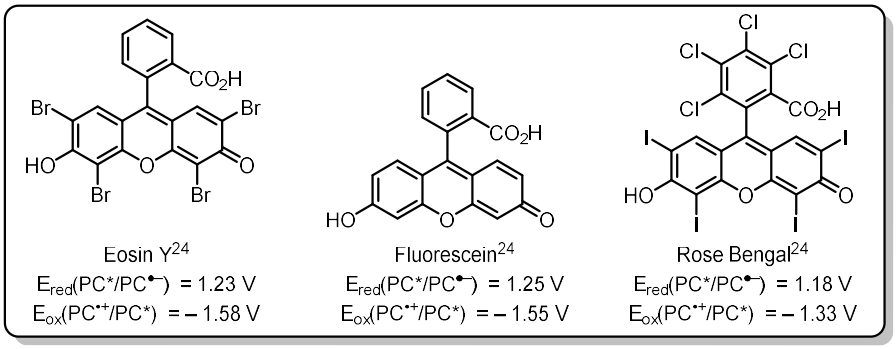

Figure 1.4 Examples of organic PCs with excited state redox properties reported vs SCE.[24]

1.2 Thermally Activated Delayed Fluorescence (TADF)

1.2.1 TADF Definition and Donor-Acceptor Strategy

ISC is typically slow for fluorescent compounds,[25] so any emission or quenching of the excited state will predominantly occur from S_1 with minimal contribution from T_1 (Figure 1.5). This has important implications for photocatalysis as whether PC* is in the singlet or triplet excited state may impact the outcome of the reaction. This is particularly clear for PEnT reactions because if PC* is in the S_1 state then the reaction will proceed through FRET and the excited state substrate that is generated will also be in the S_1 state. Alternatively, if the PC* is in the T_1 state then the reaction will proceed through DET and the excited state substrate that is generated will also be in the T_1 state. This is important because some PEnT reactions proceed via the singlet excited state of the substrate,[15] while others require the triplet excited state,[26] so a fluorescent PC would not be the optimal choice in this latter case. The nature of the excited state can also be important for photoredox catalysis. The S_1 state will be of higher energy than the T_1 state, so the magnitude of the corresponding excited state redox potentials will be greater, and the activation of more challenging substrates will be easier than if the T_1 state were used. This greater driving force also results in increased SET quenching rates, which can lead to shorter

reaction times.[27] Phosphorescent compounds typically exploit the heavy-atom effect to increase H_{SOC} and therefore increase the rate of ISC, so that any additional reactivity of PC* will occur from T_1, which allows them to promote PEnT reactions that require the substrate to be in the triplet excited state. While some of the excitation energy is lost through the ISC process, T_1 states also tend to have slower BET rates than S_1 states,[28] which is a competitive process that can impede reaction progression. An alternative method for recruiting T_1 states is to design a compound with a small ΔE_{ST}. In accordance with equation 1.1, this relaxes the spin-selection rules and allows for ISC and RISC between the S_1 and T_1 states, giving access to both for photocatalysis. The first organic molecules observed to have this property were eosin-derived compounds,[29] so this emission mechanism was coined E-type fluorescence but it is also called thermally activated delayed fluorescence because the magnitude of the delayed fluorescence component of the emission after RISC is temperature sensitive. While it is not yet known whether the nature of TADF compounds has any specific benefits for photocatalysis, there are some potential advantages that can be postulated. For example, having access to both singlet and triplet excited states should allow for both FRET and DET mechanisms to be possible, which could broaden the applicability for photocatalysed PEnT reactions. Furthermore, if the triplet state is required, due to the small ΔE_{ST}, there is less energy lost from the initial excitation than for standard 4d/5d organometallic complexes, which could help activate more challenging substrates. Another consequence of ΔE_{ST} being small is that there is little difference in driving force for SET from S_1 or T_1, so which state is active in SET will likely be down to a comparison of the relative rates of ISC, RISC, SET and BET.

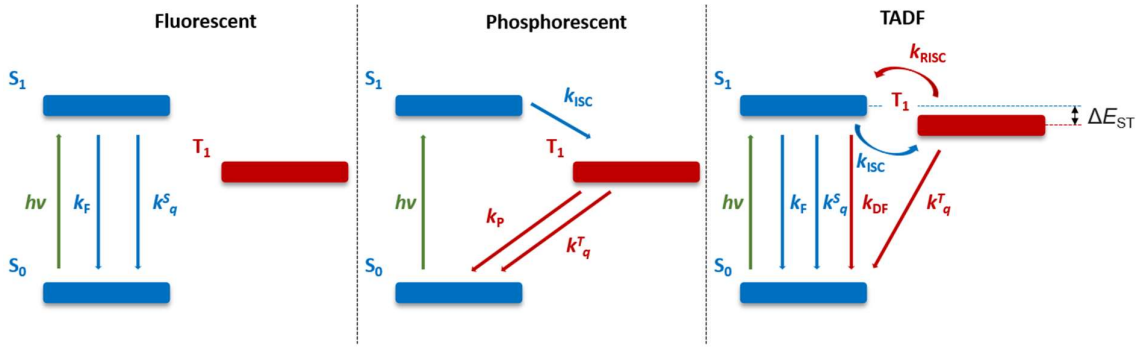

Figure 1.5 Simplified Jablonski diagrams for fluorescent, phosphorescent and TADF compounds acting as PCs. Where k_F, k_P and k_{DF} are the rate constants for fluorescence, phosphorescence, and delayed fluorescence, respectively, k_{ISC} and k_{RISC} are the rate constants for ISC and RISC, respectively, k^S_q and k^T_q are the quenching rate constants of the singlet and triplet states, respectively.

In Adachi's[30] ground-breaking work, a series of D-A TADF compounds were designed to have a significant twist between the donor and acceptor groups, so that they were largely electronically decoupled, resulting in low ΔE_{ST} values (< 0.3 eV) and high efficiencies in OLEDs (Figure 1.6).

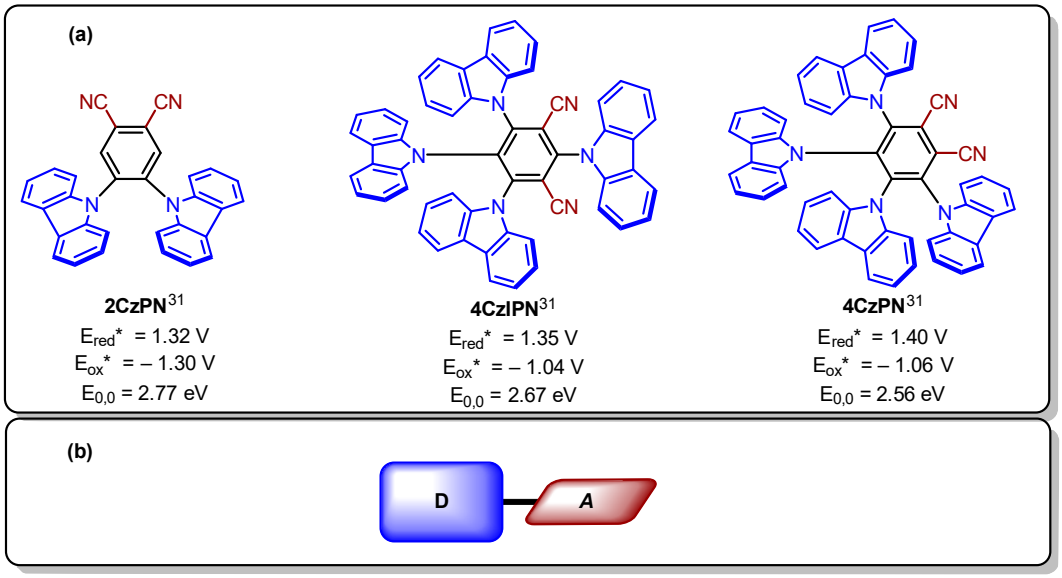

Figure 1.6 (a) Some of the first TADF OLEDs with excited state redox properties reported vs SCE in MeCN.[31] (b) Depiction of twist between donor and acceptor groups.

The rationale for this design strategy is due to the relationship between ΔE_{ST} and the exchange integral, J (Equation 1.9).[32,33] J is in turn dependent on the orbital overlap between the frontier orbitals involved in the transitions to S_1/T_1, where ψ and φ are usually the HOMO and the LUMO, respectively, and e is the electron charge (Equation 1.10). Therefore, minimization of this overlap will lead to a reduction in J and a small ΔE_{ST}.[32] This design strategy has now been employed by many research groups to develop an enormous range of different emitters.[34]

$$\Delta E_{\mathrm{ST}} = E_{\mathrm{S}} - E_{\mathrm{T}} = 2J \tag{1.9}$$

$$J = \iint \varphi(r_1)\psi(r_2)\left(\frac{e^2}{r_1 - r_2}\right)\varphi(r_2)\psi(r_1)\mathrm{d}r_1 r_2 \tag{1.10}$$

As a consequence of the D-A strategy, the lowest S_1 and T_1 states have a significant LRCT character as opposed to LE character. In the former, the electron density is displaced from the donor region of the molecule to the acceptor, while in the latter the electron density remains in the same portion of the molecule. LRCT states also have lower oscillator strengths, *f*, than LE states, as *J* is smaller, which is an indicator for the probability of transitions to or from these states to occur. This is because of the poor overlap between the HOMO and LUMO, which is a key part of the design to achieve low ΔE_{ST}. Emitters used for OLEDs must have a high photoluminescence quantum yield (Φ_{PL}), which is itself dependant on *f* for the transition from the S_1 state. Therefore, a significant weakness of this strategy is that it is difficult to achieve a D-A TADF compound that has both a high Φ_{PL} and a small ΔE_{ST}. Another weakness is that emission from LRCT states results in very broad emission profiles, due to a large degree of vibrational and conformational motion, which results in poor colour purity.

1.2.2 Multi-Resonance TADF

To address the issues detailed in Section 1.2.1, an alternative strategy for the development of TADF OLEDs was developed, by exploiting the opposing resonance effects of p- and n- dopants in nanographenes and has been termed MR-TADF.[35] By fusing the donor and acceptor groups into a single polycyclic aromatic system, the HOMO and LUMO orbitals are offset by one atom (Figure 1.7). The S_1 and T_1 electron density is therefore delocalised over the entire arene, with alternating electron rich and electron poor regions, leading to an SRCT state. This results in both a small ΔE_{ST} and a high oscillator strength, which in turn leads to a high Φ_{PL}. Furthermore, the rigidity of the compounds allows for significantly reduced vibrational motion so that a much narrower emission profile is observed and a resulting improvement in colour purity.

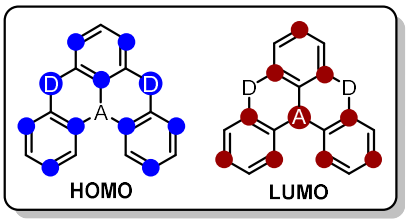

Figure 1.7 Generic MR-TADF compound design with HOMO and LUMO orbital distributions.

Another significant difference between D-A TADF and MR-TADF compounds is their differing degrees of positive solvatochromism. Solvatochromism is the term used when there is a change in position of an electronic emission or absorption band due to a change in the polarity of the medium.[3] This occurs when the permanent dipole moments of the solvent interact with the transition dipole moment of the excited state. If the molecule in the S_1 state has a larger transition dipole moment than in the S_0 state, then the S_1 state will be lowered in energy, thus narrowing the energy gap between S_1 and S_0. The degree of stabilization is increased when solvents with larger dipoles are used, resulting in positive solvatochromism. The LRCT states present in D-A compounds have large transition dipole moments so are stabilised significantly by solvents of increased polarity, resulting in a red-shifted emission and lower energy excited states (Figure 1.8a).[36] However, the SRCT states present in MR-TADF compounds have much smaller transition dipole moments and are therefore much less effected by solvent polarity changes and a solvatochromic study is one of the methods used to identify MR-TADF compounds (Figure 1.8b).[37] This will have implications for photocatalysis as discussed further in chapter 3.

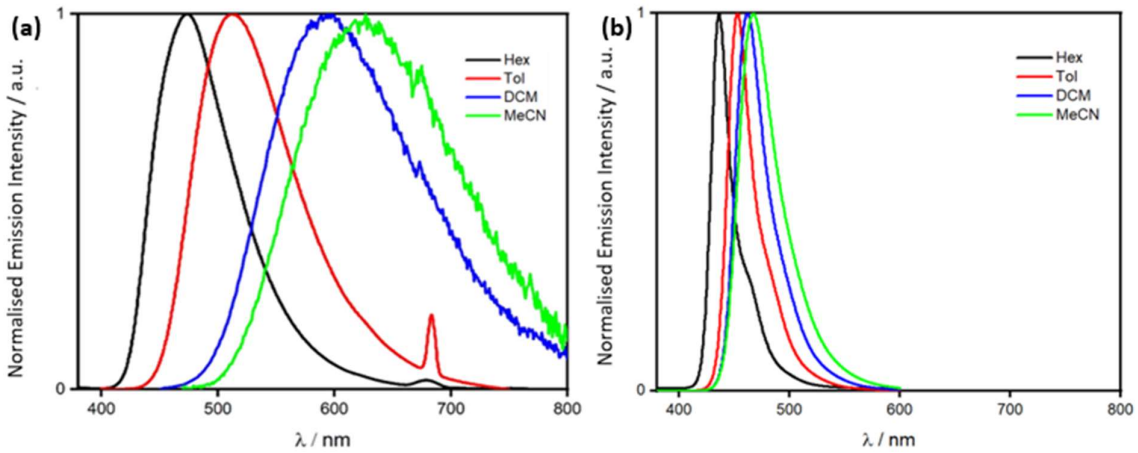

Figure 1.8 Solvatochromic study for a (a) representative D-A TADF emitter[36] (b) representative MR-TADF emitter.[37]

Following these design principles, Hatakeyama and co-workers[38] successfully developed B,O-doped polycyclic compound **10**, which has the desired MR-TADF properties (Figure 1.9). Further development replaced the oxygen atoms with tricoordinate nitrogen atoms to give compounds such as **DABNA-1**,[39] which have a slightly red-shifted emission relative to **10**. If the DABNA structure is inverted and the nitrogen donor atom is placed in the centre, then an alternative acceptor unit can be used. This is exemplified in the compound **DiKTa** and its analogues,[40] which contain bridging ketone groups that act as the acceptors. **DiKTa** had been synthesised previously by Venkataraman and co-workers[41] to investigate its structure. These scaffolds have now been explored rather extensively,[35] and other examples that deviate from these design principles have also now been reported, such as **DiICzMes$_4$**, which achieves MR-TADF without an acceptor unit.[42]

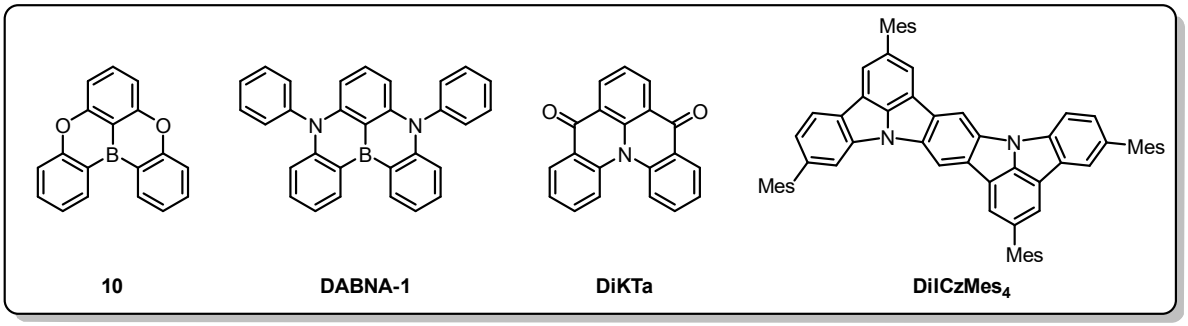

Figure 1.9 Representative examples of the different donors and acceptors used in MR-TADF emitter design.

The synthesis of **DiKTa** is relatively straightforward and begins with the Ullmann coupling of methyl 2-iodobenzoate **11** and aniline to give triarylamine **12** (Scheme 1.4). A subsequent hydrolysis and

Friedel-Crafts acylation sequence furnishes the desired compound in good overall yields. Analogues of **DiKTa** are also simply prepared through the bromination of **12** and subsequent cyclisation to give **Br_3DiKTa**, which can then be further functionalised through various coupling reactions, such as in the synthesis of **Mes_3DiKTa**.[37]

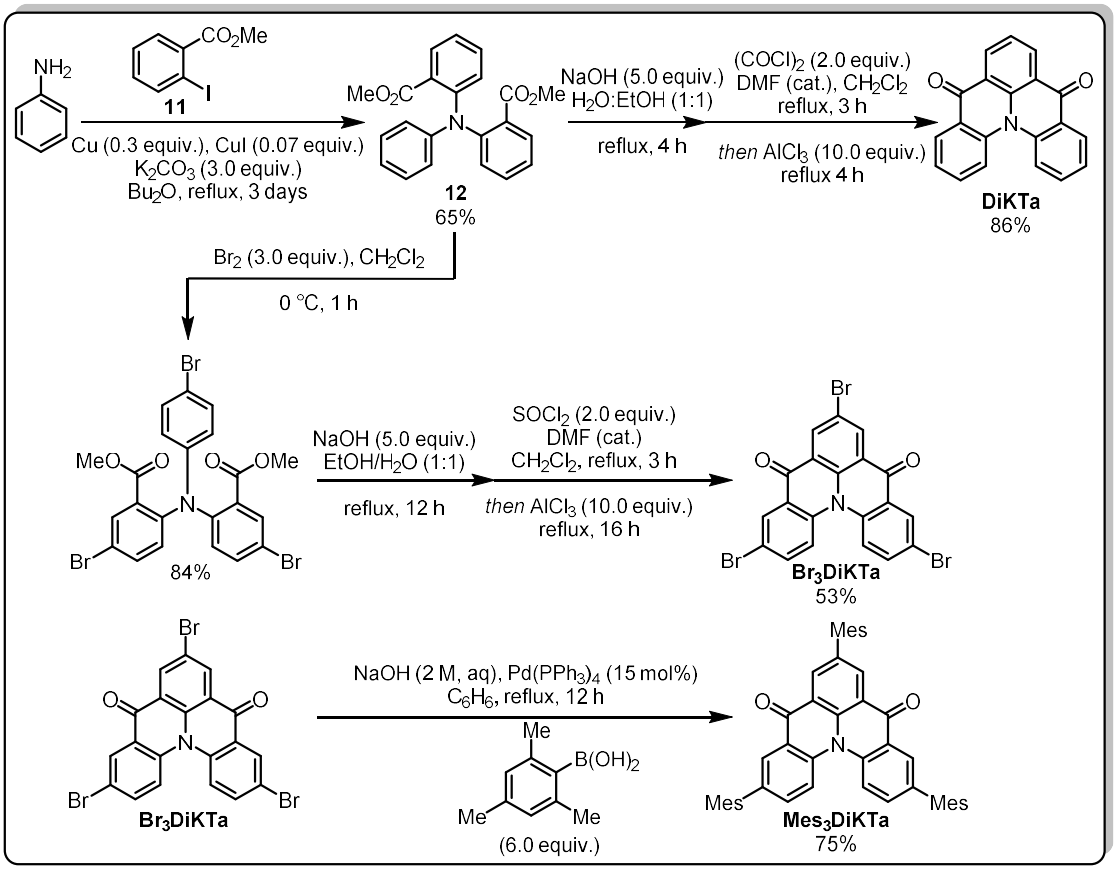

Scheme 1.4. Synthesis of **DiKTa** and **Mes_3DiKTa**.

1.2.3 TADF Compounds in Photocatalysis

Given the ideal properties for a good PC outlined in Section 1.1.4, it is unsurprising that TADF emitters are also proficient PCs.[31] The first example of a TADF compound being used as a PC was reported by Zhang and co-workers[43] using **4CzIPN** with nickel in a dual catalytic sp^2–sp^3 coupling reaction between *N*-boc-proline **13** and aryl bromide **14** (Scheme 1.5). Since then, a relatively small number of different TADF compounds have been used, and **4CzIPN** has become commonplace in many photocatalytic reaction optimizations.[31]

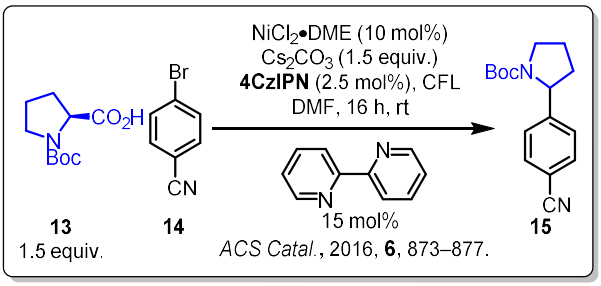

Scheme 1.5 First example of TADF photocatalysis.[43]

Zeitler and co-workers[44] utilised the tunability of D-A TADF compounds by varying the donor and acceptor strengths on a series of compounds similar to **4CzIPN** (Figure 1.10). For example, by changing the number of carbazole groups, as in **2CzIPN**, or adding methoxy groups to the carbazoles, as in **5CzBNOMe**, the excited state oxidation potential can be varied from – 1.04 to – 1.79 V (vs SCE).

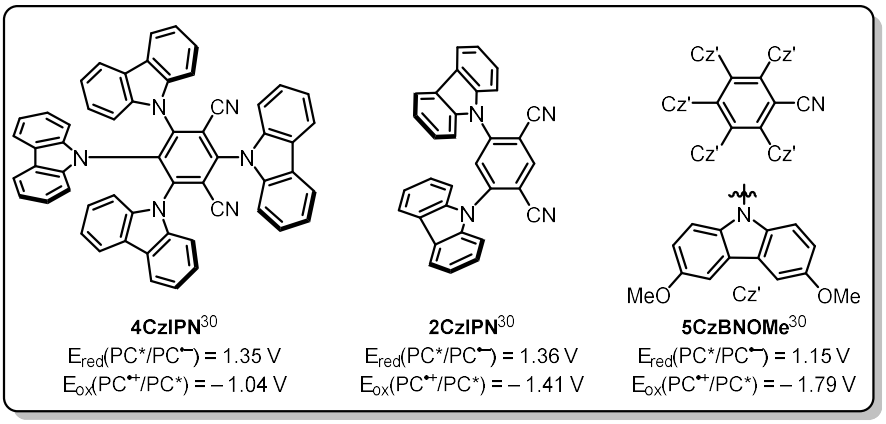

Figure 1.10 Tunability of D-A compounds with excited state redox properties reported vs SCE.[31]

Zeitler and co-workers[44] then showcased the synthetic diversity of TADF compounds as PCs in a series of different reactions. These included the oxidative bromination of anisole **16** (Scheme 1.6a) and the double reduction/pinacol coupling of lignin derivatives **17** (Scheme 1.6b). Together, these reactions demonstrate that TADF PCs are proficient in both oxidative and reductive photoredox catalysis. For each reaction a different PC was found to be optimal, showing the versatility afforded to this class of PC by its tunability.

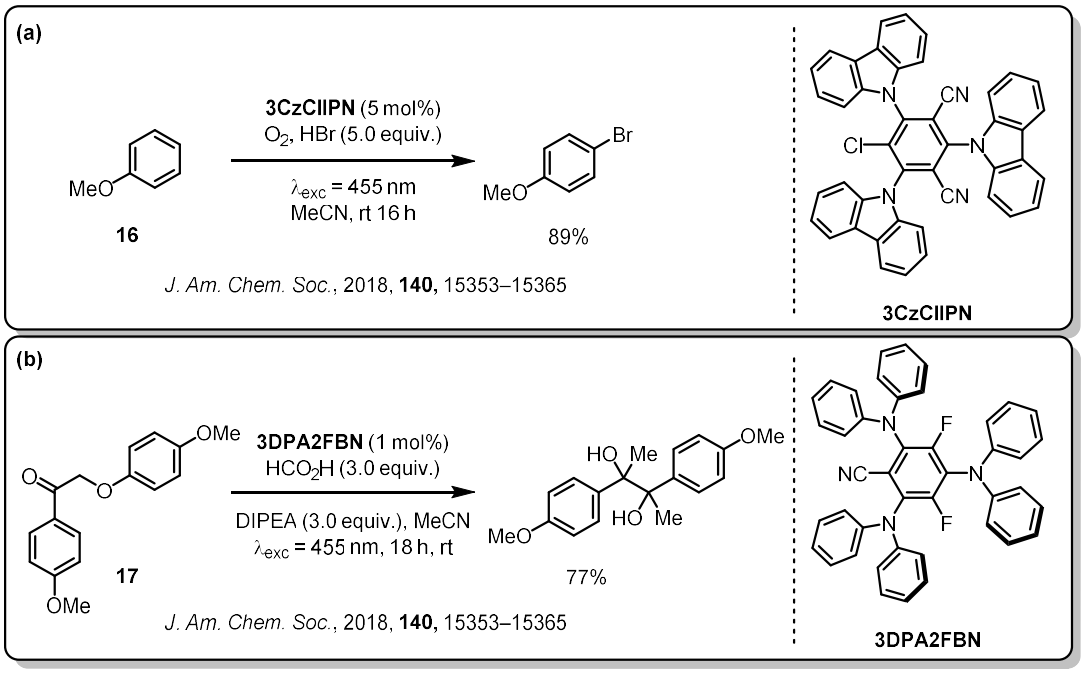

Scheme 1.6 (a) Photocatalytic bromination of anisole. (b) Photocatalytic pinacol coupling of lignin derivatives.

Zhang and co-workers[45] also demonstrated the ability of TADF compounds to enable DET reactions using the well-known photoisomerization of (*E*)-stilbene **18** (Scheme 1.7). **4CzPN** was their optimal PC for this reaction, which gave yields comparable to $[Ru(bpy)_3](PF_6)_2$. In combination with other works,[31] this demonstrates that TADF photocatalysts can perform many different transformations and can compete with organometallic catalysts.

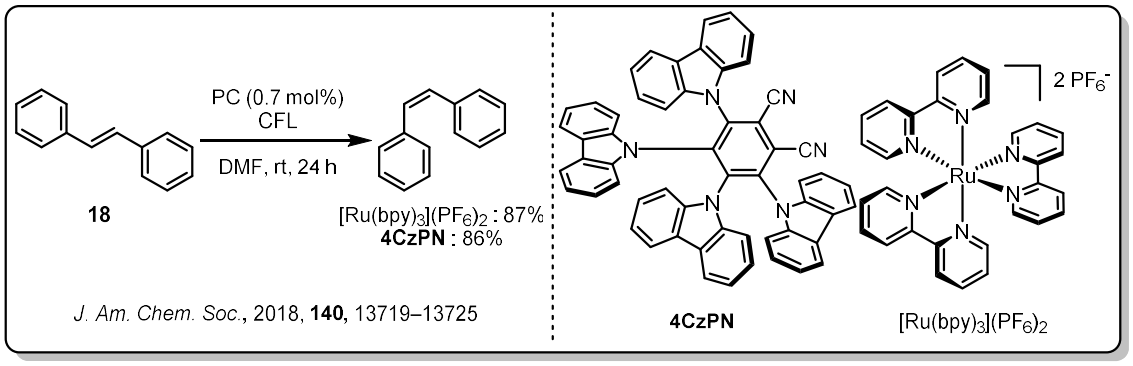

Scheme 1.7 DET catalysed isomerization of (*E*)-stilbene.

Considering the plethora of donors and acceptors that exist in TADF emitter design for applications in OLEDs, it is somewhat surprising that most TADF compounds used in photocatalysis thus far are based around the cyanoarene core with either carbazole or diphenylamine donors.[31] However, there are some exceptions to this trend, such as the recent work developed by Bryden and co-workers[46] that

used **pDTCz-DPmS** as a PC, which has a pyrimidyl sulfone acceptor unit (Scheme 1.8). A series of test reactions were performed to compare the performance of **pDTCz-DPmS** to the widely used **4CzIPN**. These included the ATRA between tosyl chloride **19** and styrene **20** (Scheme 1.8a), the pinacol coupling of benzaldehyde **21** (Scheme 1.8b), the (*E*)/(*Z*)-isomerization of both **18** and diisopropyl fumarate **22** (Scheme 1.8c), and the dual catalytic sp^2–sp^3 coupling reaction between *N*-Cbz-proline **23** and aryl bromide **14** (Scheme 1.8d). The results of this work showed that it is indeed possible to move away from the cyanoarene core for TADF photocatalysts and this can come with certain benefits, such as increased triplet energies and greater photostability.

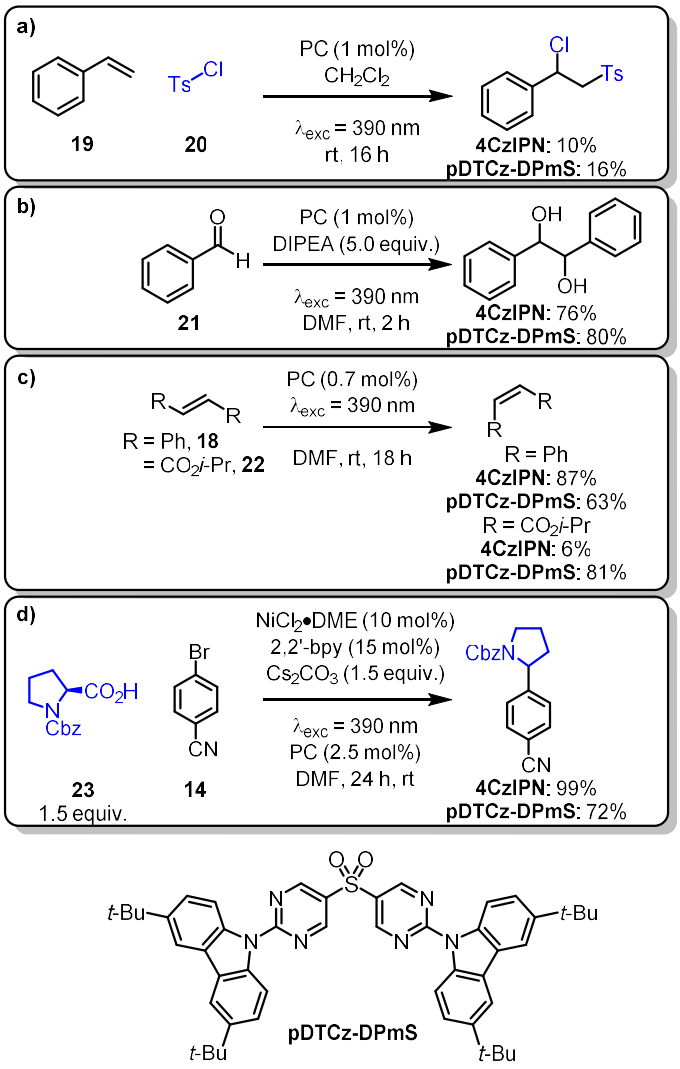

J. Org. Chem., 2022, DOI:10.1021/acs.joc.2c01137

Scheme 1.8 (a) ATRA reaction between tosyl chloride and styrene. (b) Pinacol coupling of benzaldehyde. (c) DET catalysed isomerization of (*E*)-stilbene or diisopropyl fumarate. (d) Dual catalytic sp^2–sp^3 coupling reaction.

A similar series of compounds developed by Lalevée and co-workers[47] also containing a sulfone acceptor and carbazole donor groups were used for the cationic polymerization of epoxy resin and the free radical polymerization of methacrylate (Figure 1.11). The results showed comparable or improved efficiencies when compared to non-TADF benchmarks.

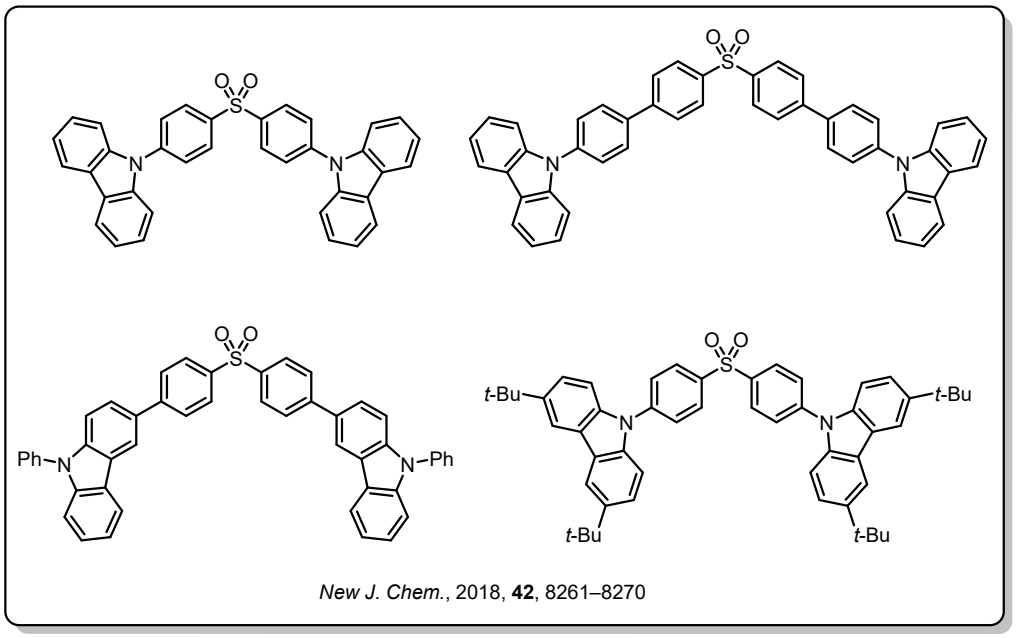

Figure 1.11 D-A TADF compounds used for photopolymerization.

Another example of alternative D-A design for photocatalysis was reported by Hudson and co-workers[48] using **ACR-IMAC**, which contains DMAC as a donor and an imidazoacridine acceptor (Scheme 1.9). **ACR-IMAC** was shown to be the optimal PC in a DET reaction for the synthesis of cyclobutanes **24** via a [2+2] cycloaddition between indole **25** and alkene **26** with comparable product yields to $[Ir(dF(Me)ppy)_2(dtbbpy)](PF_6)$.

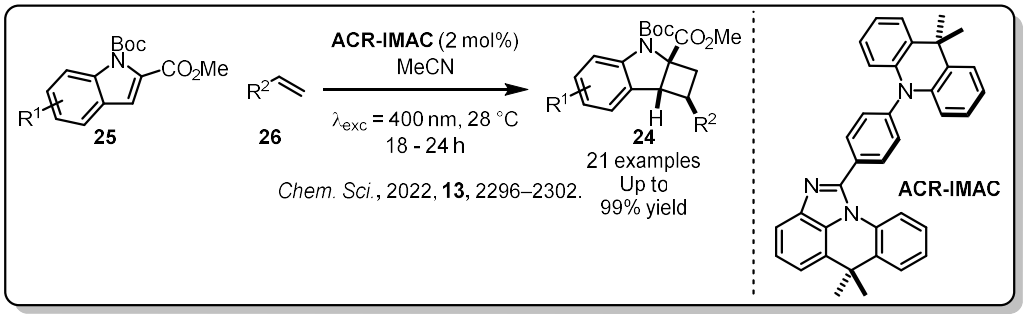

Scheme 1.9 DET catalysed [2+2] cycloaddition.

1.3 Lewis Base Catalysis

A Lewis base can be defined as a compound capable of donating an electron pair.[49] Therefore, Lewis base catalysis involves a chemical reaction that is accelerated by the donation of an electron pair to an appropriate acceptor without the consumption of the donor.[50] Some examples of Lewis base catalysts include secondary amines,[51] phosphines,[52] isothioureas (ITUs),[53,54] and N-heterocyclic

carbenes (NHCs)[55] (Figure 1.12). The classes of Lewis base catalyst relevant to this thesis are ITUs and NHCs, which will be discussed in further detail in the following sections.

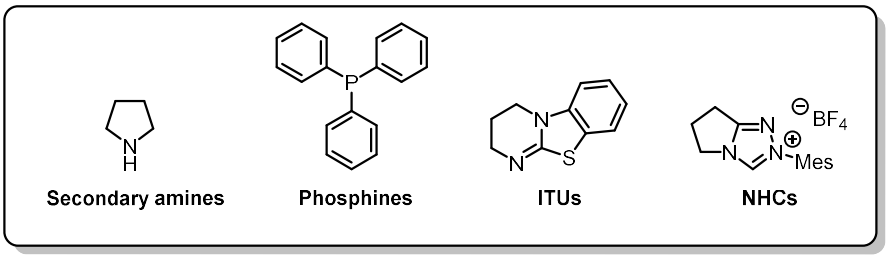

Figure 1.12 Examples of Lewis base catalysts.

1.3.1 Isothiourea Catalysis

Since Birman and co-workers' initial report of enantioselective ITU catalysis[56] using tetramisole and benzotetramisole (BTM) in enantioselective acyl transfer reactions, there has been further catalyst development to include HBTM, HBTM-2, HyperBTM, Se-HyperBTM and others (Figure 1.13).

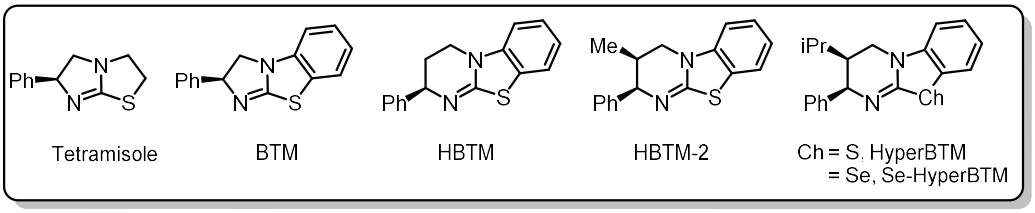

Figure 1.13 Examples of ITU catalysts and one selenium analogue.

Within ITU catalysis, four different modes of reactivity are commonly exploited (Figure 1.14). Acyl ammonium intermediates were the first to be explored,[56] using their ability to promote enantioselective acyl transfer reactions, by increasing the reactivity of the acyl group (Figure 1.14a). The acyl ammonium enolate intermediate can be generated from an acyl ammonium with an acidic α-proton,[53] which offers a nucleophilic site as well as a latent electrophilic site of the acyl ammonium (Figure 1.14b). When the acylating reagent used has a conjugated double bond, α,ß-unsaturated acyl ammoniums can be formed, which have a new electrophilic centre at the ß-position as well as a latent nucleophilic centre at the α-position (Figure 1.14c).[54] ITUs can also be used as a silyl transfer reagent, through silyl ammonium intermediates analogous to acyl ammoniums (Figure 1.14d).[57]

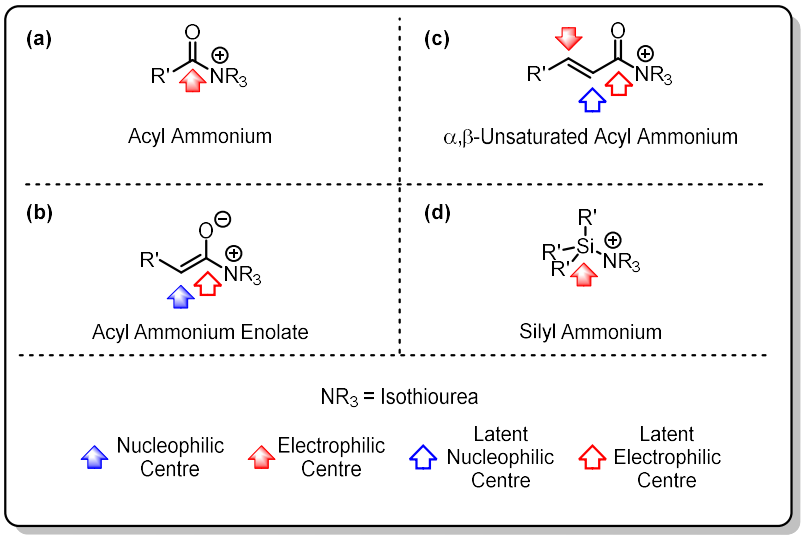

Figure 1.14 Different ITU intermediates.

The relevant intermediate to this thesis is the α,ß-unsaturated acyl ammonium. The first example of this chemistry used acyl fluorides **27** for a formal [2,3]-cycloaddition with 1,3-dipole precursor **28** (Scheme 1.10).[58] However, the results were poor with only 35% yield and 14% ee as their optimal results.

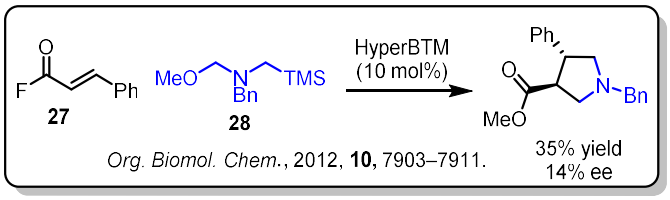

Scheme 1.10 First use of α,ß–Unsaturated Acyl Ammonium intermediates.[58]

Another example, reported by Robbinson and co-workers,[59] used homoanhydride **29** as the precursor for the key α,ß-unsaturated acyl ammonium intermediate **30** (Scheme 1.11). Reaction of **30** with deprotonated 1,3-dicarbonyls and subsequent proton transfers gives acyl ammonium **31**, which can cyclise to form lactone products **32**.

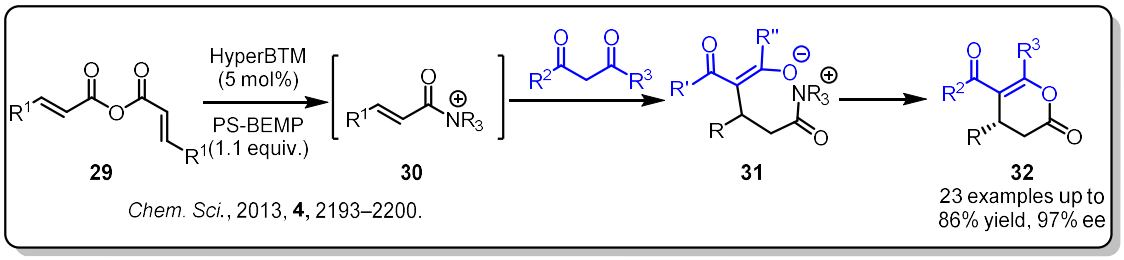

Scheme 1.11 Formal [4+2] cycloaddition *via* α,ß-unsaturated acyl ammonium intermediate.[59]

Abbasov and co-workers[60] used the α,ß-unsaturated acyl ammoniums generated from acyl chlorides **33** in combination with diene **34** in an innovative highly enantioselective [4+2] cycloaddition, to give complex bicyclic products **35** (Scheme 1.12). This reaction showed for the first time that these intermediates could act as a dienophile in Diels-Alder reactions.

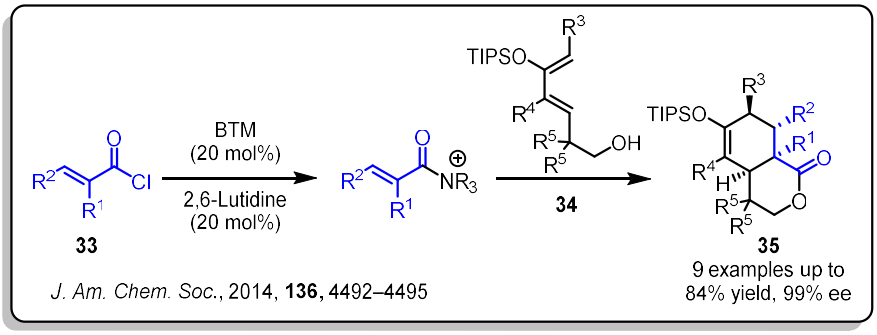

Scheme 1.12 ITU catalysed Diels-Alder reaction.[60]

Further development again came when using PNP esters, as a cyclisation is no longer required to turn over the ITU. Investigations performed by Matviitsuk and co-workers[61] showed that combining PNP ester **36** with ITU catalysis and an excess of nitromethane with base, forms the desired Michael addition products **37** with turnover facilitated by an aryloxide (Scheme 1.13). This reactivity has since been further developed to include other nucleophiles.[62]

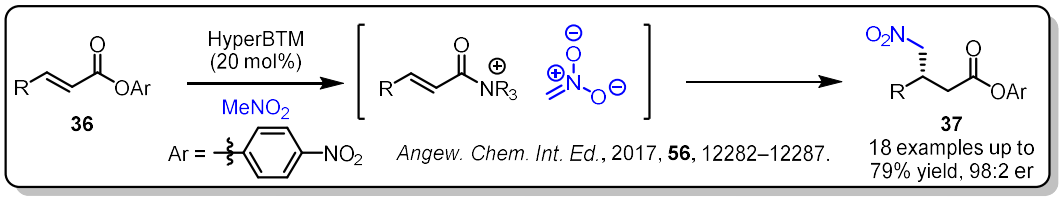

Scheme 1.13 PNP mediated Michael addition of α,ß-unsaturated ammoniums.[61]

1.3.2 N-Heterocyclic Carbenes

A carbene is a molecule containing an electronically neutral divalent carbon atom which bears two non-bonding electrons (Figure 1.15).[63] The two non-bonding electrons can be arranged into either a singlet or triplet configuration, which defines the two major categories of carbene.

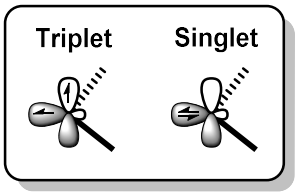

Figure 1.15 Different electronic configurations of carbenes.

The central carbon atom in a carbene is sp^2 hybridized, so of its four AOs, three are sp^2 hybridized and one is a *p* orbital (Figure 1.16).[64] Therefore, after formation of a divalent carbene molecule (RCR) there will be two bonding σ MOs, two non-bonding orbitals (in *p* and sp^2 orbitals) and two antibonding σ* orbitals. According to Hund's rules, the 6 available electrons would fill the available MOs to give a triplet carbene. However, the sp^2 orbital will not be degenerate with the *p* orbital. If this energy gap (ΔE_{nb}) is larger than the energy required to pair the two valence electrons, then a singlet carbene is preferred to a triplet carbene.

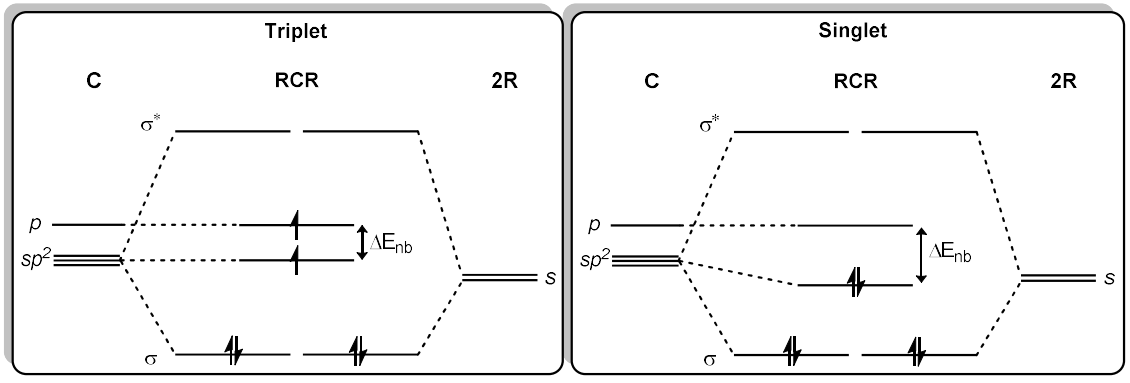

Figure 1.16 Generic MO diagrams of singlet and triplet carbenes.

Using this understanding of the bonding in carbenes, Arduengo and co-workers[65] successfully synthesised and isolated a stable free-carbene in the form of *N*,*N*'-diadamantyl imidazolinylidene (Figure 1.17).

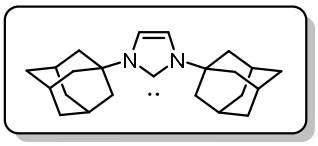

Figure 1.17 Stable free-carbene.[65]

N,*N*'-diadamantyl imidazolinylidene is an example of an NHC. The π donation from the nitrogen atom lone pairs increases ΔE_{nb}, which favours the singlet configuration and lowers the electrophilicity of the carbene, resulting in a more stable molecule (Scheme 1.18a). Additionally, there is a σ-electron-withdrawing effect from the electronegative nitrogen atoms, which further stabilises the system. The combination of these two effects is often called the "push-pull" effect and has been used extensively to design NHCs. Additional kinetic stability of NHCs is gained through the use of extremely large nitrogen-bound substituents, such as adamantyl or 2,6-diisopropylphenyl, as this helps prevent undesired dimerization (Scheme 1.18b).

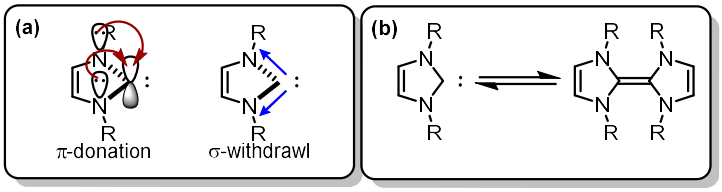

Figure 1.18 Methods for stabilization of carbenes. (a) Push-pull effect. (b) Large *N*-substituents to avoid dimerization.

As triplet carbenes have two unpaired electrons, they typically behave as diradicals. However, singlet carbenes such as NHCs, have nucleophilic lone pairs that allow them to act as Lewis bases. Therefore, NHCs have been used as both ligands in metal complexes[66] and as Lewis base catalysts,[55] which has led to a wide range of designs to produce the desired properties for differing applications (Figure 1.19).

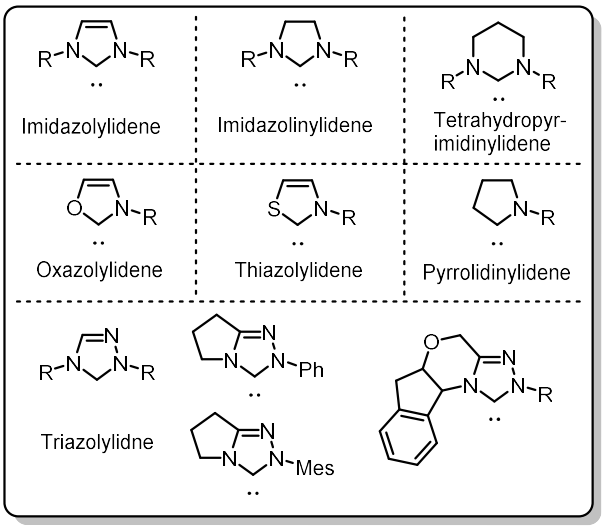

Figure 1.19 Some examples of different NHC structures.

NHCs as Lewis base catalysts can be found in nature in the form of a thiazolium ion precatalyst, thiamine **38** (vitamin B_1), which is important in a variety of biochemical processes.[67] Thiazolium **38** and its simpler analogue **39** were first used by Ukai and co-workers[68] to catalyse the acyloin condensation of furfural, which was the first example of NHC Lewis base catalysis (Scheme 1.14).

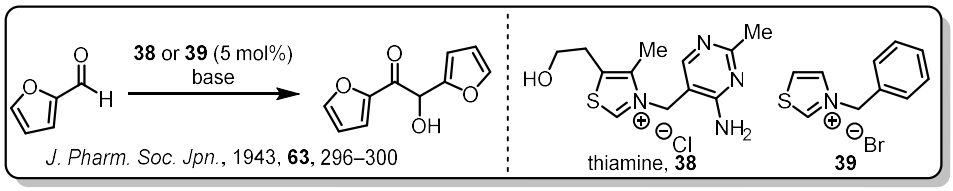

Scheme 1.14 Acyloin condensation of furfural catalysed by an NHC catalyst.[68]

The mechanism for this type of transformation was later investigated by Breslow and co-workers,[69] who proposed that the reaction began with the deprotonation of the thiazolium salt to give a free carbene **40** (Scheme 1.15). Subsequent addition to benzaldehyde **41** produced an initial adduct **42**, which after *O*-protonation and *C*-deprotonation gives an enaminol species **43** that would go on to be termed the Breslow intermediate. The Breslow intermediate can then add to a second molecule of **41** to give the corresponding adduct **44**, which collapses to release the NHC catalyst and the desired benzoin condensation product **45**.

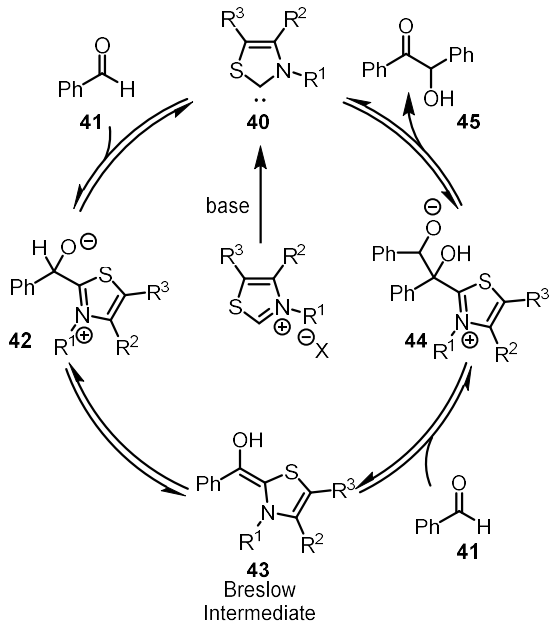

Scheme 1.15 Mechanism for the benzoin condensation.[69]

As with ITU catalysis, there are many different reactive intermediates that can be generated using NHC catalysis, depending on the starting material that is used (Figure 1.20). As described above, the Breslow intermediate has a nucleophilic centre and is used for umpolung chemistry of aldehydes. If an alkene is included in conjugation, then a homoenolate can be formed, which can act as a nucleophile from an alternative site. Analogous to the intermediates described for ITU catalysis, azolium enolates, acyl azoliums and α,ß-unsaturated acyl azoliums are also used for similar applications. Additionally, extension of the π-system for azolium enolates results in a dienolate, which now has two possible nucleophilic sites and a latent electrophilic site.

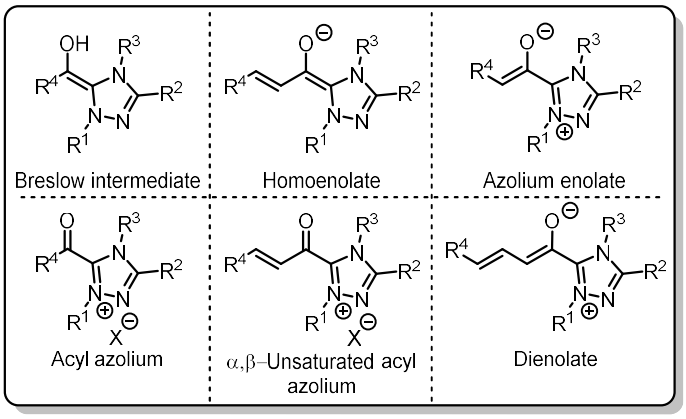

Figure 1.20 Some examples of NHC intermediates.

1.4 N-Heterocyclic Carbene and Photoredox Dual Catalysis

Dual catalysis is an excellent way to combine the unique reactivity of two different modes of catalysis together to achieve transformations otherwise impossible with either mode independently. Photocatalysis is particularly interesting as it provides a mild way of producing high-energy intermediates such as radicals; however, due to the nature of these intermediates and their interactions with the photocatalyst, selectivity can be difficult to control. Therefore, the use of an additional catalyst can be extremely beneficial for controlling this selectivity,[70] particularly enantioselectivity.[71] For NHC/PC dual catalysis,[72] the reactions developed thus far can be split into three categories. First, the interaction of an NHC-based intermediate with a separate photocatalytically generated intermediate is considered. Secondly, the PC can interact with an NHC-based intermediate to generate a different NHC-based intermediate (typically radical in nature). Thirdly, the use of a photoactive NHC-based intermediate that itself absorbs light to promote photocatalysed reactions can be harnessed.

1.4.1 Interaction of NHC Intermediates with Photocatalytically Generated Intermediates

A representative example of this type of dual NHC/PC catalysis is represented by the report of Rovis and co-workers[73] who developed a method for the α-acylation of tertiary amines **46** (Scheme 1.16). The proposed mechanism proceeds via the photocatalytic generation of iminium ions **47** using 1,3-dinitrobenzene (1,3-DNB) as a sacrificial oxidant. These could then be intercepted by a Breslow

intermediate **48**, formed between the NHC catalyst and an aldehyde **49**, to generate the adduct **50**, which can then collapse to give the desired product **51** and complete the catalytic cycle.

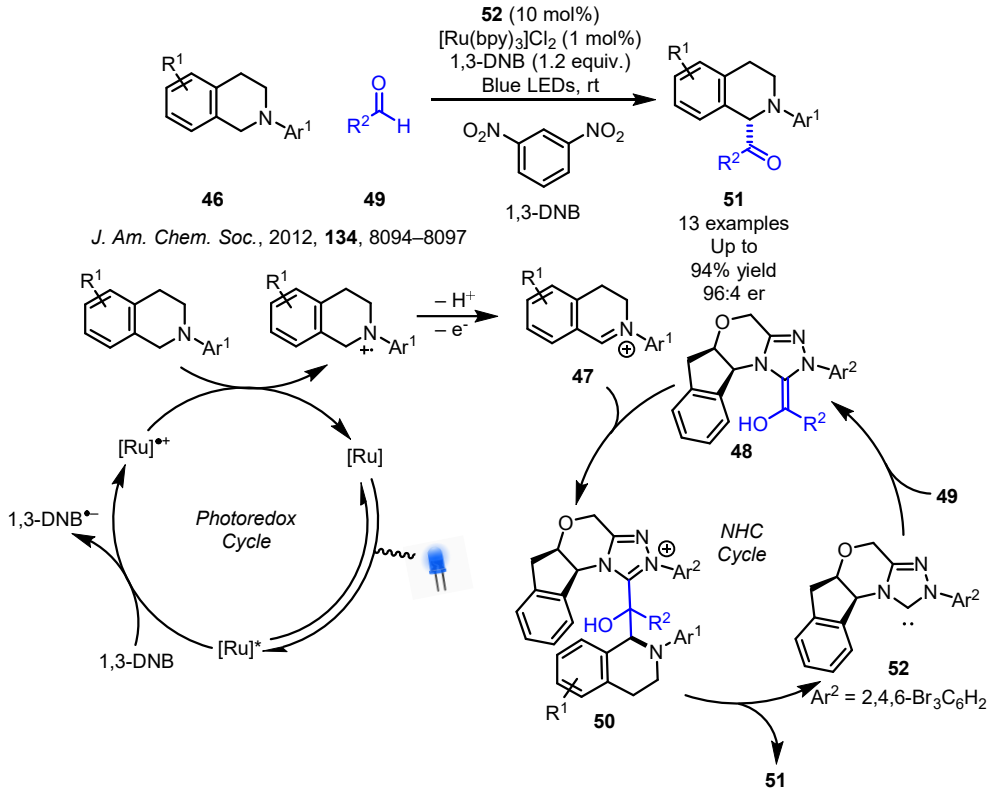

Scheme 1.16 Catalytic cycle for the α-acylation of tertiary amines.[73]

As another representative example, Ye and co-workers[74] developed the γ-alkylation of enals **53** using electron deficient alkyl halides **54** (Scheme 1.17). The proposed mechanism proceeds via the photocatalytic generation of electrophilic alkyl radicals **55**, which then add to the dienolate **56** formed between the NHC catalyst and **53** to give the desired α,ß-unsaturated esters **57**.

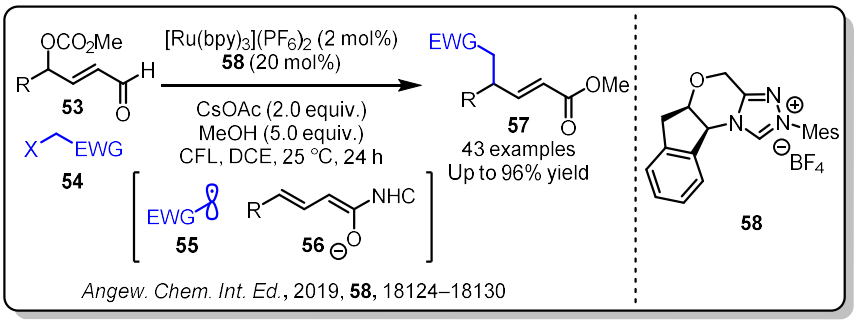

Scheme 1.17 γ-Alkylation of enals.[74]

1.4.2 Interaction of NHC Intermediates with Photocatalysts

This category of NHC/PC dual catalysis is dominated by reactions that involve the single electron reduction of acyl azolium intermediates by the PC. This was first demonstrated by Bay and co-workers[75] using acyl imidazoles **59** as the acyl azolium precursor and Hantzsch esters **60** as the radical precursor (Scheme 1.18). The proposed mechanism begins with the reductive quench of PC* by **60** to generate $PC^{\bullet-}$ and an alkyl radical **61**. $PC^{\bullet-}$ will then reduce the acyl azolium generated between the NHC catalyst and **59** to give the corresponding NHC-stabilised ketyl radical **62**, which can then undergo radical-radical coupling with **61** to generate the corresponding adduct **63**. **63** can then collapse to release the desired ketone product **64** and complete the catalytic cycle.

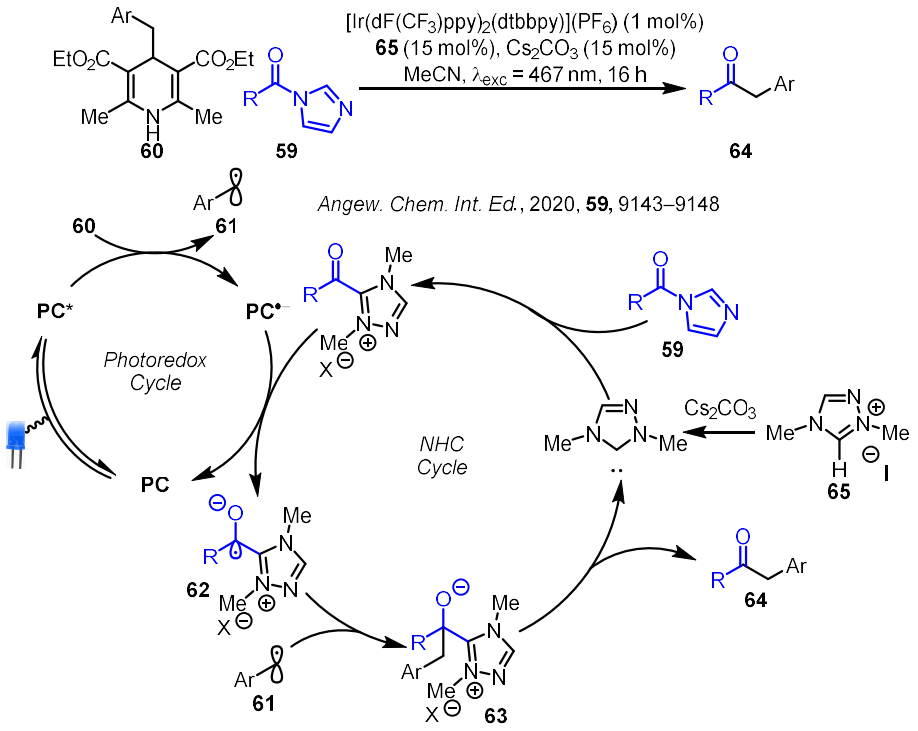

Scheme 1.18 Catalytic cycle for the synthesis of ketones.[75]

Since this seminal work, there have been numerous other examples using the general principal of combining an acyl azolium precursor with a radical precursor under appropriate NHC/PC dual catalytic conditions.[76] Of particular note is the extension to a three-component radical relay process developed by Studer and co-workers,[77] which combined a trifluoromethyl radical precursor **66**, an aroyl fluoride **67** as the acyl azolium precursor, and an alkene **68** to synthesise ketones **69** (Scheme 1.19).

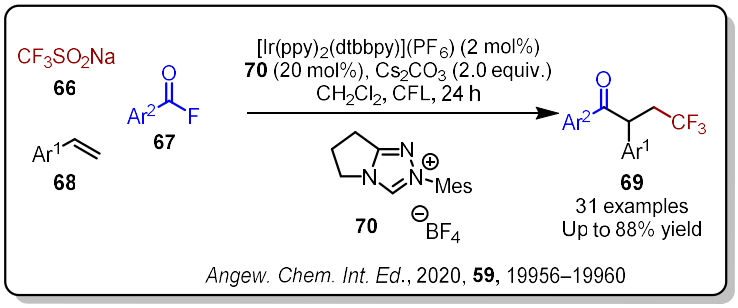

Scheme 1.19 Synthesis of extended ketones via a three-component radical relay process.[77]

1.4.3 Direct Excitation of NHC Intermediates

NHC/PC dual catalysis is typically achieved by using two distinct catalysts; however, there are examples where an NHC intermediate is directly excited and acts as a bifunctional NHC/PC catalyst to achieve similar reactivity. For example, Chi and co-workers[78] combined PNP esters **71** with Hantzsch

esters **72** under visible light irradiation using NHC catalysis to synthesise the corresponding ketones **73** without the addition of a traditional PC (Scheme 1.20). The proposed mechanism proceeds via the excitation of acyl azolium **74**, which is formed from the NHC catalyst and **71**, to generate **74*** that is then reductively quenched by **72** to give **74**$^{\bullet-}$ and an alkyl radical **75**. These two radical species can then couple together to generate the corresponding adduct **76**, which collapses to release **73** and complete the catalytic cycle.

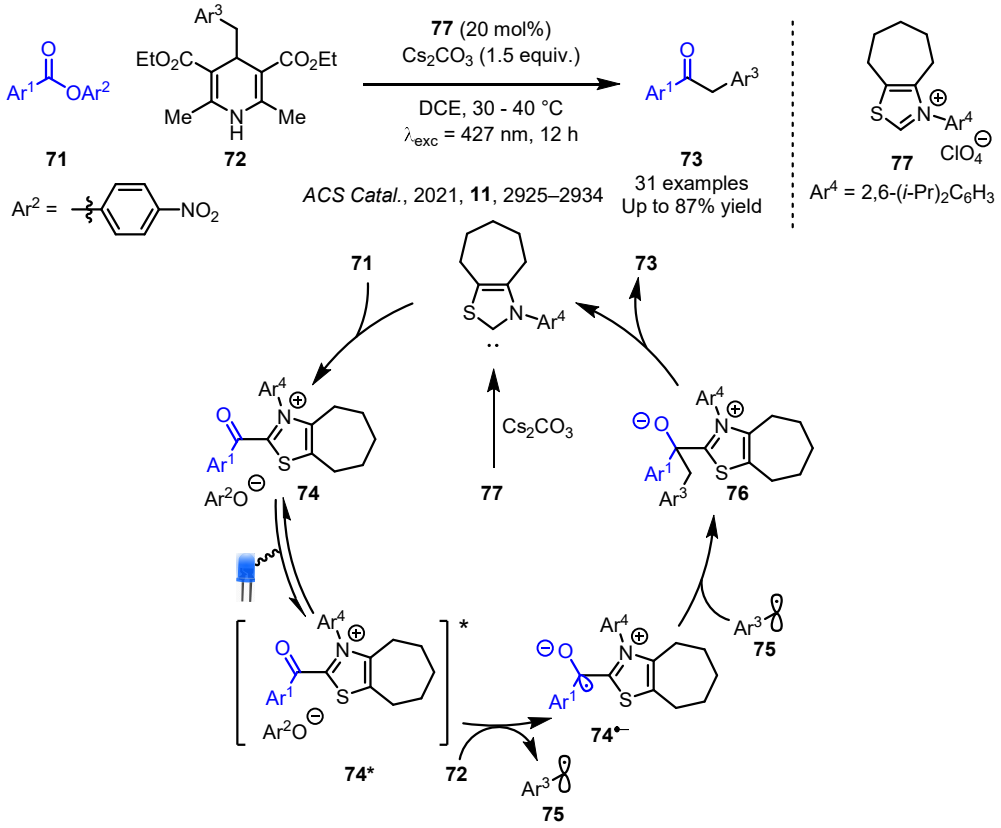

Scheme 1.20 Catalytic cycle for the bifunctional NHC/PC synthesis of ketones.[78]

Similarly to the previous section, this type of catalytic system was successfully applied to a three-component radical relay process by Larionov and co-workers[79] using diketone oxime **78** as an acyl radical precursor, an aldehyde **79** and an alkene **80** (Scheme 1.21). However, the proposed mechanism for this reaction is suggested to proceed via the excitation of an EDA complex **81** between Breslow intermediate **82** and **78** to give **81***. An EDA complex is an aggregate formed of an electron donor substrate and an electron acceptor molecule, which typically absorbs in the visible region while the individual components do not, with the resulting electronic excitation triggering a SET event to

generate radical intermediates.[80] Decomposition of this excited state intermediate will generate acyl radicals **83** and also an NHC-stabilised ketyl radical **84**. **83** can then add to **80** to give a benzylic radical intermediate **85**, which will undergo radical-radical coupling with **84** to form the corresponding adduct **86**. Finally, **86** collapses to release the desired ketone product **87** and complete the catalytic cycle.

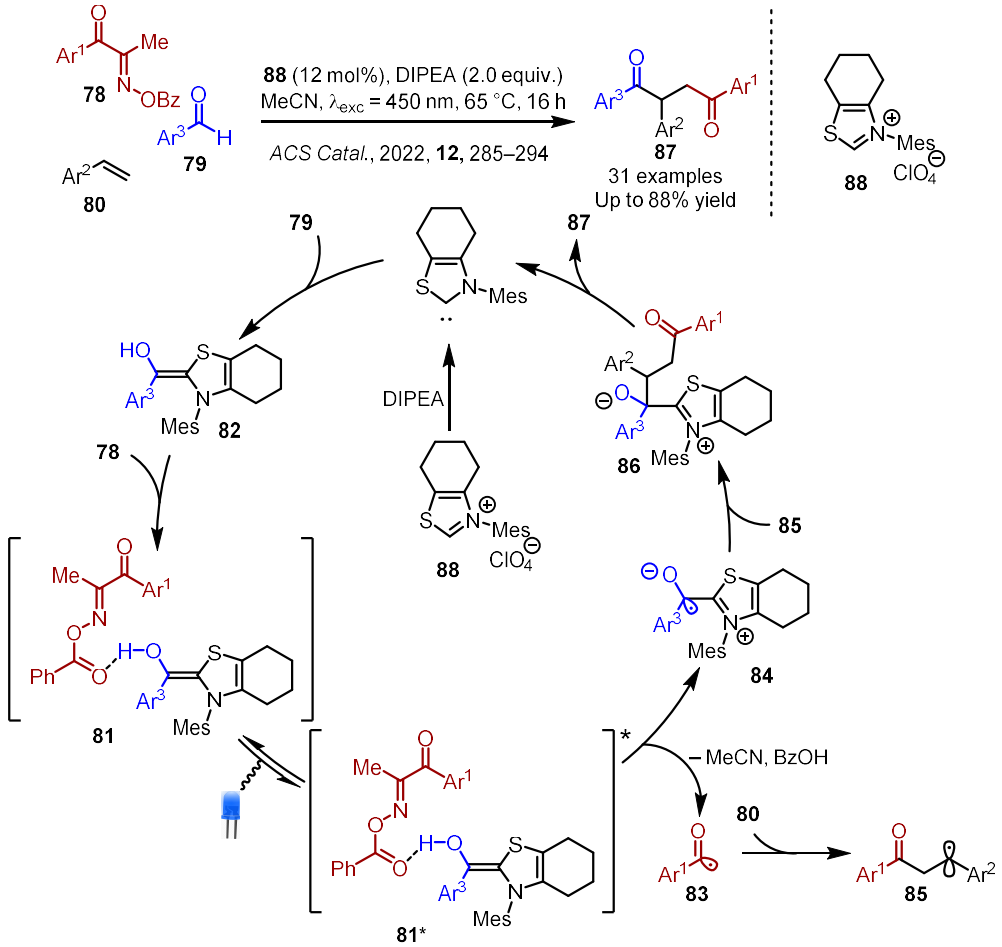

Scheme 1.21 Catalytic cycle for the bifunctional NHC/PC three component synthesis of ketones.[79]

1.5 Aims and Objectives

There are three key objectives for this thesis that together aim to investigate the benefits of TADF photocatalysis and its combination with Lewis base catalysis.

1.5.1 ITU/Photoredox Dual Catalysis

Utilising the complementary experience of the Smith group in ITU catalysis and the Zysman-Colman group in the use of TADF compounds for photocatalysis, this project aimed to develop a general platform for dual ITU/photoredox catalysis. This would include the synthesis of a bifunctional ITU/PC catalyst with the photocatalytic moiety having TADF properties. This bifunctional catalyst would then be applied for the enantioselective radical-conjugate addition reaction of α,ß-unsaturated esters **89**, to synthesise the corresponding enantioenriched products **90** (Scheme 1.22). This work would greatly expand the capabilities of ITU catalysis, which currently is limited to two-electron processes.

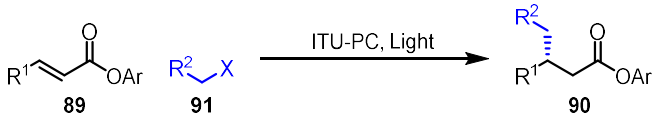

Scheme 1.22 Proposed PC/ITU dual catalysed RCA reaction.

1.5.2 MR-TADF Compounds as Photocatalysts

The majority of TADF compounds used in photocatalysis are based around the cyanoarene core and all of them are D-A in design. The aim of this project is to expand the use of TADF compounds as PCs to include MR-TADF emitters and explore whether their unique properties could result in certain advantages over typical D-A TADF photocatalysts. This work will focus on the use of **DiKTa** and its mesitylated analogue **Mes$_3$DiKTa** in various standard photocatalytic reactions, using the widely used D-A TADF photocatalyst **4CzIPN** as a benchmark (Figure 1.21).

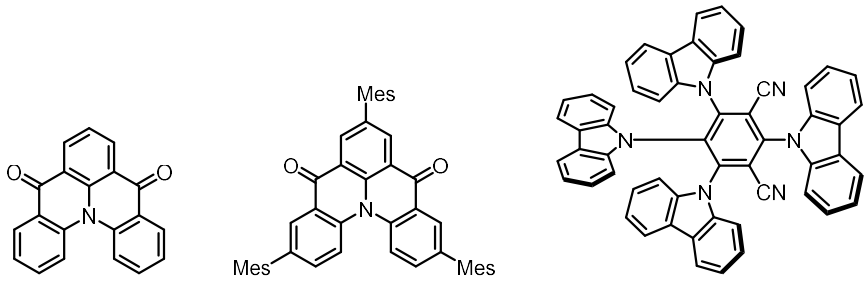

DiKTa **Mes_3DiKTa** **4CzIPN**

Figure 1.21 MR-TADF photocatalysts to be tested against a benchmark D-A TADF photocatalyst.

1.5.3 NHC/MR-TADF Dual Catalysis

NHC/photoredox catalysis is now a widely studied area of research. The aim of this project is to use the previously developed MR-TADF photocatalysts in combination with NHC Lewis base catalysts to develop new reactivity and further demonstrate the utility of MR-TADF photocatalysts. This will be explored through the development of a novel synthetic methodology for the synthesis of 1,4-diketones **92** using α-ketoacids **93** as acyl radical precursors (Scheme 1.23).

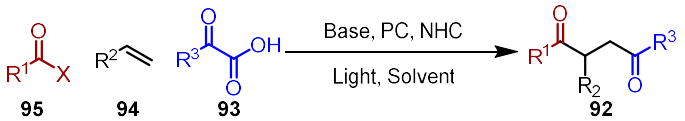

Scheme 1.23 Proposed NHC/PC synthesis of 1,4-diketones using MR-TADF PCs.

2 Synthesis and Evaluation of a Potential Bifunctional Lewis Base / Photocatalyst; Hyper2CzPN

2.1 Introduction

As discussed in the introduction, a common method for enantioselective photocatalytic processes is to combine photocatalysis with another catalyst mode that is enantioselective in a dual catalytic system. While PCs can be used in combination with a molecularly distinct enantioselective catalyst in a dual catalytic system, a limitation that arises is the necessary interaction of a low concentration chiral catalytic intermediate with a somewhat short-lived (µs time scale) excited state. One potential solution to this is to form the chiral intermediate within the same molecule as the PC using a bifunctional catalyst, so that the effective concentration of the intermediates relative to each other is much higher (Scheme 2.1).

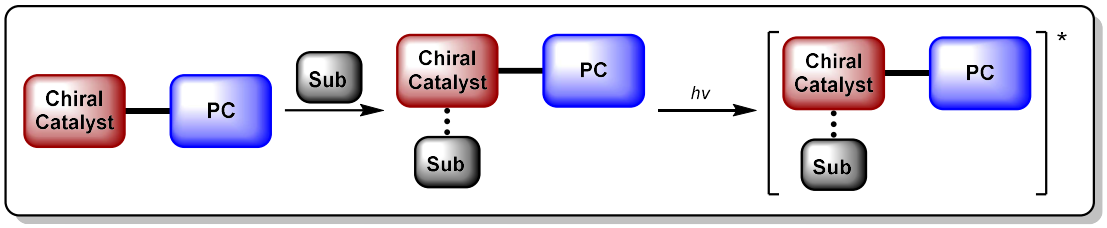

Scheme 2.1 Representation of a bifunctional PC interacting with a substrate (sub).

Catalysts **96**-**99** developed by Alemán,[81] Meggers,[82] Bach,[83] and Yoon,[84] are all bifunctional PCs (Figure 2.1). They each have a catalytic mode that can bind to a substrate to form chiral intermediates (through amine condensation, Lewis acid complexation or hydrogen bonding) and a photocatalytic moiety, which together have vastly increased the capabilities of asymmetric photocatalysis.

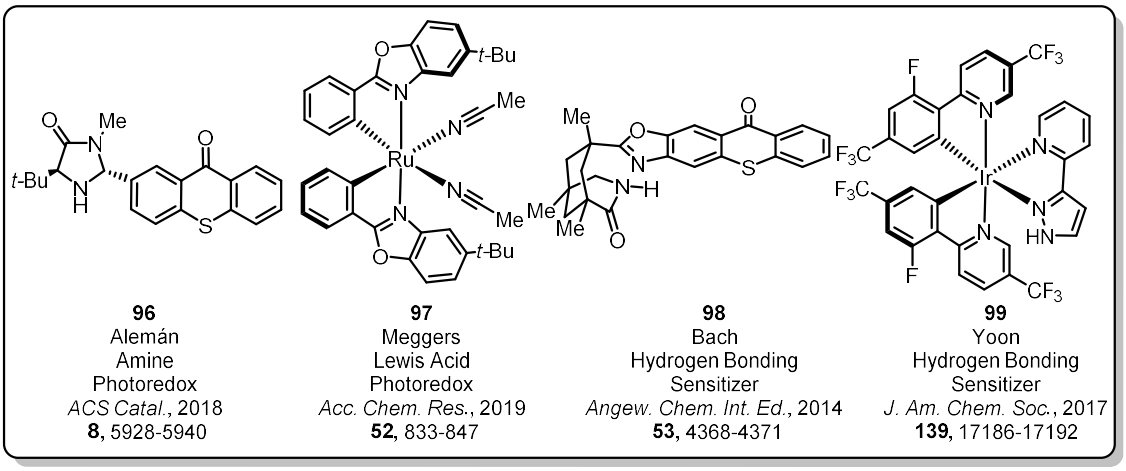

Figure 2.1 Examples of bifunctional catalysts and their known modes of action.

Looking at the precedents set and the recent development of different bifunctional PCs, we decided to expand this further using our knowledge of isothiourea catalysts. Considering the catalytic intermediates of ITU catalysis are present in very low concentrations, the aims of this research were to synthesise a bifunctional catalyst containing both an ITU and donor-acceptor PC moiety, with an initial focus on photochemical RCAs. As a starting point, previous research within the Smith group on conjugate additions to α,ß-unsaturated acyl ammonium intermediates[61] were identified as analogous to the Lewis acid complexes used by Meggers[85] and Yoon[86] in their RCA reactions. Exploitation of these α,ß-unsaturated acyl ammonium intermediates as reactive electrophiles for photocatalytically generated radicals would simultaneously expand the capabilities of both isothiourea and photoredox catalysis to include new functionalities (Scheme 2.2).

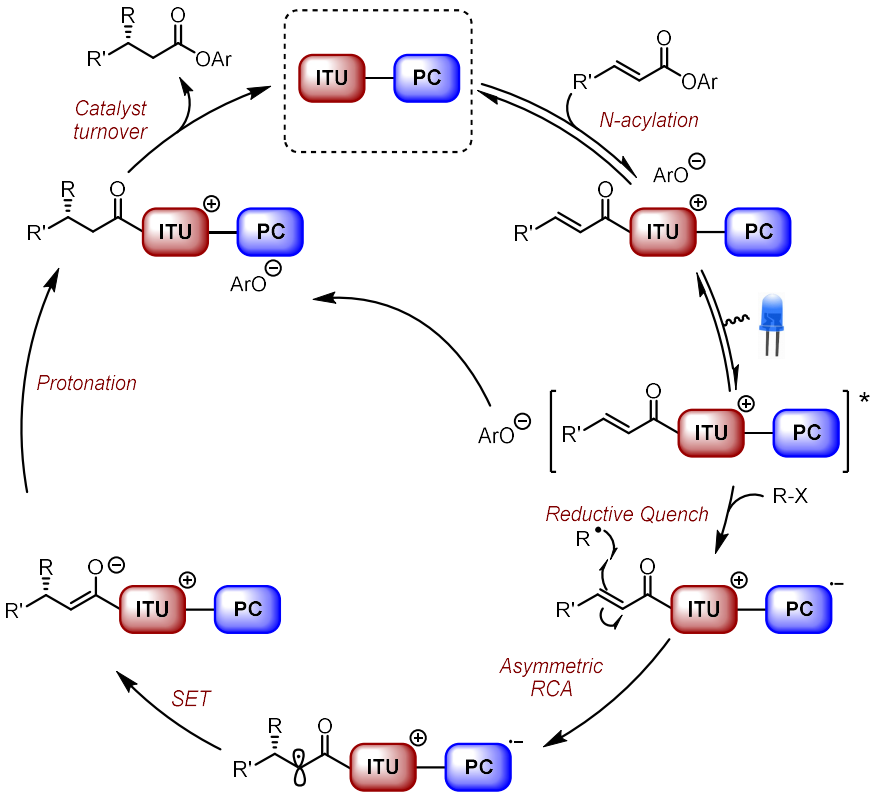

Scheme 2.2 Proposed bifunctional catalyst RCA cycle.

2.2 Results and Discussion

2.2.1 Synthetic Plan

There are three distinct sections to our design of a bifunctional catalyst, the isothiourea functional group (red), a photoactive TADF unit (blue), and a linker between them (black) (Scheme 2.3). Our initial target aimed to combine the isothiourea HyperBTM and **2CzPN** with a triazole linker to give **Hyper2CzPN**. Retrosynthetically, disconnecting the carbazole C-N bond to give a known aryl fluoride, **CzFPN**, and a carbazole **100** was envisioned. The triazole moiety could be disconnected to alkyne and azide fragments **101** and **102**, respectively. Further disconnection gave an alkyl electrophile **103** with two leaving groups which could react with known HyperBTM variant **104** and sodium azide.

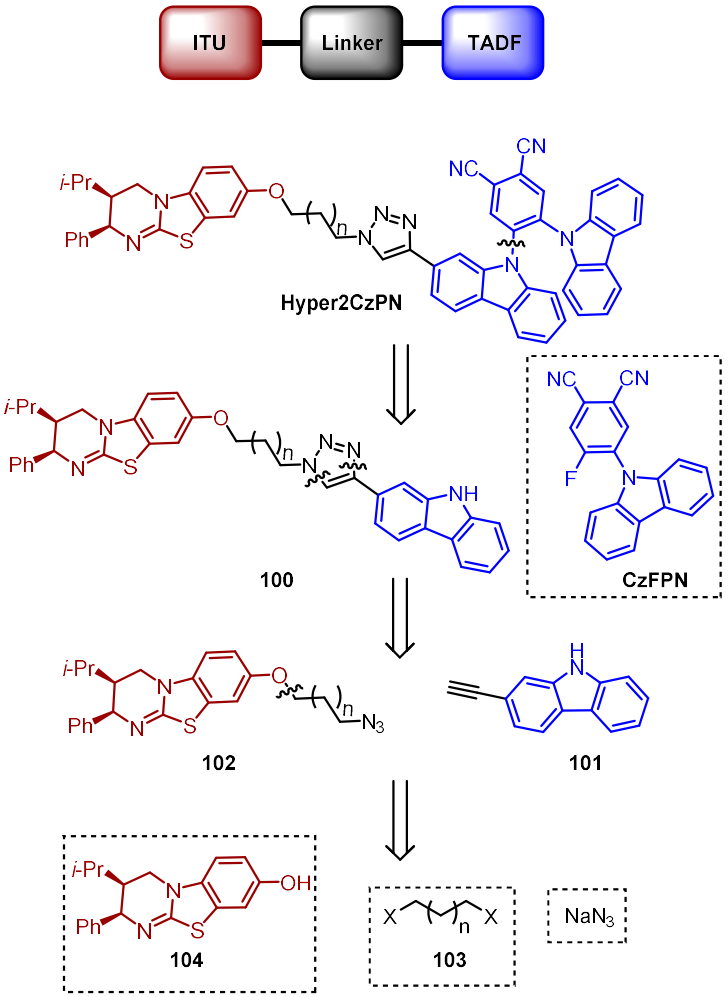

Scheme 2.3 Retrosynthesis of target molecule.

2.2.2 Synthesis of Hyper2CzPN

Synthesis began with formation of HyperBTM derivative **104•HBr** as previously reported[87] starting with the chlorination of amino benzothiazole **105** to give **106** in moderate yield (Scheme 2.4). The coupling of benzothiazole **106** with amino alcohol **107** followed by demethylation using boron tribromide gave **104•HBr** in 21% overall yield. It was possible to decrease the number of equivalents of boron tribromide required for the demethylation step from 10 equivalents in the original method,[87] to just 2 equivalents, while maintaining product yield.

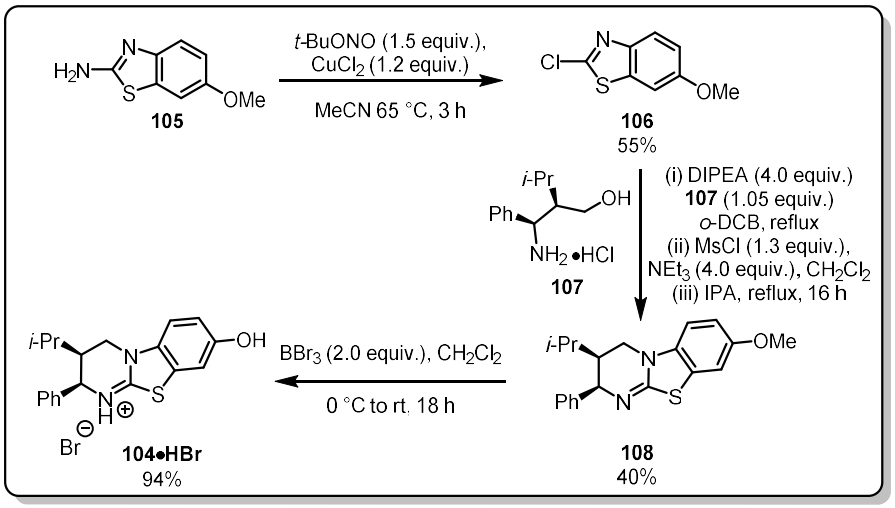

Scheme 2.4 Synthesis of **104•HBr**.

Further investigations focused on synthesising azide **102**. Initially, 1,2-dibromoethane with base and solvent was used based on the previous alkylation of **104•HBr** with propargyl bromide.[87] Unfortunately, no alkylation was observed, giving free-base **104** as the only isolated product, likely due to a competitive 1,2 elimination of dibromoethane (Scheme 2.5a). Changing to 1,3-dibromopropane showed promising reactivity, however the isolated material was shown to not be the desired product and is tentatively thought to be terminal alkene **109**, due to the characteristic terminal alkene ^{1}H NMR resonances. This side product is presumably formed through an undesired elimination step but was not fully characterised (scheme 2.5b).

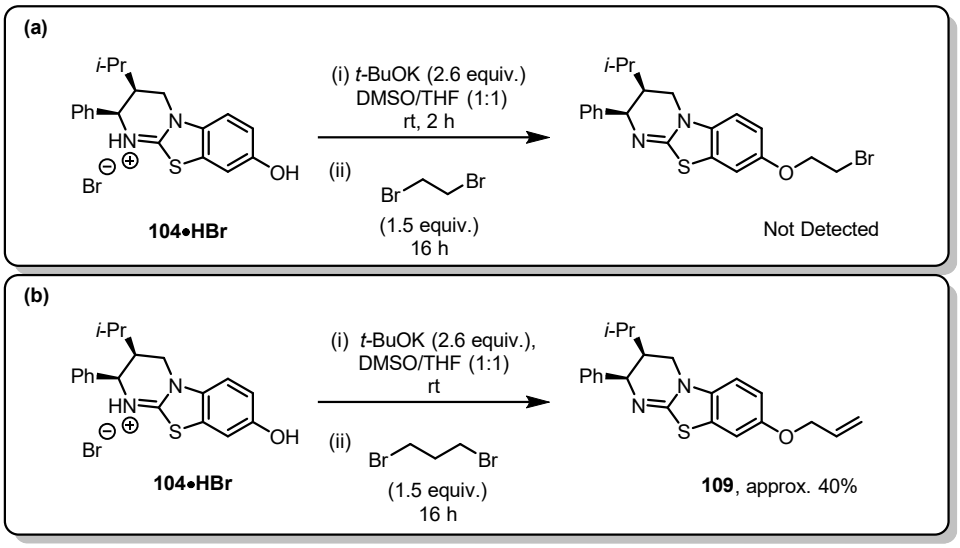

Scheme 2.5 (a) Attempted alkylation of **104•HBr** with 1,2-dibromoethane. (b) Attempted alkylation of **104•HBr** with 1,3-dibromopropane.

As the direct installation of a linker containing a second leaving group was proving problematic during the alkylation of **104•HBr**, it was decided to first install the azide functional group, starting from 3-chloro-1-propanol and NaN_3 (scheme 2.6). Azido alcohol **110** was transformed into the corresponding mesylate **111** using MsCl and NEt_3, then the crude product was used directly in reaction with **104•HBr**. Pleasingly, the desired azide **102** was formed in 61% yield, giving an overall yield of 10% for this fragment.

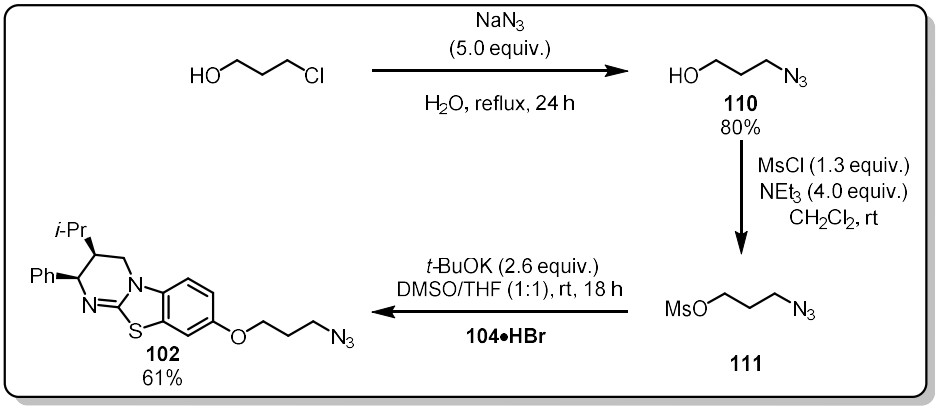

Scheme 2.6 Synthesis of azide fragment **102**.

With **102** in hand, the investigations turned to synthesising terminal alkyne **101**. Based on a procedure reported by Raithby and co-workers,[88] 2-bromo-9*H*-carbazole **112** was coupled with trimethylsilylacetylene in a Sonogashira reaction to afford TMS-alkyne **113** in 89% yield (Scheme 2.7). Proto-desilylation of **113** under basic conditions gave the desired terminal alkyne **101** in 97% yield.

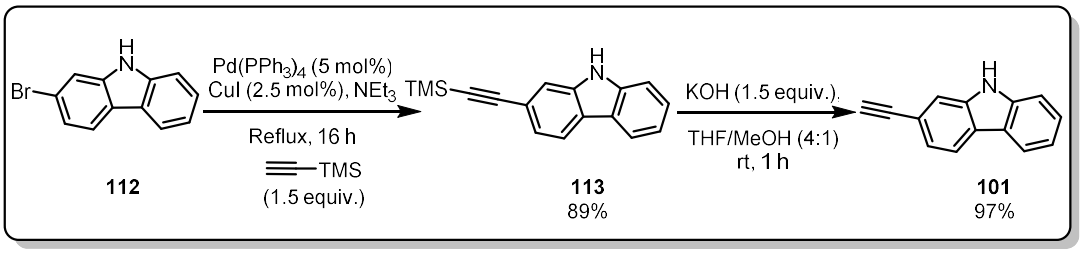

Scheme 2.7 Sonogashira reaction of **112** with trimethylsilylacetylene followed by TMS deprotection.

With both fragments in hand, the next stage in the synthesis was to perform the CuAAC reaction between the two fragments (Scheme 2.8). Initially, conditions previously reported by Smith and co-workers[87] in a synthesis of a polymer-supported catalyst were used, but gave an inseparable mixture of the desired product and other unidentified impurities. However, when the reaction was performed under anhydrous conditions and under a nitrogen atmosphere, **100** could be isolated in an 85% yield.

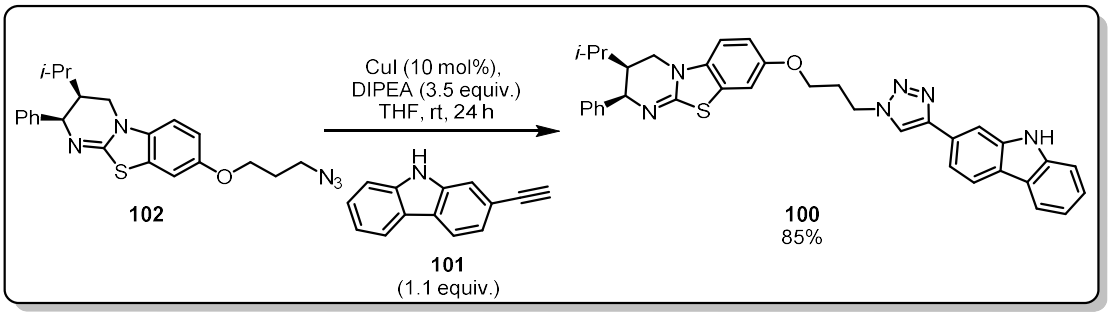

Scheme 2.8 Synthesis of **100** using CuAAC.

CzFPN has been used previously by Zysman-Colman and co-workers[89] to synthesise mixed 4,5-disubstituted phthalonitriles. The procedure first required mono-substitution of **2FPN** with carbazole. However, this proved difficult to replicate, with literature conditions giving an 8:1 mixture (**CzFPN**:**2CzPN**), which could not be separated effectively by column chromatography (Scheme 2.9). However, the mixture could be purified by recrystallization, which did provide pure **CzFPN**, but in a moderate 37% yield.

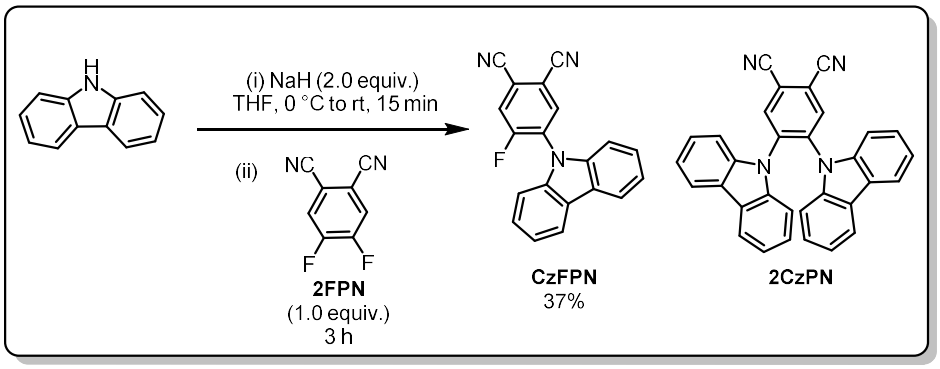

Scheme 2.9 Synthesis of **CzFPN**.

Based on the original retrosynthesis, the final step of the synthesis was proposed to be the S_NAr reaction between **CzFPN** and carbazole **100**; however, initial observations showed **100** was insoluble in many common solvents. Disappointingly, this included THF, which was the optimum solvent for similar reactions.[89] To circumvent the need for this insoluble intermediate, an alternative route was explored that switched the order of the S_NAr, CuAAC and Sonogashira reactions (Scheme 2.10). **Hyper2CzPN** was instead disconnected at the triazole moiety to give **102** and ethynyl-**2CzPN 114**, which in turn could be disconnected to give bromo-**2CzPN 115** and trimethylsilyl acetylene, with a final C-N disconnection giving **112** and **CzFPN**.

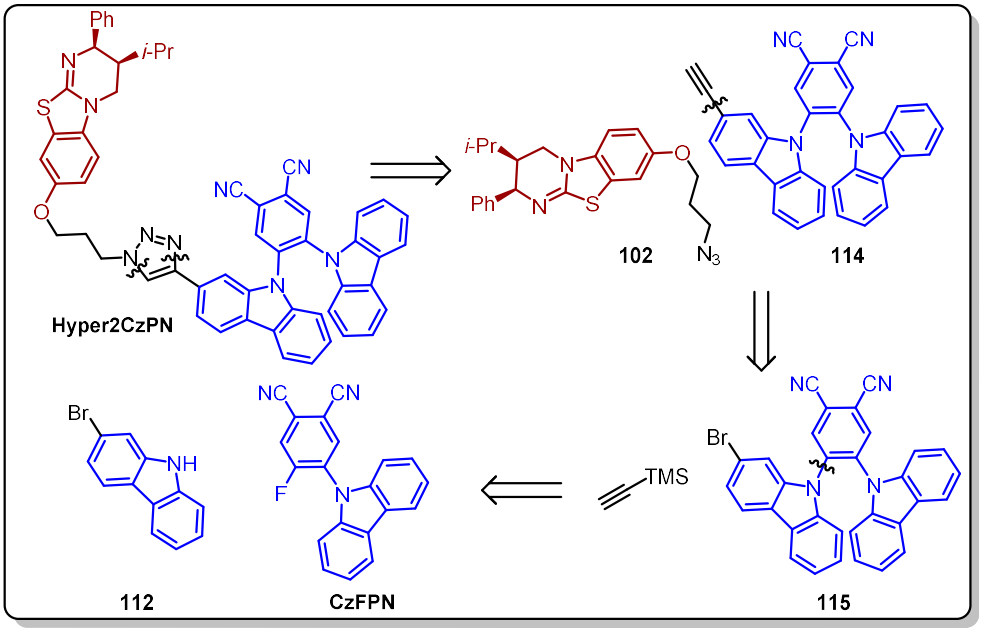

Scheme 2.10 New route to target.

This new route began with the synthesis of **115** from **CzFPN** and **112**, which proceeded with an 83% yield (Scheme 2.11).

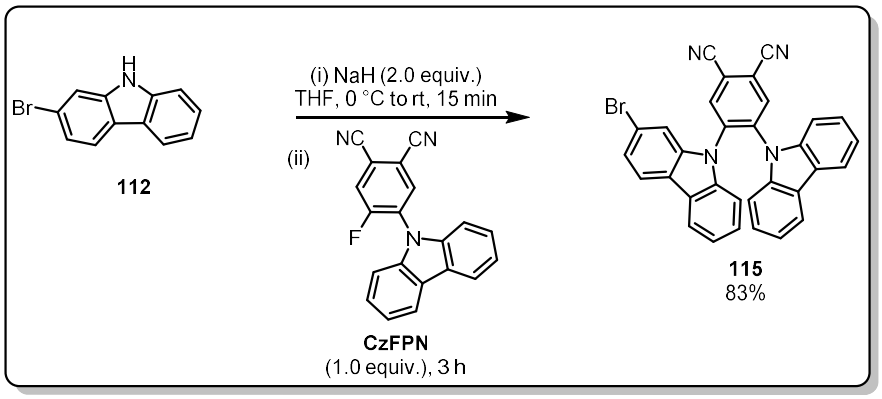

Scheme 2.11 S_NAr of **CzFPN** and **112**.

As in the previous route, a Sonogashira reaction with trimethylsilylacetylene was performed; however, when using **115**, some optimisation was required to obtain a satisfactory yield (Table 2.1). Conditions used previously to make **113** only gave trace amounts of the desired product (Table 2.1, entry 1). It was hypothesised that this was due to low solubility of **115** in neat NEt_3 and the use of co-solvents while maintaining NEt_3 as the base was considered. Using DMF improved both solubility and yield, (Table 2.1, entry 2), and further improvement was observed when using a mixture of THF and NEt_3. (Table 2.1, entry 3).

Table 2.1 Sonogashira Reaction Optimization

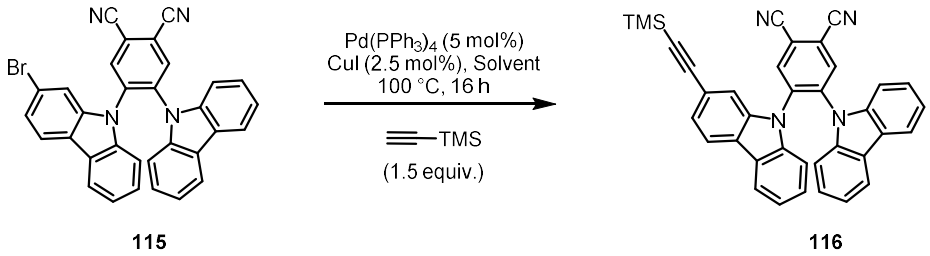

Entry[a]	Solvent	Yield / %
1	NEt_3	Trace
2	DMF:NEt_3 (1:2)	22
3	THF:NEt_3 (3:1)	60

[a] **115** (0.20 mmol, 0.08 M), trimethylsilylacetylene (0.30 mmol), $Pd(PPh_3)_4$ (6.0 µmol), CuI (0.012 mmol), THF (0.08 M), reflux, 16 h.

Under the desilylation conditions used previously, alkyne **116** was consumed but a mixture of unidentified products was obtained. However, by using TBAF deprotection, **114** could be isolated in 70% yield (Scheme 2.12a). Having synthesised both the isothiourea and TADF fragments, the final step

using CuAAC to combine them was possible. We were pleased to find that the previous conditions also worked well in this instance, furnishing the target molecule in 74% yield and an overall yield of 9% (Scheme 2.12b).

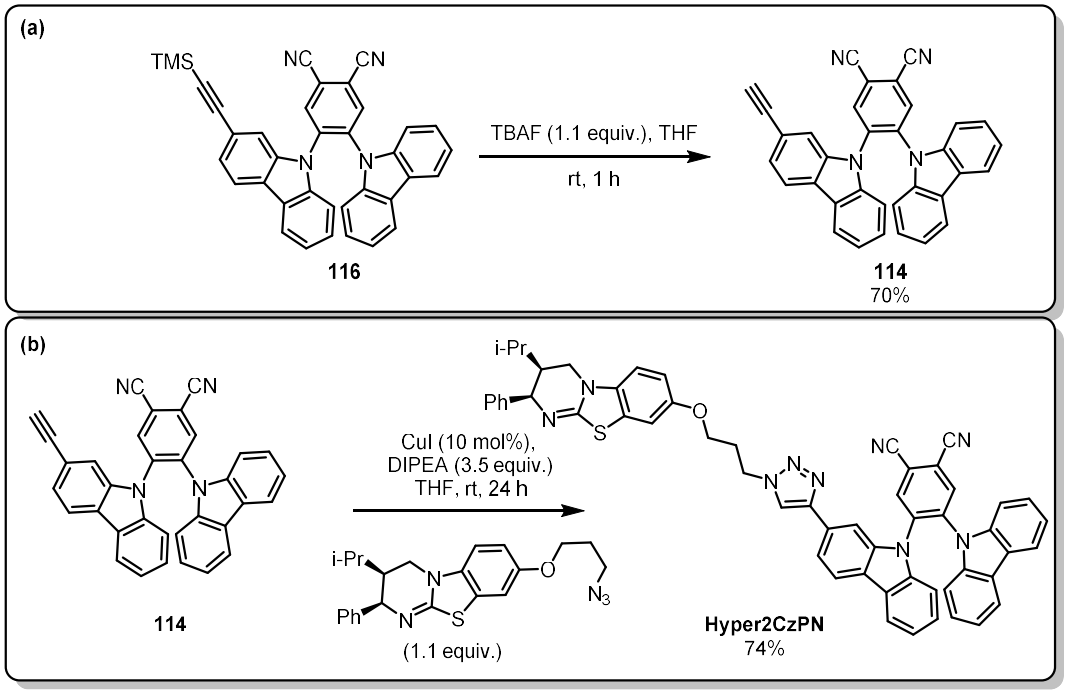

Scheme 2.12 (a) TMS deprotection of **116**. (b) CuAAC as final step.

2.2.3 Investigating the Bifunctional Catalyst

Three different experiments were performed to investigate the compatibility of the two catalysts (ITU and TADF) within the proposed bifunctional catalyst. These included CV, irradiating a solution containing both catalysts with blue LEDs (λ_{exc} = 456 nm), and adding isothioureas to known photocatalytic reactions. CV was used to determine the redox potentials of the isothiourea catalyst and the reversibility (an indication of stability to redox conditions) of their redox processes. Irradiating a solution containing just the PC and ITU was proposed as a simple test to see if the two catalyst systems were compatible. Adding isothioureas to known photoredox reactions was used to show if the catalytic cycles were likely to be able to act independently or if the ITU would inhibit these reaction processes.

Initial testing involved using CV to measure the redox potentials of HyperBTM and its analogues (Figure 2.2). As a model for the bifunctional catalyst **Hyper2CzPN**, the methoxy variant of HyperBTM

108 was first measured. The CV (CH_2Cl_2) showed no reduction waves (range scanned = – 2 to + 2 V) but a single irreversible oxidation wave at E_{PA} = 1.06 V (vs SCE) suggested significant chemical instability to oxidative conditions. Next, **Hyper2CzPN** was tested (CH_2Cl_2) showing a similar irreversible oxidation peak at E_{PA} = 1.2 V (vs SCE), which is therefore predicted to be on the isothiourea, and a reversible reduction peak at E_{red} = – 1.43 V (vs SCE) that is comparable to literature values for **2CzPN** (E_{red} = – 1.45 V in CH_2Cl_2 vs SCE),[90] so is likely on the phthalonitrile. For comparison, a model substrate **117** made with a triazole linker was also measured, which gave an identical reduction wave at E_{red} = – 1.43 V (vs SCE). These CVs showed successful production of a molecule that had the two catalysts as electronically distinct groups. However, they also suggest an inherent instability of isothioureas to oxidation, although it is still possible that the rate of regeneration of the isothiourea outcompetes decomposition under photocatalytic conditions.

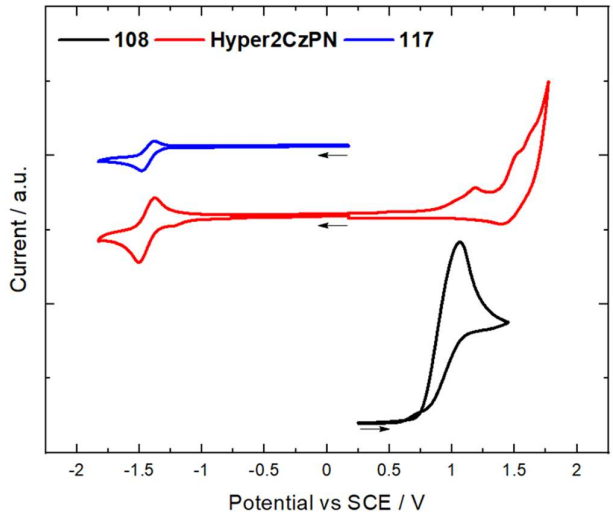

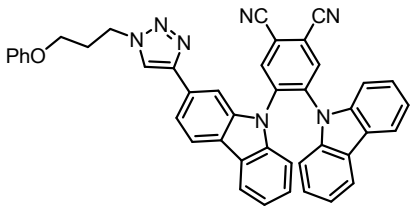

117

Figure 2.2 CVs of **108** (black), Hyper2CzPN (red), and **117** (blue) in 0.1 M solution of NBu_4PF_6 in degassed CH_2Cl_2, reported vs SCE (Fc/Fc^+ = 0.46 V in CH_2Cl_2)[91] and scan rate = 100 mV s^{-1}.

Further testing of the compatibility of isothioureas with PCs involved blue light irradiation (λ_{exc} = 456 nm) of a solution containing both an isothiourea and a PC in CH_2Cl_2 (Table 2.2). **Hyper2CzPN**

decomposed under these conditions, demonstrating a significant weakness in the bifunctional catalyst design (Table 2.2, entry 1). Further investigations probed the compatibility of isothioureas and PCs as separate molecules with the expectation that weak photooxidants would prove more favourable. Complete decomposition of HyperBTM was observed when an equimolar amount of **4CzIPN** was used (Table 2.2, entry 2). This may be expected as the excited state reduction potential of **4CzIPN** (E_{red}* = 1.35 V vs SCE)[43] is greater than the oxidation potential of HyperBTM (E_{PA} = 1.06 V vs SCE). Next, $[Ir(ppy)_2(dtbbpy)](PF_6)$, which has a less positive excited state reduction potential (E_{red}* = 0.66 V vs SCE) than **4CzIPN**, was tested with HyperBTM; however, full decomposition was again observed (Table 2.2, entry 3). Further investigations used 0.1 equivalents of PC relative to the isothiourea in an attempt to limit decomposition (Table 2.2, entry 4-8). **4CzIPN**, **2CzPN**, $[Ir(dF(CF_3)ppy)_2(dtbbpy)](PF_6)$, $[Ir(ppy)_2(dtbbpy)](PF_6)$ and $Ir(ppy)_3$ all showed complete decomposition of HyperBTM. This was expected for the strongly oxidising PCs (entries 4-6); however, even partial decomposition in the presence of $Ir(ppy)_3$ was surprising as it has a low excited state reduction potential (E_{red}* = 0.31 V vs SCE),[92] showing HyperBTM is unstable in the presence of even the mildest of photooxidants.

Table 2.2 Isothiourea Compatibility Testing.

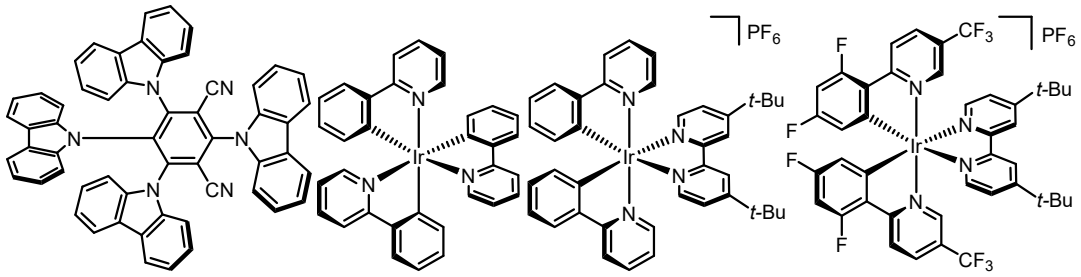

4CzIPN $Ir(ppy)_3$ $[Ir(ppy)_2(dtbbpy)](PF_6)$ [Ir-1] $[Ir(dF(CF_3)ppy)_2(dtbbpy)](PF_6)$ [Ir-2]

Entry[a]	Isothiourea	Photocatalyst	$E_{red}(P^*/P^{\bullet-})$/V	Equivalents	Decomposition
1[b]	**Hyper2CzPN**	**Hyper2CzPN**	–	–	Complete
2[b]	HyperBTM	**4CzIPN**	1.35[43]	1	Complete
3[b]	HyperBTM	[Ir-1]	0.66[21,22]	1	Complete
4	HyperBTM	**4CzIPN**	1.35[43]	0.1	Complete
5	HyperBTM	**2CzPN**	1.32[43]	0.1	Complete
6	HyperBTM	[Ir-2]	1.21[21]	0.1	Complete
7	HyperBTM	[Ir-1]	0.66	0.1	Complete
8[c[	HyperBTM	$Ir(ppy)_3$	0.31[92]	0.1	Partial
9	BTM	**4CzIPN**	1.35	0.1	Complete
10[d]	HyperBTM•HCl	**4CzIPN**	1.35	0.1	Minimal
11[d]	Tetramisole•HCl	**4CzIPN**	1.35	0.1	Minimal

[a] Isothiourea (0.1 mmol, 0.1 M), PC (0.01 mmol), λ_{exc} = 456 nm, rt for 16 h in CH_2Cl_2. (b) PC (0.1 mmol). (c) PC (0.002 mmol). (d) in deuterated DMSO.

In all cases, no decomposition products could be isolated. However, when BTM was used instead of HyperBTM with **4CzIPN** as the oxidant, full decomposition was observed, giving **118** as a single isolable product (Table 2.2, entry 9). Upon oxidation, BTM can form a fully aromatic heterocycle, likely through a similar mechanism to the iminium ion formation from tetrahydroisoquinolines,[93] where radical cation formation is followed by hydrogen abstraction and a second SET oxidation (Scheme 2.13a). Finally, protonated isothioureas were irradiated in the presence of **4CzIPN** and minimal decomposition was observed (Table 2.2, entries 10-11). This is interesting as it suggests that the cationic intermediates of isothiourea catalysis could be stable to photooxidation. However, as the equilibrium between bound and unbound catalyst would be predicted to lie heavily towards unbound "free"

catalyst (scheme 2.13b),[94] this does not necessarily provide a solution to the problem of ITU incompatibility with photoredox conditions.

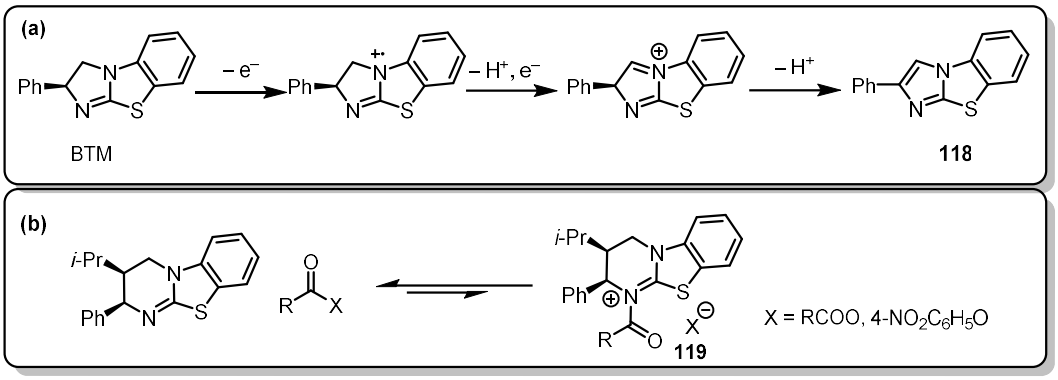

Scheme 2.13 (a) Oxidation of BTM. (b) Equilibrium of acyl ammonium formation X = RCOO or 4-$NO_2C_6H_5O$.

Further investigations were performed to determine whether the decomposition pathway could be easily outcompeted. Since an isothiourea catalysed photochemical RCA was the synthetic goal for this project, the decarboxylative addition of proline to diethyl maleate previously reported by Speckmeier and Zeitler[44] was chosen as the benchmark photoredox reaction for testing the effect of an ITU (Table 2.3). Consistent with the literature, the addition of **23** to **120** with base and **4CzIPN** as PC under blue light irradiation (λ_{exc} = 456 nm) proceeded with quantitative yield of the RCA product **121** (Table 2.3, entry 1). When HyperBTM (0.1 equivalents) was present, a small decrease in yield was observed (Table 2.3, entry 2). When 0.5 equivalents was used, full consumption of maleate and HyperBTM took place, but no formation of the desired product was observed (Table 2.3, entry 3). Unsurprisingly, increasing the HyperBTM to 1.0 equivalent gave similar results to 0.5 equivalents (Table 2.3, entry 4). If proline was excluded from the mixture, then full decomposition of both HyperBTM and diethyl maleate occured, with no identifiable products isolated (Table 2.3, entry 5). If diethyl maleate was excluded, then HyperBTM decomposition occurred but proline remained (Table 2.3, entry 6). These experiments indicate that HyperBTM outcompetes proline in SET oxidations despite having similar redox potentials (E_{PA}(HyperBTM) = 1.06 V (vs SCE), E_{PA}([Boc-Pro-O][/Cs]) = 0.95 V),[44] and indicates that the decomposition products of HyperBTM oxidation can presumably react competitively with the diethyl maleate, although products consistent with this hypothesis could not be identified. Based on these

results there are inherent stability issues with this proposed dual catalytic system and finding a general, widely applicable system of this type seems unlikely.

Table 2.3 Isothioureas in RCA Reaction.

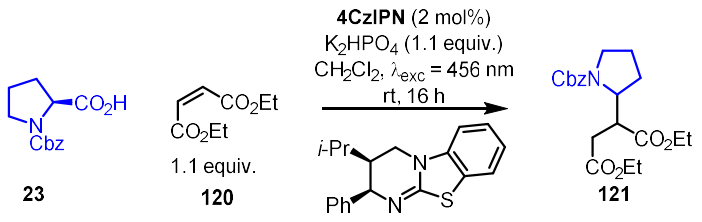

Entry[a]	Variation	Observation
1	No HyperBTM	Quant. Yield
2	0.1 equiv. HyperBTM	90% yield
3	0.5 equiv. HyperBTM	No product, decomposition
4	1.0 equiv.	No product, decomposition
5	No proline	Decomposition of both
6	No maleate	Decomposition of HyperBTM

[a] **119** (0.15 mmol, 0.8 M), **120** (0.17 mmol), K_2HPO_4 (0.17 mmol), **4CzIPN** (0.003 mmol), λ_{exc} = 456 nm, rt, 16 h.

However, subsequent work within the group[95] (Scheme 2.14a) and by Hartley *et al*.[96] (Scheme 2.14b) showed that it is possible to achieve 1,4-radical additions to α,ß-unsaturated ammonium intermediates to synthesise γ-lactams **122**. A key component of the success of these methodologies is the use of α-aminosilanes **123** or α-aminoacids **124** that proved to be more prone to oxidation than the ITU catalysts. The choice of these substrates was instructed by the compatibility testing done in this work.

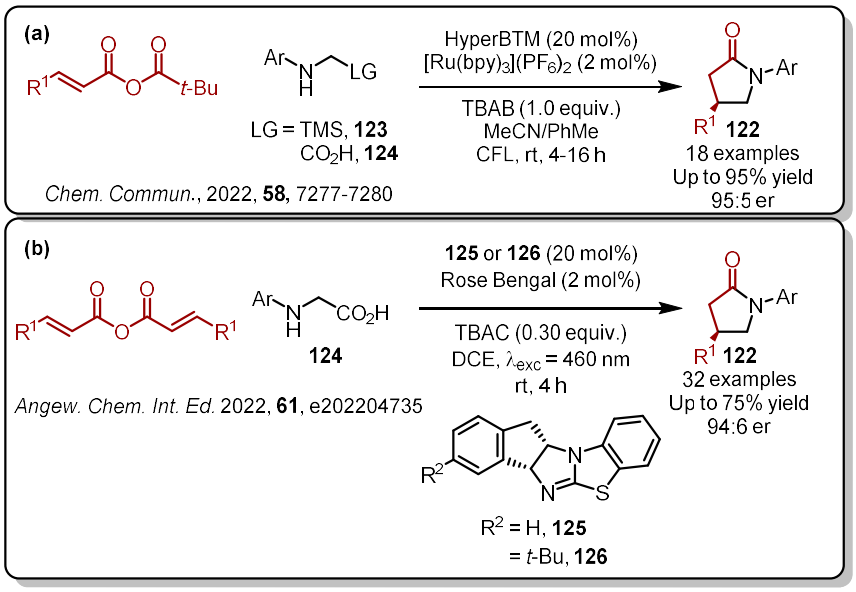

Scheme 2.14 Demonstration of enantioselective RCA reactions using dual isothiourea/photoredox catalysis reported by (a) Westwood *et al*.[95] (b) Hartley *et al*.[96]

2.3 Conclusions

The initial target for this project was to synthesise a bifunctional catalyst containing both an ITU and TADF moiety for the purpose of dual catalysis. After optimisation of the synthetic route the target molecule was successfully synthesised in a 9% overall product yield. However, subsequent testing for compatibility and stability showed significant issues with the bifunctional catalyst design. Experiments designed to test if the oxidation of the ITU could be out competed suggested that the ITU would still be degraded in the presence of other quenchers of similar oxidation potentials. While this is true, subsequent work by others in the group[95] and Hartley *et al*.[96] showed that under optimized conditions, enough of the ITU persists to achieve the desired enantioselective RCA reaction. Future work in this area should continue to explore the combination of ITU and photocatalysis as two distinct catalysts, and work towards improving enantioselectivity and broadening the scope of starting materials.

3 Evaluating MR-TADF Compounds as Photocatalysts

3.1 Introduction

Organometallic complexes based on Ru(II) and Ir(III) are the most widely used PCs (Figure 3.1a). They possess an attractive suite of properties including suitably long-lived stable excited states, absorption that extends into the visible region where most organic substrates are transparent, plus (especially for Ir(III) complexes), the capacity to modulate both the ground and excited state redox properties through ligand variation.[97] However, the scarcity, toxicity and cost of the noble metals employed has spurred intense efforts to find alternative PCs. There are now many established examples of Earth-abundant metal complexes[98] and metal-free organic PCs,[23] and numerous examples where these perform comparably to the noble metal PCs. While organic PCs, such as xanthene dyes, phenothiazines, and acridinium-based compounds are commonplace (Figure 3.1b),[23,99–101] their ground- and excited-state redox potentials are difficult to tune. D-A TADF PCs, most widely exemplified by the compound **4CzIPN**, have rapidly been adopted in the field as their properties are readily tunable through substituent variation (Figure 3.1c).[102,103] **4CzIPN**, initially developed as an emitter for organic light-emitting diodes a decade ago, luminesces via a TADF mechanism.[30]

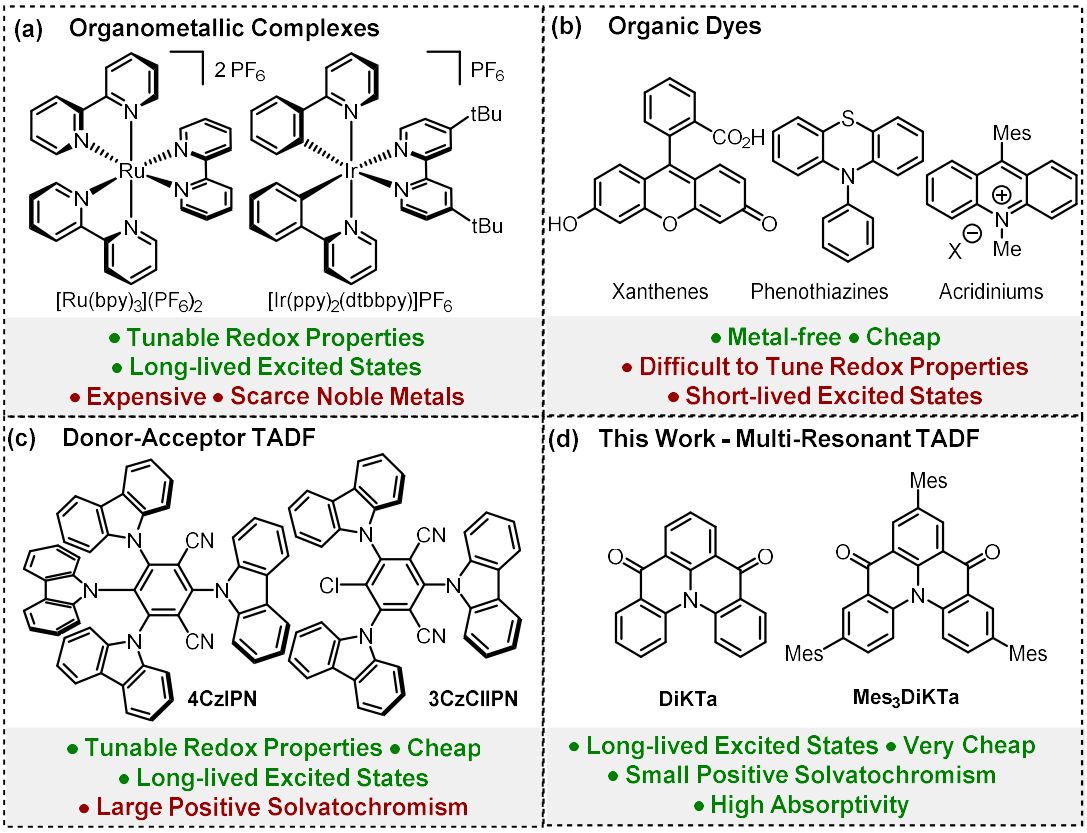

Figure 3.1 (a) Examples of organometallic PCs. (b) Examples of organic PCs. (c) Examples of D-A TADF PCs. (d) MR-TADF photocatalysts used in this work.

As a result, **4CzIPN** possesses microsecond-long emission lifetimes that, coupled with similar redox properties to that of the widely used $[Ir(dF(CF_3)ppy)_2(dtbbpy)]PF_6$, endows it with similar photochemical reactivity. **4CzIPN** was first used as a PC by Luo and Zhang to achieve a dual catalysed $(C)sp^3$-$(C)sp^2$ cross-coupling reaction.[43] Subsequent work by Speckmeier *et al.*[44] demonstrated the versatility of this class of D-A TADF PC and the tunability of their redox potentials by varying the nature and number of electron-donating and electron-accepting groups. A growing number of structurally related D-A PCs have since been reported.[104] TADF operates when the energy gap between the lowest energy singlet and triplet excited states, ΔE_{ST}, is sufficiently small such that there is an endothermic upconversion of triplet excitons into singlets via RISC (Figure 3.2a). This is possible when the exchange integral between the frontier orbitals involved in the emissive excited state is sufficiently small, which occurs in D-A compounds where the donor and acceptor groups are poorly conjugated such as when they adopt a highly twisted conformation, as is the case for **4CzIPN** and its derivatives. An alternative

molecular design strategy to reduce the exchange integral is based on the exploitation of opposing resonance effects of p- and n- dopants in nanographenes that is embodied in MR-TADF emitters.[35] Herein we present the use of two MR-TADF compounds as PCs for the first time, using **DiKTa** and **Mes$_3$DiKTa**, previously reported as emitters in OLEDs,[37] as typical examples (Figure 3.1d). Owing to their rigid structure, MR-TADF compounds typically show much narrower emission profiles and smaller Stokes shifts while also exhibiting larger molar absorptivities for the low-energy SRCT absorption band (Figure 3.2b). The emissive excited state also shows SRCT character, which is identifiable due to the modest positive solvatochromism (Figure 3.2c), in contrast to the large positive solvatochromism observed for D-A TADF compounds (Figure 3.2d).[37]

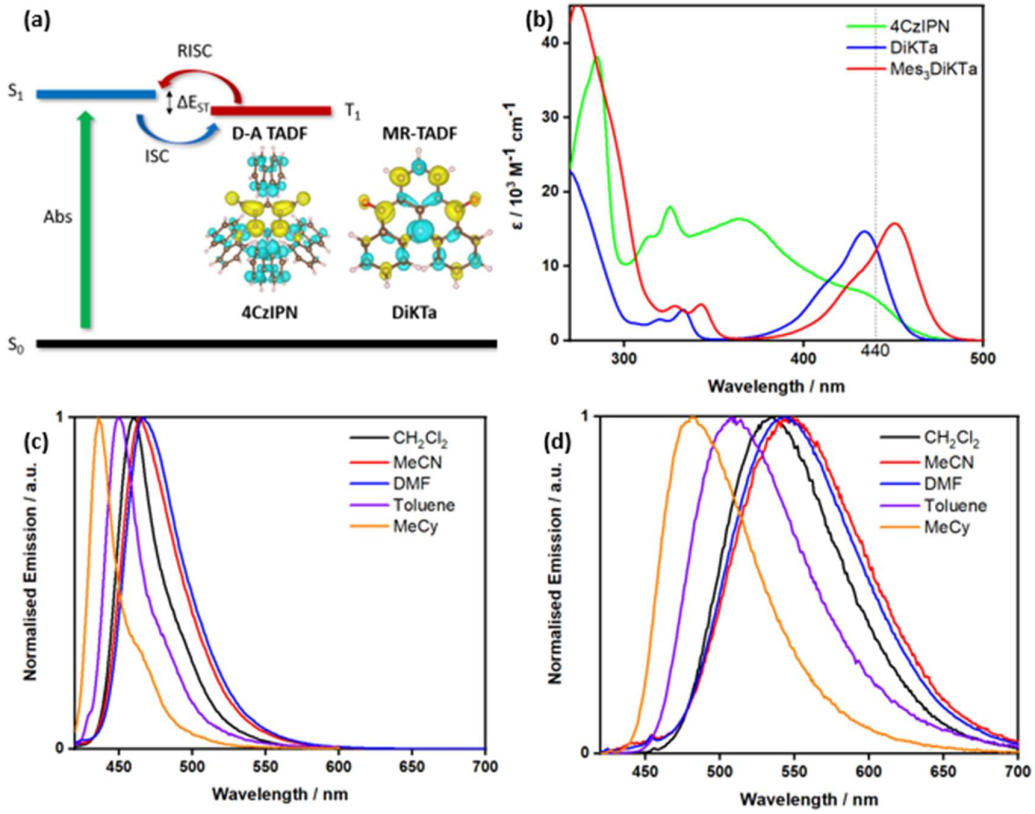

Figure 3.2 (a) Diagram depicting the TADF mechanism with S_1 plots of **4CzIPN** and **DiKTa**. (b) Absorption spectra of **4CzIPN**, **DiKTa** and **Mes$_3$DiKTa** in MeCN with wavelength of photoreactor LEDs marked as a vertical dashed line. (c) Solvatochromic study for **DiKTa** (d) Solvatochromic study for **4CzIPN.** λ_{exc} = 400 nm, measurements performed at room temperature under air.

Enhanced molar absorptivity and reduced positive solvatochromism are expected to have productive implications for photocatalysis reactivity. The higher molar absorptivity of the band that is being targeted for photoexcitation should translate to faster reaction rates and lower required

photocatalyst loadings in the absence of catalyst degradation. The attenuated positive solvatochromism of MR-TADF compounds implies that less energy is lost due to stabilization of the excited state by solvent, potentially leading to greater reactivity of the PC, particularly in commonly used polar aprotic solvents such as MeCN and DMF. **DiKTa** and its mesitylated analogue **Mes$_3$DiKTa**, were chosen for investigation as PCs because of their similar redox potentials to those of **4CzIPN** (Figure 3.3).[37,44]

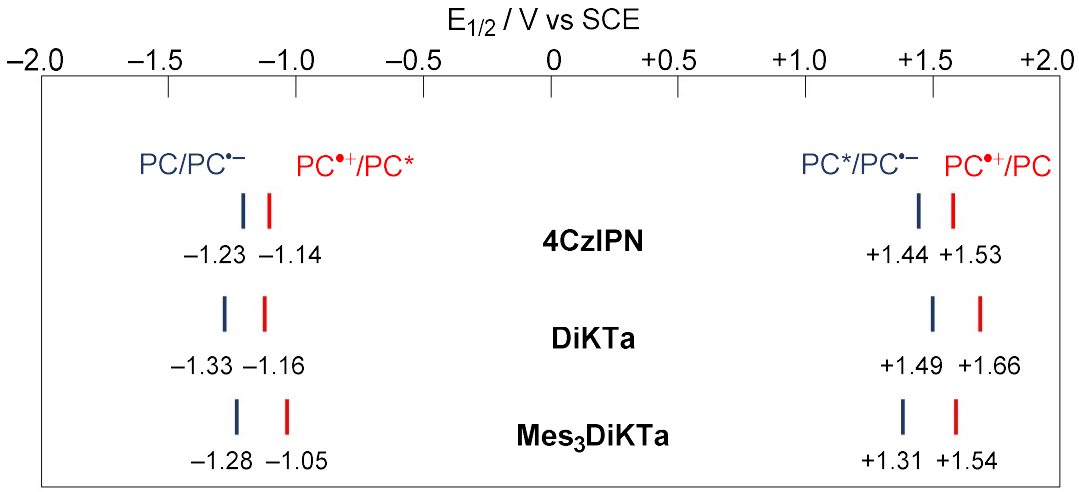

Figure 3.3 Excited state and ground state redox potentials of **4CzIPN** in MeCN.[105] Ground state redox potentials of **DiKTa** and **Mes$_3$DiKTa** in MeCN.[37] Excited state redox properties of **DiKTa** and **Mes$_3$DiKTa** calculated from the experimentally determined E_{ox}/E_{red} and $E_{0,0}$ values in MeCN, using $E_{ox}(PC^{\bullet+}/PC^*) = E_{ox} - E_{0,0}$ and $E_{red}(PC^*/PC^{\bullet-}) = E_{red} + E_{0,0}$.[37]

An additional benefit is that the raw material cost per mmol is significantly lower for **DiKTa** (£0.94/mmol) than for **4CzIPN** (£3.26/mmol).* These PCs were assessed across a diverse range of transformations including reductive quenching reactions, oxidative quenching reactions, energy transfer reactions, nickel dual catalysis and HAT dual catalysis. The result of this assessment shows that **DiKTa** and **Mes$_3$DiKTa** are attractive alternatives to the widely used **4CzIPN**. Further work explores the use of **DiKTa** as a heterogeneous PC by attaching it to a mesoporous silica polymer support and separately a water-soluble variant of **DiKTa** for aqueous photocatalysis.

*Calculated based on 12/05/2022 prices, see experimental section for further details.

3.2 Results and Discussion.

3.2.1 Reductive Quench – Decarboxylative Photo-Giese Reaction.

Our investigations began with a decarboxylative photo-Giese reaction. This process has previously been reported by Ji *et al*.[101] for their comparison of the effectiveness of different acridinium PCs and also by Speckmeier *et al*.[44] for their comparison of the suitability of alternative D-A photocatalysts. In the latter study Speckmeier *et al.* found that when **4CzIPN** was used, a superior isolated yield of 80% is achieved compared to the previously reported best acridinium PC (73% isolated yield). The proposed mechanism for this reaction begins with the reductive quenching of the PC* by the carboxylate **127** to give the reduced photocatalyst ($PC^{\bullet-}$) and an alkyl radical **128** after decarboxylation. The alkyl radical that is formed then adds to the electron-deficient alkene **120** to generate an α-carbonyl radical **130**, that is subsequently reduced to the corresponding enolate **131** by $PC^{\bullet-}$ to complete the photocatalytic cycle (Scheme 3.1).

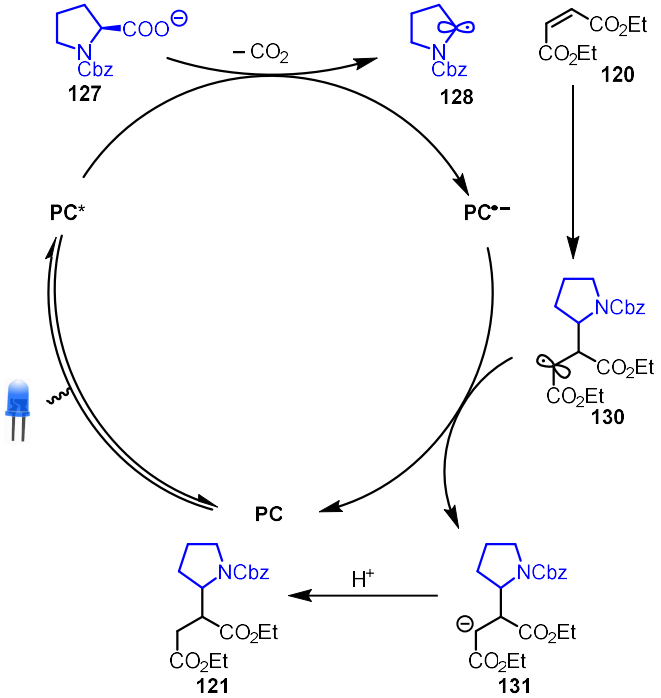

Scheme 3.1 Proposed mechanism for the decarboxylative photo-Giese reaction.

Using *N*-Cbz protected proline **23a** as the carboxylic acid substrate and diethyl maleate **120** as the electron deficient alkene, both **DiKTa** and **Mes$_3$DiKTa** gave comparable NMR yields to that of **4CzIPN**

(Table 3.1, entries 1-3). *N*-protected prolines have relatively low oxidation potentials [E_{ox}([Boc-Pro-O][/Cs]) = 0.95 V vs SCE in MeCN];[106] therefore, the more challenging iso-butyric acid, **23b**, and propanoic acid, **23c**, ([E_{ox}[*i*-PrCO_2][/NBu_4]) = 1.31 V and E_{ox}([EtCO_2][/NBu_4]) = 1.25 V)[107] were also investigated in order to differentiate the photooxidation ability of the PCs. With iso-butyric acid both **DiKTa** and **Mes$_3$DiKTa** showed improved NMR yields of 78% and 79%, respectively (Table 3.1, entries 4 and 5), relative to the 64% achieved using **4CzIPN** (Table 3.1, entry 6). Changing to the primary radical formed when using propanoic acid resulted in lower yields for all three PCs (Table 3.1, entries 7-9). This is likely due to the decreased nucleophilicity of primary radicals relative to secondary radicals, leading to alternative and undesired reaction pathways becoming competitive. Notwithstanding the lower yields, both **DiKTa** and **Mes$_3$DiKTa** still outperformed **4CzIPN**.

Table 3.1 Decarboxylative photo-Giese reaction between carboxylic acids and diethyl maleate.

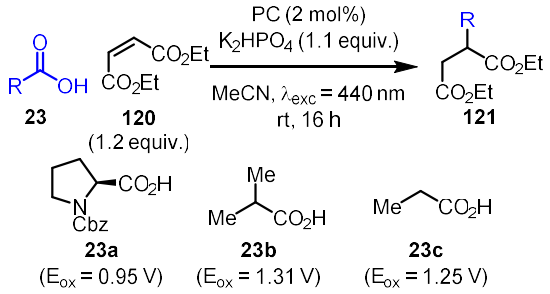

Entry[a]	Acid	PC	Yield / %[b]
1	**23a**	**DiKTa**	93 (± 3)
2	**23a**	**Mes$_3$DiKTa**	91 (± 1)
3	**23a**	**4CzIPN**	95 (± 4)
4	**23b**	**DiKTa**	78 (± 3)
5	**23b**	**Mes$_3$DiKTa**	79 (± 4)
6	**23b**	**4CzIPN**	64 (± 1)
7	**23c**	**DiKTa**	37 (± 1)
8	**23c**	**Mes$_3$DiKTa**	22 (± 3)
9	**23c**	**4CzIPN**	9 (± 1)

[a] Carboxylic acid (**23**) (0.15 mmol), diethyl maleate (**120**) (0.18 mmol), K_2HPO_4 (0.17 mmol), PC (2 mol%), MeCN (3 mL), irradiation with 440 nm LEDs, rt. [b] Yield determined by ^{1}H NMR, using 1,3,5-trimethoxybenzene as the internal standard, averaged over two separate experiments.

PC loading was next investigated as a discriminating parameter. The reaction using *N*-Cbz-proline **23a** as starting material was therefore repeated at 1 mol%, 0.5 mol%, 0.25 mol% and 0.1 mol% (Table 2). Yields remained largely the same for all three PCs down to 0.5 mol% (Table 3.2, entries 1-6). Contrastingly, differences in NMR yield were observed at 0.25 mol%, with **4CzIPN** only achieving an average yield of 28% (Table 3.2, entry 7), while **DiKTa** and **Mes$_3$DiKTa** maintained an average yield of 80% (Table 3.2, entries 8 and 9). When using 0.1 mol% PC loading, the use of both **4CzIPN** and **DiKTa** produced poor average yields of 9% and 18%, respectively (Table 3.2, entries 10 and 11), while **Mes$_3$DiKTa** achieved a significantly higher yield of 59% (Table 3.2, entry 12). The evidence suggests that **DiKTa** and **Mes$_3$DiKTa** perform better than **4CzIPN** at lower catalyst loadings, which is consistent with the higher molar absorptivity of **DiKTa** and **Mes$_3$DiKTa** relative to **4CzIPN** at the excitation wavelength used.

Table 3.2 Catalyst loading variation of photo-Giese reaction.

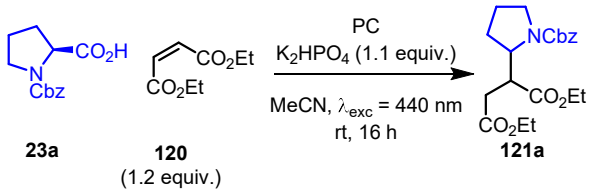

23a **120** (1.2 equiv.) **121a**

Entry[a]	Catalyst Loading / mol%	PC	Yield / %[b]
1	1	**4CzIPN**	90 (± 1)
2	1	**DiKTa**	88 (± 2)
3	1	**Mes$_3$DiKTa**	91 (± 1)
4	0.5	**4CzIPN**	89 (± 3)
5	0.5	**DiKTa**	78 (± 4)
6	0.5	**Mes$_3$DiKTa**	89 (± 1)
7	0.25	**4CzIPN**	28 (± 5)
8	0.25	**DiKTa**	80 (± 2)
9	0.25	**Mes$_3$DiKTa**	80 (± 4)
10	0.1	**4CzIPN**	9 (± 3)
11	0.1	**DiKTa**	18 (± 5)
12	0.1	**Mes$_3$DiKTa**	59 (± 7)

[a] Cbz-Pro-H (**23a**) (0.15 mmol), diethyl maleate (**120**) (0.18 mmol), K_2HPO_4 (0.17 mmol), PC, MeCN (3 mL), irradiation with 440 nm LEDs, rt. [b] Yield determined by ^{1}H NMR, using 1,3,5-trimethoxybenzene as the internal standard, averaged over three separate experiments.

3.2.2 Oxidative Quench – Atom Transfer Radical Addition.

Subsequent studies assessed these PCs in an oxidative quenching process. Initial attempts focused on the reduction of bromoacetonitrile **132** and trapping of the corresponding radical with 1-methylindole **133** (Scheme 3.2a).[108] However, attempts at reproducing this literature reactivity resulted in complex mixtures so this reaction was discarded. Subsequent attempts were based upon the ATRA reaction between tosyl chloride **20** and styrene **19** (Scheme 3.2b).[109] Repeating known conditions using $[Ru(bpy)_3](PF_6)_2$ provided the desired ATRA product **135** in near quantitative NMR yields. However, when using **4CzIPN** or **DiKTa**, significantly reduced product yields were observed with many other side reactions apparent and so this process was not probed further.

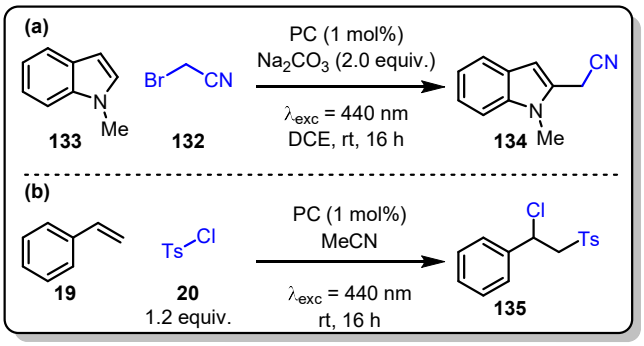

Scheme 3.2 (a) Cyanomethylation of 1-methylindole. (b) ATRA of tosyl chloride with styrene.

Next, a different ATRA reaction developed by Pirtsch *et al.*[110] was attempted (Scheme 3.3). The proposed mechanism for this reaction begins with the oxidative quenching of the PC* by the alkyl halide **136** to give the oxidised photocatalyst ($PC^{\bullet+}$) and an alkyl radical **137**. The alkyl radical that is formed then adds to the alkene **138** to generate another alkyl radical **139**, that is then oxidised to the corresponding cation **140** by $PC^{\bullet+}$ to complete the photocatalytic cycle. **140** is then trapped by the halide to produce the desired ATRA product **141**.

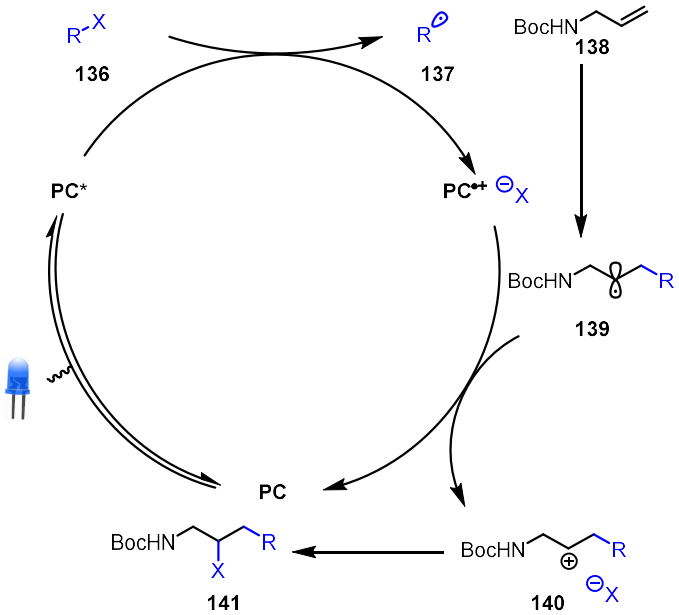

Scheme 3.3 Proposed mechanism for the photocatalytic ATRA reaction.

Using perfluorobutyl iodide **136a** (E_p^{red} = – 1.42 V vs SCE in MeCN)[111] and *tert*-butyl-*N*-allyl carbamate **138** as the substrates in DCE with **4CzIPN** produced the desired ATRA product **141a** in 83% yield (Table 3.3, entry 1). Interestingly, when using **DiKTa** and **Mes$_3$DiKTa**, near quantitative yields of 97% and 93%, respectively, could be achieved (Table 3.3, entries 2-3). Phenacyl bromide **136b** and diethyl

bromomalonate **136c** were then chosen as additional substrates with reduction potentials of E_p^{red} = – 1.21 V vs SCE and E_p^{red} of – 1.41 V vs SCE in DMF, respectively (Figure 3.4).

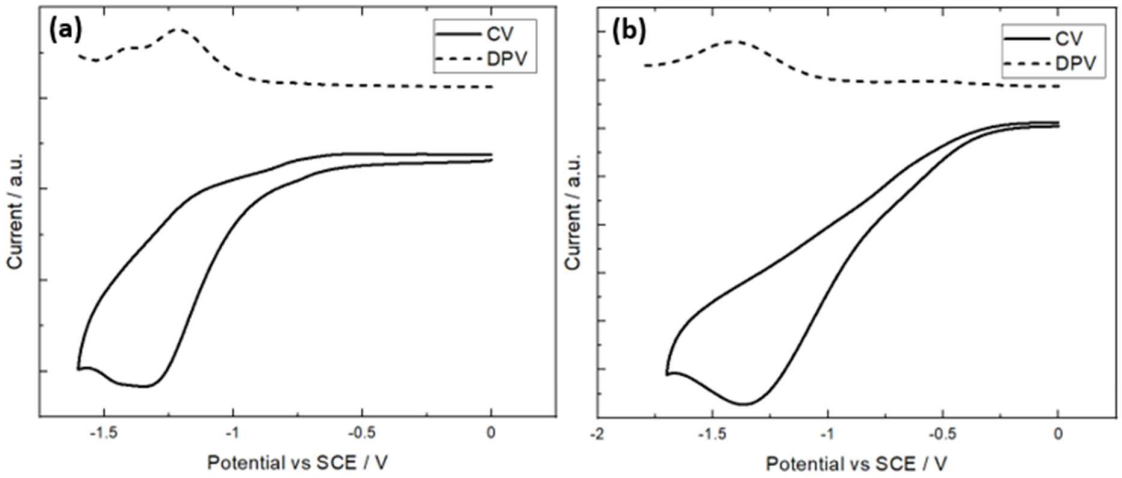

Figure 3.4 (a) CV and DPV of diethyl bromomalonate in DMF, reported vs SCE at scan rate of 50 mV s^{-1}. (b) CV and DPV of phenacyl bromide in DMF, reported vs SCE at scan rate of 50 mV s^{-1}.

When using phenacyl bromide **136b**, as observed by Pirtsch *et al*.,[110] the optimal solvent was a 1:2 mixture of DMF/H_2O. **4CzIPN**, **DiKTa** and **Mes$_3$DiKTa** performed similarly, generating **141b** in 71%, 77% and 76% yields, respectively (Table 3.3, entry 4-6). However, when using **136c**, **4CzIPN** gave marginally improved product yields, affording **141c** in 76% compared to 69% and 71% for **DiKTa** and **Mes$_3$DiKTa**, respectively, although the difference between them is within the error observed for this reaction (Table 3.3, entries 7-9).

Table 3.3 Oxidative quench ATRA reaction between alkyl halides and alkene.

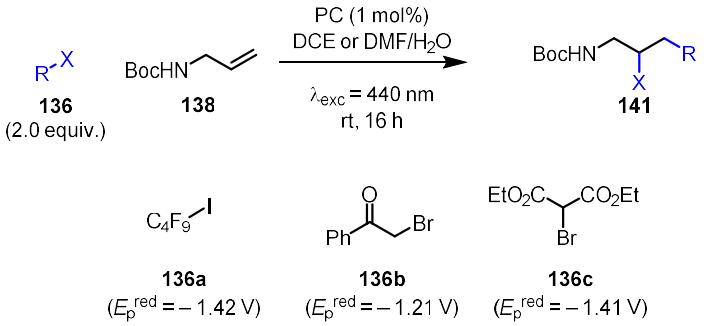

Entry	Alkyl Halide	PC	Yield / %[c]
1[a]	**136a**	**4CzIPN**	83 (± 1)
2[a]	**136a**	**DiKTa**	97 (± 2)
3[a]	**136a**	**Mes$_3$DiKTa**	93 (± 0)
4[b]	**136b**	**4CzIPN**	71 (± 4)
5[b]	**136b**	**DiKTa**	77 (± 1)
6[b]	**136b**	**Mes$_3$DiKTa**	76 (± 2)
7[b]	**136c**	**4CzIPN**	76 (± 4)
8[b]	**136c**	**DiKTa**	69 (± 3)
9[b]	**136c**	**Mes$_3$DiKTa**	71 (± 1)

[a] Alkyl halide (**136**) (0.60 mmol), *tert*-butyl *N*-allylcarbamate (**138**) (0.30 mmol), PC (1 mol%), DCE (1.5 mL), irradiation with 440 nm LEDs, rt, 24 h. [b] Alkyl halide (**136)** (0.50 mmol), *tert*-butyl *N*-allylcarbamate (**138**) (0.25 mmol), PC (1 mol%), DMF/H_2O (1:2) (0.6 mL), irradiation with 440 nm LEDs, rt. [c] Yield determined by ^{1}H NMR, using 1,3,5-trimethoxybenzene as the internal standard, averaged over two separate experiments.

The reduction potential noted by Pirtsch *et al*. for **136b** of $E_p^{red} = -0.49$ V vs SCE was originally reported by Tanner *et al*.[112] and is commonly used in the literature; however, this value is erroneous and occurs only as a result of electrochemical degradation (Figure 3.5).

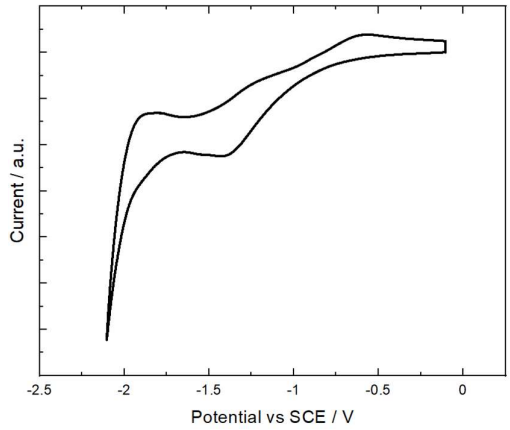

Figure 3.5 CV of phenacyl bromide in DMF, reported vs SCE at scan rate of 100 mV s^{-1}, observed peak at – 0.6 V is due to electrochemical degradation.

Indeed, a previous report by Bahamonde *et al*.[113] found that the peak reduction potential is significantly more negative E_p^{red} = – 1.39 vs SCE in MeCN, and our own measurements have found it to be E_p^{red} = – 1.21 V vs SCE in DMF from the peak of the DPV (Figure 3.4b). Similarly, literature values for the reduction potential of **136c** vary significantly from E_p^{red} = – 1.0 V vs SCE[114] in DMF to E_p^{red} = – 1.74 V vs SCE[113] in MeCN; our own measurements indicate that E_p^{red} = – 1.41 V vs SCE in DMF from the peak of the DPV (Figure 3.4a). Such a negative reduction potential would be predicted to be beyond the ability of any of these PCs to reduce via oxidative quenching; however, quenching experiments with both **4CzIPN** and **DiKTa** show quenching to occur in the presence of **136c** in DMF, showing that while endergonic, oxidative quenching does occur (Figure 3.6).

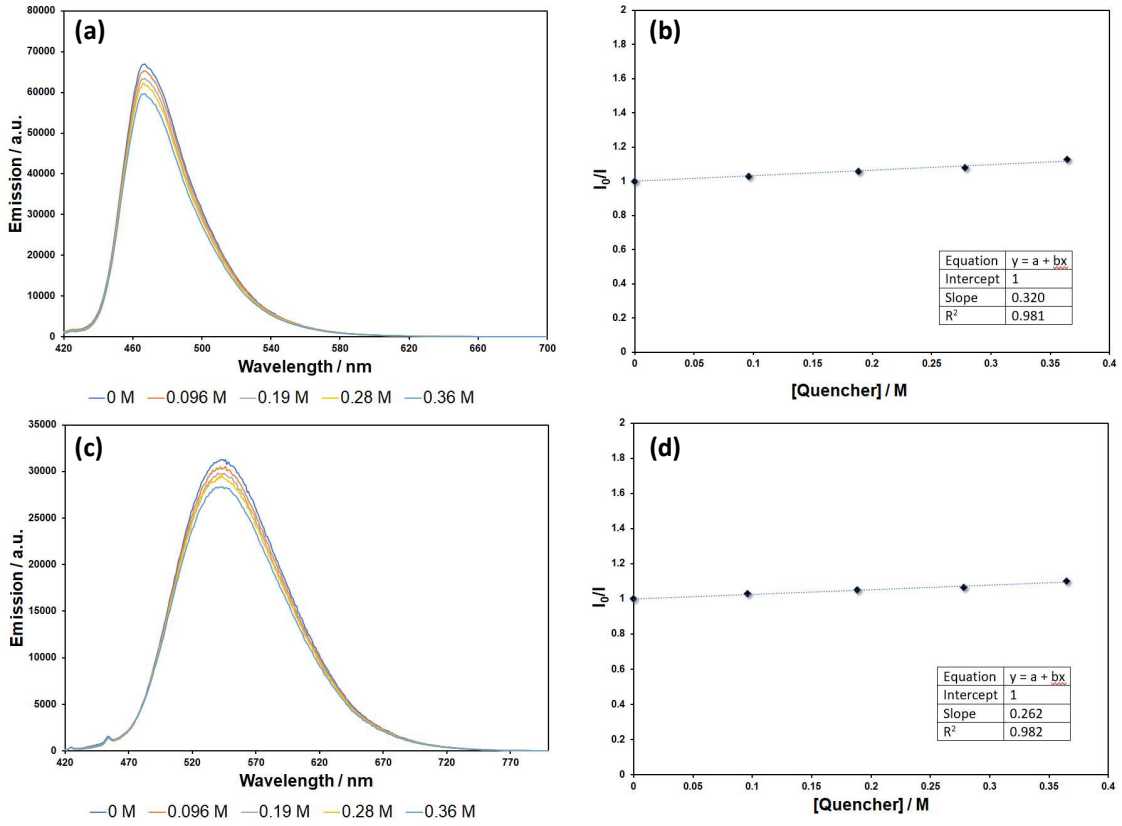

Figure 3.6 (a) Emission quenching data of **DiKTa** by sequential addition of diethyl bromomalonate in DMF. λ_{exc} = 400 nm. (b) Stern-Volmer plot of the quenching of the emission of **DiKTa** in DMF by sequential addition of diethyl bromo malonate. (c) Emission quenching data of **4CzIPN** by sequential addition of diethyl bromomalonate in DMF. λ_{exc} = 400 nm. (d) Stern-Volmer plot of the quenching of the emission of **4CzIPN** in DMF by sequential addition of diethyl bromo malonate.

The Stern-Volmer quenching relationship can be used to calculate the quenching rate constant (k_q) by plotting the ratio of the emission intensity without quencher present (I_0) and the emission intensity observed (I) against the concentration of the quencher ([Q]) (Equation 3.1). The slope of a Stern-Volmer plot is equal to the product of k_q and the lifetime (τ_0) of the emitter in the absence of quencher. Therefore, to obtain values for k_q, the lifetimes of both **4CzIPN** and **DiKTa** were extracted from time-resolved emission measurements (Figure 3.7).

$$\frac{I^0}{I} = 1 + k_q \tau_0 [Q] \tag{3.1}$$

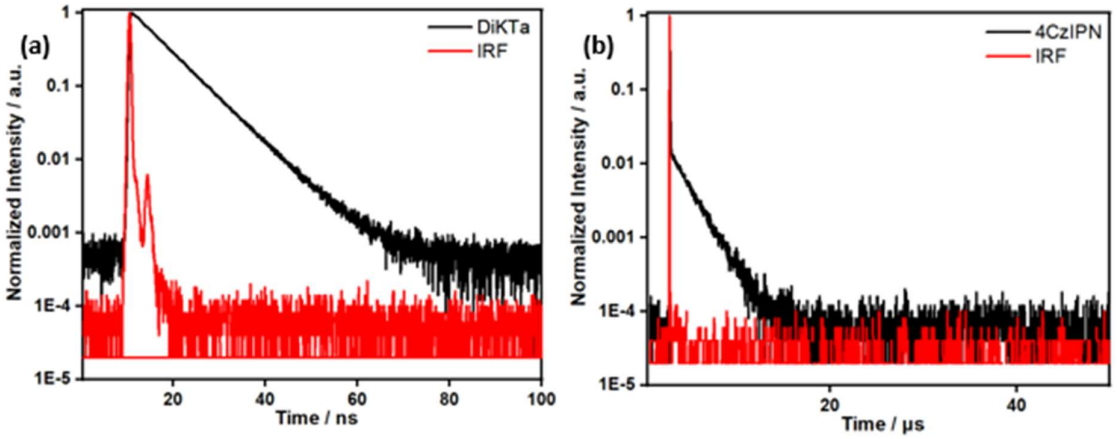

Figure 3.7 Time-resolved PL decay of (a) DiKTa and (b) 4CzIPN recorded in DMF under N_2 in 10^{-5} M solutions with λ_{exc} = 375 nm

As no delayed emission is observed in DMF for **DiKTa**, the prompt fluorescence lifetime has been used and quenching is expected to occur from the S_1 state (Table 3.4). However, for **4CzIPN** delayed emission is observed in DMF so two quenching constants can be calculated. Both k_q are at least an order of magnitude larger for **DiKTa** than for **4CzIPN**, which could have interesting implications for reaction rates.

Table 3.4 Stern-Volmer data summary.

PC	τ_p / ns	τ_d / µs	$\tau \bullet k_q$ / $mol^{-1}\,dm^3$	$k_{q,1}$ / $10^7\,mol^{-1}\,dm^3\,s^{-1}$	$k_{q,2}$ / $10^7\,mol^{-1}\,dm^3\,s^{-1}$
DiKTa	8.2	-	0.320	3.9	-
4CzIPN	32.8	1.91	0.262	0.80	0.14

τ_p = prompt fluorescence lifetime, τ_d = delayed fluorescence lifetime, $\tau \bullet k_q$ = Stern-Volmer constant taken from the gradient of the slope, $k_{q,1}$ = quenching constant using τ_p, $k_{q,2}$ = quenching rate constant using τ_d.

3.2.3 Dexter Energy Transfer – Isomerization of Alkenes.

Having shown that **DiKTa** and **Mes_3DiKTa** are capable photoredox catalysts, attention turned to their application in DET. One of the simplest examples of DET processes is the (*E*)/(*Z*) isomerization of alkenes. The proposed mechanism begins with the excitation of the PC, followed by a DET process to the (*E*)-alkene **142** to give the triplet alkene **[142]^3** and the ground state PC (Scheme 3.4). **[142]^3** is now able to rotate to conformer **[143]^3**, which upon relaxation forms the (*Z*)-isomer **143**.

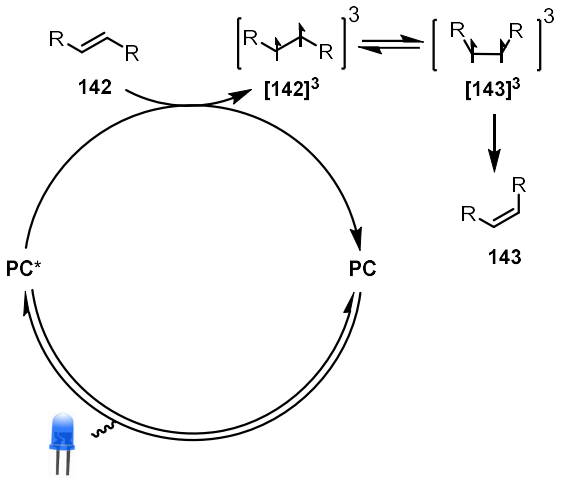

Scheme 3.4 Proposed mechanism for the photocatalytic isomerization of (*E*)-alkenes.

The isomerization of (*E*)-stilbene **18** was used effectively by Lu *et al*. to compare various D-A TADF emitters and then correlate the results with their triplet energies (E_T) relative to that of (*E*)-stilbene (E_T = 2.2 eV) and (*Z*)-stilbene (E_T = 2.5 eV).[45,115] The crucial determinant for the efficiency of DET reactions is the degree of spectral overlap between the emission of the PC and the spin-forbidden $S_0 \rightarrow T_1$ absorption of the substrate.[11] As these absorption measurements are typically difficult to obtain, a cross-comparison of the triplet energies of the reactant and PC are typically used as a crude handle to assess whether the reaction is likely to proceed. Thus, to maximize the yield for the isomerization of the substrate by limiting the reverse reaction, E_T(Substrate) ≤ E_T(PC) < E_T(Product). Using similar reaction conditions to those of Lu *et al.* $[Ru(bpy)_3](PF_6)_2$ (E_T = 2.13 eV)[116] achieved a (*Z*)/(*E*) ratio of 94:6 and **4CzIPN** (E_T = 2.53 eV)[45] performed comparably with a (*Z*)/(*E*) ratio of 92:8 (Table 3.5, entry 1 and 2). When using **DiKTa** (E_T = 2.61 eV)[37] as the PC a (*Z*)/(*E*) ratio of only 59:41 was observed (Table 3.5, entry 3), consistent with the high triplet energy of this PC, although a (*Z*)/(*E*) ratio of 61:39 was achieved with **Mes$_3$DiKTa** (E_T = 2.49 eV),[37] despite having a similar triplet energy to that of **4CzIPN** (Table 3.5, entry 4). Lu *et al.* observed similar off-trend examples in their study, revealing the limitations of using E_T alone to evaluate the efficiency of DET photocatalysts. While not as effective as **4CzIPN**, these initial reactions did show that **DiKTa** and **Mes$_3$DiKTa** can be used as DET photocatalysts. Diisopropyl fumarate **22** (E_T = 2.7 eV)[45] was used by Lu *et al*. as a more challenging substrate due to its higher E_T. $[Ir(dF(CF_3)ppy)_2(dtbbpy)]PF_6$ (E_T = 2.67 eV)[116] was used as the reference PC for this reaction

and achieved a (*Z*)/(*E*) ratio of 95:5 (Table 3.5, entry 5). Matching with previous reports, **4CzIPN** only achieved trace amounts of isomerization, giving a (*Z*)/(*E*) ratio of 4:96 (Table 3.5, entry 6). Pleasingly, **DiKTa** gave a (*Z*)/(*E*) ratio of 90:10, which is comparable to that of the iridium PC (Table 3.5, entry 7). **Mes$_3$DiKTa** afforded a lower (*Z*)/(*E*) ratio of 58:42 (Table 3.5, entry 8). Due to its higher E_T, **DiKTa** should be considered as a complementary PC to **4CzIPN**, capable of engaging in more energetically demanding DET reactions.

Table 3.5 (*E*)/(*Z*) Isomerization of alkenes.

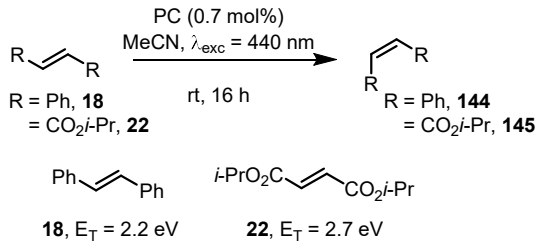

Entry[a]	Alkene	PC	E_T / eV	(*Z*)/(*E*)[b]
1	**18**	$[Ru(bpy)_3](PF_6)_2$	2.13	94:6 (± 0)
2	**18**	**4CzIPN**	2.53	92:8 (± 0)
3	**18**	**DiKTa**	2.62	59:41 (± 1)
4	**18**	**Mes$_3$DiKTa**	2.49	61:39 (± 2)
5	**22**	$[Ir(dF(CF_3)ppy)_2(dtbbpy)]PF_6$	2.67	95:5 (± 1)
6	**22**	**4CzIPN**	2.53	6:94 (± 1)
7	**22**	**DiKTa**	2.62	90:10 (± 0)
8	**22**	**Mes$_3$DiKTa**	2.49	57:43 (± 0)

[a] Alkene (0.60 mmol), PC (0.7 mol%), MeCN (3 mL), irradiation with 440 nm LEDs, rt. [b] Determined using ^{1}H NMR, averaged over two separate experiments.

3.2.4 Dual Catalysis – Nickel and Hydrogen Atom Transfer Catalysis.

Metallaphotoredox catalysis is a fast growing area of research as it often offers a mild alternative to existing transition metal catalytic reactions and give access to different redox couples of the co-catalyst, resulting in new reactivity.[117] Nickel in particular has been paired with photocatalysts for a wide range of different coupling reactions with Luo and Zhang[43] reporting the first use of **4CzIPN** as a PC in a dual-mode catalysed (C)sp^3-(C)sp^2 cross-coupling. The proposed mechanism for this reaction begins with the reductive quenching of the PC by carboxylate **127** to give alkyl radical **128** and PC$^{\bullet-}$

(Scheme 3.5). Simultaneously, Ni(0) oxidatively adds to aryl bromide **14** to give Ni(II) complex **146**, which is then intercepted by **128** to form Ni(III) complex **147**. Reductive elimination of **147** produces the desired coupling product **148** and a Ni(I) intermediate, which is reduced to Ni(0) by $PC^{\bullet-}$ to complete both catalytic cycles. However, this mechanism does not include details of how the Ni(0) is generated from the Ni(II) precursor. Ma and co-workers[118] have investigated this step computationally for a different reaction system and postulated that the PC also plays a role in reducing the Ni(II) precursor to Ni(0).

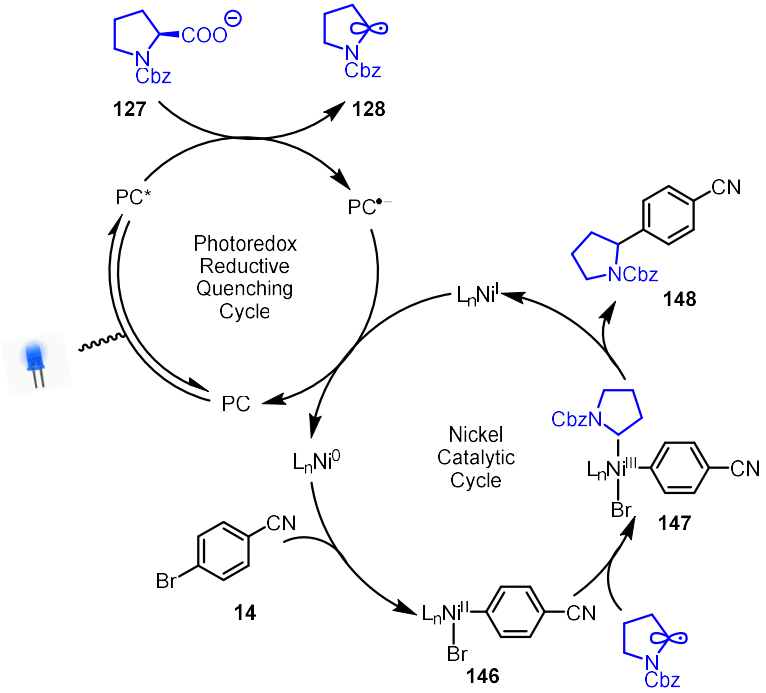

Scheme 3.5 Proposed mechanism for photoredox/nickel dual catalysed (C)sp^3-(C)sp^2 cross-coupling.

Employing a modified version of this reaction to assess the performance of **DiKTa** and **Mes$_3$DiKTa**, using **4CzIPN**, the coupling reaction between **23a** and aryl bromide **14** gave the desired product **148** in 78% yield (Table 3.6, entry 1). Both **DiKTa** and **Mes$_3$DiKTa** gave similar results of 78% and 72%, respectively (Table 3.6, entries 2 and 3), providing further evidence of the versatility of these two PCs.

Table 3.6 Dual catalysed (C)sp^3-(C)sp^2 cross-coupling reaction.

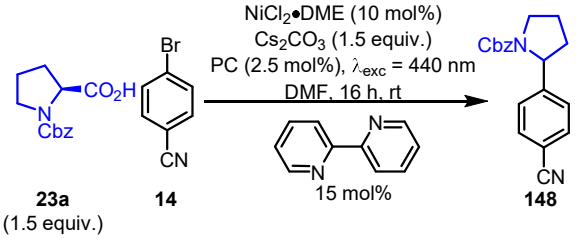

Entry[a)]	PC	Yield / %[b)]
1	**4CzIPN**	78 (± 2)
2	**DiKTa**	78 (± 2)
3	**Mes$_3$DiKTa**	72 (± 1)

[a] Cbz-Pro-H (**23a**) (0.225 mmol), 4-bromobenzonitrile (**14**) (0.15 mmol), $NiCl_2$•DME (10 mol%), Cs_2CO_3 (0.225 mmol), 2,2'-bipyridine (15 mol%) PC (2.5 mol%), DMF (3.5 mL), irradiation with 440 nm LEDs, rt. [b] Yield determined by ^{1}H NMR, using 1,3,5-trimethoxybenzene as the internal standard, averaged over two separate experiments.

HAT catalysts are also commonly partnered with PCs and have been used for dehalogenation reactions. A recent example, reported by Constantin *et al.*,[119] used the alkyl radicals **149** generated after the reductive quenching between PC* and triethylamine to abstract iodine atoms from alkyl iodides **150** to generate alkyl radicals **151** that typically would require a far more potent reductant (E_{red}(R-I) < – 2 V). **151** can then be trapped by a thiol HAT catalyst **152** to generate the dehalogenation products **153** and sulfur-centred radical **154**, which is reduced by $PC^{\bullet-}$ to complete both catalytic cycles (Scheme 3.6).

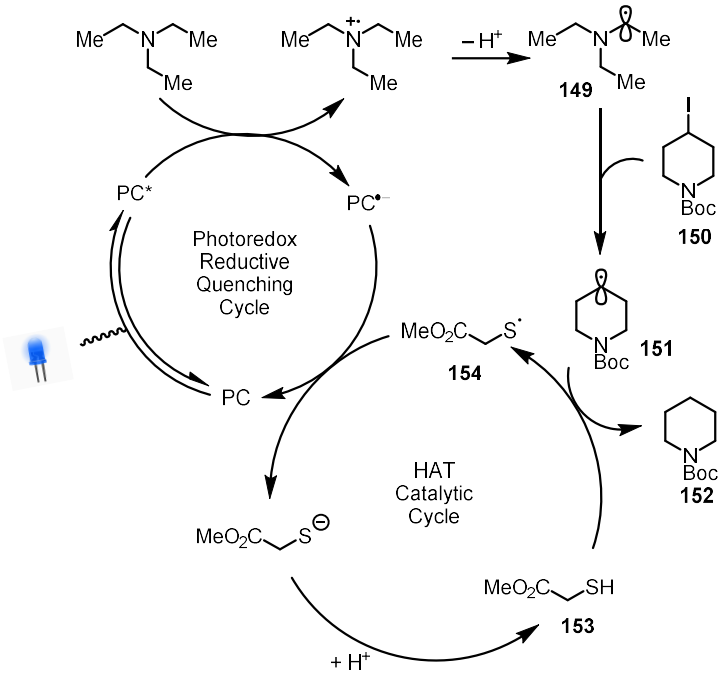

Scheme 3.6 Proposed mechanism for photoredox/HAT dual catalysed deiodination.

An 85% yield of **152** was obtained under the literature conditions and using **4CzIPN** (Table 3.7, entry 1). Both **DiKTa** and **Mes$_3$DiKTa** were able to achieve comparable average yields of 88% and 86%, respectively (Table 3.7, entries 2 and 3).

Table 3.7 Dual catalysed deiodination.

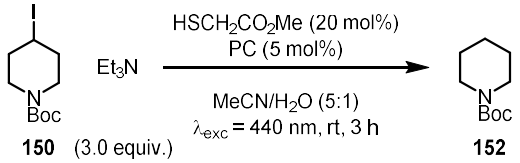

Entry[a]	PC	Yield / %[b]
1	**4CzIPN**	85 (± 0)
2	**DiKTa**	88 (± 3)
3	**Mes$_3$DiKTa**	86 (± 6)

[a] Alkyl iodide (**150**) (0.15 mmol), triethylamine (0.45 mmol), methyl 2-mercaptoacetate (20 mol%), PC (5 mol%), MeCN/H_2O (5:1) (1.5 mL), irradiation with 440 nm LEDs, rt. [b] Yield determined by ^{1}H NMR, using 1,3,5-trimethoxybenzene as the internal standard, averaged over two separate experiments.

3.2.5 Kinetics Studies.

Reactions in the previous sections have used the yield of the reaction after a given time to compare the efficiency of the PCs. While useful, this provides an incomplete picture of these reaction processes

as it does not allow comparison of relative rates of product formation. This prompted an investigation into the reaction kinetics of the formation of product using the various PCs for a model transformation. The reaction chosen for initial attempts was the photocatalytic decarboxylation of aryl acetic acid **155** in the presence of diphenyl disulfide to give 4-methylanisole **156** (Scheme 3.7).[120]

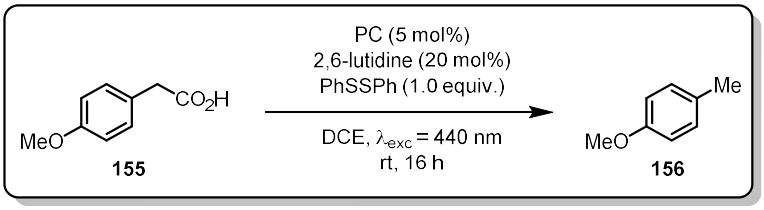

Scheme 3.7 Photocatalytic decarboxylation.

The reaction progress was monitored by taking aliquots at known time intervals and measuring them by GCMS in the presence of an internal standard. Therefore, using biphenyl as the internal standard, a calibration curve for the product was developed (Figure 3.8a). Unfortunately, the carboxylic acid starting material gave inconsistent results in different GCMS runs, so only the formation of product could be calibrated with sufficient accuracy. Using this curve, test reactions indicated that **DiKTa**, **Mes$_3$DiKTa** and **4CzIPN** performed well in this reaction giving similar GC yields of 63%, 59%, and 64%, respectively. Therefore, formation of **156** over time was successfully measured when using **DiKTa** as the PC (Figure 3.8b). However, when using **4CzIPN**, taking aliquots from the reaction mixture resulted in only trace reactivity, which is assumed to be due to a sensitivity to air as a consequence of the sampling process.

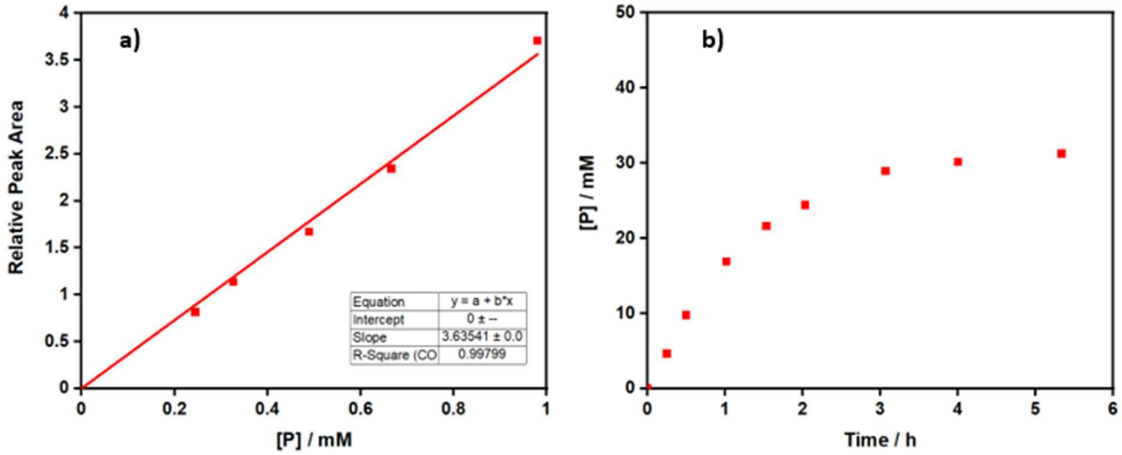

Figure 3.8 a) Calibration curve for 4-methylanisole (P) using biphenyl as internal standard. b) Product formation over time of the decarboxylation of 4-methoxyphenylacetic acid using **DiKTa** as PC.

Since air sensitivity was identified as the issue, the next reaction chosen to be monitored was the oxidative hydroxylation of phenyl boronic acid **157** to phenol **158**, which requires oxygen in the air as a reactant (Scheme 3.8).[121] Pleasingly, test reactions with **DiKTa** showed full conversion to **158** under standard conditions, so reaction monitoring was attempted using methodology developed by Pitre *et al*.[121] for this reaction.

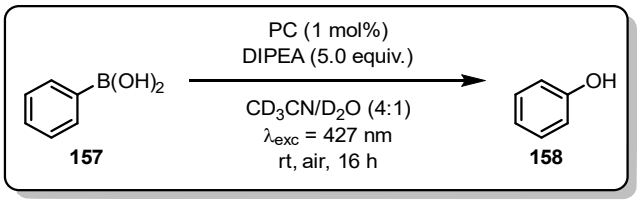

Scheme 3.8 Oxidative hydroxylation of phenyl boronic acid.

Using deuterated solvents, aliquots of the reaction were taken every hour and analysed by ^{1}H NMR to give conversions of **157** to **158** using both **DiKTa** and **4CzIPN** (Figure 3.9). Interestingly, almost identical rate profiles for both catalysts were observed up until 5 hours, where **DiKTa** continues on to full conversion after 6 hours, while **4CzIPN** seems to plateau and requires much longer to reach completion. The cause for this difference is not yet understood, although a plausible explanation is catalyst instability leading to slower reaction rates near the end of the reaction. While this does suggest **DiKTa** is slightly superior for this reaction than **4CzIPN**, a third reaction was sought for further evidence.

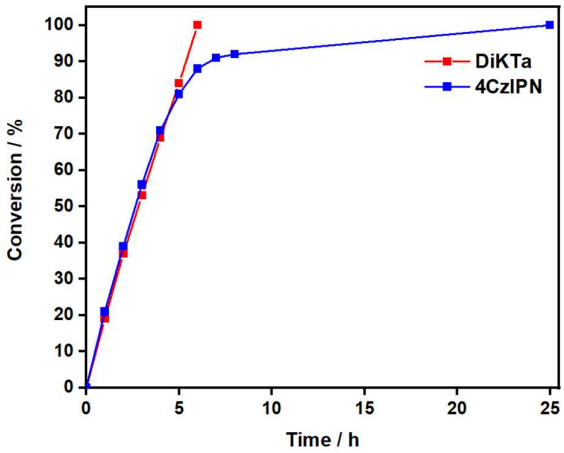

Figure 3.9 Reaction profile of the oxidative hydroxylation of phenylboronic acid using **DiKTa** and **4CzIPN**.

The third reaction chosen for the kinetics study was the ATRA reaction between nonafluoro-1-iodobutane **136a** and alkene **138** shown previously in table 3.3. Taking inspiration from work done by Ji and co-workers[122] to determine quantum yields of photochemical reactions, this reaction was monitored using in-situ NMR using the set-up shown in Figure 3.10.

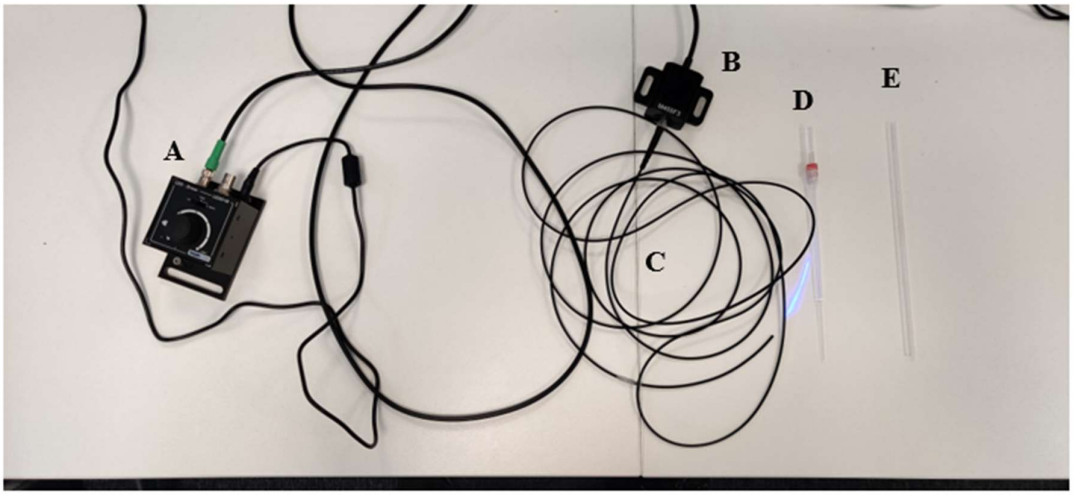

Figure 3.10 Equipment used for in-situ NMR experiments. A = LED Driver, B = Fibre-coupled LED, C = Optical Fibre, D = coaxial insert, E = NMR tube.

Notably, using this experimental set-up, the reaction reached completion for all three PCs in less than 3 hours, significantly faster than using a photoreactor, presumably due to more efficient irradiation within the in-situ NMR set-up (Figure 3.11). Furthermore, when catalysed by **Mes$_3$DiKTa** or **DiKTa** the rate of product formation is significantly enhanced than with **4CzIPN**. To quantify these differences, initial rates of the reaction with each PC were extracted and compared, with the use of **DiKTa** giving a

slightly larger initial rate (5 x 10^{-4} M s^{-1}) than **Mes$_3$DiKTa** (3.7 x 10^{-4} M s^{-1}), but with both an order of magnitude larger than that of **4CzIPN** (0.6 x 10^{-4} M s^{-1}). While our original hypothesis was that increased molar absorptivity at the excitation wavelength for **DiKTa** and **Mes$_3$DiKTa** compared to **4CzIPN** would lead to increased reaction rates, at 455 nm the molar absorptivity for **DiKTa** and **4CzIPN** are similar. Therefore, it is not directly evident what is the cause for the divergence in reaction rates between the two PCs. However, a possible explanation could be that **4CzIPN** decomposes under these reaction conditions resulting in an altered molar absorptivity, which is studied further in the next section.

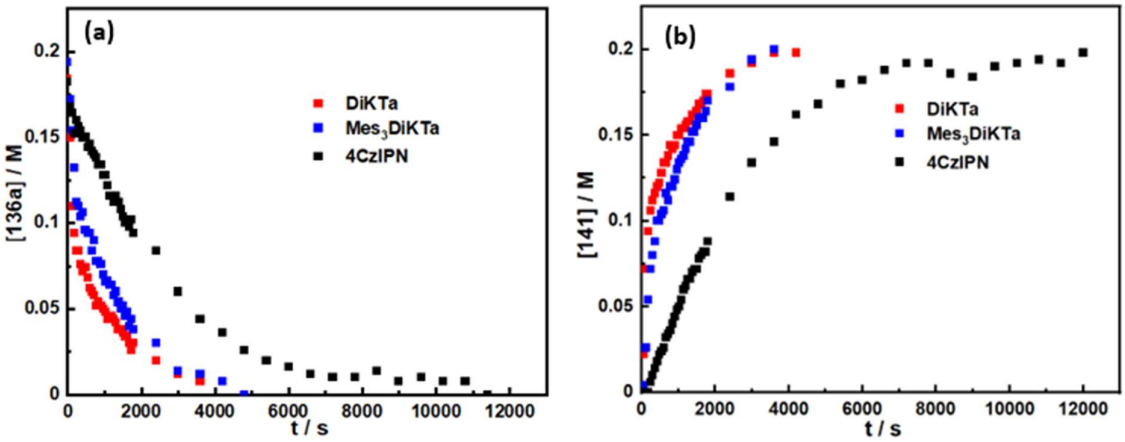

Figure 3.11 Reaction progress kinetics over time for the ATRA between **136a** and **138**, replacing DCE with CD_2Cl_2 as solvent and using λ_{exc} = 455 nm with 1,4-bis(trimethylsilyl)benzene as internal standard. a) Concentration of **138** over time. b) Concentration of **141** over time.

3.2.6 Photostability Studies

A study by Grotjahn and König[105] showed that D-A phthalonitrile-containing PCs such as **4CzIPN** photodecompose when irradiated in the presence of alkyl carboxylic acids *via* photosubstitution of one of the cyanide groups by an alkyl radical (Scheme 3.9). Due to the loss of one of the electron-accepting groups, the monocyano product **159** possesses significantly altered optoelectronic properties, including a much larger optical gap and more negative excited state redox potentials. For example, the photosubstitution product **159** between **4CzIPN** and 2-phenylpropanoic acid **160** is a stronger photoreductant [E_{ox}(**159**$^{\bullet+}$/**159***) = – 1.43 V] but a weaker photooxidant [E_{red}(**159***/**159**$^{\bullet-}$) =

1.27 V] compared to –1.23 V/1.44 V for **4CzIPN**. This increase in reducing power was exploited previously by König[123] to generate carbanions from aryl acetic acids as the active PC was in fact the photosubstitution product, rather than **4CzIPN** itself. However, photoinstability of the PC is not desirable and it could be envisaged that the decreased oxidative power of **4CzIPN** resulting from the photosubstitution could hinder the reaction. Furthermore, the observed blueshift in the absorption spectrum of the photosubstituted **4CzIPN** results in a lower molar absorptivity during the photoexcitation using a blue-light excitation source (λ_{exc} ~ 450 nm), potentially resulting in slower reaction kinetics. Given this precedent, similar photodecomposition studies were performed on **DiKTa** and **Mes$_3$DiKTa**.

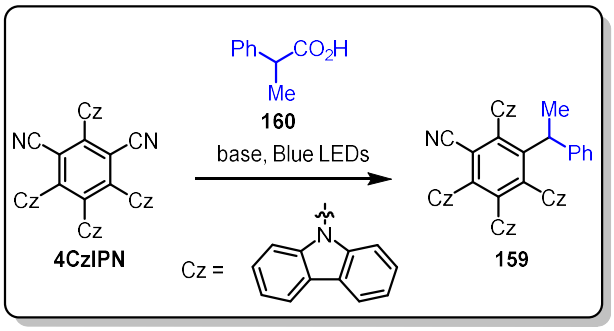

Scheme 3.9 Photosubstitution of **4CzIPN** with an aryl acetic acid.

To test the photostability of **4CzIPN**, **DiKTa** and **Mes$_3$DiKTa**, UV-vis absorption spectra before and after irradiation of the decarboxylative photo-Giese reaction mixture were monitored (Figure 3.12). As expected, a significant blueshift of **4CzIPN** was observed due to the corresponding photosubstitution product (Figure 3.12a). However, a smaller blue shift was also observed for both **DiKTa** and **Mes$_3$DiKTa** (Figures 3.12b-c), suggesting decomposition also occurs for these PCs; however, the decomposition products were not able to be identified.

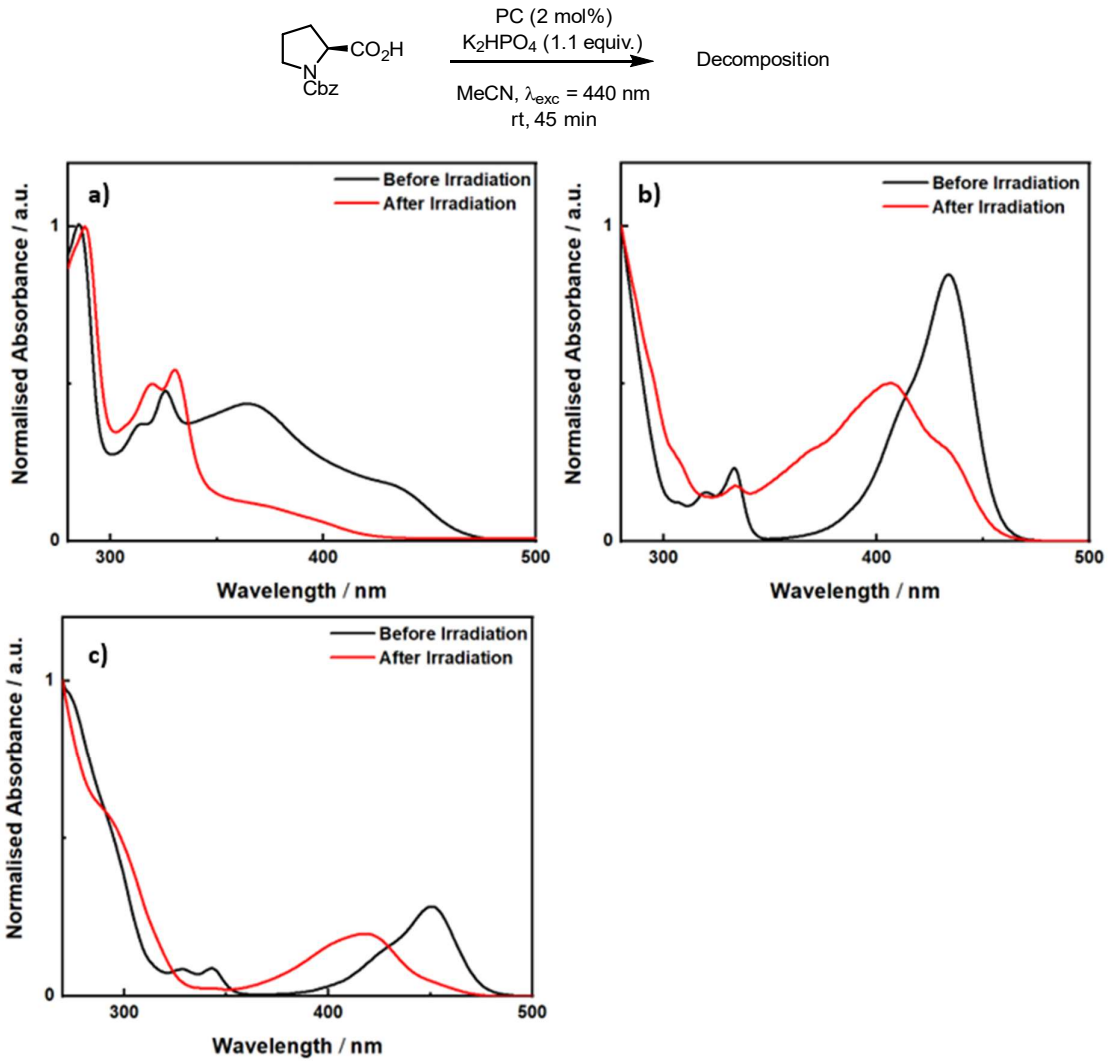

Figure 3.12 Photodecomposition study of a) **4CzIPN** b) **DiKTa** c) **Mes$_3$DiKTa**.

3.2.7 Polymer-supported DiKTa.

Homogeneous photocatalysis for organic transformations has seen rapid development in recent years. However, heterogeneous photocatalysis has received much less attention,[124] despite the many successful applications in the fields of pollutant degradation,[125] water splitting[126] and CO_2 reduction.[127] One method for the development of heterogeneous PCs is to attach a known homogeneous PC to a solid support such as mesoporous silica.[128,129] Mesoporous silica materials have now become widely used for this application due to their high stability, inertness and large surface area.[130] Considering the apparent instability of **DiKTa** we envisaged that immobilization on a polymer support could confer additional photostability and ideally allow for improved reusability of the PC. Therefore, a modified

DiKTa with an attached carboxylic acid group **161** was synthesised to allow for attachment to the polymer support via an amide coupling. First, Iodo-**DiKTa** **162** was synthesised using known procedures[131] from aniline **163** and methyl 2-iodobenzoate **11** via an Ullman coupling, iodination, and Friedel-crafts acylation sequence (Scheme 3.10a). Separately, boronic acid **164** was synthesised via the oxidation and esterification of 4-tolyl boronic acid (Scheme 3.10b).[132,133]

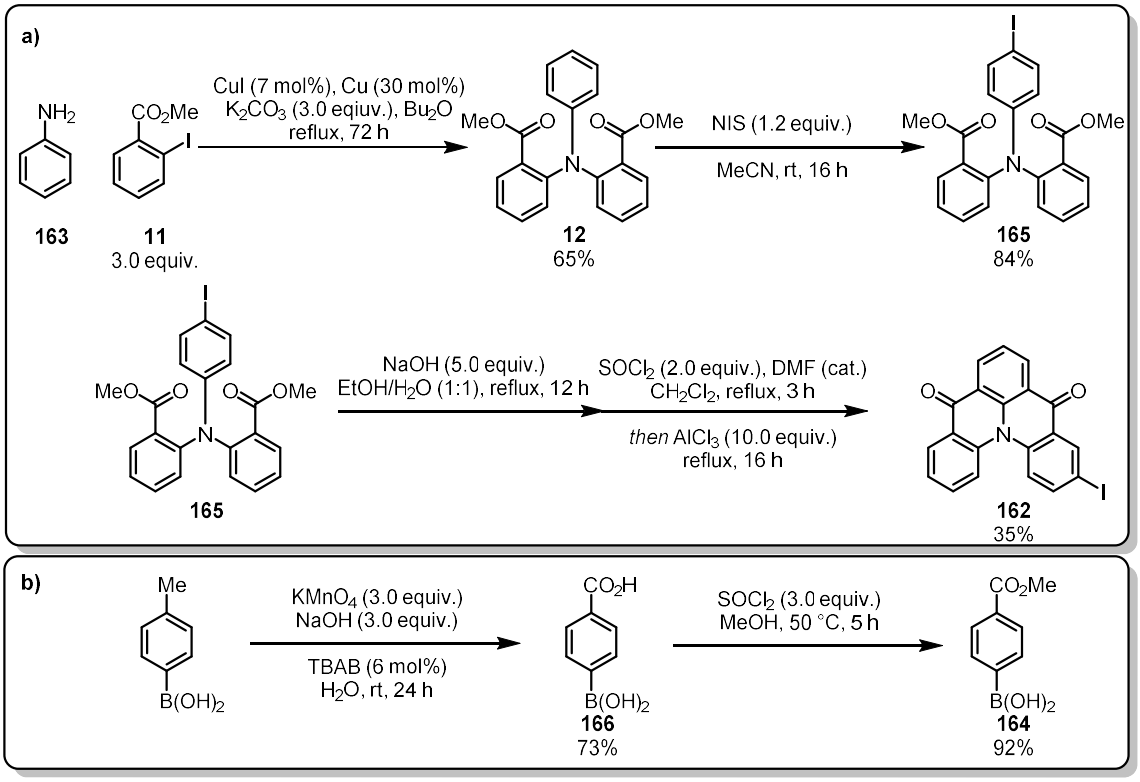

Scheme 3.10 a) Synthesis of Iodo-**DiKTa**. b) Synthesis of boronic acid **164**.

A subsequent Suzuki-Miyaura cross-coupling and hydrolysis furnished **161** in an overall yield of 13% (Scheme 3.11a). Finally, an amide coupling with polymer-supported amine (MS-AP) or hexan-1-amine provided the desired heterogeneous PCs on two different types of mesoporous silica (MSN and SBA-15) and also a homogeneous **DiKTa** variant **167** with the amide modification for comparison (Scheme 3.11b).

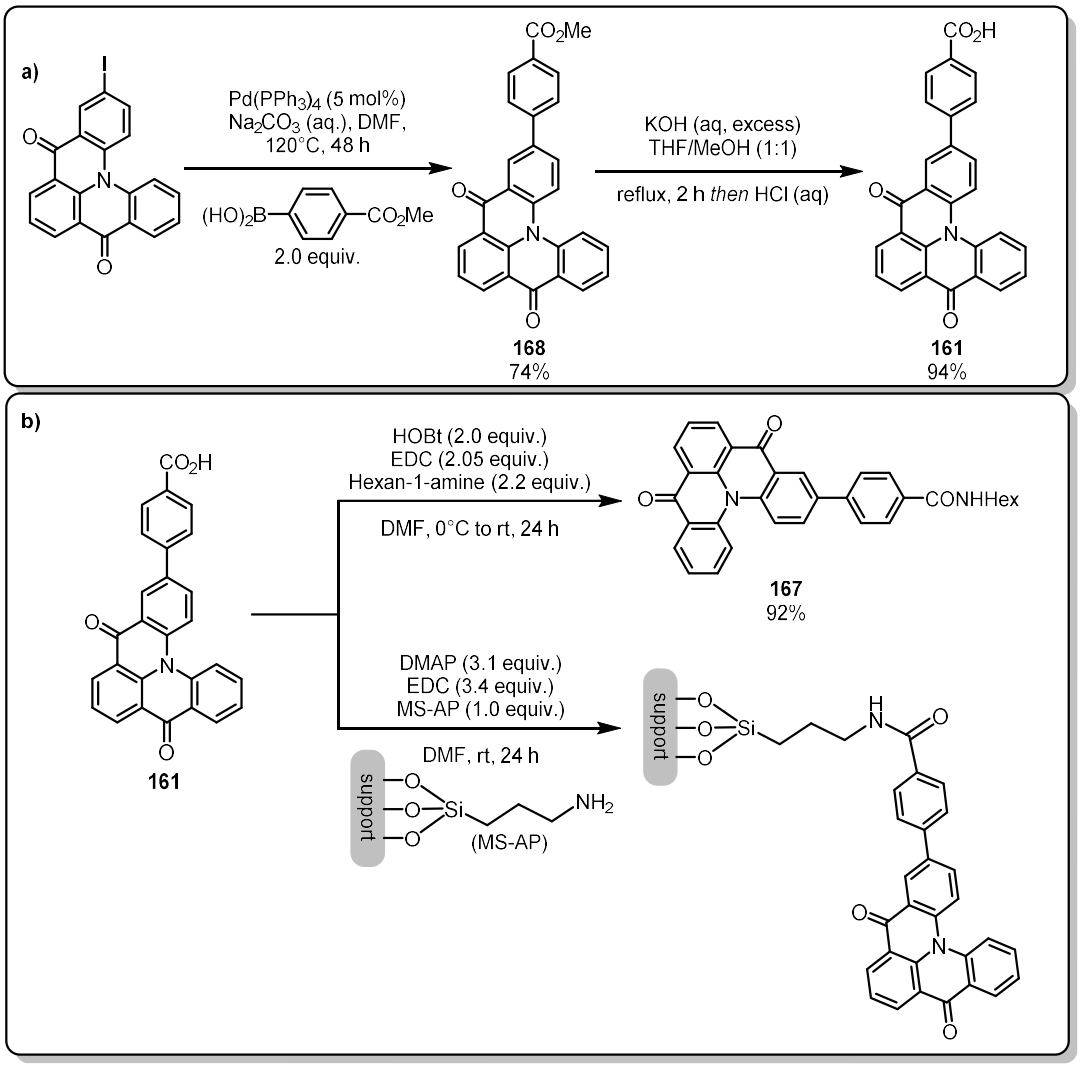

Scheme 3.11 a) Synthesis of carboxylic acid **161**. b) Amide coupling of **161**.

Characterization of the immobilised PCs using elemental analysis allowed for the calculation of the amount of PC per gram of material (mmol/g) so that catalyst loading could be known. Absorption and photoluminescence measurements of both **167** and the polymer-supported PC were also obtained. As expected, **167** shows similar absorption and emission to **DiKTa** (Figure 3.13a). Absorption measurements on a suspension of SBA-15 polymer-supported **DiKTa** (**SBA-DiKTa**) in EtOH resulted in broad uniform absorption so the excitation spectrum was used instead (Figure 3.13b). Pleasingly, the excitation and emission spectra of **SBA-DiKTa** were also similar to homogeneous **DiKTa**.

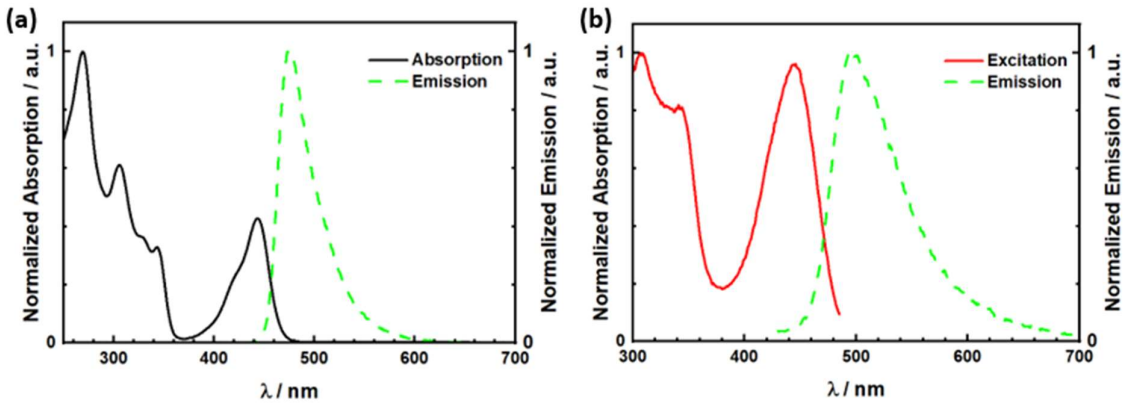

Figure 3.13 (a) Absorption and photoluminescence spectra of **167** in CH_2Cl_2 (λ_{exc} = 400 nm). (b) Excitation (λ_{em} = 495 nm)and photoluminescence spectra of **SBA-DiKTa** suspended in EtOH (λ_{exc} = 400 nm).

With this information, the polymer-supported PCs could be screened in the model reactions established in the previous sections with **167** as a homogeneous comparison. First, the decarboxylative photo-Giese reaction between proline **23a** and diethyl maleate **120** was attempted (Table 3.8). **167** achieved similar results to that of **DiKTa** with a near quantitative NMR yield (Table 3.8, entries 1-2). However, the polymer-supported version using MSN (**MSN-DiKTa**) only reached an NMR yield of 38% (Table 3.8, entry 3), and when using **SBA-DiKTa** no reaction was observed (Table 3.8, entry 4). Variation to a smaller substrate was considered with isobutyric acid in case **23a** was too large to fit through the pores of the polymer. As previously stated, when using **DiKTa** in this reaction an NMR yield of 78% was observed (Table 3.8, entry 5). However, when using **167** only a 6% NMR yield was achieved and no reaction was observed with either **MSN-DiKTa** or **SBA-DiKTa** (Table 3.8, entries 6-8).

Table 3.8 Decarboxylative photo-Giese reaction between carboxylic acids and diethyl maleate.

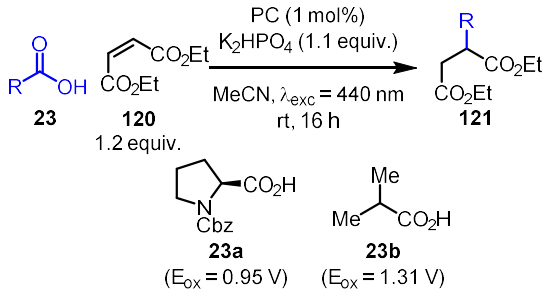

Entry[a]	Acid	PC	Yield / %[b]
1	**23a**	**DiKTa**	93 (± 3)
2	**23a**	**167**	99
3	**23a**	**MSN-DiKTa**	38
4	**23a**	**SBA-DiKTa**	N.R.
5	**23b**	**DiKTa**	78 (± 3)
6	**23b**	**167**	6
7	**23b**	**MSN-DiKTa**	N.R.
8	**23b**	**SBA-DiKTa**	N.R.

[a] Carboxylic acid (**23**) (0.15 mmol), diethyl maleate (**120**) (0.18 mmol), K_2HPO_4 (0.17 mmol), PC (1 mol%), MeCN (3 mL), irradiation with 440 nm LEDs, rt. [b] Yield determined by ^{1}H NMR, using 1,3,5-trimethoxybenzene as the internal standard.

Next the oxidative quenching ATRA between **136a** and **138** was tested with each PC (Table 3.9). When using **DiKTa** a 97% NMR yield is observed, which falls to 62% when using **167** (Table 3.9, entries 1-2). With a similar trend to the previous reaction, **MSN-DiKTa** gave a further reduced yield of 30% and **SBA-DiKTa** even lower with 12% (Table 3.9, entries 3-4).

Table 3.9 Oxidative quench ATRA reaction between alkyl halides and alkene.

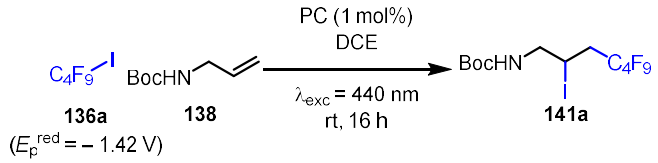

Entry[a]	PC	Yield / %[b]
1	**DiKTa**	97 (± 2)
2	**167**	62
3	**MSN-DiKTa**	30
4	**SBA-DiKTa**	12

[a] Alkyl halide (**4**) (0.60 mmol), *tert*-butyl *N*-allylcarbamate (**5**) (0.30 mmol), PC (1 mol%), DCE (1.5 mL), irradiation with 440 nm LEDs, rt, 24 h. [b] Yield determined by ^{1}H NMR, using 1,3,5-trimethoxybenzene as the internal standard.

Considering the relatively poor performances of the polymer-supported PCs in photoredox catalysis, the next reactions tested operate via DET. Beginning with the (*E*)/(*Z*)-isomerization of diisopropyl fumarate, **DiKTa** achieved a (*Z*):(*E*) ratio of 90:10 (Table 3.10, entry 1). However, it seems with the amide modification **167** behaves similarly to **Mes$_3$DiKTa** and only a 52:48 ratio was observed (Table 3.10, entry 2). Following the previously observed trend, **MSN-DiKTa** gave a reduced amount of the (*Z*) isomer with a ratio of 17:83 and **SBA-DiKTa** lower still with a ratio of 5:95 (Table 3.10, entries 3-4). Next, the (*E*)/(*Z*)-isomerization of (*E*)-stilbene was tested and interestingly, on this occasion all PCs gave similar values with **167**, **MSN-DiKTa** and **SBA-DiKTa** all achieving slightly higher (*Z*):(*E*) ratios relative to **DiKTa** (Table 3.10, entries 5-8).

Table 3.10 (*E*)/(*Z*) Isomerization of alkenes.

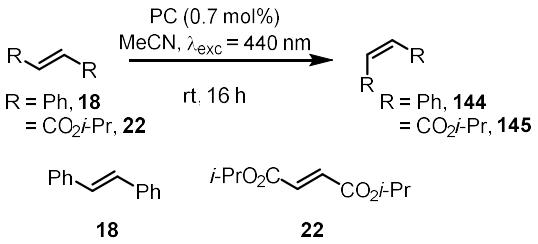

Entry[a]	Alkene	PC	(*Z*)/(*E*)[b]
1	**22**	**DiKTa**	90:10 (± 0)
2	**22**	**167**	52:48
3	**22**	**MSN-DiKTa**	17:83
4	**22**	**SBA-DiKTa**	5:95
5	**18**	**DiKTa**	59:41 (± 1)
6	**18**	**167**	64:36
7	**18**	**MSN-DiKTa**	63:37
8	**18**	**SBA-DiKTa**	64:36

[a] Alkene (0.60 mmol), PC (0.7 mol%), MeCN (3 mL), irradiation with 440 nm LEDs, rt. [b] Determined using ^{1}H NMR.

In conclusion, the polymer-supported PCs **MSN-DiKTa** and **SBA-DiKTa** have been prepared and tested in a variety of photocatalytic reactions. The results of these tests showed a significant reduction in photocatalytic efficiency when immobilised onto mesoporous silica relative to their homogeneous counterpart **167**. Future work should focus on alternative methods for immobilization.

3.2.8 Water-soluble DiKTa.

Photocatalytic reactions are typically thought of as 'green' processes as they use visible light to promote radical processes rather than heat or stoichiometric amounts of strong chemical redox reagents. However, as with many branches of organic synthesis, photocatalytic reactions typically use unsustainable organic solvents that can be toxic, volatile and flammable, which leads to increased hazards.[134] The ideal solvent for a chemical reaction is of course water, as it is environmentally benign, non-toxic, non-flammable and has a high specific heat capacity. While photocatalysis has been widely used in aqueous media for the degradation of pollutants,[125] there has been much less investigation into its use in the synthesis of organic compounds under aqueous conditions.[135,136] This is largely due

to the insolubility of both the organic starting materials of interest and also the PCs themselves. A number of solutions have been explored towards this goal. For example, using known PCs that themselves are partially water soluble, such as Eosin Y,[137] $[Ru(bpy)_3]Cl_2 \bullet 6H_2O$,[138] or Rose Bengal.[139] Another solution is to use additives that form micelles in the aqueous media for the organic PCs and substrates to react inside.[140] Alternatively, others have modified known PCs with water solubilising groups such as sulfonates[141,142] and used water-soluble substrates. Considering these options, we envisaged a modified version of **DiKTa** that would be soluble in water that could transfer all the benefits observed so far for MR-TADF PCs to aqueous photocatalysis. Given the success of the previous synthetic route to **DiKTa** with a single carboxylic acid group attached, the target of choice in this case would be **DiKTa** with 6 carboxylate groups **169** (Figure 3.14).

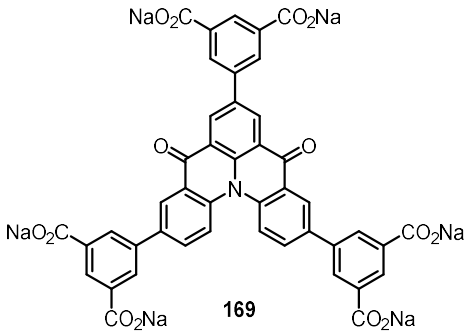

Figure 3.14 Target compound for a water soluble **DiKTa**-based PC.

The synthesis of the target compound began with the synthesis of **Br_3DiKTa** using known procedures[37] from aniline and methyl 2-iodobenzoate via an Ullman coupling, bromination, and Friedel-crafts acylation sequence (Scheme 3.12a). Separately, the boronic ester **170** was synthesised via a Miyaura borylation reaction of the corresponding aryl bromide **171** (Scheme 3.12b)[143] and used without further characterization in a subsequent Suzuki-Miyaura coupling and hydrolysis that furnished **169** in an overall yield of 19% (Scheme 3.12c). Pleasingly, **169** proved to be soluble in water.

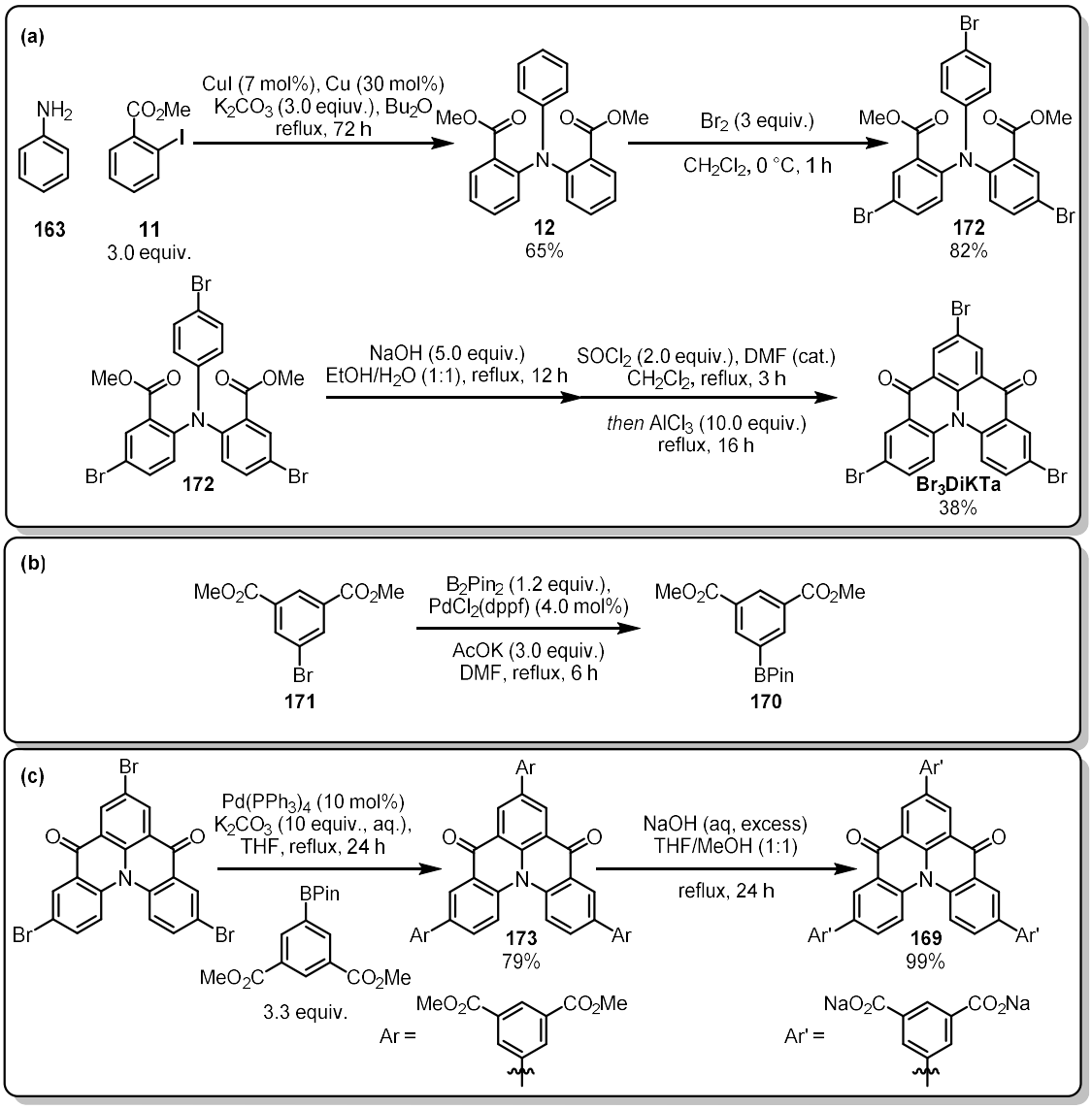

Scheme 3.12 (a) Synthesis of **Br$_3$DiKTa**. (b) Synthesis of boronic ester **170**. (c) Synthesis of water soluble **DiKTa** variant **169**.

With the synthesis of the target compound complete, the absorption and photoluminescence spectra of both **173** and **169** was obtained. Unsurprisingly the spectra of **173** are similar to that of **DiKTa** with a slight red-shift due to the added electron withdrawing groups (Figure 3.15). Next, **169** was measured in water and an even greater red-shift of both absorption and emission was observed, accompanied by a broadening of the emission.

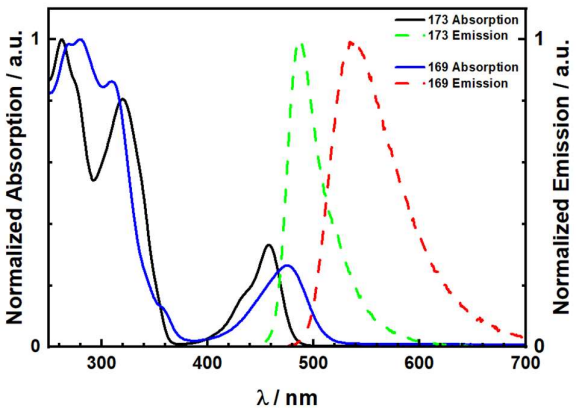

Figure 3.15 Absorption and photoluminescence spectra of **173** in CH_2Cl_2 (λ_{exc} = 400 nm) and **169** in H_2O (λ_{exc} = 420 nm).

Having completed the initial characterization of **169**, it was tested in known aqueous photocatalytic reactions. The first reaction chosen was the (*E*)/(*Z*) isomerization of cinnamic acid **174**, which was also used by Bertrams and Kerzig[141] in their evaluation of a different water soluble PC, **SO_2TDS** (Scheme 3.13). The proposed mechanism is a DET process analogous to the previous (*E*)/(*Z*) isomerizations of stilbene and fumarate described in scheme 3.4. Cinnamic acid and **169** were dissolved in a basic aqueous solution and irradiated with λ_{exc} = 440 nm and an average (*Z*):(*E*) ratio of 24:76 was observed over two separate runs. This is significantly lower than the 71:29 ratio achieved by Kerzig using **SO_2TDS** but is similar to their result with 4-carboxybenzophenone which achieved a 27:73 ratio.

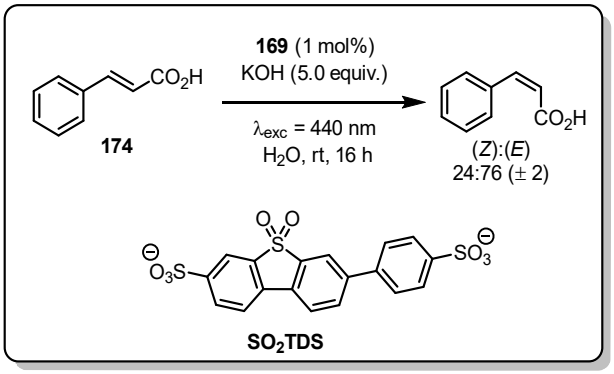

Scheme 3.13 (*E*)/(*Z*) isomerization of cinnamic acid.

Another reaction used in Bertrams and Kerzig's study[141] of SO_2TDS is the pinacol coupling of acetophenone in the presence of sodium ascorbate (NaHAsc), which was previously reported by Naumann and Goez (Scheme 3.14).[144] The proposed mechanism proceeds via the reductive quenching of the PC by NaHAsc to generate $PC^{\bullet-}$, which can then reduce acetophenone via SET to give the desired

ketyl radical **175** and complete the catalytic cycle. Two molecules of **175** can then couple together to produce the desired product **176**. However, when using **169** no conversion was observed. Potential reasons for this are inefficient quenching of **169*** with NaHAsc, or perhaps **169**$^{\bullet-}$ is not sufficiently reducing to reduce acetophenone.

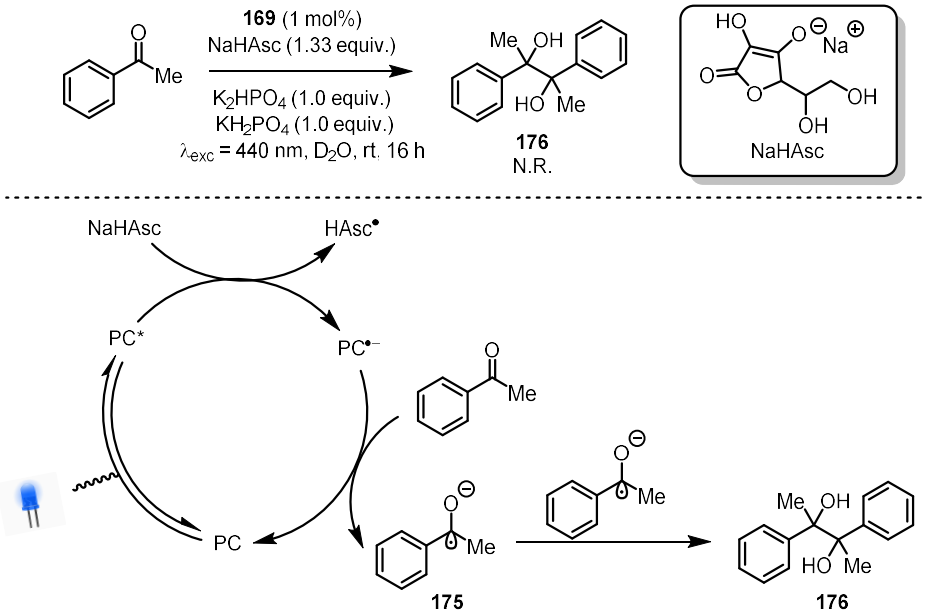

Scheme 3.14 Photocatalytic pinacol coupling of acetophenone in water.

Diazonium salts **177** are particularly useful as aryl radical precursors due to their low reduction potentials (– 0.16 V vs SCE in MeCN).[145] Xue and co-workers[146] showed that diazoniums can be used for the arylation of *N*-heteroarenes **178** in aqueous media under photocatalytic conditions (Scheme 3.15). This seemed to be a useful test reaction for **169** so the reproducibility of this reaction was investigated. Pleasingly, under literature conditions a satisfactory 52% NMR yield was observed. However, a similar NMR yield of 41% was also observed in the absence of a PC. Therefore, this reaction was not investigated further with **169**.

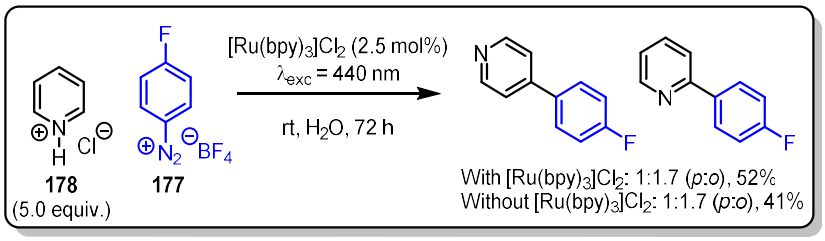

Scheme 3.15 Arylation of N-heteroarenes in water. Using 1,3,5-trifluorobenzene as ^{19}F NMR internal standard.

Considering **DiKTa** proved to be particularly capable for decarboxylative reactions, the next reaction chosen was the decarboxylative formation of ketones developed by Xu and co-workers (Scheme 3.16).[147] A full catalytic cycle has not been postulated; however, this reaction presumably proceeds through the decarboxylative formation of a benzylic radical that is subsequently trapped by O_2 in the air and the resulting intermediate collapses to yield the desired ketone products **179**. Using **SAS** as a PC, Xu and co-workers observed a 95% yield of **179**. However, when using **169** under the same conditions, a much lower NMR yield of only 6% was obtained. These results, in combination with the previous attempts described, show that **169** can act as a water-soluble PC but product yields tend to be low. Therefore, future work will focus on alternative PC designs for water-soluble variants of **DiKTa**.

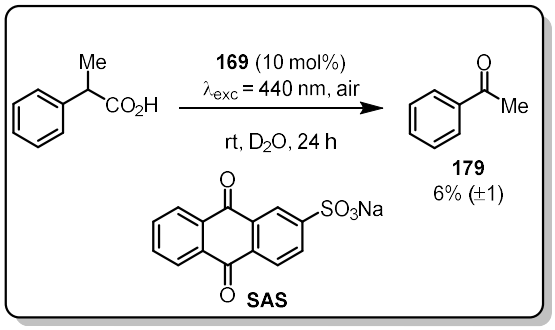

Scheme 3.16 Decarboxylative formation of acetophenone in water.

3.3 Conclusions.

In summary, this work demonstrates the potential of MR-TADF compounds as a new class of PC, using **DiKTa** and **Mes$_3$DiKTa** as examples compared with **4CzIPN** as a prototypical donor-acceptor TADF benchmark. Compared to other photocatalysts **DiKTa** stands out for its wide redox window, low molecular weight, and low cost. Multiple different classes of photocatalytic reactions were tested, including oxidative and reductive quenching reactions, DET reactions and dual catalytic reactions. Both

DiKTa and **Mes$_3$DiKTa** were shown to be comparable or superior in all examples of photoredox catalysis, particularly at low catalyst loadings, and complementary for energy transfer reactions compared to **4CzIPN** due to their higher triplet energies. In-situ NMR studies were used to probe reaction kinetics of the ATRA reaction between a perfluorinated alkyl halide and an unactivated alkene and showed a significant enhancement of the rate of reaction when using either **DiKTa** or **Mes$_3$DiKTa** over **4CzIPN**.

In an attempt to improve the stability and reusability of **DiKTa** a mesoporous silica-based polymer-supported version was synthesised. **MSN-DiKTa** and **SBA-DiKTa** were then used in the previously established standard reactions. However, a reduced photocatalytic efficiency was observed relative to the homogeneous standard **167**. Finally, a water-soluble version of **DiKTa** was synthesised, **169**, and tested in a series of known photocatalytic reactions that use water as a solvent. However, poor yields were observed. Future work in this field should expand the use of MR-TADF PCs to other structural classes such as DABNA-based emitters. Additionally, further work on the **DiKTa** core could be to investigate alternative solubilizing groups for aqueous photocatalysis.

4 NHC/Photoredox Catalytic Synthesis of 1,4-Diketones Using an MR-TADF Photocatalyst.

4.1 Introduction

The development of synthetic methodologies to produce 1,4-diketones is a well-studied area of research,[148–150] in large part due to their utility as precursors of various heterocycles such as furans,[151] thiophenes,[152] and pyrroles.[153] While a number of disconnections are possible, perhaps the most commonly used synthetic strategy follows the umpolung approach of disconnecting the 1,4-diketone into a nucleophilic acyl group equivalent and an α,ß-unsaturated ketone, such as employed in the Stetter reaction (Scheme 4.1).[148] The Stetter reaction uses substoichiometric amounts of an NHC in the presence of an aldehyde **41** and an α,ß-unsaturated ketone **181** to furnish the desired 1,4-diketones **182** via a nucleophilic Breslow intermediate **183**.

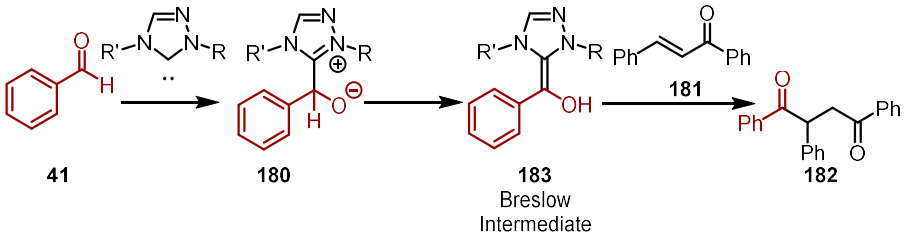

Scheme 4.1 Stetter reaction.

Another possible disconnection would involve generating the 1,4-diketone from three distinct fragments. While such processes have been developed employing conventional two electron mechanisms,[154,155] they are currently limited to the use of 1,3-diketones **184** in combination with an appropriate α-ketoaldehyde **185** and nucleophile **186** (Scheme 4.2).

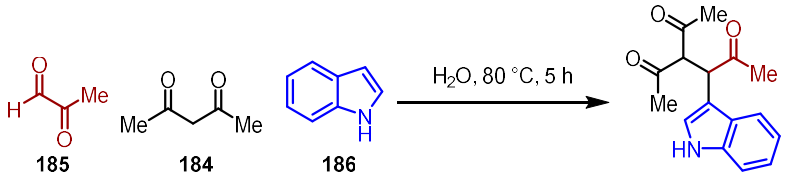

Scheme 4.2 Three-component synthesis of 1,4-diketones.

As a more general approach, the 1,4-diketone may be disconnected into two acyl radical components and an alkene, which in the forward direction would involve a radical addition of one acyl group to the alkene, followed by a subsequent radical-radical coupling (Scheme 4.3).

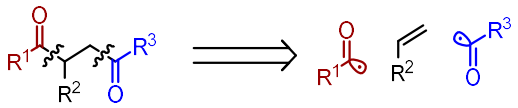

Scheme 4.3 Radical disconnection of 1,4-diketones.

This strategy has been executed successfully by the groups of Ackermann,[156] Larionov,[157] Li,[158] and Wu.[159] However, these examples are typically limited to the synthesis of symmetric 1,4-diketones, as is the case for the reaction developed by Li and co-workers[158] for the synthesis of symmetric 1,4-diketones **187** from alkenes **188** and aldehydes **189** using NHC catalysis and peroxyester **190** as a radical initiator (Scheme 4.4).

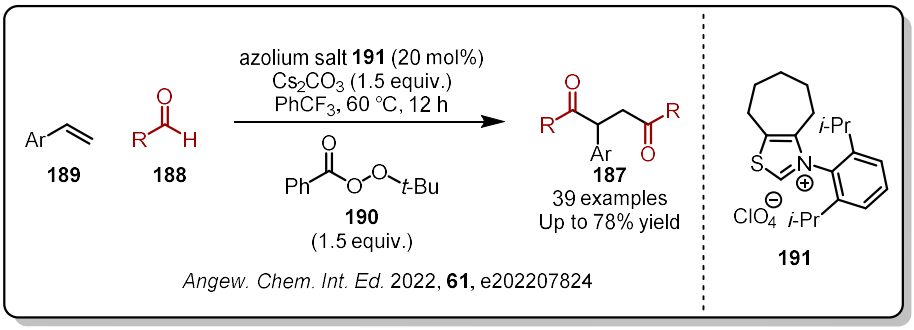

Scheme 4.4 Synthesis of symmetric 1,4-diketones through radical NHC catalysis.[158]

The challenge of making unsymmetric 1,4-diketones using this strategy is significant, as the two acyl radicals must offer distinct reactivity to avoid forming a mixture of symmetric and unsymmetric products. Therefore, to achieve selective formation of the desired unsymmetric 1,4-diketones another acyl radical, or equivalent, is required that must be generated simultaneously but itself will not react with the alkene. In a recent report, Wang and Ackermann[156] accomplished this transformation selectively through the use of metallaphotoredox catalysis using sodium decatungstate (NaDT) as the PC and a nickel co-catalyst, although electron deficient alkenes were required (Scheme 4.5).

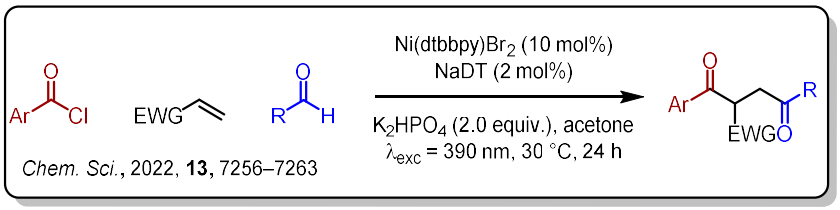

Scheme 4.5 Synthesis of unsymmetric 1,4-diketones through metallaphotoredox catalysis.[156]

As an alternative, we envisaged the photocatalytic formation of acyl radicals **192** from α-keto acids **193** via a reductive quenching mechanism,[159–161] which would add to the alkene **194** to give radical **195** (Scheme 4.6). Subsequently, an acyl azolium intermediate **196**, generated from an NHC catalyst and an appropriate electrophile **197**, could be reduced through SET to the corresponding NHC-stabilised ketyl radical **198**,[77,162,163] which could act as the second acyl radical required for this transformation. Radical-radical coupling between **195** and **198** would generate intermediate **199**, which would then collapse to complete the NHC cycle and release the desired unsymmetric 1,4-diketone product **200**.

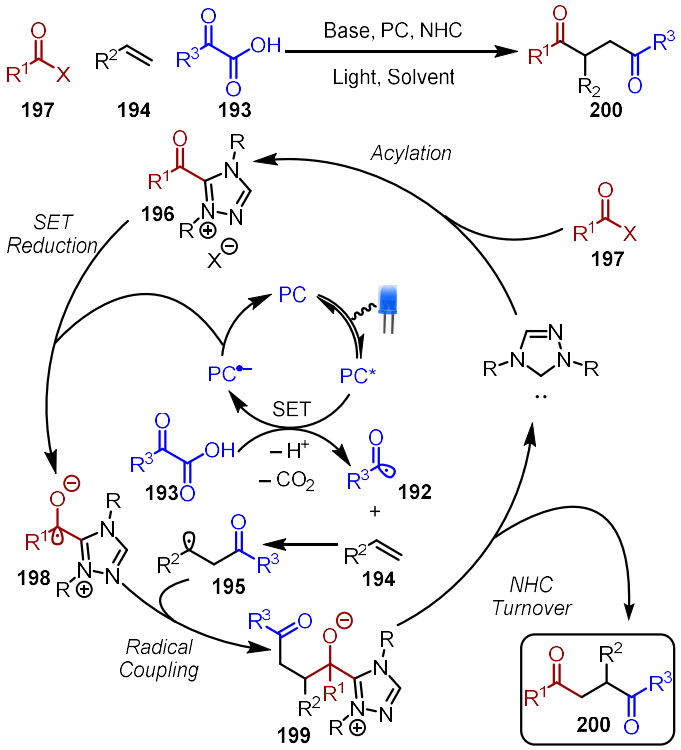

Scheme 4.6 Proposed catalytic cycle.

During the course of our investigations Feng *et al.*[164] published the use of triphenylphosphine in combination with NHC/photoredox dual catalysis using an iridium(III) PC for the generation of acyl

radicals from benzoic acids **201**. However, to achieve the challenging synthesis of unsymmetric 1,4-diketones **202**, the use of stoichiometric acyl azoliums **203** was required (Scheme 4.7a). Building upon this work, we considered that using an α-keto acid **193** in combination with the MR-TADF photocatalyst **DiKTa** (introduced in chapter 3),[165] would allow for the preparation of unsymmetric 1,4-diketones **200** in a modular, metal-free, three-component relay reaction using NHC/photoredox dual catalysis (Scheme 4.7b). Zhang *et al.*[166] have now also published a similar but independent study that relied upon the use of an Ir-based PC (Scheme 4.7c).

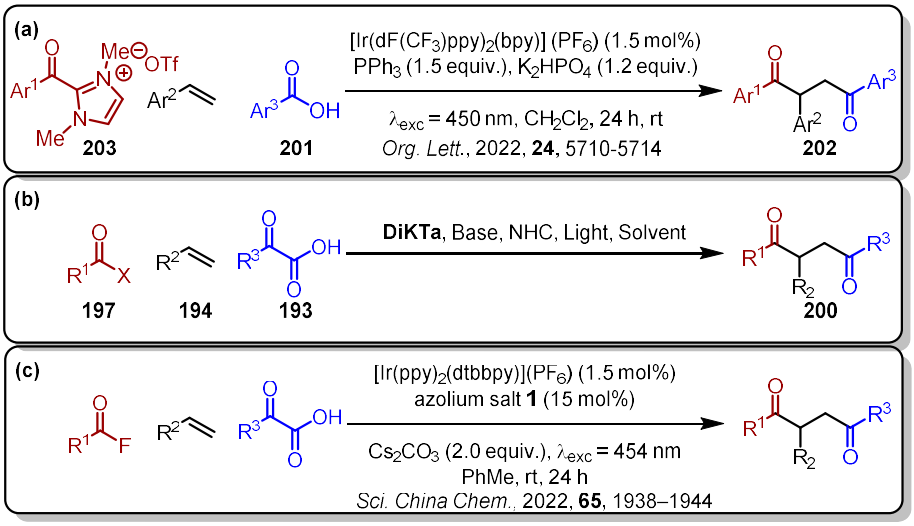

Scheme 4.7 (a) Synthesis of unsymmetric 1,4-diketones using stoichiometric acyl azoliums.[164] (b) Proposed synthesis of unsymmetric 1,4-diketones using NHC catalysis. (c) Synthesis of unsymmetric 1,4-diketones using an iridium photocatalyst.[166]

4.2 Results and Discussion

4.2.1 Optimization

Initial exploration used the reaction of commercially available benzoyl fluoride **204**, styrene **19**, and phenylglyoxylic acid **205** (Scheme 4.8). Using azolium salt **2** in the presence of Cs_2CO_3 as a base and **DiKTa** as the PC, under photoexcitation using a 427 nm LED, the corresponding 1,4-diketone **182** was generated in a promising 38% NMR yield, using 1,3,5-trimethoxybenzene as an internal standard. The choice of these initial conditions were guided by previous reports on similar NHC/photoredox catalytic systems such as the work by Studer and co-workers.[77] While an initial hit of 38% was promising, the

complete consumption of **19** but moderate product yields indicated significant side reactivity was occurring and so further optimization was required.

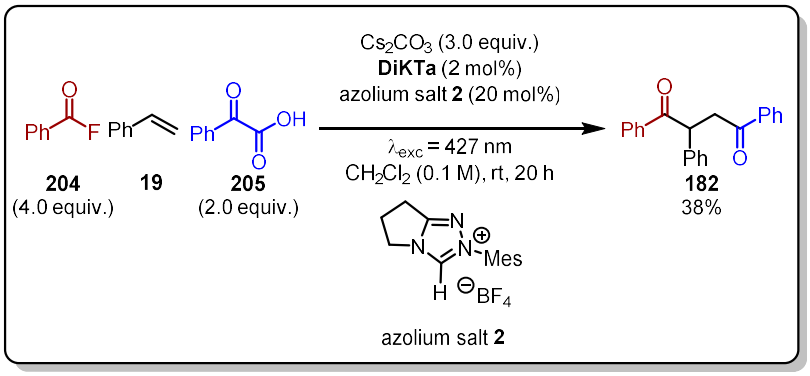

Scheme 4.8 Initial hit. ^{1}H NMR yield with 1,3,5-trimethoxybenzene as standard.

Firstly, other commonly used photocatalysts were tested (Table 4.1). [Ir(dF(CF$_3$)ppy)$_2$(dtbbpy)](PF$_6$), [Ir(ppy)$_2$(dtbbpy)](PF$_6$) and **4CzIPN**, also all managed complete consumption of **19** and gave similar product yields of 29-30% (Table 4.1, entries 1-3), which are slightly lower than that observed with **DiKTa** (Table 4.1, entry 4). Eosin Y was also tested and only starting materials were detected (Table 4.1, entry 5).

Table 4.1 Photocatalyst Optimization.

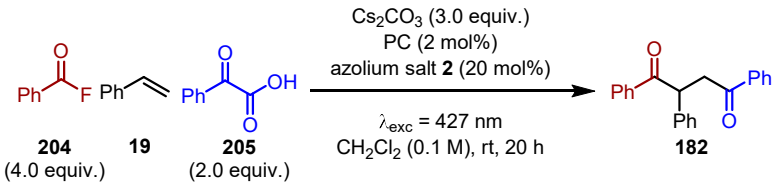

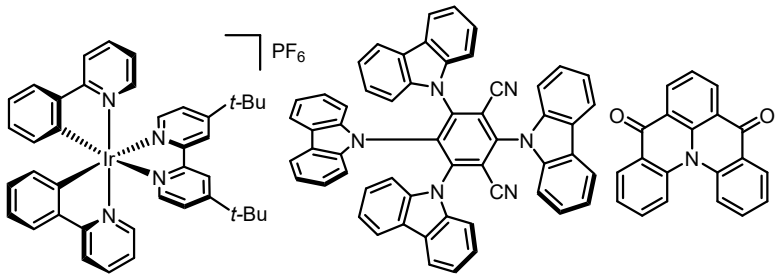

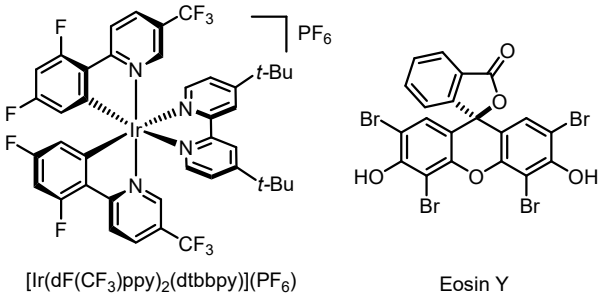

Entry[a]	PC	Yield / %[b]
1	$[Ir(dF(CF_3)ppy)_2(dtbbpy)](PF_6)$	30
2	$[Ir(ppy)_2(dtbbpy)](PF_6)$	30
3	**4CzIPN**	29
4	**DiKTa**	38
5	Eosin Y	0

[a] Benzoyl fluoride (**204**) (0.4 mmol), styrene (**19**) (0.10 mmol), phenylglyoxylic acid (**205**) (0.2 mmol), Cs_2CO_3 (0.3 mmol), azolium salt **2** (20 mol%), PC (2 mol%), CH_2Cl_2 (1 mL), irradiation with 427 nm LED, rt. [b] Yield determined by ^1H NMR, using 1,3,5-trimethoxybenzene as internal standard.

Next, the stoichiometry of the starting materials was varied (Table 4.2). Changing the limiting agent from styrene to **205** gave an improved yield of 46% (Table 4.2, entries 1-2). However, when using a larger excess of styrene, a reduced yield of 30% was observed (Table 4.2, entry 3). Finally, using **204** as the limiting reagent gave poor product yields (Table 4.2, entries 4-5), so the conditions from entry 2 were taken forward.

Table 4.2 Starting Material Ratio Optimization.

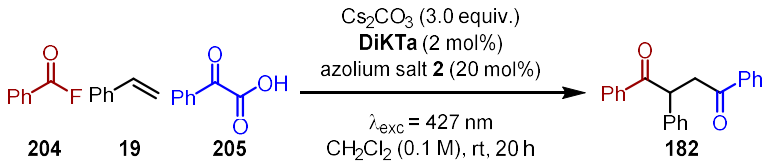

Entry[a]	Benzoyl Fluoride Equiv.	Styrene Equiv.	Acid Equiv.	Yield / %[b]
1	4	1	2	38
2	4	2	1	46
3	4	4	1	30
4	1	2	4	10
5	1	4	2	Trace

[a] Benzoyl fluoride (**204**), styrene (**19**), phenylglyoxylic acid (**205**), Cs_2CO_3, azolium salt **2** (20 mol%), **DiKTa** (2 mol%), CH_2Cl_2 (1 mL), irradiation with 427 nm LED, rt. [b] Yield determined by ^1H NMR, using 1,3,5-trimethoxybenzene as internal standard.

Further optimization focused on variation of the azolium salt. The current best conditions gave a yield of 46% using azolium salt **2** (Table 4.3, entry 1); however, when the *N*-aryl substituent is changed from mesityl to pentafluorophenyl (azolium salt **3**) only traces of **182** were observed (Table 4.3, entry 2). If 2,4,6-trichlorophenyl (azolium salt **4**) is used instead a moderate yield of 27% is achieved (Table 4.3, entry 3), therefore mesityl was maintained as the *N*-aryl substituent. Chiral azolium salt **1** developed by Bode and co-workers[167] has a similar mesityl triazolium core but an extended backbone and gave a slightly improved yield of 50% (Table 4.3, entry 4). Variation of the *N*-aryl substituent was also investigated for this different backbone; however, both the phenyl (azolium salt **5**) and pentafluorophenyl (azolium salt **6**) analogues gave poor yields of **182** consistent with the achiral catalyst variants (Table 4.3, entries 5-6). As azolium salts **1**-**6** are all triazolium salts, variation to an imidazolium salt was next investigated. However, imidazolium salt **7** with two mesityl substituents gave a poor yield of 17% (Table 4.3, entry 7). Similar to previous examples, variation away from the mesityl substituent to a 2,6-diisopropylphenyl substituent (azolium salt **8**) resulted in a lower yield of 6% (Table 4.3, entry 8). Finally, the dihydroimidazolium salt **9** and the commercially available thiazolium salt **10** generated trace amounts of **182** (Table 4.3, entries 9-10). Therefore, the conditions from entry 4 were carried forward for further optimization.

Table 4.3 Azolium Salt Optimization.

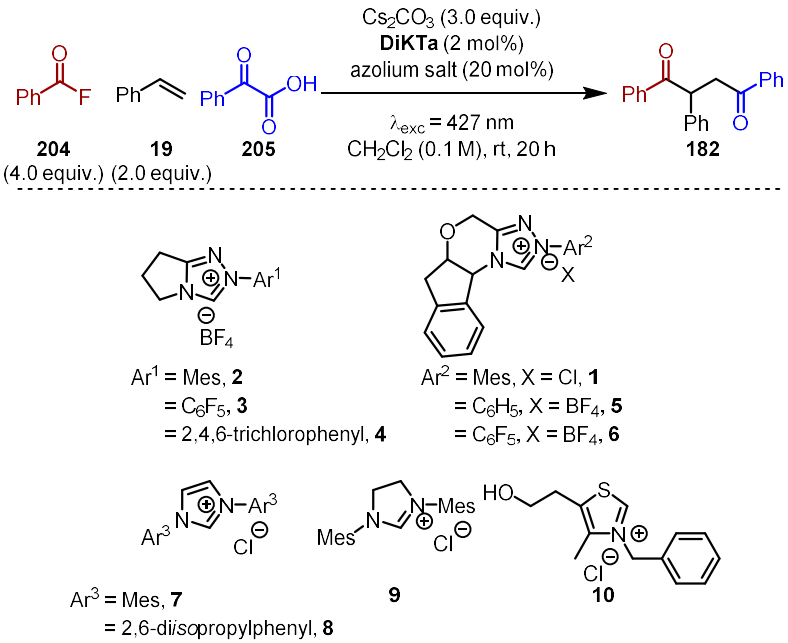

Entry[a]	Azolium Salt	Yield / %[b]
1	**2**	46
2	**3**	Trace
3	**4**	27
4	**1**	50
5	**5**	7
6	**6**	Trace
7	**7**	17
8	**8**	6
9	**9**	Trace
10	**10**	Trace

[a] Benzoyl fluoride (**204**) (0.4 mmol), styrene (**19**) (0.2 mmol), phenylglyoxylic acid (**205**) (0.1 mmol), Cs_2CO_3 (0.3 mmol), azolium salt (20 mol%), **DiKTa** (2 mol%), CH_2Cl_2 (1 mL), irradiation with 427 nm LED, rt. [b] Yield determined by ^1H NMR, using 1,3,5-trimethoxybenzene as internal standard.

To assist with the optimization, an investigation into the undesired side-products was conducted. Through GCMS analysis of the crude reaction mixture it was discovered that the major side-product was the diketone product **206** (Scheme 4.9). This is assumed to be formed through the dimerization of radical intermediate **207** after the initial addition of acyl radical **208** to styrene **19**. This issue has been observed by others in similar catalytic systems previously, such as in Wang and co-workers[163]

work on the sulfonylacylation of 1,3-enynes. Other side-products included chalcone **181** and dihydro chalcone **208**. Chalcone is presumably also formed from **207** but instead of dimerization, a subsequent single electron oxidation and deprotonation occurs. Similarly, dihydrochalcone likely also derives from **207** but has abstracted a hydrogen atom from somewhere in the reaction mixture.

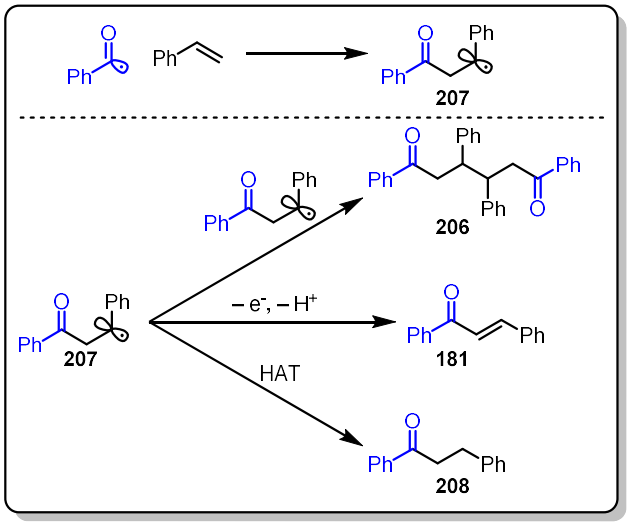

Scheme 4.9 Formation of side-products from **207**.

Another side-product that is formed is esterified benzoin **210**. Benzoin esters are known to form during the synthesis of benzoin if the flask is left open to the air under NHC catalysis (Scheme 4.10).[168] The proposed mechanism for this process is the reaction of the NHC catalyst with an aldehyde **41** to form the Breslow intermediate **183** via the adduct **180**. **183** then nucleophilically adds to another molecule of **41** to form the benzoin product **211** via adduct **212**. In the presence of air, benzoin is oxidised to the corresponding benzil **213**, which in turn oxidises another molecule of **180** to form the acyl azolium **214** and regenerate benzoin. Finally, Benzoin is esterified by **214** to form **210**. The reaction conditions optimized in this work for the synthesis of 1,4-diketones do not include any aldehydes, nor is it open to air. However, benzaldehyde could be formed from the acyl radicals generated by the decarboxylation of **205** through HAT; air would no longer be required to form the

acyl azolium as it would be formed via the addition of the NHC to **204**. Therefore, the same mechanism is likely in operation.

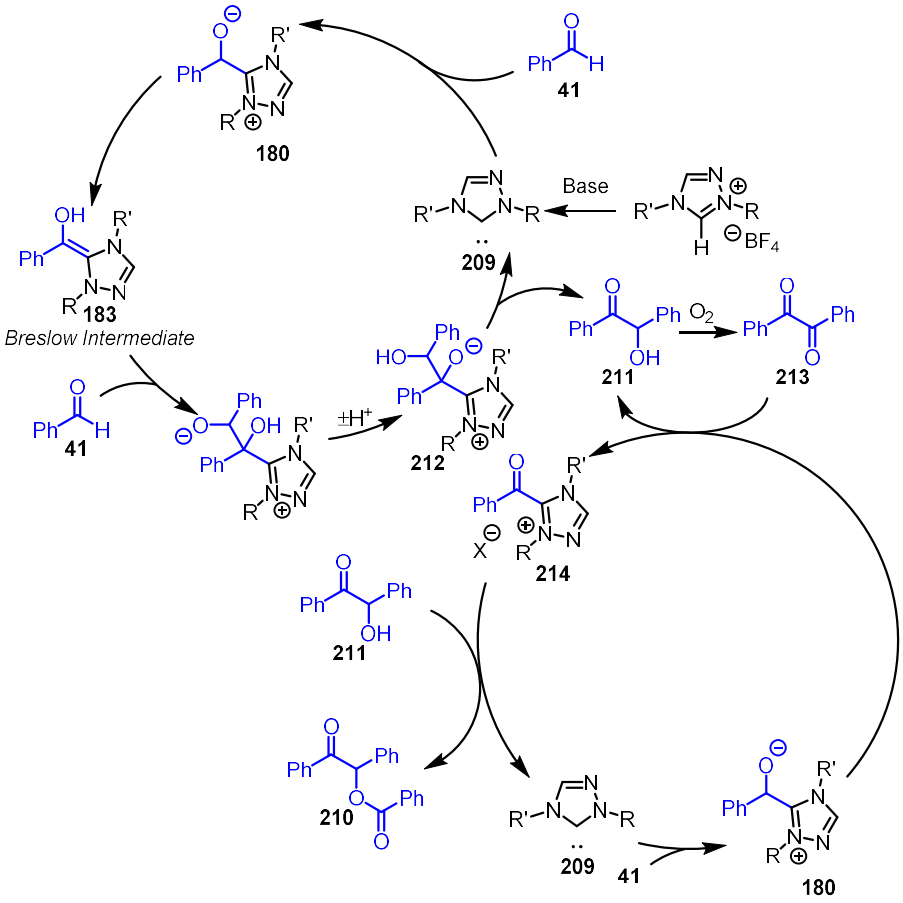

Scheme 4.10 Proposed mechanism for the formation of benzoin esters.

The key parameter Wang and co-workers[163] found that limited the formation of these undesired dimers was the concentration of the reaction, with dilution disfavouring dimerization. Therefore, the effect of different concentrations was investigated (Table 4.4). The initial concentration of 0.1 M generates **182** in a 50% yield (Table 4.4, entry 1). Unsurprisingly, increasing the concentration to 0.2 M resulted in a reduced yield of 35% (Table 4.4, entry 2). However, dilution to 0.05 M and even 0.025 M also gave reduced yields of 30% and 33%, respectively (Table 4.4, entries 3-4). Therefore, the concentration was maintained at 0.1 M for further optimization.

Table 4.4 Concentration Optimization.

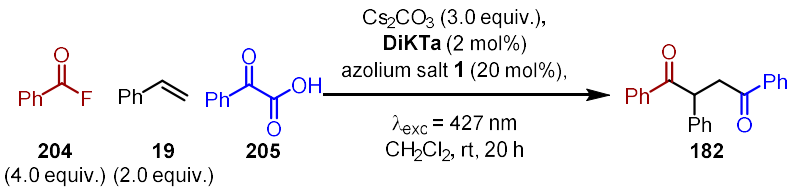

Entry[a]	Concentration / M	Yield / %[b]
1	0.1	50
2	0.2	35
3	0.05	30
4	0.025	33

[a] Benzoyl fluoride (**204**) (0.4 mmol), styrene (**19**) (0.2 mmol), phenylglyoxylic acid (**205**) (0.1 mmol), Cs_2CO_3 (0.3 mmol), azolium salt **1** (20 mol%), **DiKTa** (2 mol%), CH_2Cl_2, irradiation with 427 nm LED, rt. [b] Yield determined by ^1H NMR, using 1,3,5-trimethoxybenzene as internal standard.

Considering the change that has yielded the largest improvement thus far was the changes to the ratio of starting materials, this was revisited to investigate whether further improvements could be made (Table 4.5). The current ratio of reagents (4:2:1:3, **204**:**19**:**205**:Cs_2CO_3) could achieve a 50% NMR yield (Table 4.5, entry 1). First, the requirement of such an excess of base was investigated by lowering the equivalents of Cs_2CO_3 to 1.5 equivalents, which produced a near identical result of 49% (Table 4.5, entry 2). This was repeated for the excess of styrene by lowering the equivalents to 1.5, which again gave a similar result of 48% (Table 4.5, entry 3). However, further reduction in the amount of styrene to 1.0 equivalents was not well tolerated with a 33% yield observed (Table 4.5, entry 4). Interestingly, using a ratio of 4:1:1.5:2 gave an improved yield of 61% (Table 4.5, entry 5). Therefore, this ratio of reagents was carried forward to the next stage of optimization.

Table 4.5 Starting Material Ratio Optimization.

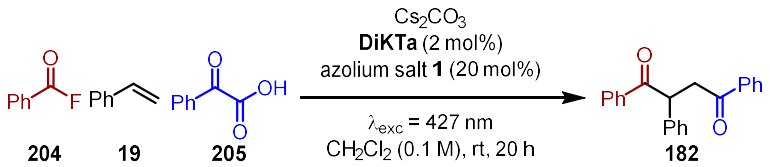

Entry[a]	Styrene Equiv.	Acid Equiv.	Cs_2CO_3 equiv.	Yield / %[b]
1	2	1	3	50
2	2	1	1.5	49
3	1.5	1	1.5	48
4	1	1	1.5	33
5	1	1.5	2	61

[a] Benzoyl fluoride (**204**) (0.4 mmol), styrene (**19**), phenylglyoxylic acid (**205**), Cs_2CO_3, azolium salt **1** (20 mol%), **DiKTa** (2 mol%), CH_2Cl_2 (1 mL), irradiation with 427 nm LED, rt. [b] Yield determined by ^1H NMR, using 1,3,5-trimethoxybenzene as internal standard.

Next, the effects of changing the solvent were explored (Table 4.6). Dichloromethane has been used throughout the optimization and achieved a 61% NMR yield (Table 4.6, entry 1). Acetonitrile and DMF were tested as examples of more polar solvents and they gave similar yields of 48% and 51%, respectively (Table 4.6, entries 2-3). Toluene produced **182** in a 54% yield (Table 4.6, entry 4), suggesting solvent polarity does not play a significant role in this reaction, which could be due to the small solvatochromism of **DiKTa**. However, THF resulted in a reduced yield of 33% (Table 4.6, entry 5). Considering there seemed to be little variation in yield depending on solvent, the use of dichloromethane was taken on as optimal.

Table 4.6 Solvent Optimization.

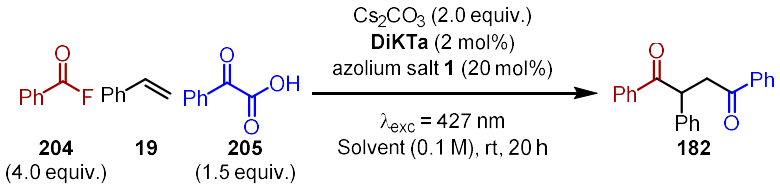

Entry[a]	Solvent	Yield / %[b]
1	CH_2Cl_2	61
2	MeCN	48
3	DMF	51
4	Toluene	54
5	THF	33

[a] Benzoyl fluoride (**204**) (0.4 mmol), styrene (**19**) (0.1 mmol), phenylglyoxylic acid (**205**) (0.15 mmol), Cs_2CO_3 (0.2 mmol), azolium salt **1** (20 mol%), **DiKTa** (2 mol%), CH_2Cl_2, irradiation with 427 nm LED, rt. [b] Yield determined by ^{1}H NMR, using 1,3,5-trimethoxybenzene as internal standard.

Cs_2CO_3 is the most commonly used base in other similar reactions, which is why it was chosen for initial testing. Since organic bases such as DIPEA, DBU or triethylamine are known to quench photocatalysts as they are potent sacrificial electron donors, only inorganic bases were considered in this study (Table 4.7). While using Cs_2CO_3 achieved a yield of 61% (Table 4.7, entry 1); variation to K_2CO_3 and Na_2CO_3 resulted in significantly lower yields of 30% and 16%, respectively (Table 4.7, entries 2-3). This is perhaps due to the weaker basicity of these compounds and indeed $NaHCO_3$, an even weaker base, only produced **182** in a yield of 8% (Table 4.7, entry 4). Since the strongest base at this point was superior, *t*-BuOK was tried; however, this also resulted in a low yield of only 22% (Table 4.7, entry 5). It seems the efficiency of this reaction is particularly sensitive to the base used, so Cs_2CO_3 remained the optimal base.

Table 4.7 Base Optimization.

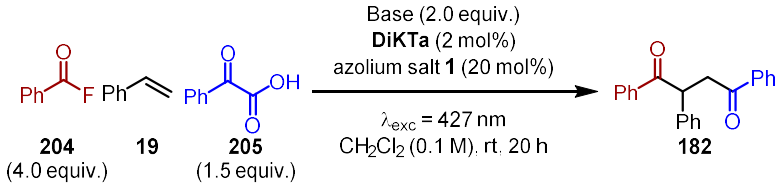

Entry[a]	Solvent	Yield / %[b]
1	Cs_2CO_3	61
2	K_2CO_3	30
3	Na_2CO_3	16
4	$NaHCO_3$	8
5	*t*-BuOK	22

[a] Benzoyl fluoride (**204**) (0.4 mmol), styrene (**19**) (0.1 mmol), phenylglyoxylic acid (**205**) (0.15 mmol), Base (0.2 mmol), azolium salt **1** (20 mol%), **DiKTa** (2 mol%), CH_2Cl_2, irradiation with 427 nm LED, rt. [b] Yield determined by ^{1}H NMR, using 1,3,5-trimethoxybenzene as internal standard.

There are two types of acylating reagents that are typically used in this type of catalytic system; aroyl fluorides[77] **204** and aroyl imidazoles[75] **215** (Table 4.8). To investigate the effect of the leaving group in this reaction benzoyl imidazole **215** was synthesised and tested. However, despite a 61% NMR yield being observed for benzoyl fluoride (Table 4.8, entry 1), no product was observed when using **215** (Table 4.8, entry 2). Interestingly, benzoic anhydride **216**, which is not typically used in NHC/photoredox catalysis, gave a moderate yield of 26% (Table 4.8, entry 3). Finally, aroyl chlorides **217** were investigated as the acylating agent, which would be convenient as aroyl fluorides are synthesised from aroyl chlorides. However, when using benzoyl chloride only traces of **182** were observed, which is consistent with observations made by others (Table 4.8, entry 4).[75] The lack of reactivity with **215** is unusual and was postulated to be due to poor reactivity with azolium salt **1**. Interestingly, when azolium salt **2** was used, much less variation was observed when using benzoyl fluoride, **215**, or benzoic anhydride as they produced **182** in 42%, 46%, and 39% yield, respectively (Table 4.8, entries 5-7). Therefore, the dependence on the acylating agent is itself dependant on the azolium salt used. However, the best result was still the 61% achieved when using azolium salt **1** with benzoyl fluoride so this remained the optimal conditions.

Table 4.8 Acyl Leaving Group Optimization.

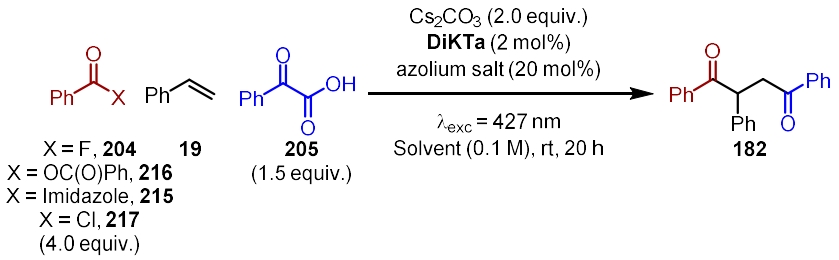

Entry[a]	Leaving Group	Azolium Salt	Yield / %[b]
1	Fluoride	**1**	61
2	Imidazole	**1**	0
3	OC(O)Ph	**1**	26
4	Chloride	**1**	Trace
5	Fluoride	**2**	42
6	Imidazole	**2**	39
7	OC(O)Ph	**2**	46

[a] Benzoyl X (0.4 mmol), styrene (**19**) (0.1 mmol), phenylglyoxylic acid (**205**) (0.15 mmol), Cs_2CO_3 (0.2 mmol), azolium salt (20 mol%), **DiKTa** (2 mol%), CH_2Cl_2, irradiation with 427 nm LED, rt. [b] Yield determined by ^1H NMR, using 1,3,5-trimethoxybenzene as internal standard.

Considering many changes had been made without any improvements to product yield, at this point control reactions were investigated (Table 4.9). With no change, an NMR yield of 61% is observed (Table 4.9, entry 1). If the PC is excluded, a trace amount of the product is observed along with a complex mixture of various other unwanted products (Table 4.9, entry 2). An explanation for this background reactivity could be due to the direct excitation of **205**,[169] or some NHC-based intermediates.[157] Similarly, if no azolium salt is added then no product formation is observed but there is a mixture of undesired products due to significant background reactivity (Table 4.9, entry 3). Considering the aryl groups used on both **204** and **205** are the same, it is feasible that one is not actually required as in the reaction reported by Wu and co-workers.[159] However, in the absence of benzoyl fluoride, trace amounts of **182** are formed (Table 4.9, entry 4). Similarly, if **205** is excluded then none of the desired product is detected (Table 4.9, entry 5). Next, the requirement of the base was investigated and as expected, if no Cs_2CO_3 is added then only trace amounts of **182** are formed (Table 4.9, entry 6). Finally, the impact of changing the wavelength of light used was explored. Using

a different wavelength (λ_{exc} = 456 nm) gave a slightly lower yield of 48% (Table 4.9, entry 7), while the use of no light resulted in no reactivity, including the previously observed background reactivity (Table 4.9, entry 8).

Table 4.9 Control Reactions.

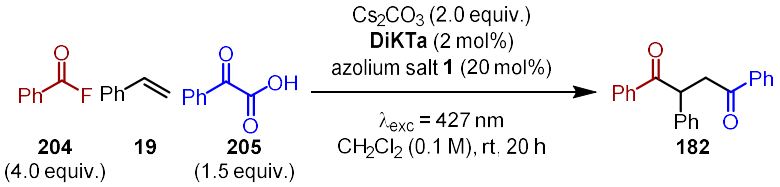

Entry[a]	Variation	Yield / %[b]
1	None	61
2	No **DiKTa**	Trace
3	No azolium salt	0
4	No **204**	Trace
5	No **205**	0
6	No Cs_2CO_3	Trace
7	λ_{exc} = 456 nm	48
8	No Light	0

[a] Benzoyl fluoride (**204**) (0.4 mmol), styrene (**19**) (0.1 mmol), phenylglyoxylic acid (**205**) (0.15 mmol), Cs_2CO_3 (0.2 mmol), azolium salt **1** (20 mol%), **DiKTa** (2 mol%), CH_2Cl_2, irradiation with 427 nm LED, rt. [b] Yield determined by ^{1}H NMR, using 1,3,5-trimethoxybenzene as internal standard.

Considering the optimal azolium salt for this reaction is chiral and typically used in enantioselective NHC catalysis,[167] the enantioselectivity of this reaction was explored using a single enantiomer of azolium salt **1** (Scheme 4.11). However, as with all other reactions that use this type of NHC/photoredox catalysis, no enantioselectivity was observed with only racemic product generated.

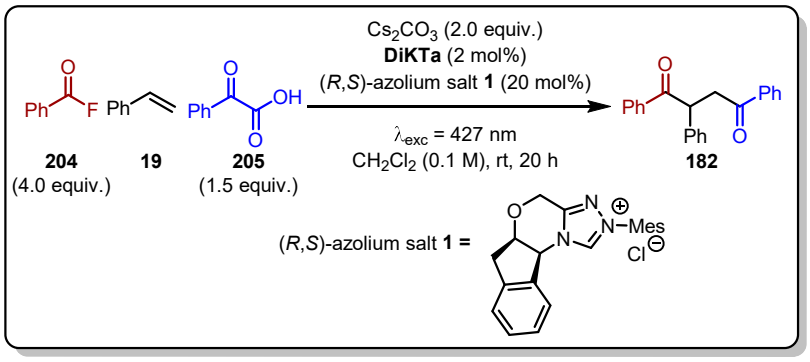

Scheme 4.11 Synthesis of 1,4-diketones using single enantiomer of the azolium salt.

4.2.2 Reaction Scope

With the optimized conditions in hand, the scope and limitations of this NHC/photoredox dual catalysed synthesis of 1,4-diketones was developed. Using benzoyl fluoride **204** and phenylglyoxylic acid **205** a variety of terminal alkene derivatives were explored in this process (Scheme 4.12). Incorporation of halogenated (*para*-Br, *para*-F) as well as electron-withdrawing (*para*-CF_3) substituents within the styrene component were tolerated, giving the desired 1,4-diketones in 42-46% yield **218**-**220**. Incorporation of the heteroaromatic 2-vinyl pyridine variant produced comparable yield of product **221**. The incorporation of alkyl substituents at the *para* position were well tolerated **222**-**224**, while *ortho* (to give **225**) or electron-donating (*para*-MeO, **226**) substituents delivered the 1,4-diketone in lower yields. However, **226** could be obtained in an improved 58% yield when using $[Ir(ppy)_2(dtbbpy)](PF_6)$ as the PC and modifying reaction stoichiometries.[166]

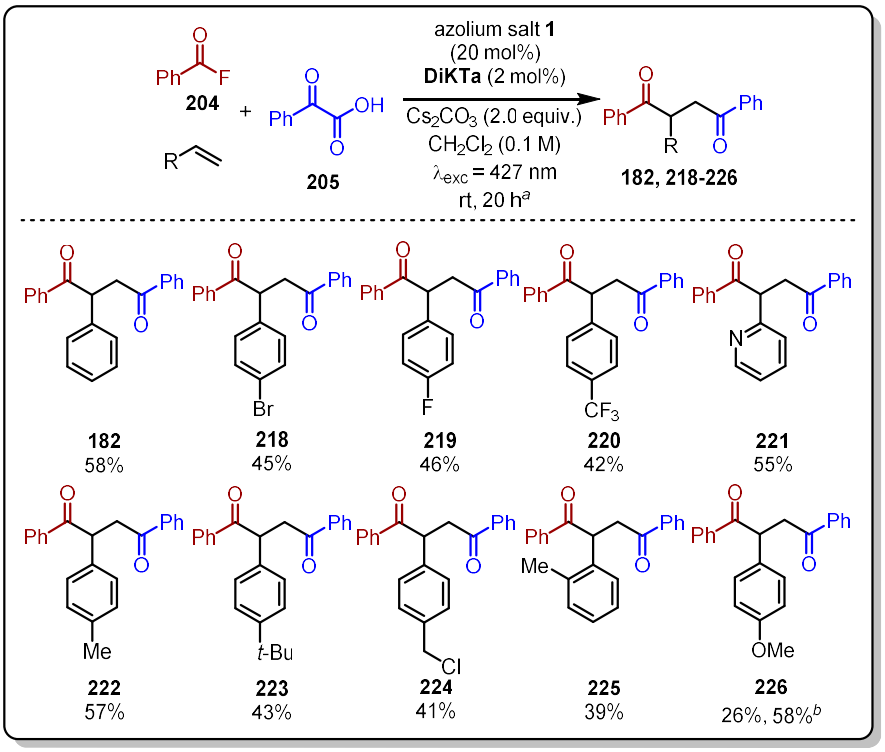

Scheme 4.12 Alkene scope. [a]All reactions performed using **204** (0.40 mmol), **205** (0.15 mmol) and an alkene (0.10 mmol). [b]Conditions: **204** (0.40 mmol), alkene (0.20 mmol), **205** (0.40 mmol), $[Ir(ppy)_2(dtbbpy)](PF_6)$ (1.5 mol%), azolium salt **1** (15 mol%), toluene (0.05 M), rt, (λ_{exc} = 456 nm), 20 h.

Substrates that proved unsuccessful under the developed conditions included α- and ß-methyl styrene, 2-vinylthiophene, oct-1-ene and 4-vinylpyridine that would have given products **227**-**232**, respectively (Figure 4.1). α- and ß-methyl styrene gave NMR yields of < 10% product and likely did not work due to increased steric congestion. However, while indene gave a moderate NMR yield of 33%, the desired product was inseparable from the corresponding dimerization side-product. The use of oct-1-ene gave a complex mixture with only traces of what is assumed to be the desired product; this was expected as unactivated alkenes are known to be more challenging for the radical-radical coupling step with the NHC-stabilised radical intermediate.[77] 2-Vinylthiophene and 4-vinylpyridine gave only moderate product conversion, with significantly reduced isolated product yields of 13% and 17%, respectively.

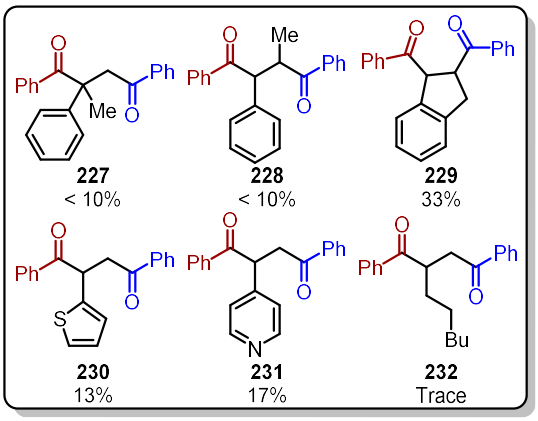

Figure 4.1 Unsuccessful alkene substrates.

With the alkene scope established, attention turned to variation of the benzoyl fluoride component and the synthesis of unsymmetric 1,4-diketones (Scheme 4.13). In each case ~5 % of the symmetrical 1,4-diketone product **182** was also observed, likely formed through the same process as reported by Wu and co-workers.[159] Trace amounts of the corresponding 1,2-dione, where effectively the styrene component has been excluded, were also detected. All aroyl fluorides were synthesised from the corresponding aroyl chloride using potassium fluoride and 18-crown-6.[170] Larger π-systems such as biphenyl **233** and 2-naphthyl **234** were well tolerated, although lower yields resulted from the use of 1-naphthyl **235**, perhaps due to increased steric congestion. *para*-Fluoro- **236** and *para*-chloro- **237** substituted benzoyl fluorides worked well; although, *para*-bromo **238** and *para*-iodo **239** derivatives gave reduced product yield. However, **238** and **239** could be obtained in improved yields using alternative conditions with $[Ir(ppy)_2(dtbbpy)](PF_6)$ as the PC.[166] Pleasingly, electron-donating groups such as *para*-methoxy **240** and *para*-*t*-Bu **241** gave good yields of the corresponding unsymmetric 1,4-diketones.

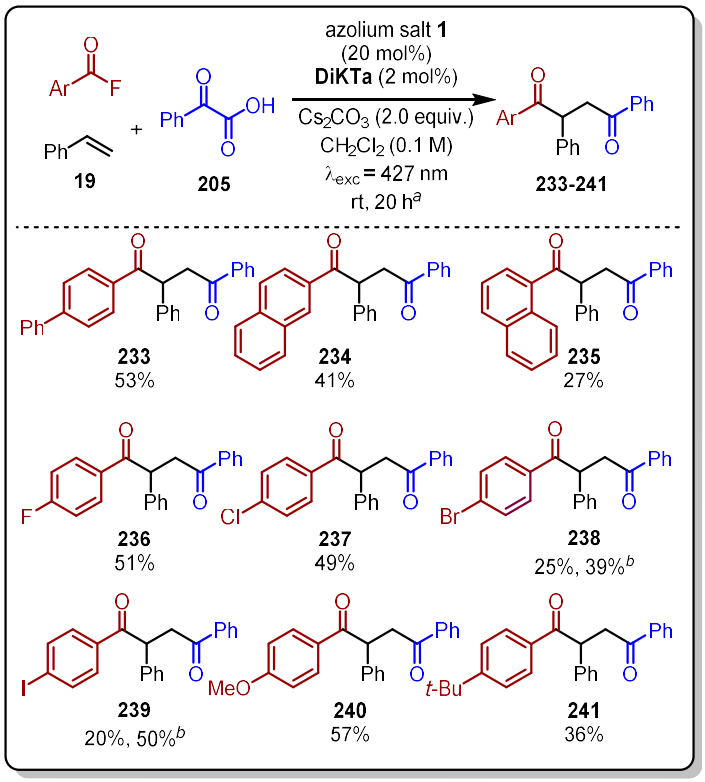

Scheme 4.13 Aroyl fluoride scope. [a]All reactions performed using aroyl fluoride (0.40 mmol), **205** (0.15 mmol) and **19** (0.10 mmol). [b]Conditions: aroyl fluoride (0.60 mmol), **19** (0.20 mmol), **205** (0.60 mmol), $[Ir(ppy)_2(dtbbpy)](PF_6)$ (1.5 mol%), azolium salt **1** (15 mol%), toluene (0.05 M), rt, (λ_{exc} = 456 nm), 20 h.

Unsuccessful substrates for the benzoyl fluoride component included *para*-cyanobenzoyl fluoride and cyclohexane carbonyl fluoride that would have given 1,4-diones **242** and **243**, respectively (Figure 4.2). When using *para*-cyanobenzoyl fluoride only traces of **242** were detected by GCMS and the dominant product was the dimerization product **206**; it is not clear why this is favoured in this case. When using cyclohexanecarbonyl fluoride only traces of **243** were detected by GCMS, with the dominant product again being **206**; this is consistent with the use of alkyl acyl fluorides that are known to be more challenging in this type of catalytic system.

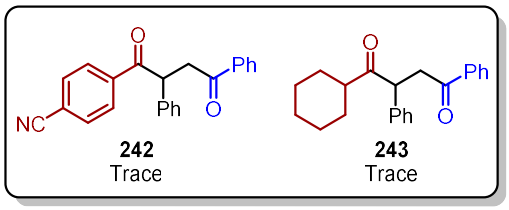

Figure 4.2 Unsuccessful aroyl fluorides.

Given these promising results in terms of the breadth of both the alkene and benzoyl fluoride components, the scope of possible α-ketoacids was evaluated next. Aryl α-ketoacids were synthesised from the corresponding acetophenone using selenium dioxide in pyridine (Scheme 4.14).[171] However, α-ketoacid **244** was synthesised via Grignard addition to dimethyl oxalate and subsequent hydrolysis.

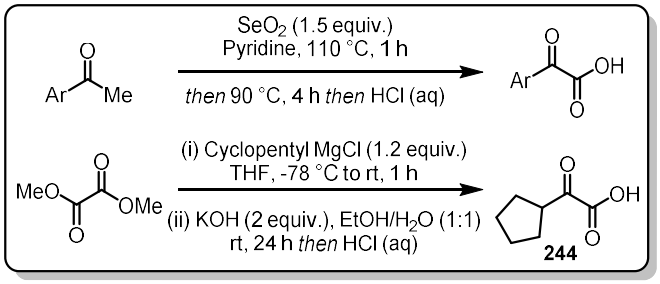

Scheme 4.14 Different methods used for the synthesis of α-ketoacids.

Surprisingly, even seemingly small changes to the structure of the α-ketoacid such as the addition of a *para*-methyl substituent gave significantly lower yields of the corresponding 1,4-dione **245** (Scheme 4.15). This also proved to be the case for other substituents such as *para*-bromo, *para*-methoxy, *para*-fluoro and *para*-trifluoromethyl **246**-**249**. However, when using the alternative catalytic conditions with $[Ir(ppy)_2(dtbbpy)](PF_6)$ as the PC, the yields for each of these substrates could be improved. Pleasingly, the use of pyruvic acid under standard conditions gave the corresponding 1,4-diketone **250** in a moderate product yield and the use of alkyl α-keto acids could be extended to **244** with the use of 2-vinyl pyridine to give the corresponding 1,4-diketone **251**. However, if a tertiary alkyl group is used such as in **252**, decarbonylation as well as decarboxylation occurs to produce *tert*-butyl radicals, so the only product observed was ketone **252**. This behaviour has previously been observed by others.[166]

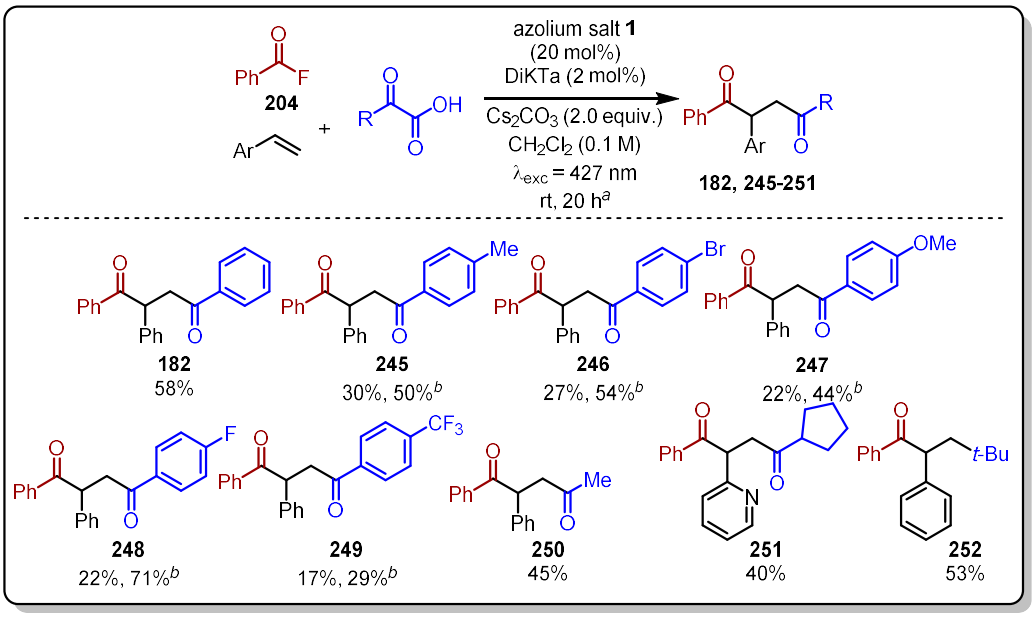

Scheme 4.15 α-Ketoacid scope. [a]All reactions performed using **204** (0.40 mmol), α-ketoacid (0.15 mmol) and an alkene (0.10 mmol). [b]Conditions: **204** (0.60 mmol), **19** (0.20 mmol), α-ketoacid (0.60 mmol), $[Ir(ppy)_2(dtbbpy)](PF_6)$ (1.5 mol%), azolium salt **1** (15 mol%), toluene (0.05 M), rt, (λ_{exc} = 456 nm), 20 h.

4.2.3 Mechanistic Investigations

At the outset of this investigation a mechanism was proposed based on previous NHC/photoredox catalysed reactions. To support this mechanistic proposal, Stern-Volmer quenching studies of benzoyl fluoride **204**, styrene **19** and phenylglyoxylic acid **205** were undertaken (Figure 4.3). These studies revealed that quenching occurs in the presence of **205** but not in the presence of **204** or **9**.

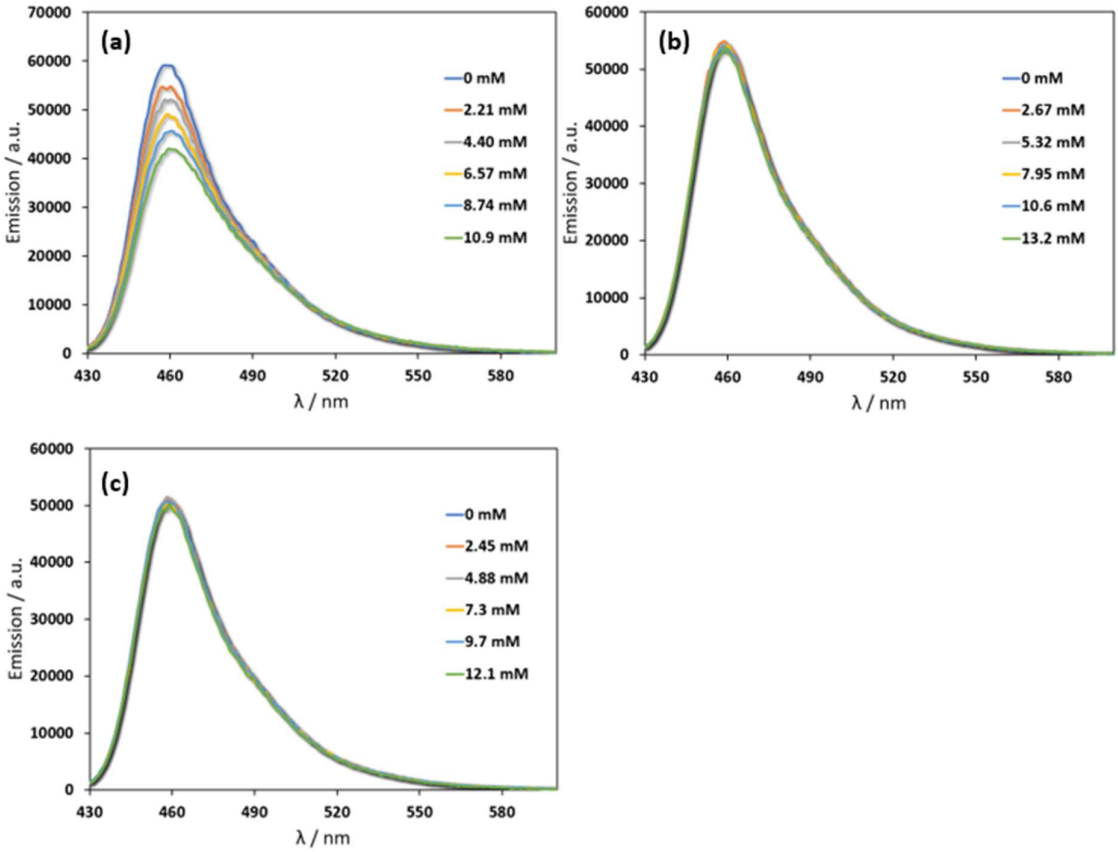

Figure 4.3 Emission quenching data of **DiKTa** by sequential addition of (a) phenyl glyoxylic acid (b) benzoyl fluoride (c) styrene in CH_2Cl_2 under air. λ_{exc} = 410 nm.

If the change in fluorescence intensity (I/I_0) is plotted against the concentration of the quencher ([Q]), using the Stern-Volmer relationship, a straight line is observed with a y-intercept of 1 and a gradient equal to the Stern-Volmer constant (K_{SV}). To obtain a quenching constant (k_q) the lifetime (τ_{PL}) of **DiKTa** was measured in the reaction solvent (CH_2Cl_2) using time-resolved photoluminescence spectroscopy and was found to be 5.6 ns (Figure 4.4a). Finally, k_q for **205** could be obtained by dividing K_{SV} by τ_{PL} to give a quenching constant of 3.8×10^9 M^{-1} s^{-1}. However, it is worth noting that these measurements were carried out under air and the reaction is not, so any contribution from the triplet state is likely lost through oxygen quenching. While these investigations support the plausibility of the proposed mechanism, they do not rule out the possibility of an alternative oxidative quenching mechanism with the acyl azolium intermediate.

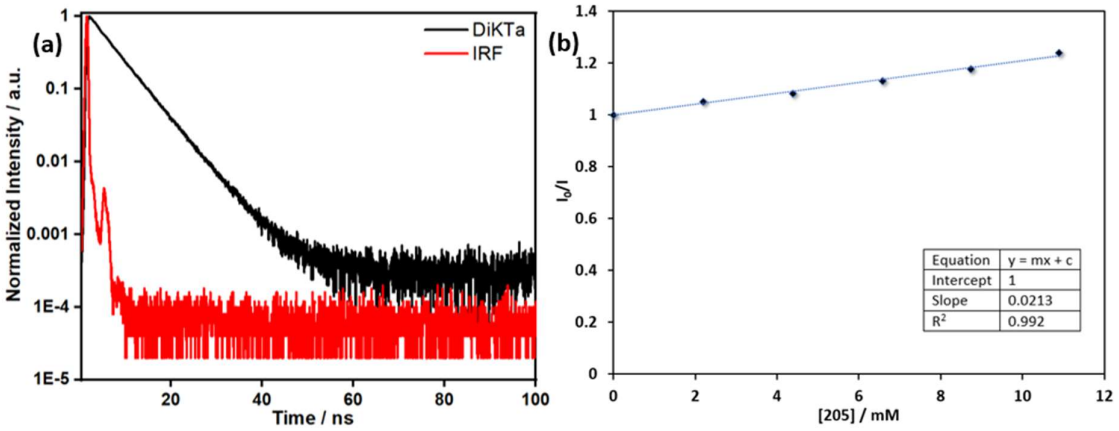

Figure 4.4 (a) Time resolved PL decay of **DiKTa** recorded in CH_2Cl_2 under air in 10^{-5} M solutions with λ_{exc} = 375 nm. (b) Stern-Volmer plot of the quenching of the emission of **DiKTa** in CH_2Cl_2 by sequential addition of phenylglyoxylic acid.

4.3 Conclusions

We have developed a modular synthetic route to unsymmetric 1,4-diketones through the combination of benzoyl fluorides, styrenes and α-keto acids catalysed by a dual catalytic NHC/photoredox system using the MR-TADF organophotocatalyst **DiKTa**.[22] During the development of this system Zhang and co-workers published a similar methodology requiring an iridium-containing PC.[20] Certain substrates performed better under their conditions, although most 1,4-diones were obtained in comparable yields using the metal-free conditions described herein.

Future work in this area can be separated into two separate objectives. The first of these objectives should involve the expansion of the use of **DiKTa** and perhaps other MR-TADF compounds in different types of dual catalysis to apply the benefits of MR-TADF photocatalysis to these areas. The second objective would focus on the further development of NHC/photoredox catalysis, either through the expansion of the scope through the use of different radical precursors, or through the exploration of different NHC-based intermediates and their interactions with photocatalysis. To expand the scope, a departure from carbon-centred radicals would be of particular interest to include heteroatoms such as phosphorous or nitrogen (Scheme 4.15).

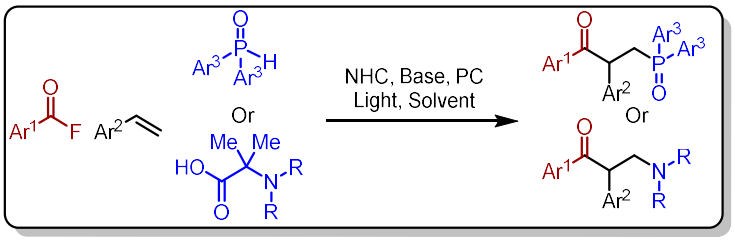

Scheme 4.16 Proposed reactions using nitrogen and phosphorous radicals in dual NHC/photoredox catalysis.

An alternative avenue of research could include the single electron oxidation of acyl azolium enolates to afford the corresponding α-carbonyl radical intermediate, which in turn could undergo radical-radical coupling reactions or radical additions to alkenes, for example (Scheme 4.16).

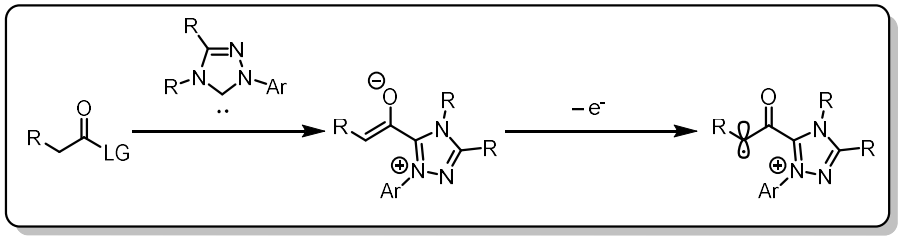

Scheme 4.17 Proposed single electron oxidation of acyl azolium enolates to generate α-carbonyl radical intermediates.

Additionally, α.ß-unsaturated acyl azoliums could be used in RCA reactions in a similar manner to ITUs in chapter 2 but with fewer issues involving decomposition of the co-catalyst (Scheme 4.17).

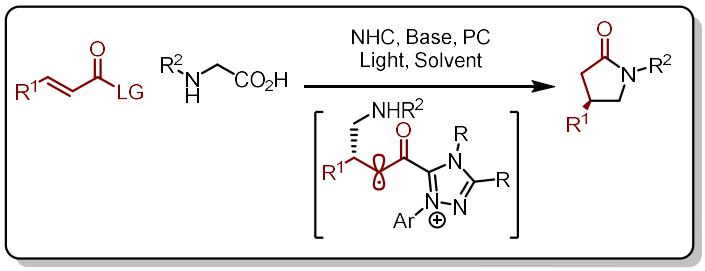

Scheme 4.18 Proposed NHC/photoredox catalysis for the synthesis of γ-lactams.

5 Photocatalytic Synthesis and Functionalization of Cubane.

5.1 Introduction

Cubane was first theorised to exist by Thorpe and Beesley[172] over 100 years ago and consists of eight nominally sp^3-hybridized carbon atoms bonded together to produce a highly strained cubic structure.[173] Cubane is not only interesting because of its peculiarity as a hydrocarbon Platonic solid, but it is also a useful bioisostere for the benzene ring due to its similar size and shape (Figure 5.1a).[174–176] Therefore, the 1,4-substitution pattern of a cubane molecule could replace a *para*-substituted phenyl ring in a molecule and potentially offer improved properties including a departure from "flat-land".[177] This hypothesis was confirmed by Williams and co-workers[174] through the synthesis of cubane variants of a range of pharmaceutical and agrochemical compounds such as leteprinim, benzocaine and diflubenzuron (Figure 5.1b). Furthermore, there are other uses for cubane and its derivatives such as its ability to rearrange into cunenes,[178] its utilization in explosives[179] and its incorporation into polymers.[180]

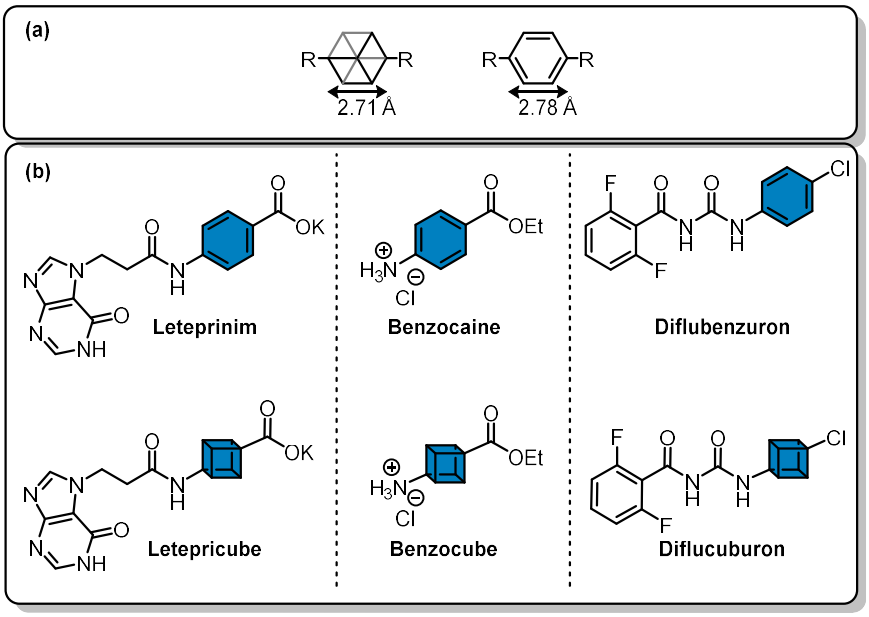

Figure 5.1 (a) Body diagonals of cubane and benzene. (b) Selected examples of cubane as a benzene bioisostere.

The first successful synthesis of cubane was accomplished by Eaton and Cole[181] to give dimethyl cubane-1,4-dicarboxylate **253** in 8 steps with a 12% overall yield from cyclopentenone. Subsequent

routes by Chapman (route I)[182] and Tsanaktsidis (route II)[183] allowed for cyclopentanone to be used as starting material at comparable synthetic efficiency and overall yield (Scheme 5.1 and Scheme 5.2). Further optimizations of Tsanaktsidis's route by Collin and co-workers allowed for the synthesis of decagram quantities of **253** in overall yields of between 33-40%.[184] The synthesis begins with the ketal protection of cyclopentanone under acidic conditions. Subsequent tribromination, elimination and dimerization generates the bisethylene ketal **254** (Scheme 5.1).

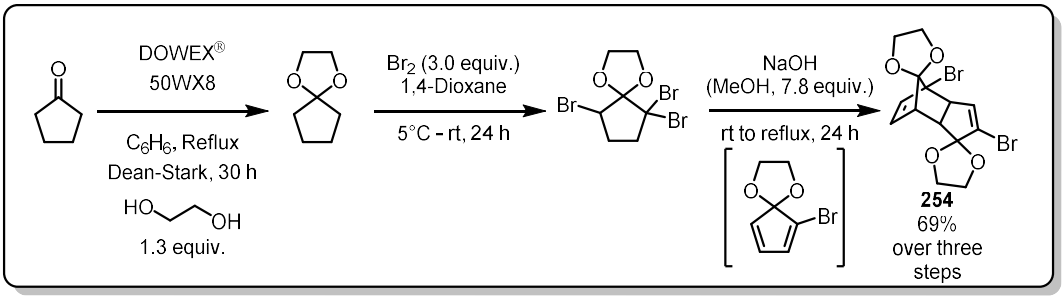

Scheme 5.1 Synthetic route to bisethylene ketal **254** used by Collin and co-workers.[184]

At this point the two routes diverge, with route I opting to perform a mono-deprotection with HCl in THF to give monoketal **255**, while route II uses neat H_2SO_4 to deprotect both ketals to give the diketone **256** (Scheme 5.2). Both **255** and **256** can undergo a photochemical [2+2] cycloaddition using Hg lamps or UV-B irradiation (λ_{exc} = 311 nm) to the corresponding products **257** and **258**, respectively. To transform **257** into **258** a second deprotection is required making route I slightly longer than route II.

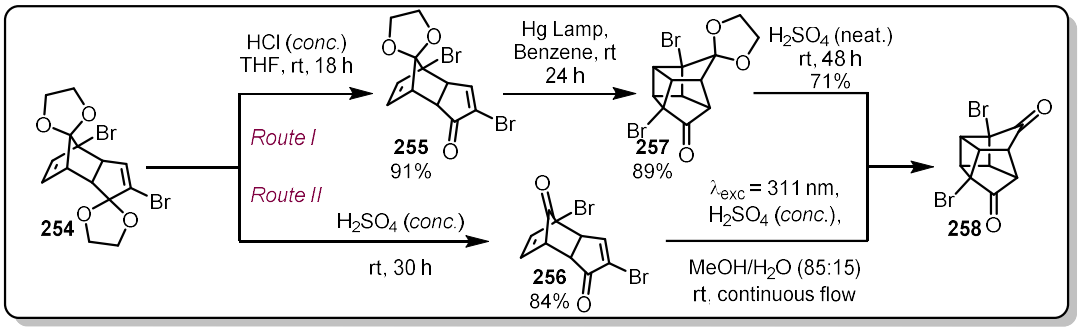

Scheme 5.2 Two synthetic routes to cubane precursor **258**. The conditions shown for route I are those reported by Chapman and co-workers[182] while route II uses conditions reported by Collin and co-workers.[184]

Compound **258** exists in an equilibrium with the corresponding monohydrate **258a** and dihydrate **258b** but to simplify things throughout this section this mixture will be referred to as **258** (Scheme 5.3). To complicate things further, route II requires an acidic methanol solution to make **258** so there are also

methyl ketals present. Therefore, route II requires an initial water hydrolysis of these methyl ketals before moving on to the cubane-forming step. Finally, a Favorskii rearrangement generates 1,4-cubane dicarboxylic acid and a subsequent esterification gives the diester **253**, which is easily purified by column chromatography.

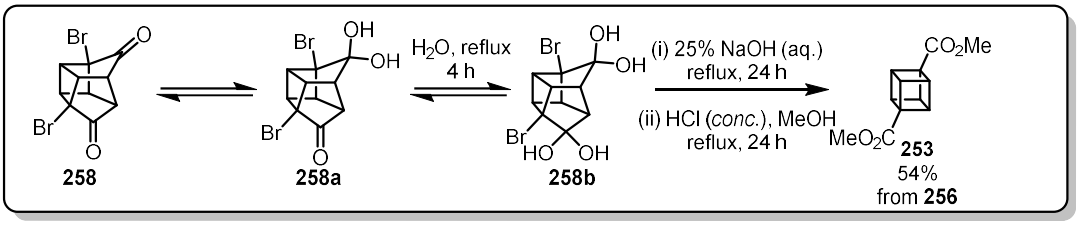

Scheme 5.3 Synthesis of 1,4-dimethylcubane dicarboxylate as reported by Collin and co-workers.[184]

While these synthetic routes have been refined over decades and can now be scaled-up to produce large quantities of **253** using flow chemistry,[184] the key [2+2] cycloaddition step still requires the use of UV-B lamps and uncommon glassware. With this in mind, we set out to identify and optimize alternative conditions that would allow for lower energy light to be used. Two different strategies to achieve this were considered: the use of Lewis acid coordination to **256** to bathochromically shift the absorption into the visible region where it could be directly photoexcited (Scheme 5.4a), or the use of an appropriate photosensitiser to generate the same excited state intermediate required but via DET instead of direct photoexcitation (Scheme 5.4b).

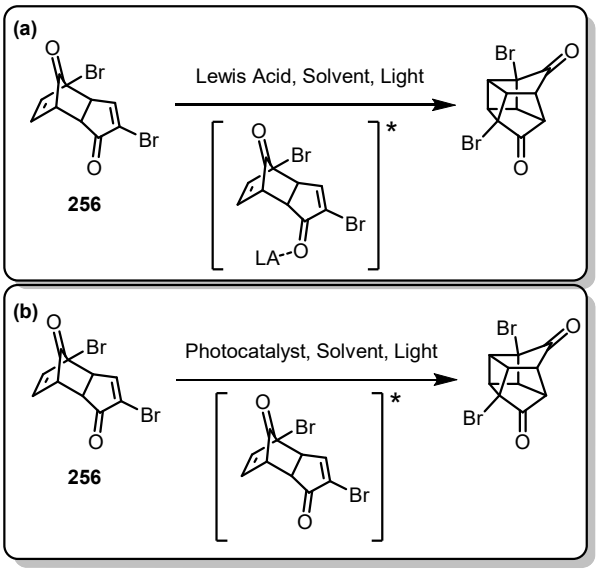

Scheme 5.4 Idea for the photochemical [2+2] cycloaddition of **256** using (a) a Lewis acid catalyst (b) a photocatalyst.

5.2 Results and Discussion

5.2.1 Synthesis of Starting Materials and Lewis Acid Testing

Investigations began with the synthesis of both **255** and **256**,[182,184] to allow for flexibility between these starting materials depending on which proved to be more synthetically viable. Initial exploration of the photochemical [2+2] cycloaddition focused on the use of Lewis acids to shift the absorption spectra of **256** closer to the visible region. This has been demonstrated previously for simpler α,ß-unsaturated ketones by Bach and coworkers[185] using oxazaborolidine-based catalysts for enantioselective reactions and boron trichloride in the racemic version, which achieved bathochromic shifts of nearly 70 nm. To test if this was possible for **256**, UV-vis absorption spectra were obtained in the presence and absence of BCl_3 (Figure 5.2). Without BCl_3, **256** shows a band with a λ_{abs} of 250 nm. Pleasingly, in the presence of BCl_3 a new band appears at λ_{abs} of 300 nm with a tail into the visible region. However, attempts at direct photoexcitation of **256** in the presence of boron trichloride with a 370 nm LED showed no reactivity and only returned unreacted starting material. Therefore, even though the Lewis acid shifts the absorption of **256** as hypothesised, this strategy did not prove productive, and investigation turned to the use of a photocatalytic DET reaction.

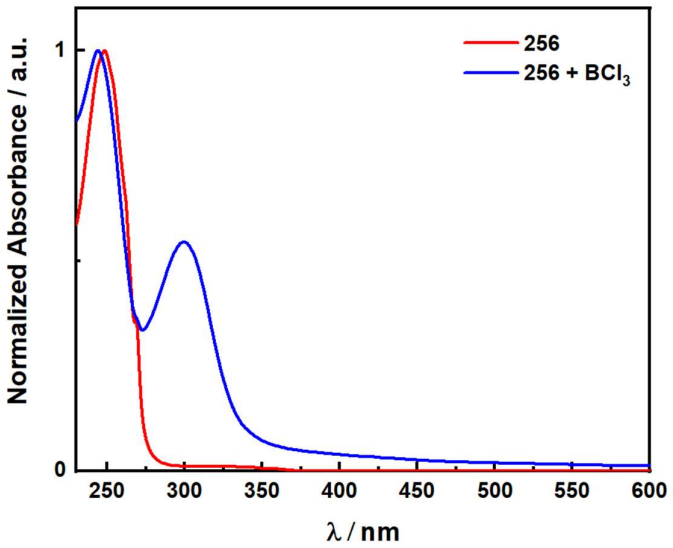

Figure 5.2 Absorption spectrum of **256** with and without BCl_3 in CH_2Cl_2.

5.2.2 DET Optimization

A DET reaction is possible if there is spectral overlap between the $S_0 \rightarrow T_1$ absorption spectrum of the acceptor and the $T_1 \rightarrow S_0$ emission spectrum of the donor.[11] However, such absorption spectra are not easily obtained, so instead the triplet energies (E_T) of the donor and acceptor are often used as a rough predictive guide. If E_T(donor) > E_T(acceptor) then the DET is predicted to occur. Density functional theory (DFT) calculations were therefore employed to predict the E_T of **255** and **256**. A small validation study was undertaken to determine the best combination of functional and basis set to accurately model the triplet energy of the system by cross-comparison with the experimentally determined E_T. Cyclohexenone was chosen as the test molecule as it has a similar structure to the molecules of interest and has an experimentally determined triplet energy (E_T = 62.4 kcal mol^{-1}).[186] The most accurate methodology used was at the BLYP/6-31G(d,p) level of theory, which predicted an E_T of 62.5 kcal mol^{-1} (Table 5.1, entry 1). Other functionals tested included B3LYP and PBE0 but they significantly overestimated the E_T (Table 5.1, entries 2-3). The E_T of **255** and **256** was thus calculated at the BLYP/6-31G(d,p) level to be 66.8 and 67.3 kcal mol^{-1}, respectively (Table 5.1, entries 4-5). While these values make them more challenging substrates than cyclohexenone to engage in DET, we hypothesised that the commonly used and commercially available photosensitiser, benzophenone (E_T = 69.0 kcal mol^{-1}),[187] could promote the DET and subsequent cyclisation.

Table 5.1 Optimization of functional to calculate E_T.

Entry[a]	Functional	Compound	E_T / kcal mol^{-1}
1	BLYP	Cyclohexenone	62.5
2	B3LYP	Cyclohexenone	72.4
3	PBE0	Cyclohexenone	73.1
4	BLYP	**255**	66.8
5	BLYP[a]	**256**	67.3

[a] Calculations for benzophenone at the same level of theory underestimate E_T = 62.5 kcal mol^{-1}.

Initial optimization of the reaction procedure focused on route I to avoid the use of **256** as it contains an α-bromo carbonyl component which had potential to be unstable under photocatalytic conditions. Therefore, **255** and stoichiometric benzophenone were dissolved in dry degassed CH_2Cl_2 and irradiated (λ_{exc} = 370 nm) for 24 hours on a 0.1 mmol scale (Table 5.2, entry 1). Pleasingly, complete conversion of the starting material was observed and the ^{1}H NMR of the crude material matched that reported by Chapman and co-workers.[182] Next, the catalyst loading was lowered to investigate if stoichiometric benzophenone was required, and full conversion was also observed if 0.5 or 0.2 equivalents were used (Table 5.2, entries 2-3). However, if the loading was lowered further to 0.1 equivalents, the conversions dropped slightly to 91% (Table 5.2, entry 4). To verify whether such a high triplet energy PC was truly required, [Ir(dF(CF_3)ppy)$_2$(dtbbpy)](PF_6) was also tested in this reaction under similar conditions. However, no consumption of starting material was observed at all, presumably due to the much lower triplet energy (E_T = 61.6 kcal mol^{-1})[116] (Table 5.2, entry 5).

Table 5.2 Optimization of [2+2] cycloaddition with **255**

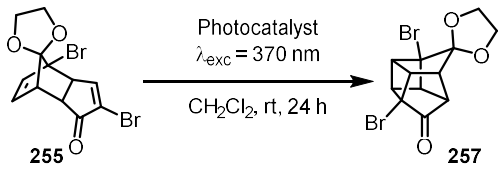

Entry[a]	PC	Catalyst Equivalents	Conversion / %[b]
1	Benzophenone	1.0	100
2	Benzophenone	0.5	100
3	Benzophenone	0.2	100
4	Benzophenone	0.1	91
5[c]	$[Ir(dF(CF_3)ppy)_2(dtbbpy)](PF_6)$	0.02	0

[a] Conditions: **255** (36.2 mg ,0.1 mmol), PC, CH_2Cl_2 (0.1 M), N_2, LED (λ_{exc} = 370 nm), rt. [b] From ^{1}H NMR of crude material calculated without internal standard. [c] λ_{exc} = 390 nm.

Given these promising results our attention turned to whether this reaction could be scaled up to generate useful quantities of the desired product for the subsequent steps to make **253**. However, on a 0.5 mmol scale, 0.2 equivalents of benzophenone only achieved 57% conversion (Table 5.3, entry 1). Extending the reaction time to 72 h allowed 97% conversion to be achieved (Table 5.3, entry 2). However, to get full conversion, 0.5 equivalents of benzophenone and a 72 h reaction time were required (Table 5.3, entry 3).

Table 5.3 Scale-up optimization.

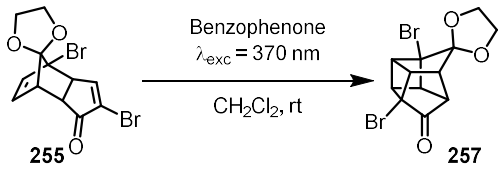

Entry[a]	Reaction time / h	Catalyst Equivalents	Conversion / %[b]
1	24	0.2	57
2	72	0.2	97
3	72	0.5	100

[a] Conditions: **255** (181 mg, 0.5 mmol), benzophenone, CH_2Cl_2 (0.1 M), N_2, LED (λ_{exc} = 370 nm), rt. [b] From ^{1}H NMR of crude material calculated without internal standard.

Considering the success of route I, the shorter route II was evaluated next. However, if **256** is irradiated (λ_{exc} = 370 nm) in CH_2Cl_2 in the presence of stoichiometric benzophenone for 72 hours on a 0.1 mmol

scale, only a 94% conversion is observed (Table 5.4, entry 1). Fortunately, this issue can be resolved if the solvent is changed to acetonitrile (Table 5.4, entry 2). Given the direct excitation method using UV-B lamps was performed in methanol, this solvent was also attempted but this resulted in a mixture of starting material and unknown side-products (Table 5.4, entry 3). Therefore, acetonitrile was carried forward for further optimization of route II.

Table 5.4 Optimization of [2+2] cycloaddition with **256**.

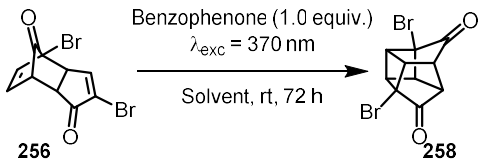

256 **258**

Entry[a]	Solvent	Conversion / %[b]
1	CH_2Cl_2	94
2	MeCN	100
3	MeOH	0

[a] Conditions: **256** (31.8 mg, 0.1 mmol), benzophenone (18.2 mg, 0.1 mmol), Solvent (0.1 M), N_2, LED (λ_{exc} = 370 nm), rt. [b] From ^{1}H NMR of crude material calculated without internal standard.

At this point the best conditions for route II's [2+2] cycloaddition step used stoichiometric benzophenone, long reaction times and small scale. Therefore, to make this step more synthetically useful, the equivalents of benzophenone were reduced to 0.5, the reaction time was reduced to 24 h, and the scale was increased to 0.5 mmol but this resulted in poor conversions (Table 5.5, entry 1). However, if the reaction vessel were irradiated outside the photoreactor, (Figure 5.3), these conditions could achieve full conversion (Table 5.5, entry 2).

(a)

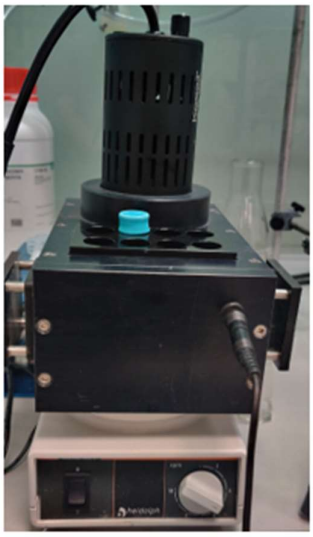

(b)

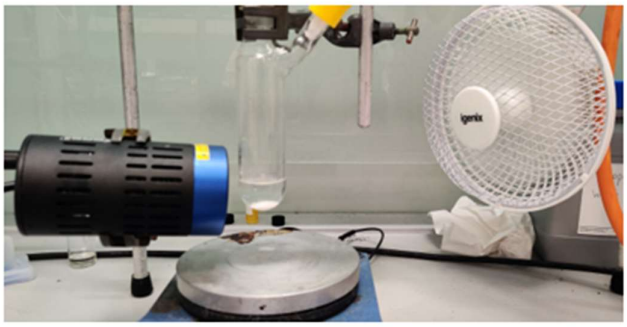

Figure 5.3 Experimental set-up for photocatalysis reactions using PR160L – Kessil LED lights (λ_{exc} = 390 nm) (a) in a photoreactor, (b) outside of a photoreactor.

Unfortunately, when using this reaction set-up, a significant background reaction was observed in the absence of benzophenone (Table 5.5, entry 3), suggesting if the light is intense enough, 370 nm lamps can promote the direct excitation pathway.

Table 5.5 Scale-up Optimization

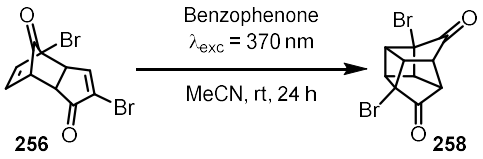

Entry[a]	Reaction Set-up	Catalyst Equivalents	Conversion / %[b]
1	In photoreactor	0.5	18
2	Outside photoreactor	0.5	100
3[c]	Outside photoreactor	0	93

[a] Conditions: **256** (159 mg, 0.5 mmol), benzophenone, MeCN (0.1 M), N_2, LED (λ_{exc} = 370 nm), rt. [b] From ^{1}H NMR of crude material calculated without internal standard. [c] 0.1 mmol scale.

Since the goal was to use lower energy light for this step (and also considering that using lower energy light would be expected to typically result in reduced background reactivity), the optimization was redone with 390 nm excitation. A solution of **256** and 0.25 equivalents of benzophenone in MeCN was irradiated with a 390 nm LED over 24 h in our standard photoreactor (Table 5.6, entry 1). Pleasingly, partial conversion to **258** was observed, showing that 390 nm excitation is viable. Increasing the

catalyst loading gave increased product conversion over the same period but fell short of complete conversion to **258** (Table 5.6, entries 2-3). As before, direct irradiation and at least 0.5 equivalents of benzophenone were required to achieve full conversion (Table 5.6, entry 4-6). At this point, control reactions were again carried out to confirm the necessity of benzophenone. When using the photoreactor in the absence of benzophenone, no conversion to the desired product was observed, which is consistent with our previous attempts with BCl_3 (Table 5.6, entry 7). However, upon direct irradiation, a modest conversion to **258** was observed in the absence of benzophenone (Table 5.6, entry 8). This suggests that if the light is sufficiently intense, then photoirradiation at 390 nm should promote the [2+2] cycloaddition via direct excitation of **256**, albeit much less efficiently. To obtain useful quantities of **258** the reaction was scaled up to a 0.5 mmol scale. Similar results were observed, with full conversion to **258** requiring 0.5 equivalents of benzophenone (Table 5.6, entries 9-11). Further increase in scale to a 1.0 mmol reaction could also be achieved using the same conditions and an NMR yield of 93% was observed (Table 5.6, entry 12).

Table 5.6 Optimization with 390 nm excitation.

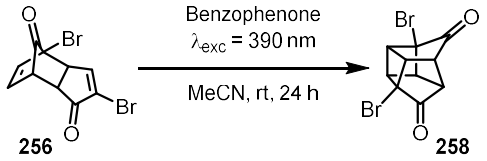

256 258

Entry[a]	Reaction Set-up	**256** / mmol	Catalyst Equivalents	Conversion / %[b]
1	In photoreactor	0.1	0.25	66
2	In photoreactor	0.1	0.5	73
3	In photoreactor	0.1	1.0	95
4	Outside photoreactor	0.1	0.25	93
5	Outside photoreactor	0.1	0.5	100
6	Outside photoreactor	0.1	1.0	100
7	In photoreactor	0.1	0	0
8	Outside photoreactor	0.1	0	28
9	Outside photoreactor	0.5	0.25	87
10	Outside photoreactor	0.5	0.50	100
11	Outside photoreactor	0.5	1.0	100
12	Outside photoreactor	1.0	0.5	100 (93)[c]

[a] Conditions: **256**, benzophenone, MeCN (0.1 M), N_2, LED (λ_{exc} = 390 nm), rt. [b] From ^{1}H NMR of crude material calculated without internal standard. [c] Using 1,3,5-trimethoxybenzene as the internal standard.

With optimized conditions for the synthesis of **258** in hand (Table 5.6, entry 12), the synthesis of dimethyl cubane-1,4-dicarboxylate was then completed (Scheme 5.5). Collin and co-workers[184] reported that crude **258** could only be subjected to the Favorskii rearrangement conditions after being refluxed in water to hydrolyse any methyl ketals present. As our method avoids the formation of any methyl ketals, crude **258** could undergo the desired Favorskii rearrangement without the water hydrolysis step to give crude **259**. To allow for facile purification, **259** was then converted to the methyl ester using an acidic methanol solution to give the final compound **253** in 20% yield over three steps from **256**. Although this represents a lower overall yield than the 54% achieved by Collin and coworkers,[184] considering the high conversion and NMR yield for the formation of **256** through the [2+2] cycloaddition, we hypothesise this is due to difficulties in preparing **253** on a much smaller scale.

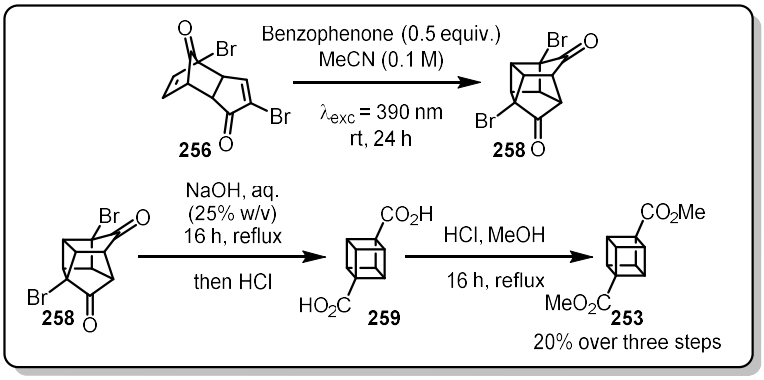

Scheme 5.5 Synthesis of **253**.

5.2.3 Towards the Photocatalytic Functionalization of Cubane

Having completed the synthesis of **253**, our attention turned to the photocatalytic functionalization of cubane using cubane carboxylic acids as convenient cubyl radical precursors. Evidence for the stability and utility of the cubyl radical can be seen in the synthesis of unsubstituted cubane **260**, which goes via a double Barton decarboxylation of **259** (Scheme 5.6a).[188] Furthermore, Baran and co-workers successfully used a redox active ester variant of cubane **261** as a radical precursor in an iron catalysed coupling reaction with aryl zinc reagents (Scheme 5.6b).[189]

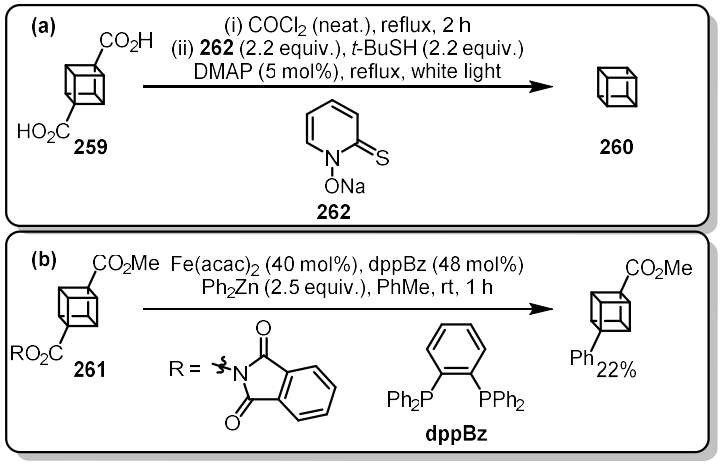

Scheme 5.6 (a) Synthesis of cubane via a double Barton decarboxylation. (b) Fe-catalysed decarboxylative coupling of **261**.

First, **262** was synthesised via hydrolysis of **253** in 50% yield, with 44% of the unreacted diester being recovered (Scheme 5.7a). Then, **262** was subjected to a photocatalytic decarboxylation procedure known to work efficiently with other tertiary carboxylic acids such as 1-adamantylcarboxyclic acid;[190] however, only trace amounts of the desired product, **263**, was observed (Scheme 5.7b). Other

decarboxylation conditions[107,120] were also attempted but these failed to provide detectable amounts of **263**.

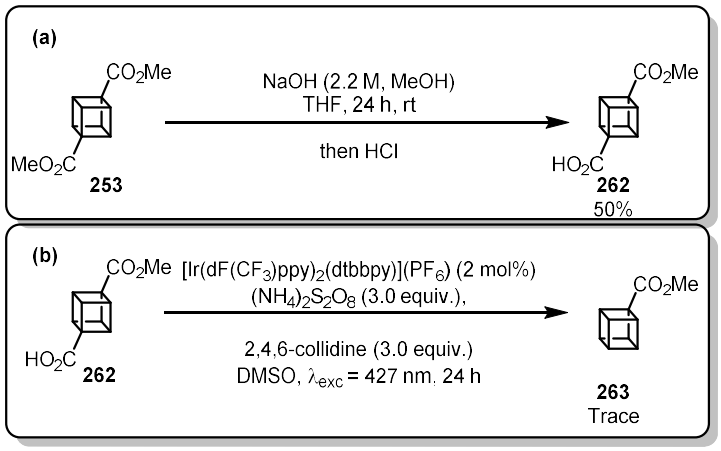

Scheme 5.7 (a) Synthesis of **262**. (b) Attempted photocatalytic decarboxylation of **262**.

After the conclusion of this work, MacMillan and co-workers[191] published an elegant way to utilise **262** as a cubyl radical precursor through its activation using $MesI(OAc)_2$ via intermediate **264**. Within the same publication, new routes to 1,3 and 1,2-cubane dicarboxylates were also developed, which in combination with this work greatly improves the chemist's ability to access the cubane functional group.

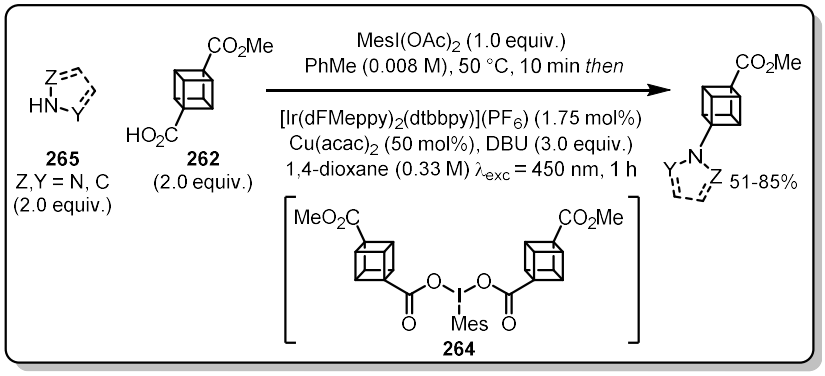

Scheme 5.8 Use of **262** as a cubyl radical precursor for the functionalization of cubane.

5.3 Conclusion

In summary, we have developed a synthetic route to dimethyl cubane-1,4-dicarboxylate where the key photochemical [2+2] cycloaddition is catalysed by the cheap and widely available photosensitiser benzophenone to give near quantitative yields of the desired product **258** from dione **256**. This allowed for the use of much lower energy light (λ_{exc} = 390 nm) than previous direct excitation methods

that required a high-power Hg lamp or UV-B irradiation. Finally, attempts at photocatalytic decarboxylation of **262** were made using conditions known to work for tertiary carboxylic acids; however, these were unsuccessful.

There are two main points of improvement to this reaction on which future work could focus. Firstly, the scale of this reaction is somewhat limited due to the inherent weaknesses of photocatalysis in batch reactors. Therefore, the application of flow chemistry to this process should improve its viability greatly. Furthermore, this should also improve the overall yields of **253** as it seems the final steps are easier on larger scale. Secondly, an alternative PC could be sought with a similar triplet energy but a more red-shifted absorption spectra so that even lower energy light could be used and ideally a lower catalyst loading.

6 Concluding Remarks

The objectives set out at the beginning of this thesis were to investigate the benefits of using TADF compounds as PCs with an additional interest in their use for photoredox/Lewis base dual catalysis. Towards this goal, in chapter 2 **Hyper2CzPN** was synthesised and investigated as a bifunctional ITU/photoredox catalyst. However, the two components when incorporated in the same molecule proved to be incompatible and led to the decomposition of the catalyst under photocatalytic conditions. Further investigation into ITU/photoredox dual catalysis using a separate ITU catalyst and PC also pointed to an issue of incompatibility. However, subsequent investigations by others[95,96] showed that this catalytic system can be utilised effectively if a suitable radical precursor is identified that quenches the PC faster than the ITU. Further work in this area should continue to explore this new mode of dual catalysis to broaden the potential scope.

Investigations in chapter 3 focused on evaluating the benefits of using MR-TADF compounds as photocatalysts as up to this point only D-A TADF compounds had been explored. This was achieved by testing **DiKTa** and **Mes$_3$DiKTa** in a variety of photocatalytic reactions that included reductive quenching reactions, oxidative quenching reactions, DET reactions and dual catalytic reactions. The product yields of these test reactions were then compared to the results when using a benchmark D-A TADF photocatalyst, **4CzIPN**. Further comparisons were made through the analysis of the rates of reaction using the three different catalysts. Initial attempts to monitor a photocatalytic decarboxylation proved challenging and the results from monitoring an oxidative hydroxylation were inconclusive. However, the monitoring of an ATRA reaction using in-situ NMR techniques showed a significant rate enhancement when using either **DiKTa** or **Mes$_3$DiKTa** rather than **4CzIPN**. Future work on MR-TADF photocatalysis should investigate other MR-TADF emitters as potential PCs, particularly those that are either highly photooxidising or photoreducing.

Having successfully demonstrated the utility of **DiKTa** as an excellent PC, it was then applied to the development of a new NHC/photoredox catalysed synthesis of unsymmetric 1,4-diketones through a three-component radical relay process. The optimized conditions combined aroyl fluorides, α-

ketoacids and styrenes in the presence of **DiKTa**, azolium salt **1** and caesium carbonate to generate the desired 1,4-diketones in moderate yields. Subsequent investigation of the scope was achieved by varying the substituents of each starting material. Finally, Stern-Volmer analysis was performed to support the proposed mechanism. Future work in this area should look to expand the scope of radical precursors and also to investigate other ways of combining NHC intermediates with photocatalysis.

In chapter 5 of this thesis a photocatalytic method was developed, using the cheap and widely available benzophenone organophotocatalyst, to perform the key [2+2] cycloaddition step in the synthesis of dimethyl cubane-1,4-dicarboxylate. This allowed for the use of significantly lower energy light (λ_{exc} = 390 nm) than previously reported (λ_{exc} = 311 nm),[184] which meant a simpler reaction set-up could be used that does not require Hg lamps or specialist quartz glassware. Further work on this reaction should improve the scale-up potential through the use of flow chemistry and also investigate the use of other PCs to try and lower the necessary catalyst loading.

7 Experimental

7.1 General Synthetic Procedures.

Flash column chromatography was carried out using silica gel (Silia-P from Silicycle, 60 Å, 40-63 μm). Analytical thin-layer-chromatography (TLC) was performed with silica plates with aluminum backings (250 μm with F-254 indicator). TLC visualization was accomplished by 254/365 nm UV lamp. GCMS analysis was conducted using a Shimadzu QP2010SE GC-MS equipped with a Shimadzu SH-Rtx-1 column (30 m × 0.25 mm). ^{1}H, ^{13}C and ^{19}F NMR spectra were recorded on a Bruker Advance spectrometer (500 MHz for ^{1}H, 125 MHz for ^{13}C, 471 MHz for ^{19}F). The following abbreviations have been used for multiplicity assignments: “s” for singlet, “d” for doublet, “t” for triplet, “q” for quartet, “br” for broad, “m” for multiplet. ^{1}H and ^{13}C NMR spectra were referenced residual solvent peaks with respect to TMS (δ = 0 ppm). Melting points were measured using open-ended capillaries on an Electrothermal 1101D Mel-Temp apparatus and are uncorrected. High-resolution mass spectrometry (HRMS) was performed by SIRCAMS at University of Edinburgh. Infra-red spectra were recorded on a Shimadzu IRAffinity-1 Fourier transform IR spectrophotometer fitted with a Specac Quest ATR accessory (diamond puck). Spectra were recorded of either thin films or solids, with characteristic absorption wavenumbers (ν_{max}) reported in cm^{-1}. Reactions involving moisture sensitive reagents were carried out in flame or oven-dried glassware under an inert atmosphere (nitrogen) using standard vacuum line techniques. Anhydrous solvents (MeCN, Et_2O, CH_2Cl_2, THF and PhMe) were obtained after passing through an alumina column (Mbraun SPS-800). Petrol is defined as petroleum ether 40–60 °C. All other solvents and commercial reagents were used as received without further purification unless otherwise stated.

Photophysical measurements. Optically dilute solutions of concentrations on the order of 10^{-5} or 10^{-6} M of the photocatalysts were prepared in spectroscopic or HPLC grade solvents for absorption and emission analysis. Absorption spectra were recorded at room temperature on a Shimadzu UV-2600 double beam spectrophotometer with a 1 cm quartz cuvette. Molar absorptivity determination was

verified by linear regression analysis of values obtained from five independent solutions at varying concentrations with absorbance ranging from 5.11×10^{-5} to 1.18×10^{-5} M. Steady-state emission, excitation spectra and time-resolved emission spectra were recorded at 298 K using an Edinburgh Instruments F980 or a Perkin Elmer LS55 spectrofluorometer, equipped with a Hamamatsu R928 phototube or an Edinburgh Instruments FS5 spectrofluorometer. Samples were excited at the wavelength specified for steady-state measurements and time-resolved measurements. Fitting of time-resolved luminescence measurements: Time-resolved PL measurements were fitted to a sum of exponentials decay model, with chi-squared ($\chi 2$) values between 1 and 2, using the EI FLS980, Edinburgh FLS920 or Edinburgh FS5 software.

Electrochemistry measurements. Cyclic Voltammetry (CV) analysis was performed on an Electrochemical Analyzer potentiostat model 620E from CH Instruments at a sweep rate of 100 mV/s. Samples were prepared as solutions, which were degassed by sparging with solvent-saturated nitrogen gas for 5 minutes prior to measurements. All measurements were performed using 0.1 M solution of tetra-*n*-butylammonium hexafluorophosphate ($[n\text{Bu}_4\text{N}]\text{PF}_6$). An Ag/Ag^+ electrode was used as the reference electrode while a platinum electrode and a platinum wire were used as the working electrode and counter electrode, respectively. The redox potentials are reported relative to a saturated calomel electrode (SCE) with a ferrocenium/ferrocene (Fc/Fc^+) redox couple as the internal standard.[91]

Photocatalytic Reactors. Three types of photocatalytic set-up were used throughout (Figure 7.1). Which set-up is used is specified for each reaction.

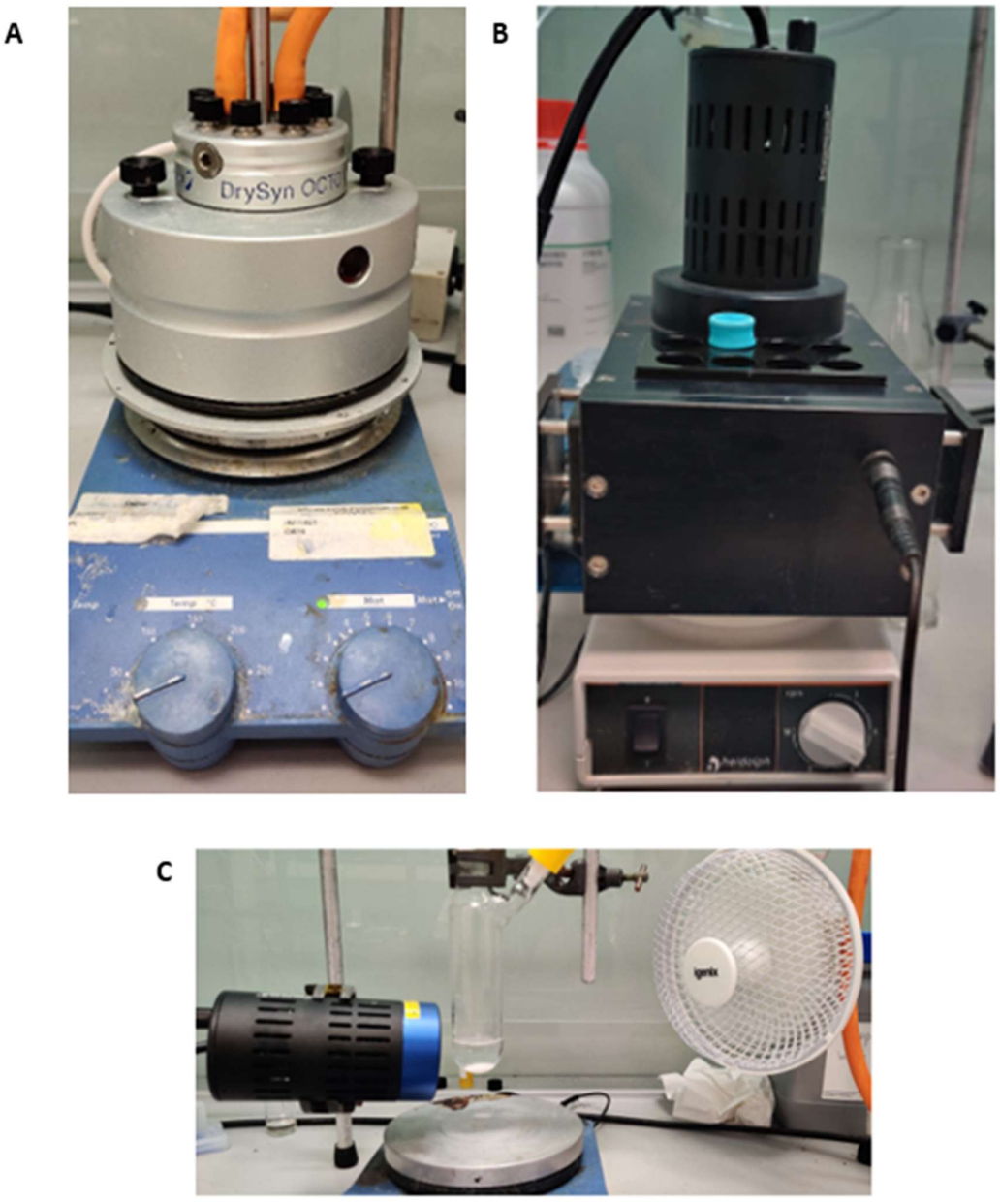

Figure 7.1 Different photocatalytic reaction set-ups used. (A) Asynt's LightSyn Illumin8 photoreactor. (B) Custom photoreactor made in-house. (C) Outside of a photoreactor.

7.2 Experimental procedures and characterization for Chapter 2.

(4*r*,5*S*)-4-(9*H*-carbazol-9-yl)-5-(2-(1-(3-(((2*R*,3*S*)-3-isopropyl-2-phenyl-3,4-dihydro-2*H*-benzo[4,5]thiazolo[3,2-*a*]pyrimidin-8-yl)oxy)propyl)-1*H*-1,2,3-triazol-4-yl)-9*H*-carbazol-9-yl)phthalonitrile (Hyper2CzPN):

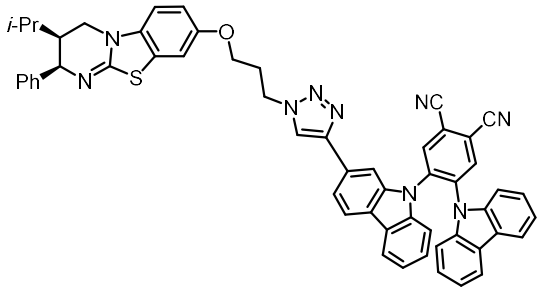

Based on a procedure reported by Neyyappadath *et al*.[87] **102** (135 mg, 0.28 mmol. 1.0 equiv.), **86** (azide) (137 mg, 0.34 mmol, 1.2 equiv.) and Copper (I) Iodide (5 mg, 0.028 mmol, 0.1 equiv.) were added to a flame dried flask then evacuated and backfilled with nitrogen three times. Anhydrous THF (5 mL) and *i*Pr_2NEt (0.17 mL, 0.98 mmol, 3.5 equiv.) were then added and the solution was stirred under nitrogen at room temperature for 24 h. The reaction was quenched with H_2O (5 mL) and the aqueous phase extracted with CH_2Cl_2 (3 × 10 mL). The organic layers were dried (Na_2SO_4) and concentrated *in vacuo*. Purification by silica column chromatography (50% EtOAc/CH_2Cl_2) to afford Hyper2CzPN as a yellow solid (185 mg, 74%)

Rf: 0.15 (50% EtOAc/CH_2Cl_2). **Infra-red (ν max, cm^{-1})**: 2234 (C≡N, w), 1622 (C=N, s), 1450, 748. **^{1}H NMR (400 MHz, $CDCl_3$) δ (ppm):** 0.83 (3H, d, *J* = 6.7 Hz, CH_3), 1.13 (3H, d, *J* = 6.4 Hz, CH_3), 1.24 – 1.34 (1H, m, C*H*(CH_3)$_2$), 1.91 – 1.98 (1H, m, C(3)*H*), 2.43 (2H, p, *J* = 6.4 Hz, C(2)H_2), 3.33 (1H, td, *J* = 11.4, 3.8 Hz, C(4)H^AH^B), 3.79 – 3.86 (1H, m, C(4)H^A*H*^{B}), 4.00 (2H, dt, *J* = 9.5, 5.8 Hz, OC(1)H_2), 4.52 – 4.58 (2H, m, NC(3)H_2), 4.93 (1H, d, *J* = 4.6 Hz, C(2)*H*), 6.72 (1H, d, *J* = 8.7 Hz, ArC(6)*H*), 6.76 – 6.84 (3H, m, Ar*H*), 6.87 (1H, tdd, *J* = 7.2, 4.5, 1.2 Hz, Ar*H*), 6.96 (1H, dd, *J* = 10.9, 2.5 Hz, Ar*H*), 7.03 (1H, ddd, *J* = 8.9, 7.4, 1.8 Hz, Ar*H*), 7.13 (1H, dd, *J* = 13.5, 1.3 Hz, Ar*H*), 7.17 – 7.34 (10H, m, Ar*H*), 7.45 (1H, t, *J* = 8.2 Hz, Ar*H*), 7.57 (1H, ddd, *J* = 7.8, 5.8, 1.3 Hz, Ar*H*), 7.73 (1H, d, *J* = 7.7 Hz, Ar*H*), 7.80 (1H, d, *J* = 8.0 Hz, Ar*H*), 7.87 (1H, d, *J* = 7.6 Hz, Ar*H*), 8.35 (2H, d, *J* = 12.6 Hz, Ar*H*). **^{13}C{^{1}H} NMR (126 MHz, $CDCl_3$) δ (ppm):** 20.0

(*C*H_3), 22.0 (*C*H_3), 26.9 (*C*H(CH_3)$_2$), 30.1 (*C*(2)H_2, app. d), 40.8 (*C*(3)H, app. d), 42.1 (*C*(4)H_2), 47.1 (N*C*(3)H_2, app d), 65.2 (O*C*(1)H_2, app. d), 106.28 (Ar*C*), 106.30 (Ar*C*), 108.2 (Ar*C*), 109.0 (Ar*C*), 109.1 (Ar*C*), 109.2 (Ar*C*), 109.3 (Ar*C*), 112.4 (Ar*C*), 114.5 (Ar*C*), 114.7 (Ar*C*), 114.8 (Ar*C*), 119.6 (Ar*C*), 120.0 (Ar*C*), 120.1 (Ar*C*), 120.4 (Ar*C*), 120.7 (Ar*C*), 120.8 (Ar*C*), 120.9 (Ar*C*), 121.6 (Ar*C*), 121.7 (Ar*C*), 122.2 (Ar*C*), 123.77 (Ar*C*), 123.79 (Ar*C*), 124.0 (Ar*C*), 124.4 (Ar*C*), 124.5 (Ar*C*), 124.8 (Ar*C*), 126.3 (Ar*C*), 126.7 (Ar*C*), 127.3 (Ar*C*), 128.0 (Ar*C*), 128.4 (Ar*C*), 128.8 (Ar*C*), 135.4 (Ar*C*), 135.7 (Ar*C*), 137.9 (Ar*C*), 137.97 (Ar*C*), 138.00 (Ar*C*), 138.03 (Ar*C*), 138.4 (Ar*C*), 138.6 (Ar*C*), 139.0 (Ar*C*), 147.4 (Ar*C*).

HRMS (ESI) $C_{56}H_{44}N_9OS$ [M+H]$^+$ found 890.3358, theoretical 890.3384 (-2.9 ppm)

4-(9*H*-carbazol-9-yl)-5-fluorophthalonitrile (CzFPN):

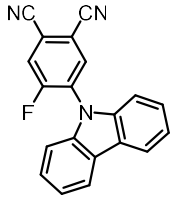

Based on a procedure reported by Chen *et al.*[89] carbazole (2.0 g, 12.0 mmol, 1.0 equiv.) was added to a flame dried round bottom flask and then evacuated and backfilled with nitrogen three times. Anhydrous THF (40 mL) was added followed by portionwise addition of NaH (0.96 g, 24.0 mmol, 60 wt%, 2.0 equiv.). The suspension was stirred at room temperature for 15 minutes. 4,5-Difluorophthalonitrile (1.97 g, 12.0 mmol, 1.0 equiv.) was added. An immediate colour change from white to red was observed. The reaction was stirred for a further 3 h. The mixture was then poured onto cold H_2O (40 mL) and the aqueous phase extracted with CH_2Cl_2 (3 × 20 mL). The organic layers were combined, dried (Na_2SO_4) and concentrated *in vacuo*. Purification by silica column chromatography (30% to 60% CH_2Cl_2/Pet. ether) afforded a mixture of CzFPN and 2CzPN. Recrystallization from $CHCl_3$ afforded CzFPN as a pale green solid (1.36 g, 37%).

Mp 222-224 °C {Lit.[89] 225 °C}. **Rf:** 0.20 (50% CH_2Cl_2/Pet. Ether). **^{1}H NMR (400 MHz, $CDCl_3$) δ (ppm):** 7.22 (2H, ddt, *J* = 8.2, 2.7, 0.9 Hz, Ar*H*), 7.39 (2H, ddd, *J* = 8.2, 7.3, 1.0 Hz, Ar*H*), 7.48 (2H, ddd, *J* = 8.3, 7.3, 1.3 Hz, Ar*H*), 7.86 (1H, d, *J* = 9.0 Hz, Ar*H*), 8.10 – 8.18 (3H, m, Ar*H*); **^{19}F NMR (376 MHz, $CDCl_3$) δ (ppm):** – 103.4.

Data matches that previously reported.[89]

2-ethynyl-9*H*-carbazole (101):

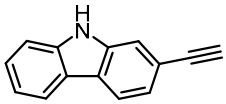

Based on a procedure reported by Al-Balushi *et al*.[88] KOH (0.57 mL, 0.57 mmol, 1 M in H_2O, 1.5 equiv.) was added to a solution of 2-((trimethylsilyl)ethynyl)-9H-carbazole (100 mg, 0.38 mmol, 1.0 equiv.) in a mixture of THF:MeOH (4 mL, 4:1) and then stirred at room temperature for 1 h. The reaction was then concentrated *in vacuo*. Purification by silica column chromatography (10% EtOAc/Pet. Ether) afforded the desired product as a colourless solid (71 mg, 98%).

Mp 166-168 °C. **Rf:** 0.20 (5% EtOAc/Pet. Ether). **^{1}H NMR (400 MHz, $CDCl_3$) δ (ppm):** 3.13 (1H, s, C≡C-*H*), 7.23 – 7.29 (2H, m, N*H* & ArC*H*), 7.38 (1H, dd, *J* = 8.1, 1.3 Hz, ArC*H*), 7.44 (2H, dt, *J* = 4.0, 0.9 Hz, ArC*H*), 7.59 (1H, dd, *J* = 1.4, 0.7 Hz, ArC*H*), 8.01 (1H, dt, *J* = 8.0, 0.8 Hz, ArC*H*), 8.05 – 8.12 (2H, m, ArC*H*). Data matches that previously reported.[88]

(2*R*,3*S*)-8-(3-azidopropoxy)-3-isopropyl-2-phenyl-3,4-dihydro-2*H*-benzo[4,5]thiazolo[3,2-*a*]pyrimidine (102):

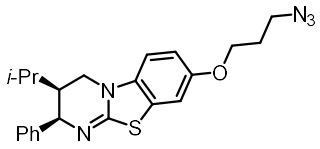

Based on a procedure reported by Neyyappadath *et al*.[87] potassium *tert*-butoxide was added to a solution of **104•HBr** (850 mg, 2.10 mmol, 1.0 equiv.) in DMSO/THF (18 mL, 1:1) at 0 °C and stirred for 2 h. In a separate flame dried flask methane sulfonyl chloride (0.26 mL, 3.3 mmol, 1.6 equiv.) was added to a solution of 3-azidopropan-1-ol (255 mg, 2.5 mmol, 1.2 equiv.) and triethylamine (1.4 mL, 10 mmol, 4.8 equiv.) in CH_2Cl_2 (10 mL) at 0 °C. The solution was then allowed to warm to room temperature and stirred for 30 minutes. The reaction was quenched with $NaHCO_3$ (10 mL), and the aqueous phase extracted with CH_2Cl_2 (2 × 10 mL). The organic layers were combined, washed with H_2O (10 mL), dried ($MgSO_4$) and concentrated *in vacuo* to afford 3-azidopropyl methanesulfonate as a crude product. 3-azidopropyl methanesulfonate was then transferred directly to the solution of **104•HBr** in DMSO/THF (1:1) and the reaction was left to stir for 16 h at room temperature. The reaction was diluted with EtOAc (20 mL) and washed with brine (20 mL). The aqueous phase was then extracted with EtOAc (2 × 20 mL). The combined organic phases were dried ($MgSO_4$) and concentrated *in vacuo*. Purification through silica column chromatography (20% to 50% EtOAc/CH_2Cl_2) afforded the desired product as a pale yellow solid (571 mg, 67%).

Mp 106-109 °C. **Rf:** 0.10 (30% EtOAc/Pet. Ether). **Infra-red (ν max, cm^{-1}):** 2099 (N=N=N), 1610 (C=N), 1490,1260, 1206, 1037, 800. **^{1}H NMR (400 MHz, $CDCl_3$) δ (ppm):** 0.84 (3H, d, *J* = 6.7 Hz, CH_3), 1.13 (3H, d, *J* = 6.5 Hz, CH_3), 1.24 – 1.34 (1H, m, C*H*$(CH_3)_2$), 1.90-1.99 (1H, m, C(3)*H*), 2.02 – 2.09 (2H, m, C(2)H_2), 3.32 (1H, t, *J* = 11.5 Hz, C(4)H^AH^B), 3.53 (2H, t, *J* = 6.6 Hz, NC(3)H_2), 3.83 (1H, ddd, *J* = 11.6, 5.3, 1.8 Hz, C(4)H^A*H*^{B}), 4.03 (2H, t, *J* = 5.9 Hz, OC(1)H_2), 4.90 (1H, dd, *J* = 4.5, 1.7 Hz, C(2)*H*), 6.71 (1H, d, *J* = 8.6 Hz, ArC(6)*H*), 6.78 (1H, dd, *J* = 8.7, 2.5 Hz, ArC(7)*H*), 6.95 (1H, d, *J* = 2.5 Hz, ArC(9)*H*), 7.18 – 7.33 (5H, m, PhC*H*); **^{13}C{^{1}H} NMR (126 MHz, $CDCl_3$) δ (ppm):** 20.1 (*C*H_3), 22.1 (*C*H_3), 27.0 (*C*H$(CH_3)_2$), 28.9 (*C*(2)H_2),

40.9 (*C*(3)H), 42.1 (*C*(4)H_2), 48.3 (N*C*(3)H_2), 61.2 (*C*(2)H), 65.6 (O*C*(1)H_2), 108.0 (Ar*C*(6)H), 109.2 (Ar*C*(9)H), 112.4 (Ar*C*(7)H), 124.3 (Ar*C*(5a)), 127.3 (Ph*C*(4)H), 128.1 (Ph*C*(3,5)H), 128.4 (Ph*C*(2,6)H), 135.2 (Ar*C*(9a)), 140.8 (Ph*C*(1)), 154.4 (Ar*C*(8)), 158.6 (*C*=N).

HRMS: $C_{22}H_{26}N_5OS$ **(ESI) [M+H]$^+$**, found 408.1839, theoretical 408.1853 (– 3.4 ppm).

(2*R*,3*S*)-8-hydroxy-3-isopropyl-2-phenyl-3,4-dihydro-2*H*-benzo[4,5]thiazolo[3,2-*a*]pyrimidin-1-ium (104•HBr):

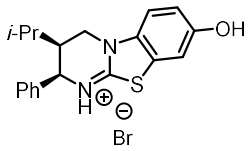

Based on a procedure reported by Neyyappadath *et al*.[87] BBr_3 (3 mL, 3 mmol, 1 M in CH_2Cl_2, 2 equiv.) was added dropwise to a solution of **108** (500 mg, 1.48 mmol, 1 equiv.) in CH_2Cl_2 (10 mL) at 0 °C in a flame dried flask under nitrogen. The solution was stirred at 0 °C for 2 h then warmed to room temperature and stirred for 16 h. The reaction was carefully quenched with MeOH (6 mL). Water (10 mL) was added, and the aqueous phase was extracted with CH_2Cl_2 (3 × 10 mL). A precipitate formed which was filtered and added to the combined organic layers after they were dried ($MgSO_4$), the suspension was then concentrated *in vacuo* to afford **104•HBr** as a colourless solid (567 mg, 93%).

Mp 190-192°C {Lit.[37] 194-196 °C}. **^{1}H NMR (400 MHz, DMSO-d_6) δ (ppm):** 0.80 (3H, d, *J* = 6.6 Hz, CH_3), 1.08 (3H, d, *J* = 6.5 Hz, *CH_3*), 1.17 – 1.28 (1H, m, C*H*(CH_3)$_2$), 2.27 – 2.38 (1H, m, C(3)*H*), 3.64 – 3.74 (1H, m, C(4)*H*^{A}H^B), 4.40 (1H, dd, *J* = 13.4, 4.9 Hz, C(4)H^A*H*^{B}), 5.17 (1H, d, *J* = 4.7 Hz, C(2)*H*), 7.00 (1H, dd, *J* = 8.8, 2.5 Hz, C(7)*H*), 7.30-7.35 (2H, dd, *J* = 7.7, 1.9 Hz, PhC(2,6)H), 7.38 – 7.43 (3H, m, PhC(3,4,5)*H*), 7.45 (1H, d, J = 2.4 Hz, ArC(9)*H*) 7.66 (1H, d, *J* = 8.9 Hz, ArC(6)*H*), 9.99 (1H, s, O*H*), 11.12 (1H, s, N*H*).

Data matches that previously reported.[87]

2-chloro-6-methoxybenzo[*d*]thiazole (106)

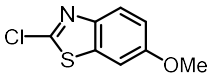

Based on a procedure reported by Neyyappadath *et al*.[87] $CuCl_2$ (13.6 g, 100 mmol, 1.2 equiv.) was added to a round bottomed flask and dried under vacuum at 110 °C for 1 h. After cooling to 40–50 °C, MeCN (500 mL) and *tert*-butyl nitrite (15.0 mL, 126 mmol, 1.5 equiv.) were added, followed by a suspension of 6-methoxybenzo[*d*]thiazol-2-amine (15.2 g, 84 mmol, 1.0 equiv.) in MeCN (15 mL), which was added portionwise using a pipette (nitrogen gas evolution was observed as a froth). Upon complete addition, the reaction was heated at 65 °C for 3 h. After the reaction cooled to room temperature it was poured into 4 M HCl (200 mL) and extracted using Et_2O (2 × 200 mL). The organic layers were combined, dried ($MgSO_4$) and concentrated *in vacuo*. Purification by silica column chromatography (2.5% EtOAc/Pet. ether) afforded 2-chloro-6-methoxybenzo[d]thiazole as a colourless solid (9.25 g, 55%).

Rf: 0.30 (2.5% EtOAc/Pet. ether). **^{1}H NMR (400 MHz, $CDCl_3$) δ (ppm):** 3.87 (3H, s, OCH_3), 7.07 (1H, dd, *J* = 9.0, 2.6 Hz, ArC(5)*H*), 7.23 (1H, d, *J* = 2.5 Hz, ArC(7)*H*), 7.82 (1H, d, *J* = 9.0 Hz, ArC(4)*H*).

Data matches that previously reported.[192]

(2*R*,3*S*)-3-isopropyl-8-methoxy-2-phenyl-3,4-dihydro-2*H*-benzo[4,5]thiazolo[3,2-*a*]pyrimidine (108):

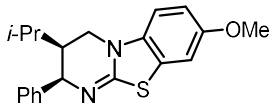

Based on a procedure reported by Daniels *et al*.[193] **106** (4.0 g, 20 mmol, 1 equiv.) was added to a solution of (*R*)-2-((*R*)-amino(phenyl)methyl)-3-methylbutan-1-ol hydrochloride (4.81 g, 21 mmol, 1.05 equiv.) and *i*-Pr_2NEt (10.45 mL, 60 mmol, 4 equiv.) in *o*-dichlorobenzene (7.5 mL, 2.0 M). The resulting pale-yellow suspension was heated at reflux until completion. The resulting mixture was cooled to room temperature, H_2O (15 mL) was added, and the aqueous phase extracted with CH_2Cl_2 (3 × 20 mL). The organic layers were combined, washed with brine, dried ($MgSO_4$), and concentrated *in vacuo* to afford the crude product which was triturated with hexane to afford the amino alcohol intermediate as a brown solid which was used in the next step without further purification. To a slurry of crude amino alcohol (5.43 g, 15.2 mmol, 1 equiv.) in anhydrous CH_2Cl_2 (80 mL, 0.2 M) was added Et_3N (8.47 mL, 60.8 mmol, 4 equiv.) and the reaction mixture was cooled to 0 °C. Methanesulfonyl chloride (1.53 mL, 19.8 mmol, 1.3 equiv.) was added and the reaction mixture was stirred at room temperature for 30 mins. Once complete consumption of the amino alcohol was observed, *i*-PrOH (1 mL) was added, and the reaction was heated at reflux for 16 h. The reaction was quenched with 1 M aq. NaOH (20 mL) and the biphasic mixture stirred vigorously for 30 mins. The aqueous layer was extracted with CH_2Cl_2 (3 × 20 mL). The organic layers were combined, washed with brine (50 mL), dried ($MgSO_4$) and concentrated *in vacuo* to afford the crude product. Purification by silica column chromatography (20% to 50% EtOAc/Pet. ether) afforded an off white solid that was recrystallised from 50% EtOAc/hexane to give **108** as a colourless solid (2.05 g, 40%)

Mp 143-145°C {Lit.[87] 139-141 °C}. **Rf:** 0.10 (20% EtOAc/Pet. ether). **^{1}H NMR (400 MHz, $CDCl_3$) δ (ppm):** 0.84 (3H, d, *J* = 6.7 Hz, CH_3), 1.13 (3H, d, *J* = 6.5 Hz, CH_3), 1.23 – 1.35 (1H, m, C$H(CH_3)_2$), 1.88 – 2.00 (1H, m, C(3)*H*), 3.32 (1H, t, *J* = 11.5 Hz, C(4)H^AH^B), 3.81 (3H, s, OCH_3), 3.82 – 3.85 (1H, m, C(4)H^AH^B), 4.90

(1H, dd, *J* = 4.5, 1.7 Hz, C(2)*H*), 6.71 (1H, d, *J* = 8.6 Hz, ArC(6)*H*), 6.78 (1H, dd, *J* = 8.7, 2.5 Hz, ArC(7)*H*), 6.95 (1H, d, *J* = 2.4 Hz, ArC(9)*H*), 7.18 – 7.33 (5H, m, PhC*H*).

Data matches that previously reported.[87]

(2R,3S)-8-(allyloxy)-3-isopropyl-2-phenyl-3,4-dihydro-2H-benzo[4,5]thiazolo[3,2-a]pyrimidine (109):

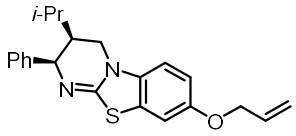

Based on a procedure reported by Neyyappadath *et al*.[87] potassium *tert*-butoxide was added to a solution of **104•HBr** (50 mg, 0.12 mmol, 1.0 equiv.) in DMSO/THF (0.9 mL, 1:1) at 0 °C and stirred for 2 h. Then, 1,3-dibromopropane (19 µl, 0.18 mmol, 1.5 eqiuv.) was added and the reaction was left to stir for 16 h at room temperature. The reaction was diluted with EtOAc (5 mL) and washed with brine (5 mL). The aqueous phase was then extracted with EtOAc (2 × 5 mL). The combined organic phases were dried ($MgSO_4$) and concentrated *in vacuo*. Characterisation of this crude mixture by ^{1}H NMR showed characteristic signals for a terminal alkene at 5.27 – 5.35 (1H, m, $CH_2HC=CH_2$), 5.37 – 5.46 (1H, m, $CH_2HC=CH_2$) and 5.98 – 6.11 (1H, m, $CH_2HC=CH_2$).

3-azidopropan-1-ol (110):

3-Chloropropan-1-ol (4.23 g, 44.8 mmol, 1.0 equiv.) was added dropwise to a solution of sodium azide (11.63 g, 179 mmol, 4.0 equiv.) in 70 mL H_2O. The mixture was then heated to reflux and stirred overnight. After the reaction cooled to room temperature it was extracted with CH_2Cl_2 (3 × 70 mL). The organic layers were combined, dried (Na_2SO_4) and concentrated *in vacuo* to afford **110** as a colourless oil (3.61 g, 80%)

^{1}H NMR (500 MHz, $CDCl_3$) δ (ppm): 1.65 (1H, s, O*H*), 1.83 (2H, app. p, *J* = 6.3 Hz, C(2)H_2), 3.45 (2H, t, *J* = 6.6 Hz, NC(3)H_2), 3.75 (2H, t, *J* = 6.0 Hz, OC(1)H_2); **^{13}C{^{1}H} NMR (126 MHz, $CDCl_3$) δ (ppm):** 31.4 (*C*(2)), 48.5 (*C*(3)), 60.0 (*C*(1)).

Data matches that previously reported.[194]

2-((trimethylsilyl)ethynyl)-9*H*-carbazole (113):

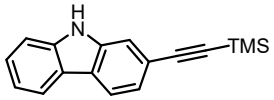

Based on a procedure reported by Al-Balushi *et al*.[88] 2-Bromo-9*H*-carbazole (500 mg, 2.0 mmol, 1.0 equiv.), $Pd(PPh_3)_4$ (125 mg, 0.1 mmol, 0.05 equiv.), CuI (25 mg, 0.05 mmol, 0.025 equiv.) were added to a flame dried round bottom flask. The mixture was then evacuated and flushed with nitrogen three times. Degassed triethylamine (26 mL) and trimethylsilylacetylene (0.44 mL, 3.0 mmol, 1.5 equiv.) were added and the solution was heated to reflux and stirred for 16 h. The reaction was cooled to room temperature and concentrated *in vacuo.* Purification by silica column chromatography (8% EtOAc/Pet. ether) afforded **113** as a brown solid (477 mg, 89%).

Mp 222-223 °C. {Lit.[88] 218 °C}. **Rf:** 0.20 (5% EtOAc/Pet. ether). **^{1}H NMR (500 MHz, $CDCl_3$) δ (ppm):** 0.29 (9H, s, Si(C*H*$_3$)$_3$), 7.27 – 7.23 (1H, m, ArC*H*), 7.36 (1H, dd, *J* = 8.0, 1.3 Hz, ArC*H*), 7.43 (2H, d, *J* = 3.8 Hz, ArC*H*), 7.56 (1H, s, ArC*H*), 7.99 (1H, d, *J* = 8.0, ArC*H*), 8.09 – 8.02 (2H, m, N*H* & ArC*H*).

Data matches that previously reported.[88]

(**4*r*,5*S*)-4-(9*H*-carbazol-9-yl)-5-(2-ethynyl-9*H*-carbazol-9-yl)phthalonitrile (114):**

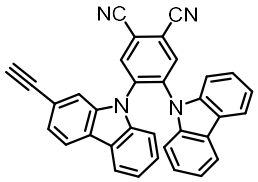

116 (239 mg, 0.43 mmol, 1.0 equiv.) was added to a flame dried round bottom flask then evacuated and flushed with nitrogen three times. Anhydrous THF (5 mL) and tetrabutylammonium fluoride (0.47 ml, 0.47 mmol, 1 M in THF, 1.1 equiv.) were added, an immediate colour change from yellow to dark green was observed. The reaction mixture was stirred at room temperature for 1 h. H_2O (10 mL) was added, and the aqueous phase extracted with CH_2Cl_2 (3 × 10 mL). The organic layers were combined, dried ($MgSO_4$) and concentrated *in vacuo*. Purification by silica column chromatography (60% CH_2Cl_2/Pet. ether) afforded **114** as a yellow solid (145 mg, 70%).

Mp 240-244 °C (decomp.). **Rf:** 0.10 (50% CH_2Cl_2/Pet. ether). **Infra-red (ν max, cm^{-1}):** 2235 (C≡N, w), 1591, 1504, 1221. **^{1}H NMR (500 MHz, $CDCl_3$) δ (ppm):** 2.98 (1H, s, C≡C-*H*), 6.99 – 7.16 (9H, m, Ar*H*), 7.18 (1H, s, Ar*H*), 7.23 (1H, dd, *J* = 8.0, 1.2 Hz, Ar*H*), 7.71 (1H, d, *J* = 8.0 Hz, Ar*H*), 7.74 – 7.84 (3H, m, Ar*H*), 8.32 (2H, d, *J* = 13.9 Hz, Ar*H*).; **^{13}C{^{1}H} NMR (126 MHz, $CDCl_3$) δ (ppm):** 77.6 (C≡*C*-H), 83.6 (*C*≡C-H), 109.0 (Ar*C*), 109.0 (Ar*C*), 109.2 (Ar*C*), 113.0 (Ar*C*), 114.6 (Ar*C*), 114.9 (Ar*C*), 115.2 (Ar*C*), 119.8 (Ar*C*), 120.4 (Ar*C*), 120.59 (Ar*C*), 120.62 (Ar*C*), 120.8 (Ar*C*), 121.8 (Ar*C*), 122.0 (Ar*C*), 122.1 (Ar*C*), 123.8 (Ar*C*), 124.3 (Ar*C*), 124.4 (Ar*C*), 124.7 (Ar*C*), 125.7 (Ar*C*), 126.2 (Ar*C*), 126.6 (Ar*C*), 127.0 (Ar*C*), 135.5 (Ar*C*), 135.7 (Ar*C*), 137.8 (Ar*C*), 138.0 (Ar*C*), 138.2 (Ar*C*), 138.5 (Ar*C*), 138.9 (Ar*C*).

HRMS (ESI) $C_{34}H_{19}N_4$ $[M+H]^+$ found 483.1597, theoretical 483.1604 (– 1.5 ppm).

(4*S*,5*r*)-4-(2-bromo-9*H*-carbazol-9-yl)-5-(9*H*-carbazol-9-yl)phthalonitrile (115):

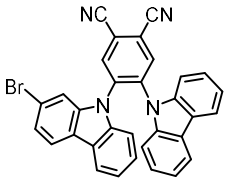

2-Bromo-9*H*-carbazole (246 mg, 1.0 mmol, 1.0 equiv.) was added to a flame dried round bottom flask and then evacuated and flushed with nitrogen three times. Anhydrous THF (3.3 mL) was added followed by portionwise addition of NaH (80 mg, 2.0 mmol, 60 wt%, 2.0 equiv.). The suspension was stirred at room temperature for 15 minutes. CzFPN (311 g, 1.0 mmol, 1.0 equiv.) was added. An immediate colour change from white to red was observed. The reaction was stirred for a further 3 h. The mixture was then poured onto cold H_2O (5 mL) and the aqueous phase extracted with CH_2Cl_2 (3 × 10 mL). The organic layers were combined, dried (Na_2SO_4) and concentrated *in vacuo*. Purification by silica column chromatography (30% to 60% CH_2Cl_2/Pet. ether) afforded **115** as a yellow solid (448 mg, 83%).

Mp 269-272 °C. **Rf:** 0.20 (50% CH_2Cl_2/Pet. ether). **Infra-red (ν max, cm^{-1}):** 2237 (C≡N, w), 1447, 752. **^{1}H NMR (400 MHz, $CDCl_3$) δ (ppm):** 6.79 (1H, dt, *J* = 8.3, 0.9 Hz, Ar*H*), 6.84 – 6.89 (1H, m, Ar*H*), 6.98 (1H, dd, *J* = 1.6, 0.5 Hz, Ar*H*), 7.02 – 7.06 (1H, m, Ar*H*), 7.14 (1H, dd, *J* = 8.3, 1.6 Hz, Ar*H*), 7.19 – 7.33 (6H, m, Ar*H*), 7.58 (1H, dd, *J* = 8.3, 0.5 Hz, Ar*H*), 7.75 – 7.81 (2H, m, Ar*H*), 7.88 (1H, dt, *J* = 7.5, 1.0 Hz, Ar*H*), 8.33 (2H, dd, *J* = 15.1, 0.4 Hz, Ar*H*); **^{13}C{^{1}H} NMR (126 MHz, $CDCl_3$) δ (ppm):** 108.7 (Ar*C*), 108.9 (Ar*C*), 109.0 (Ar*C*), 112.5 (Ar*C*), 114.39(Ar*C*), 114.41 (Ar*C*), 114.8 (Ar*C*), 115.2 (Ar*C*), 119.8 (Ar*C*), 120.4 (Ar*C*), 120.6 (Ar*C*), 120.7 (Ar*C*), 121.2 (Ar*C*), 121.6 (Ar*C*), 122.16 (Ar*C*), 122.22 (Ar*C*), 122.9 (Ar*C*), 123.7 (Ar*C*), 124.2 (Ar*C*), 124.4 (Ar*C*), 124.7 (Ar*C*), 125.9 (Ar*C*), 126.8 (Ar*C*), 126.9 (Ar*C*), 135.3 (Ar*C*), 135.6 (Ar*C*), 137.7 (Ar*C*), 137.8 (Ar*C*), 138.3 (Ar*C*), 138.3 (Ar*C*), 138.5 (Ar*C*), 138.6 (Ar*C*).

HRMS $C_{32}H_{17}BrN_4Na$ (ESI) $[M+Na]^+$ found 559.0522, theoretical 559.0529 (– 1.3 ppm).

(4*r*,5*S*)-4-(9*H*-carbazol-9-yl)-5-(2-((trimethylsilyl)ethynyl)-9*H*-carbazol-9-yl)phthalonitrile (116):

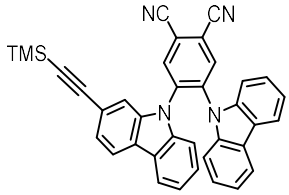

115 (430 mg, 0.8 mmol, 1.0 equiv.), $Pd(PPh_3)_4$ (48 mg, 0.04 mmol, 0.05 equiv.), CuI (25 mg, 0.02 mmol, 0.025 equiv.) were added to a flame dried round bottom flask. The mixture was then evacuated and flushed with nitrogen three times. In separate Schlenk flask THF/NEt_3 (3:1) was sparged with nitrogen for 15 minutes then added to the flask (14 mL). Then trimethylsilylacetylene (0.17 mL, 1.2 mmol, 1.5 equiv.) was added and the solution was heated to reflux and stirred for 16 h. The reaction was cooled to room temperature and concentrated *in vacuo.* Purification by silica column chromatography (50% CH_2Cl_2/Pet. ether) afforded **116** as a bright yellow solid (269 mg, 60%).

Mp 157-160 °C. **Rf:** 0.30 (50% CH_2Cl_2/Pet. ether). **Infra-red (ν max, cm^{-1}):** 2235 (C≡N, w), 2154 (C≡C, w), 1506, 748. **^{1}H NMR (400 MHz, $CDCl_3$) δ (ppm):** 0.26 (9H, s, Si(CH_3)$_3$), 6.99 – 7.16 (10H, m, Ar*H*), 7.22 (1H, dd, *J* = 8.0, 1.3 Hz, Ar*H*), 7.70 (1H, dd, *J* = 8.0, 0.7 Hz, Ar*H*), 7.75 – 7.85 (3H, m, Ar*H*), 8.33 (2H, d, *J* = 11.1 Hz, Ar*H*); **^{13}C{^{1}H} NMR (126 MHz, $CDCl_3$) δ (ppm):** 0.1 (Si(CH_3)$_3$), 94.5(C≡*C*-Si), 104.9(*C*≡C-Si), 109.1 (Ar*C*), 109.2 (Ar*C*), 112.7 (Ar*C*), 114.57 (Ar*C*), 114.61 (Ar*C*), 114.9 (Ar*C*), 115.1 (Ar*C*), 120.3 (Ar*C*), 120.6 (Ar*C*), 120.6 (Ar*C*), 120.8 (Ar*C*), 120.9 (Ar*C*), 121.8 (Ar*C*), 122.0 (Ar*C*), 122.1 (Ar*C*), 123.9 (Ar*C*), 124.3 (Ar*C*), 124.41 (Ar*C*), 124.44 (Ar*C*), 125.8 (Ar*C*), 126.2 (Ar*C*), 126.6 (Ar*C*), 126.9 (Ar*C*), 135.5 (Ar*C*), 135.7 (Ar*C*), 137.8 (Ar*C*), 138.1 (Ar*C*), 138.2 (Ar*C*), 138.2 (Ar*C*), 138.5 (Ar*C*), 139.0 (Ar*C*).

HRMS (ESI) $C_{37}H_{26}N_4NaSi$ [M+Na]$^+$ found 577.1811, theoretical 577.1819 (– 1.4 ppm).

4-(9*H*-carbazol-9-yl)-5-(2-(1-(3-phenoxypropyl)-1*H*-1,2,3-triazol-4-yl)-9*H*-carbazol-9-yl)phthalonitrile (117):

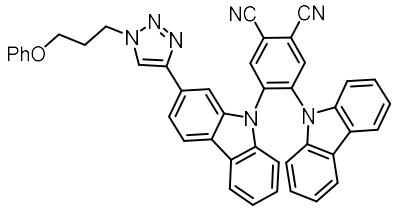

Based on a procedure reported by Neyyappadath *et al.*[87] **102** (97 mg, 0.2 mmol. 1.0 equiv.) and copper (I) iodide (3.8 mg, 0.02 mmol, 0.1 equiv.) were added to a flame dried flask then evacuated and flushed with nitrogen three times. (3-Azidopropoxy)benzene (53 mg, 0.3 mmol, 1.5 equiv.), anhydrous THF (4 mL) and *i*Pr_2NEt (0.12 mL, 0.7 mmol, 3.5 equiv.) were then added and the solution was stirred under nitrogen at room temperature for 24 h. The reaction was quenched with H_2O (5 mL) and the aqueous phase extracted with CH_2Cl_2 (3 × 10 mL). The combined organic phases were dried (Na_2SO_4) and concentrated *in vacuo*. Purification by silica column chromatography (0% to 20% EtOAc/CH_2Cl_2) to afford **117** as a yellow solid (97 mg, 73%)

Mp 130-133 °C. **Rf:** 0.25 (20% EtOAc/CH_2Cl_2). **Infra-red (ν max, cm^{-1})**: 2232 (C≡N, w), 1595, 1506, 1221. **^{1}H NMR (500 MHz, $CDCl_3$) δ (ppm):** 2.42 (2H, p, *J* = 6.4 Hz, C(2)H_2), 3.94 – 4.05 (2H, m, OC(3)H_2), 4.48 – 4.61 (2H, m, NC(1)H_2), 6.67 (1H, s, Ar*H*), 6.74 (1H, d, *J* = 8.3 Hz, Ar*H*), 6.82 (1H, t, *J* = 7.7 Hz, Ar*H*), 6.94 (2H, d, *J* = 8.5 Hz, Ar*H*), 6.97 – 7.04 (2H, m, Ar*H*), 7.16 – 7.22 (1H, m, Ar*H*), 7.24 – 7.38 (8H, m, Ar*H*), 7.58 (1H, d, *J* = 8.2 Hz, Ar*H*), 7.71 (1H, d, *J* = 7.7 Hz, Ar*H*), 7.78 (2H, d, *J* = 8.0 Hz, Ar*H*), 7.88 (1H, d, *J* = 7.6 Hz, Ar*H*), 8.34 (1H, d, *J* = 11.6 Hz, Ar*H*); **^{13}C{^{1}H} NMR (126 MHz, $CDCl_3$) δ (ppm):** 30.1 (*C*(2)H_2), 47.1 (N*C*(1)H_2), 63.9 (O*C*(3)H_2), 106.3 (Ar*C*), 108.9 (Ar*C*), 109.0 (Ar*C*), 109.3 (Ar*C*), 114.5 (Ar*C*), 114.6 (Ar*C*), 114.7 (Ar*C*), 119.6 (Ar*C*), 120.3 (Ar*C*), 120.4 (Ar*C*), 120.72 (Ar*C*), 120.74 (Ar*C*), 121.01, 121.29, 121.66, 121.69, 122.19, 123.73, 123.85, 124.47, 124.90, 126.19, 126.35, 126.76, 128.80, 129.70, 135.33, 135.61, 137.85, 137.89, 137.94, 138.33, 138.55, 139.01, 147.28, 158.45.

HRMS (ESI) $C_{43}H_{30}N_7O$ [M+H]$^+$ found 660.2497, theoretical 660.2506 (– 1.4 ppm).

2-phenylbenzo[*d*]imidazo[2,1-*b*]thiazole (118):

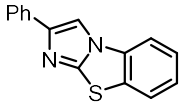

BTM (25.2 mg, 0.1 mmol, 1.0 equiv.) and 4CzIPN (1.6 mg, 0.002 mmol, 0.02 equiv.) were added to a vial. In a separate Schlenk flask CH_2Cl_2 was sparged with nitrogen for 10 minutes then added to the vial (1 mL). The solution was then irradiated with 456 nm LEDs using photoreactor set-up B for 16 h and then concentrated *in vacuo*. Purification by silica column chromatography (20% EtOAc/Pet. Ether) gave **118** as a colourless solid.

Mp 136-140 °C {Lit.[195] 142-146}. **Rf:** 0.15 (20% EtOAc/Pet. ether). **^{1}H NMR (400 MHz, $CDCl_3$) δ (ppm):** 7.28 – 7.37 (2H, m, *m*-Ph*H*), 7.40 – 7.48 (3H, m, *o*,p-Ph*H*), 7.60 (1H, ddd, *J* = 8.0 Hz, 1.3 Hz, 0.6 Hz, Ar*H*), 7.70 (1H, ddd, *J* = 8.0 Hz, 1.2 Hz, 0.6 Hz, Ar*H*), 7.86 – 7.90 (2H, m, Ar*H*), 7.97 (1H, s, NC(3)*H*).

Data matches that previously reported.[195]

((benzyloxy)carbonyl)proline (23):

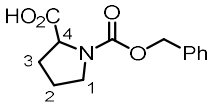

L-Proline (5.0 g, 43.5 mmol, 1.0 equiv.), $NaHCO_3$ (18.26 g, 217.4 mmol, 5.0 equiv.) and water (240 mL) were added to a round bottom flask and cooled to 0 °C. Benzyl chloroformate (6.8 mL, 47.8 mmol, 1.1 equiv.) was then added dropwise and the reaction stirred at room temperature for 16 h. The pH of the reaction mixture was adjusted to 2 using dilute hydrochloric acid. The reaction was extracted with EtOAc (3 × 50 mL). The organic layers were combined, washed with brine (50 mL), dried (Na_2SO_4) and concentrated *in vacuo*. Purification using silica column chromatography (25% to 50% EtOAc/Pet. Ether) gave **23** as a viscous oil that later solidified to a colourless solid (8.36 g, 77%).

Mp 77-81°C {Lit.[196] 78 °C}. **Rf:** 0.10 (20% EtOAc/Pet. ether). **^{1}H NMR (400 MHz, $CDCl_3$) δ (ppm):** 1.80 – 2.31 (4H, m, C(2)H_2 + C(3)H_2), 3.40 – 3.66 (2H, m, C(1)H_2), 4.35 (1H, m, C(2)*H*), 5.08 – 5.19 (2H, m, OCH_2), 7.22 – 7.37 (5H, m, Ph*H*).

Data matches that previously reported.[196]

diethyl 2-(1-((benzyloxy)carbonyl)pyrrolidin-2-yl)succinate (121):

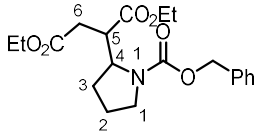

Based on a procedure reported by Speckmeier *et al*.[44] ((Benzyloxy)carbonyl)proline (37.4 mg, 0.15 mmol, 1.0 equiv.), K_2HPO_4 (31.4 mg, 0.18 mmol, 1.1 equiv.), 4CzIPN (2.4 mg, 0.003 mmol, 0.02 equiv.), diethyl maleate (25 µL, 0.17 mmol, 1.1 equiv.) and acetonitrile (3.75 mL) were added to a vial then sparged with nitrogen for 10 minutes. The reaction was stirred under 456 nm irradiation at room temperature for 20 h using photoreactor set-up B. Water (5 mL) was added then the mixture was extracted with CH_2Cl_2 (3 × 5 mL). The organic phases were combined, dried (Na_2SO_4) and concentrated *in vacuo*. Purification by silica column chromatography (10% to 20% EtOAc/Pet. Ether) afforded **121** as a pale-yellow oil (44 mg, 76%).

R_f: 0.2 (20% EtOAc/Pet. Ether). **^{1}H NMR (500 MHz, $CDCl_3$) δ (ppm):** 1.21 – 1.31 (6H, m, OCH_2CH_3), 1.75 – 2.00 (4H, m, C(2)H_2 + C(3)H_2), 2.26 – 2.55 (1H, m, C(6)H^AH^B), 2.69 – 2.86 (1H, m, C(6)H^AH^B), 3.21 – 3.36 (1H, m, C(5)*H*), 3.47 – 3.75 (2H, m, NC(1)H_2), 4.06 – 4.20 (4H, OCH_2CH_3), 4.31 – 4.36 (1H, m, NC(4)*H*), 5.07 – 5.27 (2H, OCH_2Ph), 7.30 – 7.45 (5H, m, Ph*H*).

GCMS $C_{11}H_{20}O_4$ $[M]^+$ found 377.3, theoretical 377.2, retention time = 10.5 min.

Data matches that previously reported.[44]

7.3 Experimental procedures and characterization for Chapter 3.

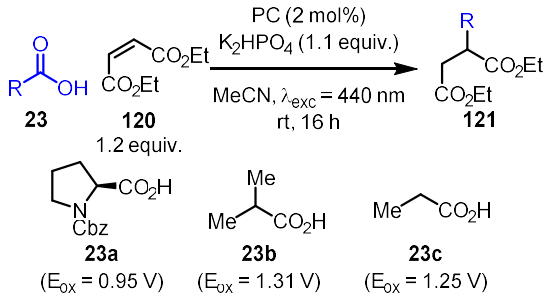

General Procedure A

Based on a procedure reported by Speckmeier *et al.*[44] carboxylic acid (0.15 mmol, 1.0 equiv.), K_2HPO_4 (31.4 mg, 0.17 mmol, 1.1 equiv.), photocatalyst (3.0 µmol, 0.02 equiv.) and diethyl maleate (27 µL, 0.18 mmol, 1.2 equiv.) were added to a vial in the photoreactor then evacuated and backfilled with nitrogen three times. In a separate Schlenk flask acetonitrile was sparged for 10 minutes and then added to the reaction vial (3 mL). The reaction was then stirred under 440 nm irradiation at room temperature for 16 h using photoreactor set-up A. Water (5 mL) was added then the mixture was extracted with CH_2Cl_2 (3 × 5 mL). The organic phases were combined and dried (Na_2SO_4) then concentrated *in vacuo*. Purification by silica column chromatography EtOAc/Pet. Ether afforded the desired products.

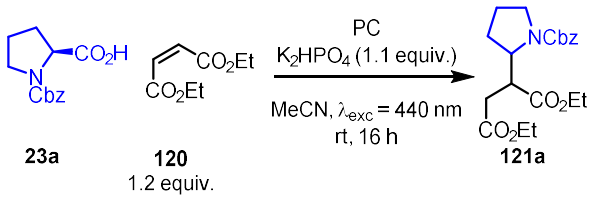

General Procedure B

A stock solution of the photocatalyst (0.5 mM) was prepared in acetonitrile and diluted to the appropriate concentrations for each catalyst loading (1 mol%, 0.5 mol%, 0.25 mol% and 0.1 mol%). The diluted solution was then added to a Schlenk flask and degassed *via* three freeze-pump-thaw cycles. ((Benzyloxy)carbonyl)proline (37.4 mg, 0.15 mmol, 1.0 equiv.), K_2HPO_4 (31.4 mg, 0.17 mmol, 1.1 equiv.) and diethyl maleate (27 µL, 0.18 mmol, 1.2 equiv.) were added to three vials in the

photoreactor then evacuated and backfilled with nitrogen three times. The photocatalyst solution was added (3 mL) and the solution stirred under 440 nm irradiation at room temperature for 16 h using photoreactor set-up A. Then 0.5 mL of a stock solution of 1,3,5-trimethoxybenzene in acetonitrile (0.1 M) was added and the solution stirred for 5 minutes. A sample was taken and concentrated *in vacuo* then dissolved in $CDCl_3$ to obtain an NMR yield.

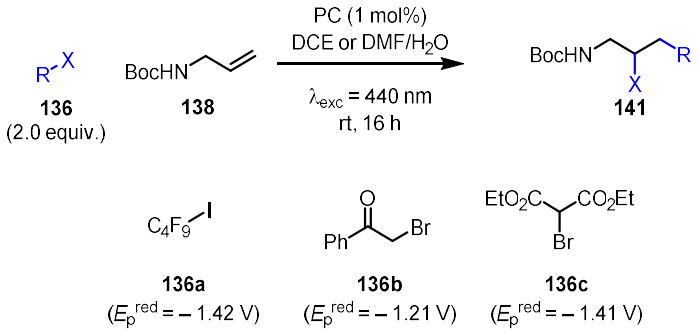

General Procedure C

Based on a procedure reported by Pirtsch *et al.*[110] *tert*-butyl allyl carbamate (39.3 mg, 0.25 mmol, 1.0 equiv.), alkyl halide (0.50 mmol, 2.0 equiv.) and the photocatalyst (2.5 µmol, 0.01 equiv.) were added to a vial in the photoreactor then evacuated and backfilled with nitrogen three times. In a separate Schlenk flask a DMF/H_2O (1:2) solution was sparged for 10 minutes and then added to the reaction vial (0.6 mL). The reaction was then stirred under 440 nm irradiation at room temperature for 16 h using photoreactor set-up A. Water (5 mL) and EtOAc (5 mL) were added, and the mixture was extracted with EtOAc (3 × 5 mL). The organic phases were combined and dried (Na_2SO_4) then concentrated *in vacuo*. Purification by silica column chromatography EtOAc/Pet. Ether afforded the desired products.

General Procedure D

Based on a procedure reported by Pirtsch *et al.*[110] *tert*-butyl allyl carbamate (47.2 mg, 0.30 mmol, 1.0 equiv.), alkyl halide (0.60 mmol, 2.0 equiv.) and the photocatalyst (3.0 µmol, 0.01 equiv.) were added to a vial in the photoreactor then evacuated and backfilled with nitrogen three times. In a separate Schlenk flask DCE was sparged for 10 minutes and then added to the reaction vial (1.5 mL). The reaction was then stirred under 440 nm irradiation at room temperature for 16 h using photoreactor

set-up A. The reaction was then transferred to a round-bottom flask and concentrated *in vacuo*. Purification by silica column chromatography EtOAc/Pet. Ether afforded the desired product.

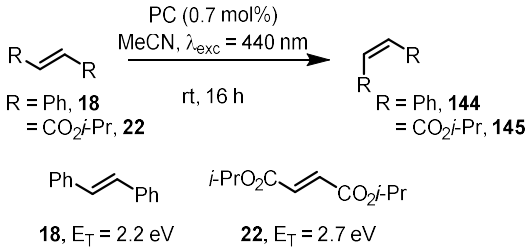

General Procedure E

Based on a procedure reported by Lu *et al*.[45] the alkene (0.40 mmol) and the photocatalyst (2.8 µmol) were added to a vial in the photoreactor then evacuated and backfilled with nitrogen three times. In a separate Schlenk flask acetonitrile was sparged for 20 minutes and then added to the reaction vial (2 mL). The reaction was then stirred under 440nm irradiation at room temperature for 16 h using photoreactor set-up A. The reaction mixture was then transferred to a round-bottom flask and concentrated *in vacuo*. Purification by silica column chromatography EtOAc/Pet. Ether afforded the desired products.

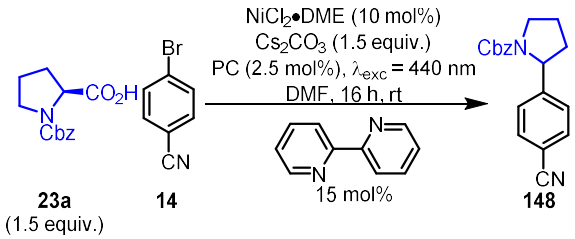

General Procedure F

Based on a procedure reported by Luo *et al*.[43] 4-bromobenzonitrile (27.3 mg, 0.15 mmol, 1.0 equiv.), *N*-Cbz-L-proline (56.1 mg, 0.225 mmol, 1.5 equiv.), Cs_2CO_3 (73.3 mg, 0.225 mmol, 1.5 equiv.), 2,2'-bipyridine (3.5 mg, 0.0225 mmol, 0.15 equiv.), $NiCl_2$•DME (3.3 mg, 0.015 mmol, 0.10 equiv.) and the photocatalyst (3.75 µmol, 0.01 equiv.) were all added to a vial in the photoreactor and evacuated then backfilled with nitrogen three times. In a separate Schlenk flask DMF was sparged for 10 minutes with nitrogen and then added to the reaction vial (3.5 mL). The reaction was then stirred under 440nm irradiation at room temperature for 16 h using photoreactor set-up A. Water (5 mL) and EtOAc (5 mL)

were added, and the mixture was extracted with EtOAc (3 × 5 mL). The organic phases were combined and dried (Na_2SO_4) then concentrated *in vacuo*. Purification by silica column chromatography EtOAc/Pet. Ether afforded the desired product.

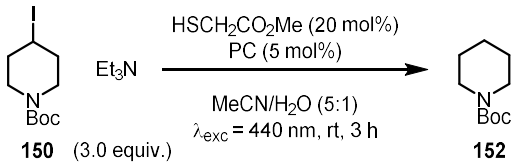

General Procedure G

Based on a procedure reported by Constantin *et al*.[119] 4-iodo-*N*-*boc*-piperidine (46.7 mg, 0.15 mmol, 1.0 equiv.) and the photocatalyst (7.50 µmol, 0.05 equiv.) were added to a vial in the photoreactor and evacuated then backfilled with nitrogen three times. In a separate Schlenk flask a solution of triethylamine (62.7 µl, 0.45 mmol, 3.0 equiv.), acetonitrile (1.25 mL) and water (0.25 mL) was degassed *via* three freeze-pump-thaw cycles then transferred to the vial in the photoreactor. In a separate vial methyl thioglycolate (2.7 µl, 30 µmol. 0.2 equiv.) was sparged with nitrogen for 5 minutes before being added to the vial in the photoreactor. The reaction was then stirred under 440nm irradiation at room temperature for 4 h using photoreactor set-up A. Then 0.5 mL of a stock solution of 1,3,5-trimethoxybenzene in acetonitrile (0.1 M) was added and the solution stirred for 5 minutes. A sample was taken and concentrated in vacuo then dissolved in $CDCl_3$ to obtain an NMR yield. A reference sample was prepared for comparison from piperidine using a known literature procedure.[197]

Sample Preparation for Kinetics Experiments:

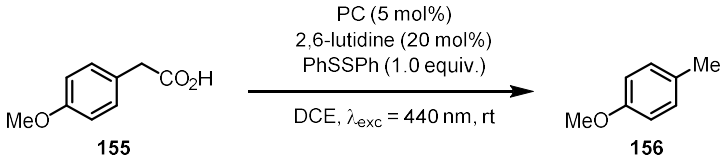

Based on a procedure reported by Cassani *et al*.[120] 4-methoxyphenylacetic acid (74.8 mg, 0.45 mmol, 1.0 equiv.), the photocatalyst (22.5 µmol, 0.05 equiv.), diphenyl disulfide (98.2 mg, 0.45 mmol, 1.0 equiv.) and biphenyl (17.3 mg, 0.11 mmol, 0.25 equiv.) were added to a Schlenk flask and evacuated then backfilled with nitrogen three times. Then 2,6-lutidine (10.4 µl, 90 µmol, 0.2 equiv.) and DCE (9.0

mL) were added, and the reaction mixture was sparged with nitrogen for 10 minutes. The reaction mixture was stirred until homogeneous then 4 mL portions were added to two separate vials in the photoreactor. The reactions were then stirred under 440 nm irradiation at room temperature using photoreactor set-up A, with samples taken regularly for GCMS analysis.

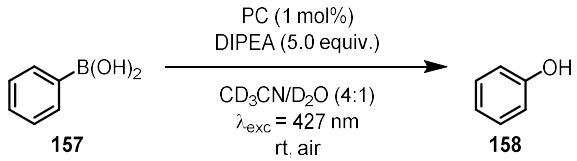

Based on a procedure reported by Pitre *et al*.[121] phenylboronic acid (73.2 mg, 0.60 mmol, 1.0 equiv.), photocatalyst (6 µmol, 0.01 equiv.), DIPEA (0.52 mL, 3.0 mmol, 5.0 equiv.), CD_3CN (8.0 mL) and D_2O (2.0 mL) were added to a schlenk a flask open to air and stirred under 427 nm irradiation at room temperature using photoreactor set-up B with samples taken regularly for ^1H NMR analysis.

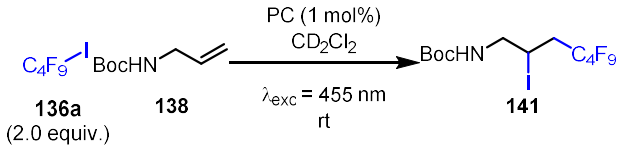

tert-Butyl allyl carbamate (70.1 mg, 0.45 mmol, 1.0 equiv.), 1,4-bis(trimethylsilyl)benzene (25.0 mg, 0.113 mmol, 0.25 equiv.) and the photocatalyst (4.5 µmol, 0.01 equiv.) were added to a vial and sealed with a septum then evacuated and backfilled with nitrogen three times. Then nonafluoro-1-iodobutane (0.15 mL, 0.90 mmol, 2.0 equiv.) was added. In a separate Schlenk flask CD_2Cl_2 was sparged for 15 minutes with DCM saturated nitrogen and then added to the vial (2.25 mL). The solution was stirred until complete dissolution then 0.45 mL transferred into an NMR tube. The coaxial insert is then quickly inserted, secured with parafilm and both wrapped in aluminium foil to block ambient light. The optical fibre is then inserted into the coaxial insert and secured in place with parafilm. Finally, the NMR loop and light source are turned on simultaneously.

Photodecomposition Study:

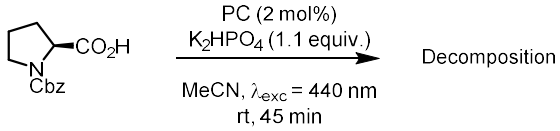

Following general procedure A with compound **23a** but in the absence of diethyl maleate and before and after 45 minutes of irradiation an asborbance measurement is taken.

Aqueous Photocatalysis:

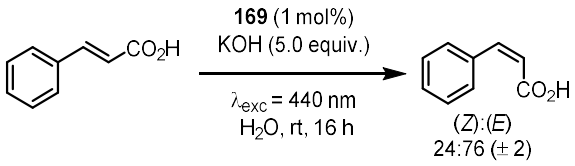

Based on a procedure reported by Bertrams *et al.*[141] cinnamic acid (14.8 mg, 0.10 mmol, 1.0 equiv.) and **169** (1.02 mg, 1.0 µmol, 1 mol%) were added to a vial in the photoreactor then evacuated and backfilled with nitrogen three times. In a separate schlenk flask a potassium hydroxide solution (0.1 M, 5 mL) was sparged with nitrogen for 15 minutes then added to the vial. Then, the reaction miture was stirred at room temperature under 440 nm irradiation for 16 h. The reaction mixture was then concentrated *in vacuo* and ^{1}H NMR analysis was used to determine the (*Z*):(*E*) ratio.

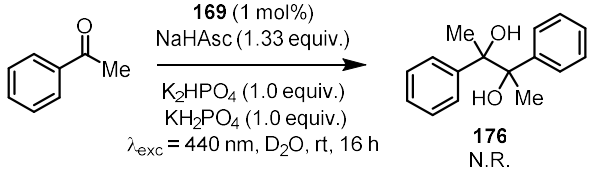

Based on a procedure reported by Bertrams *et al.*[141] acetophenone (8.8 µl, 75 µmol, 1.0 equiv.), NaHAsc (19.8 mg, 0.10 mmol, 1.33 equiv.), **169** (0.8 mg, 0.75 µmol, 1 mol%), K_2HPO_4 (13.1 mg, 75.0 µmol, 1.0 equiv.), KH_2PO_4 (10.2 mg, 75.0 µmol, 1.0 equiv.) and D_2O (5 mL) were added to a vial and sparged with nitrogen for 15 minutes. The reaction mixture was then stirred under 456 nm irradiation at room temperature using photoreactor set-up B for 16 h. Then an aliquot was taken for ^{1}H NMR analysis.

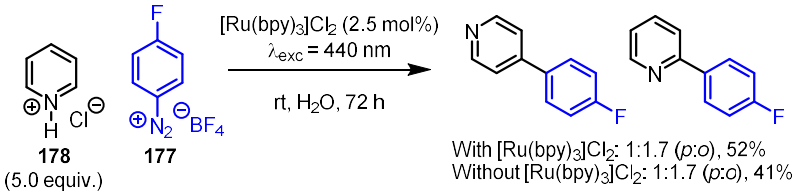

Based on a procedure reported by Xue *et al*.[198] **177** (63.0 mg, 0.30 mmol, 1.0 equiv.), **178** (173 mg, 0.15 mmol, 5.0 equiv.) and $[Ru(bpy)_3]Cl_2 \bullet 6H_2O$ (5.6 mg, 7.5 µmol, 2.5 mol%) were added to a vial in the photoreactor then evacuated and backfilled with nitrogen three times. In a separate schlenk flask, water was sparged with nitrogen for 15 minutes then added to the vial (1.0 mL). The reaction mixture was then stirred under 440 nm irradiation at room temperature for 72 h using photoreactor set-up A. Then the reaction was diluted with 5% aqeous sodium hydrogen carbonate (10 mL) and extracted with CH_2Cl_2 (3 × 10 mL). The organic layers were combined, washed with a saturated brine solution, dried (Na_2SO_4) and concentrated *in vacuo*. ^{19}F NMR analysis of the crude material with the addition of 1,3,5-trifluorobenzene (10.3 µl, 0.1 mmol, 0.33 equiv.) as an internal standard allowed for NMR yields to be collected.

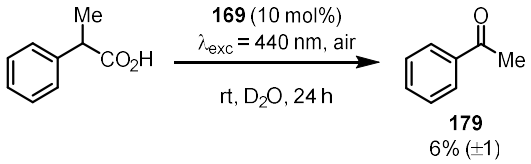

Based on a procedure reported by Xu *et al*.[147] **169** (6.1 mg, 6.0 µmol, 10 mol%) and D_2O (2.0 mL) were added to a vial. Separately 2-phenylpropanoic acid (9.0 mg, 60 µmol, 1.0 equiv.) was dissolved in MeCN (50 µL) and then added to the vial. Then the reaction mixture was stirred open to air under 440 nm irradiation for 24 h using photoreactor set-up A. Then sodium acetate (4.9 mg, 60 µmol, 1.0 equiv.) was added as an internal standard to allow for NMR yields to be collected.

diethyl 2-(1-((benzyloxy)carbonyl)pyrrolidin-2-yl)succinate (121a):

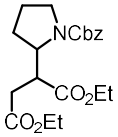

Synthesised using general procedure A.

Oil. **R_f:** 0.2 (20% EtOAc/Pet. Ether). **^{1}H NMR (500 MHz, $CDCl_3$) δ (ppm):** 1.21 – 1.31 (6H, m, OCH_2CH_3), 1.75 – 2.00 (4H, m, C(2)H_2 + C(3)H_2), 2.26 – 2.55 (1H, m, C(6)H^AH^B), 2.69 – 2.86 (1H, m, C(6)H^AH^B), 3.21 – 3.36 (1H, m, C(5)*H*), 3.47 – 3.75 (2H, m, NC(1)H_2), 4.06 – 4.20 (4H, OCH_2CH_3), 4.31 – 4.36 (1H, m, NC(4)*H*), 5.07 – 5.27 (2H, OCH_2Ph), 7.30 – 7.45 (5H, m, Ph*H*).

GCMS $C_{11}H_{20}O_4$ $[M]^+$ found 377.3, theoretical 377.2, retention time = 10.5 min.

Data matches that previously reported.[44]

diethyl 2-isopropylsuccinate (121b):

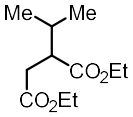

Synthesised using general procedure A.

Oil. **R_f:** 0.15 (10% EtOAc/Pet. Ether). **Infra-red (ν max, cm^{-1})**: 2964 (C-H), 1732 (C=O). **^{1}H NMR (500 MHz, $CDCl_3$) δ (ppm):** 0.92 (3H, d, *J* = 6.9 Hz, $(CH_3)^ACH(CH_3)^B$), 0.94 (3H, d, *J* = 6.9 Hz, $(CH_3)^ACH(CH_3)^B$), 1.25 (6H, dt, *J* = 7.7 Hz, 7.1 Hz, OCH_2CH_3), 1.99 (1H, m, $(CH_3)^ACH(CH_3)^B$), 2.35 – 2.45 (1H, m, CH^ACH^B), 2.66 – 2.77 (2H, m, CH^ACH^B + CH_2CH), 4.09 – 4.18 (4H, m, OCH_2CH_3). **^{13}C{^{1}H} NMR (126 MHz, $CDCl_3$) δ (ppm):** 14.1 (OCH_2CH_3), 14.2 (OCH_2CH_3), 19.6 ($CH(CH_3)_2$), 20.0 ($CH(CH_3)_2$), 30.1 ($CH(CH_3)_2$), 33.2 (C(3)CH_2), 47.5 (C(2)CH), 60.3 (OCH_2CH_3), 60.5 (OCH_2CH_3), 172.5 (COOEt), 174.3 (COOEt).

HRMS (EI) $C_{11}H_{20}O_4$ $[M]^+$ found 216.1361, theoretical 216.1356 (+2.3 ppm).

diethyl 2-ethylsuccinate (121c):

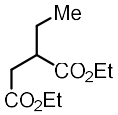

Synthesised using general procedure A.

Mixture with diethyl succinate and diethyl maleate. **R_f:** 0.10 (10% EtOAc/Pet. Ether). **^{1}H NMR (500 MHz, $CDCl_3$) δ (ppm):** 0.92 (3H, t, *J* = 7.5 Hz, CH_2CH_3), 1.25 (6H, m, OCH_2CH_3) 1.53 – 1.71 (2H, m, CH_2CH_3), 2.41 (1H, dd, *J* = 15.9 Hz, 4.6 Hz, CH^ACH^B), 2.66 – 2.81 (2H, m, CH^ACH^B + CH_2CH), 4.09 – 4.17 (4H, m, OCH_2CH_3).

GCMS $C_{11}H_{20}O_4$ $[M+H]^+$ found 203.2, theoretical 203.1, retention time = 4.5 min.

Data matches that previously reported.[199]

tert-butyl (4,4,5,5,6,6,7,7,7-nonafluoro-2-iodoheptyl)carbamate (136a):

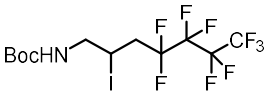

Synthesised using general procedure D.

Brown solid. **Mp** 67-69 °C {Lit.[200] 68-70 °C} **R_f:** 0.60 (40% EtOAc/Pet. Ether). **^{1}H NMR (400 MHz, $CDCl_3$) δ (ppm):** 1.46 (9H, s, $OC(CH_3)_3$), 2.69 – 2.95 (2H, m, CF_2CH_2), 3.41 – 3.52 (1H, m, $NHCH^ACH^B$), 3.54 – 3.66 (1H, m, $NHCH^ACH^B$), 4.31 – 4.43 (1H, m, CH_2CHCH_2), 4.96 (1H, s, NH). **^{19}F NMR (376 MHz, $CDCl_3$) δ (ppm):** -125.81 – - 125.95 (2F, m), -124.57 (2F q, *J* = 9.4 Hz), -113.32 (1F, t, *J* = 13.5 Hz), - 113.75 (1F, t, *J* = 13.5 Hz), -81.03 – -80.93 (3F, m).

Data matches that previously reported.[110]

tert-butyl (2-bromo-5-oxo-5-phenylpentyl)carbamate (136b):

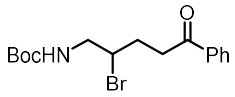

Synthesised using general procedure C.

Colourless Solid. **Mp** 112-114 °C **R_f:** 0.40 (40% EtOAc/Pet. Ether). **^{1}H NMR (400 MHz, $CDCl_3$) δ (ppm):** 1.45 (9H, s, OC(CH_3)$_3$), 2.11 – 2.29 (1H, m, C(O)CH^AH^B), 2.31 – 2.42 (1H, m, C(O)CH^AH^B) 3.10 – 3.36 (2H, m, C(O)CH_2CH_2), 3.44 – 3.57 (1H, m, NHCH^AH^B), 3.58 – 3.69 (1H, m, NHCH^AH^B), 4.17-4.36 (1H, m, NHCH_2CHBr), 5.03 (1H, s, NH), 7.48 (2H, td, J 7.6, 1.4, *m*-PhH), 7.55 – 7.61 (1H, m, *p*-PhH), 7.96 – 8.00 (2H, m, *o*-PhH).

Data matches that previously reported.[110]

diethyl 2-(2-bromo-3-((tert-butoxycarbonyl)amino)propyl)malonate (136c):

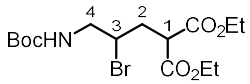

Synthesised using general procedure C.

Yellow oil. **Rf:** 0.40 (20% EtOAc/Pet. Ether). **^{1}H NMR (400 MHz, $CDCl_3$) δ (ppm):** 1.27 (6H, app. td, OCH_2CH_3, J = 7.1 Hz, 2.3 Hz), 1.44 (9H, C(CH_3)$_3$ s), 2.27 (1H, ddd, C(2)H^AH^B, J = 14.9 Hz, 10.1 Hz, 5.1 Hz), 2.47 (1H, ddd, C(2)H$^AH^B$, J = 14.9 Hz, 9.5 Hz, 3.7 Hz), 3.42 – 3.60 (2H, C(1)H + C(4)H^AH^B, m), 3.74 (1H, dd, C(4)H$^AH^B$, J = 9.5 Hz, 5.0 Hz), 4.12 (1H, q, C(3)H, J = 7.1 Hz), 4.17 – 4.27 (4H, OCH_2CH$_3$, m), 4.97 (1H, NH, br s). **^{13}C{^{1}H} NMR (126 MHz, $CDCl_3$) δ (ppm):** 14.0 (OCH$_2$CH$_3$), 14.1 (OCH$_2$CH$_3$), 28.3 (CCH$_3$), 34.6 (C(2)CH$_2$), 47.1 (C(3)CHBr), 50.2 (C(1)CH), 53.3 (C(4)CH$_2$), 61.76 (OCH$_2$) , 61.83 (OCH$_2$), 79.9 (OC(CH$_3$)$_3$), 155.6 (C(O)NH), 168.5 (COOEt), 168.9 (COOEt).

Data matches that previously reported.[110]

(*Z*)-Stilbene (144):

Synthesised using general procedure E.

Colourless oil. **Rf:** 0.3 (Hexane). **^{1}H NMR (400 MHz, $CDCl_3$) δ (ppm):** 6.61 (2H, s, *H*C=C*H*), 7.16 – 7.29 (10H, m, Ar*H*).

GCMS $C_{11}H_{20}O_4$ [M]$^+$ found 180.2, theoretical 180.1, retention time = 5.7 min.

Data matches that previously reported.[45]

Diisopropyl Fumarate (145):

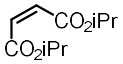

Synthesised using general procedure E.

Colourless oil. **Rf:** 0.2 (20% EtOAc/Pet. Ether). **^{1}H NMR (400 MHz, $CDCl_3$) δ (ppm):** 1.29 (12H, d, CH(C*H*$_3$)$_2$, *J* = 6.3 Hz), 5.12 (2H, p, C*H*(CH$_3$)$_2$ *J* = 6.3 Hz), 6.18 (2H, s, *H*C=C*H*).

GCMS $C_{11}H_{20}O_4$ [M+H]$^+$ found 201.2, theoretical 200.1, retention time = 4.4 min.

Data matches that previously reported.[201]

benzyl 2-(4-cyanophenyl)pyrrolidine-1-carboxylate (148):

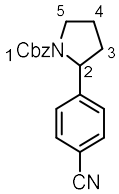

Synthesised using general procedure F.

Yellow oil. **Rf:** 0.2 (30% EtOAc/Pet. Ether). **^{1}H NMR (400 MHz, $CDCl_3$) δ (ppm):** 1.78 – 1.87 (1H, m, C(4)*H*^{A}H^B), 1.87 – 1.98 (2H, m, C(3)*H*^{A}H^B + C(4)H^A*H*^{B}), 2.30 – 2.47 (1H, m, C(3)H^A*H*^{B}), 3.60 – 3.76 (2H, m, C(5)*H*$_2$), 4.81 – 4.95 (1H, m, C(2)*H*), 4.95 – 5.21 (2H, m, CO$_2$C*H*$_2$), 6.89 (1H, d, *J* = 7.2 Hz, Ar*H*), 7.15 – 7.25 (3H, m, Ar*H*), 7.27 – 7.40 (3H, m, Ar*H*), 7.51 – 7.63 (2H, m, Ar*H*).

GCMS $C_{11}H_{20}O_4$ [M]$^+$ found 306.3, theoretical 306.1, retention time = 10.7 min.

Data matches that previously reported.[106]

***tert*-butyl piperidine-1-carboxylate (152):**

Synthesised using general procedure G.

Colourless oil. **Rf:** 0.2 (10% EtOAc/Pet. Ether) **^{1}H NMR (400 MHz, $CDCl_3$) δ (ppm):** 1.45 (9H, s. $(CH_3)_3$), 1.47 – 1.59 (6H, m, $CH_2CH_2CH_2CH_2CH_2$), 3.31 – 3.41 (4 H, m, CH_2NCH_2).

GCMS $C_{11}H_{20}O_4$ [M]$^+$ found 185.2, theoretical 185.1, retention time = 4.4 min.

Data matches that previously reported.[197]

Dimethyl 2,2'-(phenylazanediyl)dibenzoate (12):

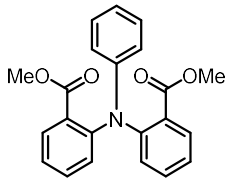

Based on a procedure reported by Hall *et al*.[37] aniline (2.28 mL, 25.0 mmol, 1.0 equiv.), methyl 2-iodobenzoate (11.0 mL, 75.0 mmol, 3.0 equiv.), copper powder (477 mg, 7.5 mmol, 0.3 equiv.), copper (I) iodide (333 mg, 1.75 mmol, 0.07 equiv.), K_2CO_3 (10.4 g, 75.0 mmol, 3.0 equiv.) and anhydrous di-*n*-butyl ether (25 mL) were added to a 3-neck flask under nitrogen. The reaction mixture was heated to reflux and stirred for 3 days. After cooling to room temperature, the reaction mixture was filtered through a pad of celite and washed through with CH_2Cl_2. The filtrate was then washed with water (3 × 50 mL). The organic layer was then dried (Na_2SO_4) and concentrated *in vacuo*. Purification by silica column chromatography (5% NEt_3, 15% EtOAc, 80% Hexane) afforded the desired product as a colourless solid (5.9 g, 65%).

Mp 139-141 °C {Lit.[37] 143-145 °C}. **R_f:** 0.1 (20% EtOAc/Hexane). **^{1}H NMR (400 MHz, $CDCl_3$) δ (ppm):** 3.41 (6H, s, OC*H*$_3$), 6.76 – 6.82 (2H, m, Ar*H*), 6.88 (1H, t, *J* = 7.3 Hz, Ar*H*), 7.18 (6H, dddd, *J* = 16.0 Hz, 8.6 Hz, 7.7 Hz, 1.5 Hz, Ar*H*), 7.44 (2H, ddd, *J* = 8.3 Hz, 7.3 Hz, 1.7 Hz, Ar*H*), 7.68 (2H, dd, *J* = 7.7 Hz, 1.7 Hz, Ar*H*).

Data matches that previously reported.[37]

DiKTa:

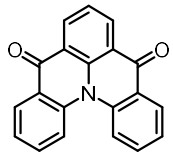

Based on a procedure reported by Hall *et al*.[37] **12** (1.80 g, 3.7 mmol, 1.0 equiv.), sodium hydroxide (739 mg, 18.5 mmol, 5.0 equiv.), EtOH (7.5 mL) and Water (7.5 mL) were added to a round bottom flask. The reaction mixture was then heated to reflux and stirred for 4 h. After cooling to room temperature the pH was adjusted to 1 by addition of dilute hydrochloric acid. The diacid precipitated from the solution and was collected through vacuum filtration then washed thoroughly with water and dried under vacuum. This solid was then suspended in CH_2Cl_2 (45 mL) under a nitrogen atmosphere. To the reaction mixture were added thionyl chloride (0.54 mL, 7.4 mmol, 2.0 equiv.) and DMF (several drops). The reaction mixture was then heated to reflux and stirred for 3 h. After the reaction cooled to room temperature, under a positive flow of nitrogen, aluminium chloride (4.93 g, 37 mmol, 10.0 equiv.) was added portionwise. The reaction mixture was then heated to reflux and stirred for 16 h. After the reaction mixture cooled to room temperature the reaction was quenched by dropwise addition of water with vigorous stirring. The resulting mixture was extracted with CH_2Cl_2 (3 × 50 mL). The organic fractions were combined and then concentrated *in vacuo*. The resulting yellow solid was then washed with MeOH and hexane to afford the desired product as a yellow solid (512 mg, 62%).

Mp 260-262 °C {Lit.[37] 257-260 °C}. **R_f:** 0.5 (50% EtOAc/Hexane). **^{1}H NMR (500 MHz, $CDCl_3$) δ (ppm):** 7.50 (2H, t, *J* = 7.5 Hz, Ar*H*), 7.65 (1H, t, *J* = 7.6 Hz, Ar*H*), 7.70 (2H, t, *J* = 7.9 Hz), 8.14 (2H, d, *J* = 8.5 Hz), 8.50 (2H, d, *J* = 7.8 Hz), 8.75 (2H, d, *J* = 8.0 Hz).

Data matches that previously reported.[37]

Dimethyl 2,2'-((4-iodophenyl)azanediyl)dibenzoate (165):

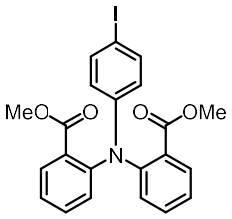

Based on a procedure reported by Sun *et al*.[131] **12** (2.0 g, 5.5 mmol, 1.0 equiv.) and MeCN (35 mL) were added to a round-bottom flask and stirred until mostly dissolved. Then *N*-iodosuccinimide (1.5g, 6.6 mmol, 1.2 equiv.) dissolved in MeCN (15 mL) was added dropwise. The reaction was stirred at room temperature for 16 h then quenched with 0.1 M sodium hydroxide (10 mL) and extracted with CH_2Cl_2 (30 mL). The organic layer was separated and washed with water (3 × 30 mL) then dried ($MgSO_4$) and concentrated *in vacuo*. Purification by silica column chromatography (10% EtOAc/Hexane) afforded the desired product as a colourless solid (2.3 g, 84%).

Mp 133-134 °C {Lit.[131] 130-131 °C}. **R_f:** 0.1 (20% EtOAc/Hexane). **^{1}H NMR (400 MHz, $CDCl_3$) δ (ppm):** 3.45 (6H, s, OC*H*$_3$), 6.46 – 6.52 (2H, m, Ar*H*), 7.16 – 7.23 (4H, m, Ar*H*), 7.37 – 7.46 (4H, m, Ar*H*), 7.69 (2H, dd, *J* = 8.2 Hz, 1.7 Hz, Ar*H*).

Data matches that previously reported.[131]

3-Iodoquinolino[3,2,1-de]acridine-5,9-dione (162):

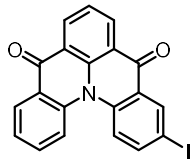

Based on a procedure reported by Sun *et al*.[131] **165** (1.80 g, 3.7 mmol, 1.0 equiv.), sodium hydroxide (739 mg, 18.5 mmol, 5.0 equiv.), EtOH (7.5 mL) and Water (7.5 mL) were added to a round bottom flask. The reaction mixture was then heated to reflux and stirred for 16 h. After cooling to room temperature the pH was adjusted to 1 by addition of dilute hydrochloric acid. The diacid precipitated from the solution and was collected through vacuum filtration then washed thoroughly with water and dried under vacuum. This solid was then suspended in CH_2Cl_2 (45 mL) under a nitrogen atmosphere. To the reaction mixture were added oxalyl chloride (0.54 mL, 7.4 mmol, 2.0 equiv.) and DMF (several drops). The reaction mixture was then heated to reflux and stirred for 3 h. After the reaction cooled to room temperature, under a positive flow of nitrogen, aluminium chloride (4.93 g, 37 mmol, 10.0 equiv.) was added portionwise. The reaction mixture was then heated to reflux and stirred for 4 h. After the reaction mixture cooled to room temperature the reaction was quenched by dropwise addition of water with vigorous stirring. The resulting mixture was extracted with CH_2Cl_2 (3 × 50 mL). The organic fractions were combined, dried (Na_2SO_4) and then concentrated *in vacuo*. The resulting yellow-brown solid was then washed with hexane and purified further using silica column chromatography (50% EtOAc/Hexane).

Mp 280 °C (decomp.) {Lit.[131] 284-285 °C}. **R_f:** 0.50 (50% EtOAc/Hexane). **^{1}H NMR (400 MHz, $CDCl_3$) δ (ppm):** 7.47 – 7.56 (1H, m, Ar*H*), 7.63 – 7.75 (2H, m, Ar*H*), 7.88 – 7.99 (2H, m, Ar*H*), 8.03 – 8.09 (1H, m, Ar*H*), 8.49 (1H, dd, *J* = 8.0 Hz, 1.7Hz, Ar*H*), 8.74 (2H, ddd, *J* = 8.2 Hz, 7.6 Hz, 1.7 Hz), 8.80 (1H, d, *J* = 2.1 Hz, Ar*H*).

Data matches that previously reported.[131]

4-Boronobenzoic acid (166):

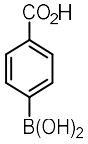

Based on a procedure reported by Dong *et al*.[132] 4-(methylphenyl)boronic acid (6.80 g, 50.0 mmol, 1.0 equiv.) and 1 M sodium hydroxide (150 mL) were added to a mixture of $KMnO_4$ (23.8 g, 150.0 mmol, 3.0 equiv.) and tetrabutyl ammonium bromide (1.0 g, 4 mmol, 0.06 equiv.) in water (500 mL). The reaction mixture was stirred at room temperature for 24 h. Then EtOH (100 mL) was added, and the reaction mixture was stirred for 1 h. The reaction mixture was then filtered, and the pH of the filtrate adjusted to 1 using concentrated hydrochloric acid. The resulting precipitate was collected through vacuum filtration and dried under vacuum to afford the desired product as a colourless solid (6.1 g, 73%).

Mp 216-218 °C {Lit.[202] 219-220 °C}. **^{1}H NMR (400 MHz, DMSO-d_6) δ (ppm):** 7.85 – 7.91 (4H, m, Ar*H*), 8.27 (2H, s, B(O*H*)$_2$), 12.93 (1H, s, CO_2H).

Data matches that previously reported.[202]

(4-(Methoxycarbonyl)phenyl)boronic acid (164):

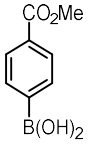

Based on a procedure reported by Kühl *et al*.[133] thionyl chloride (2.0 mL, 27.0 mmol, 3.0 equiv.) was added dropwise to a solution of **166** (1.5 g, 9.0 mmol, 1.0 equiv.) in dry MeOH (40 mL) at 0 °C. The reaction mixture was then heated to 50 °C and stirred for 5 h. After the reaction mixture cooled to room temperature it was concentrated *in vacuo* and purified through recrystallization (MeOH) to afford the desired compound as a colourless solid (1.5 g, 92%).

Mp 234-237 °C {Lit.[203] 232-233 °C}. **^{1}H NMR (400 MHz, DMSO- d_6) δ (ppm):** 3.85 (3H, s, CO_2CH_3), 7.88 – 7.93 (4H, m, Ar*H*).

Data matches that previously reported.[203]

Methyl 4-(5,9-dioxo-5,9-dihydroquinolino[3,2,1-de]acridin-3-yl)benzoate (168):

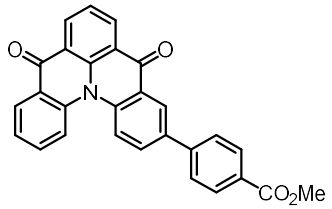

162 (42.3 mg, 0.10 mmol, 1.0 equiv.), **164** (36.0 mg, 0.20 mmol, 2.0 equiv.) and $Pd(PPh_3)_4$ (5.8 mg, 5 µmol, 0.05 equiv.) were added to a Schlenk flask and evacuated then back filled with nitrogen three times. Then Na_2CO_3 (2 M, 0.15 mL) and DMF (2.5 mL) were added. The reaction mixture was then heated to 120 °C and stirred for 48 h. After the reaction mixture cooled to room temperature it was diluted with CH_2Cl_2 (20 mL) and washed with water (20 mL). The aqueous layers were then extracted with CH_2Cl_2 (3 × 15 mL). The organic layers were combined and dried (Na_2SO_4) then concentrated *in vacuo*. The resulting yellow solid was washed with EtOAc to afford the desired product as a yellow solid (32 mg, 74%).

Mp 298-299 °C. **^{1}H NMR (500 MHz, CD_2Cl_2) δ (ppm):** 3.94 (3H, s, CO_2CH_3), 7.53 (1 H, ddd, *J* = 8.0 Hz, 7.1 Hz, 0.9 Hz), 7.67 (1H, t, *J* = 7.6 Hz, Ar*H*), 7.76 (1H, ddd, *J* = 8.7 Hz, 7.1 Hz, 1.7 Hz, Ar*H*), 7.84 – 7.88 (2H, m, Ar*H*), 8.01 (1H, dd, *J* = 8.8 Hz, 2.4 Hz, Ar*H*), 8.13 – 8.20 (3H, m, Ar*H*), 8.25 (1H, d, *J* = 8.8 Hz, Ar*H*), 8.46 (1H, dd, *J* = 7.9 Hz, 1.7 Hz, Ar*H*), 8.69 – 8.75 (3H, m, Ar*H*). **^{13}C{^{1}H} NMR (126 MHz, CD_2Cl_2) δ (ppm):** 52.1 (CO_2CH_3), 120.4 (Ar*C*), 121.2 (Ar*C*), 123.5 (Ar*C*), 123.6 (Ar*C*), 123.7 (Ar*C*), 125.3 (Ar*C*), 125.6 (Ar*C*), 126.5, 126.7 (Ar*C*), 126.9 (Ar*C*), 127.5 (Ar*C*), 129.7 (Ar*C*), 130.2 (Ar*C*), 131.3 (Ar*C*), 132.0 (Ar*C*), 132.6 (Ar*C*), 132.7 (Ar*C*), 132.9 (Ar*C*), 136.5 (Ar*C*), 139.5 (Ar*C*), 139.8 (Ar*C*), 143.2 (Ar*C*), 178.3 (*C*=O).

HRMS (ESI) $C_{28}H_{18}NO_4$ $[M+H]^+$ found 432.1214, theoretical 432.1236 (-5.1 ppm).

4-(5,9-Dioxo-5,9-dihydroquinolino[3,2,1-de]acridin-3-yl)benzoic acid (161):

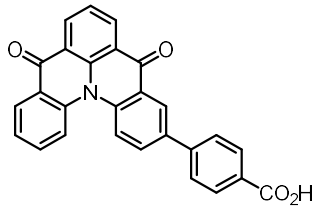

168 (0.75 g, 1.74 mmol, 1.0 equiv.) and potassium hydroxide (5.0 g, 90 mmol, excess) were suspended in THF/MeOH (1:1, 180 mL). The reaction mixture was heated to reflux and stirred for 2 h. After the reaction cooled to room temperature the pH was adjusted to 1 using dilute hydrochloric acid. The resulting orange precipitate was collected through gravity filtration on filter paper then dried in air overnight to afford the desired compound as an orange solid (0.68 g, 94%).

Mp 340 °C (decomp.). **^{1}H NMR (500 MHz, CD_3OD) δ (ppm):** 7.58 (1H, ddd, *J* = 7.9 Hz, 7.1, 0.9, Ar*H*), 7.74 (1H, t, *J* = 7.6 Hz, Ar*H*), 7.79 – 7.82 (2H, m, Ar*H*), 7.84 (1H, ddd, *J* = 8.7 Hz, 7.1 Hz, 1.7 Hz, Ar*H*), 8.09 – 8.13 (2H, m, Ar*H*), 8.15 (1H, dd, *J* = 8.9 Hz, 2.4 Hz, Ar*H*), 8.32 (2H, dd, *J* = 10.2 Hz, 8.7 Hz, Ar*H*), 8.45 (1 H, dd, *J* = 8.0 Hz, 1.6 Hz, Ar*H*), 8.70 (1H, d, *J* = 2.3 Hz, Ar*H*), 8.74 (2H, ddd, *J* = 8.7 Hz, 7.6 Hz, 1.7 Hz, Ar*H*).**^{13}C{^{1}H} NMR (126 MHz, CD_3OD) δ (ppm):** 120.7 (Ar*C*), 121.3 (Ar*C*), 123.5 (Ar*C*), 124.4 (Ar*C*), 125.2 (Ar*C*), 125.9 (Ar*C*), 126.9 (Ar*C*), 129.8 (Ar*C*), 131.5 (Ar*C*), 132.5 (Ar*C*), 132.6 (Ar*C*), 133.1 (Ar*C*). A limited number of resonances were observed in the ^{13}C NMR due to the poor solubility of this compound.

HRMS (ESI) $C_{27}H_{15}NO_4Na$ $[M+Na]^+$ found 440.0893, theoretical 440.0899 (-1.4 ppm).

4-(5,9-Dioxo-5,9-dihydroquinolino[3,2,1-de]acridin-3-yl)-N-hexylbenzamide (167):

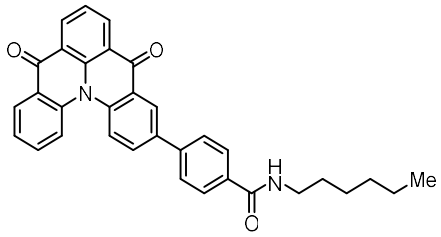

161 (41.7 mg, 0.10 mmol, 1.0 equiv.), HOBt (30.6 mg, 0.20 mmol, 2.0 equiv.), hexan-1-amine (29.1 µl, 0.22 mmol, 2.2 equiv.) and DMF (5.0 mL) were all added to a round bottom flask and cooled to 0 °C. Then EDCI (39.3 mg, 0.21 mmol, 2.1 equiv.) was added portionwise and the reaction mixture was stirred for 1 h. The reaction mixture was then allowed to warm to room temperature and stirred for 16 h. The resulting yellow precipitate was collected using vacuum filtration and washed with water and EtOAc to afford the desired product as a yellow solid (46.0 mg, 92%).

Mp 207-209 °C. **^{1}H NMR (500 MHz, CD_2Cl_2) δ (ppm):** 0.89 – 0.93 (3H, m, CH_3), 1.35 (4H, dp, *J* = 7.3 Hz, 3.2 Hz, CH_2CH_2CH$_3$), 1.39 – 1.45 (2H, m, HNCH$_2$CH$_2$CH_2), 1.61 – 1.68 (2H, m, HNCH$_2$CH_2), 3.43 – 3.48 (2H, m, HNCH_2), 6.32 (1H, t, *J* = 5.7 Hz, *H*N), 7.51 (1H, ddd, *J* = 8.0 Hz, 7.1 Hz, 0.9 Hz), 7.65 (1H, t, *J* = 7.6 Hz), 7.74 (1H, ddd, *J* = 8.7 Hz, 7.1 Hz, 1.7 Hz), 7.80 – 7.84 (2H, m), 7.85 – 7.90 (2H, m), 7.97 (1H, dd, *J* = 8.8 Hz, 2.4 Hz), 8.16 (1H, d, *J* = 8.5 Hz), 8.21 (1 H, d, *J* 8.8), 8.44 (1 H, dd, *J* 7.9, 1.7), 8.67 – 8.71 (3 H, m).**^{13}C{^{1}H} NMR (126 MHz, CD_2Cl_2) δ (ppm):** 13.8 (*C*H$_3$), 22.6 (*C*H$_2$CH$_3$), 26.7 (*C*H$_2$CH$_2$CH$_3$), 29.7 (*C*H$_2$CH$_2$CH$_2$CH$_3$), 31.6 (HNCH$_2$*C*H$_2$), 40.1 (HN*C*H$_2$), 120.4 (Ar*C*), 121.1 (Ar*C*), 123.4 (Ar*C*), 123.5 (Ar*C*), 123.6 (Ar*C*), 125.3 (Ar*C*), 126.4 (Ar*C*), 126.6 (Ar*C*), 126.9 (Ar*C*), 127.5 (Ar*C*), 127.6 (Ar*C*), 131.2 (Ar*C*), 132.6 (Ar*C*), 132.7 (Ar*C*), 132.8 (Ar*C*), 134.4 (Ar*C*), 136.5 (Ar*C*), 139.2 (Ar*C*), 139.3 (Ar*C*), 139.7 (Ar*C*), 141.5 (Ar*C*), 166.6 (*C*O$_2$NH), 178.3 (*C*=O).

HRMS (ESI) $C_{27}H_{15}NO_4Na$ [M+Na]$^+$ found 501.2173, theoretical 501.2178 (-1.0 ppm).

MSN-DiKTa/SBA-DiKTa:

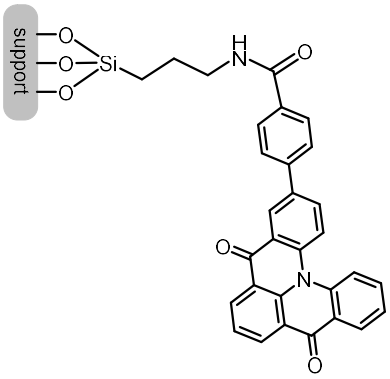

161 (1.0 equiv.) was dissolved in DMF (10 mL per 50 mg of MS-AP). Then DMAP (3.1 equiv.) and EDC (3.4 equiv.) were added, and the mixture was stirred at room temperature for 15 minutes. Finally, the MS-AP (1.0 equivalent in N) was added, and the reaction was stirred for 24 h. Then, the crude solid was collected through vacuum filtration and washed with DMF three times, EtOAc three times and Et_2O three times. The resulting material was dried under vacuum for 24 h to afford the desired products.

MSN-DiKTa: 0.295 mmol **DiKTa**/g of material.

SBA-DiKTa: 0.307 mmol **DiKTa**/g of material.

dimethyl 6,6'-((4-bromophenyl)azanediyl)bis(3-bromobenzoate) (172):

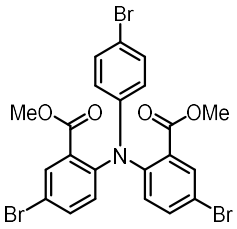

Based on a procedure reported by Hall *et al*.[37] **12** (3.0 g, 8.3 mmol, 1.0 equiv.) and CH_2Cl_2 (75 mL) were added to a round bottom flask and cooled to 0 °C. Bromine (1.3 mL, 25.0 mmol, 3.0 equiv.) was added dropwise and the reaction was stirred at 0 °C for 1 h. Then a 10% sodium hydroxide solution (50 mL) was added. The organic layer was separated, washed with water (3 × 50), dried (Na_2SO_4) and concentrated *in vacuo*. Purification by hexane trituration afforded the desired product as a pale yellow solid (4.1 g, 82%).

Mp 132-133 °C {Lit.[37] 134-136 °C}. **R_f:** 0.4 (10% EtOAc/Hexane) **^{1}H NMR (400 MHz, $CDCl_3$) δ (ppm):** 3.46 (6H, s, CO_2CH_3), 6.57 – 6.62 (2H, m, Ar*H*), 7.05 (2H, d, *J* = 8.6 Hz, Ar*H*), 7.22 – 7.25 (2H, m, Ar*H*), 7.53 (2H, dd, *J* = 8.6 Hz, 2.5 Hz, Ar*H*), 7.81 (2H, d, *J* = 2.4 Hz, Ar*H*).

Data matches that previously reported.[37]

Br_3DiKTa:

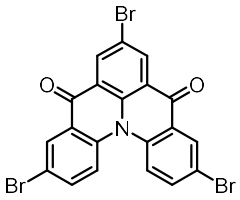

Based on a procedure reported by Hall *et al*.[37] **172** (1.80 g, 3.7 mmol, 1.0 equiv.), sodium hydroxide (739 mg, 18.5 mmol, 5.0 equiv.), EtOH (7.5 mL) and Water (7.5 mL) were added to a round bottom flask. The reaction mixture was then heated to reflux and stirred for 16 h. After cooling to room temperature the pH was adjusted to 1 by addition of dilute hydrochloric acid. The diacid precipitated from the solution and was collected through vacuum filtration then washed thoroughly with water and dried under vacuum. This solid was then suspended in CH_2Cl_2 (45 mL) under a nitrogen atmosphere. To the reaction mixture were added oxalyl chloride (0.54 mL, 7.4 mmol, 2.0 equiv.) and DMF (several drops). The reaction mixture was then heated to reflux and stirred for 3 h. After the reaction cooled to room temperature, under a positive flow of nitrogen, aluminium chloride (4.93 g, 37 mmol, 10.0 equiv.) was added portionwise. The reaction mixture was then heated to reflux and stirred for 4 h. After the reaction mixture cooled to room temperature the reaction was quenched by dropwise addition of water with vigorous stirring. The resulting mixture was diluted with CH_2Cl_2 (100 mL), and the organic layer extracted. The remaining aqueous layer was extracted further with CH_2Cl_2 (3 × 50 mL) to transfer the insoluble yellow product completely into the organic layer. The organic fractions were combined and then concentrated *in vacuo* but not to dryness. The resulting suspension was filtered, and the yellow solid was then washed with methanol and hexane to afford the desired product as a yellow solid (0.85g, 38%).

Mp 361-364 °C (decomp.) {Lit.[37] 364 °C (decomp.)}. **^{1}H NMR (500 MHz, $CDCl_3$) δ (ppm):** 7.83 (2H, dd, *J* = 9.0 Hz, 2.4 Hz, Ar*H*), 7.97 (1H, d, *J* = 9.0 Hz, Ar*H*), 8.62 (1H, d, *J* = 2.4 Hz, Ar*H*), 8.83 (1H, s, Ar*H*).

Data matches that previously reported.[37]

Mes_3DiKTa:

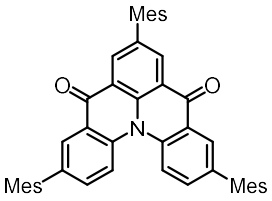

Based on a procedure reported by Hall *et al*.[37] **Br_3DiKTa** (0.3 g, 0.56 mmol, 1.0 equiv.), mesitylboronic acid (0.55 g, 3.4 mmol, 6.0 equiv.), benzene (16 mL) and sodium hydroxide (4.8 mL, 2 M) were added to a three-necked flask. The reaction mixture was sparged with nitrogen for 20 minutes. Then, under a positive flow of nitrogen, $Pd(PPh_3)_4$ (97.4 mg, 84 µmol, 0.15 equiv.) was added and the solution was heated to reflux and stirred for 16 h. After the reaction had cooled to room temperature it was diluted with EtOAc (100 mL). The organic layer was washed with water (3 × 50 mL), dried (Na_2SO_4) and concentrated *in vacuo*. Purification by silica column chromatography (10% EtOAc/Hexane) and a subsequent trituration with MeOH, afforded the desired product as a yellow solid (175 mg, 48%).

Mp 240-243 °C {Lit.[37] 249 °C}. **R_f:** 0.5 (10% EtOAc/Hexane). **^{1}H NMR (400 MHz, $CDCl_3$) δ (ppm):** 2.01 – 2.15 (18H, m, *o*-CH_3), 2.34 – 2.39 (9H, m, *p*-CH_3), 6.99 (6H, d, *J* = 5.9 Hz Ar*H*), 7.55 (2H, dd, *J* = 8.7 Hz, 2.1 Hz, Ar*H*), 8.32 – 8.35 (4H, m, Ar*H*), 8.60 (2H, s, Ar*H*).

Data matches that previously reported.[37]

Hexamethyl 5,5',5''-(5,9-dioxo-5,9-dihydroquinolino[3,2,1-de]acridine-3,7,11-triyl)triisophthalate (173):

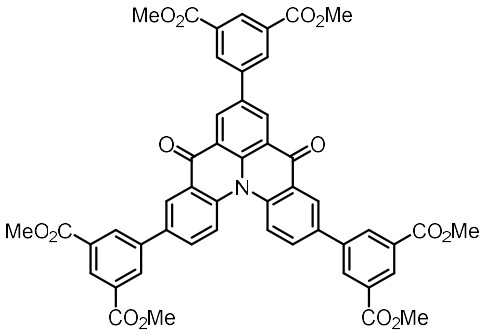

Based on a procedure reported by Ye *et al*.[143] dimethyl 5-bromoisophthalate (5.0 g, 18.3 mmol, 1.0 equiv.), B_2Pin_2 (5.6 g, 22.0 mmol, 1.2 equiv.), potassium acetate (5.4 g, 54.9 mmol, 3.0 equiv.) and DMF (100 mL) were added to a two-neck flask under nitrogen. $Pd(dppf)Cl_2$ (536 mg, 0.73 mmol, 0.04 equiv.) was then added and the reaction mixture was heated to reflux and stirred for 24 h. After the reaction mixture cooled to room temperature it was quenched with saturated aqueous ammonium chloride and extracted with CH_2Cl_2 (3 × 100 mL). The organic layers were then combined, dried (Na_2SO_4) and concentrated *in vacuo*. Purification by silica column chromatography (5% EtOAc/Hexane) afforded the desired product as a colourless solid, which was then taken onto the next step without further characterization.

Br_3DiKTa (200.0 mg, 0.37 mmol, 1.0 equiv.), **170** (395.7 mg, 1.4 mmol, 3.3 equiv.) and $Pd(PPh_3)_4$ (43.3 mg, 37.5 µmol, 0.10 equiv.) were added to a Schlenk flask and evacuated then back filled with nitrogen three times. Then Na_2CO_3 (0.75 M, 5 mL, 10.0 equiv.) and THF (15 mL) were added. The reaction mixture was then heated to reflux and stirred for 24 h. After the reaction mixture cooled to room temperature it was diluted with CH_2Cl_2 (20 mL) and washed with water (20 mL). The aqueous layer was then extracted with CH_2Cl_2 (3 × 15 mL). The organic layers were combined and dried (Na_2SO_4) then concentrated *in vacuo*. The resulting yellow solid was washed with EtOAc to afford the desired product as a yellow solid (260 mg, 79%).

Mp 385-387 °C (decomp.). **^{1}H NMR (400 MHz, $CDCl_3$) δ (ppm):** 4.03 (18H, s, CO_2CH_3), 8.07 (2H, dd, *J* = 8.8 Hz, 2.4 Hz, Ar*H*), 8.32 (2H, d, *J* = 8.8 Hz, Ar*H*), 8.61 (4H, d, *J* = 1.6 Hz, Ar*H*), 8.67 (2H, d, *J* = 1.6 Hz,

Ar*H*), 8.74 (3H, dt, *J* = 8.1 Hz, 1.6 Hz, Ar*H*), 8.82 (2H, d, *J* = 2.3 Hz, Ar*H*), 9.07 (2H, s, Ar*H*); ^{13}C NMR data could not be obtained due to poor solubility of this compound.

HRMS (ESI) $C_{27}H_{15}NO_4Na$ [M+Na]$^+$ found 874.2130, theoretical 874.2136 (-0.7 ppm).

Sodium 5,5',5''-(5,9-dioxo-5,9-dihydroquinolino[3,2,1-de]acridine-3,7,11-triyl)triisophthalate (169):

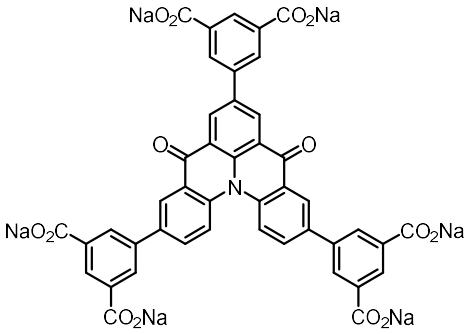

173 (80 mg, 92 µmol, 1.0 equiv.), sodium hydroxide (2 mL, 2 M, excess), THF (4 mL) and MeOH (4 mL) were added to a round bottom flask. The reaction mixture was heated to reflux and stirred for 16 h. The resulting orange precipitate was collected through vacuum filtration and washed thoroughly with THF and MeOH to afford the desired product as an orange solid (84 mg, 99%).

Mp 275-280 °C (decomp.). **^{1}H NMR (500 MHz, D_2O) δ (ppm):** 8.12 – 8.50 (15H, m, Ar*H*), 8.66 – 8.72 (1H, m), 9.04 (1H, s (br)); ^{13}C NMR data could not be obtained due to poor solubility of this compound.

HRMS (ESI) $C_{44}H_{18}NNa_6O_{14}$ $[M+H]^+$ found 922.0108, theoretical 922.0087 (+2.3 ppm).

7.3.1 Cost Comparison of DiKTa and 4CzIPN

4CzIPN:

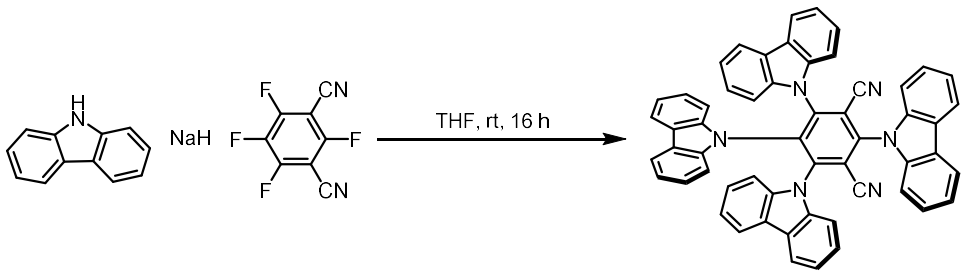

Chemical	Equivalents	Mass / g	Cost / £
Carbazole	5	1.67	0.47
NaH	7.5	0.6	0.29
Tetrafluoroisophthalonitrile	1	0.4	5.44
4CzIPN	-	1.5	6.2

Total cost / g = (0.47+0.29+5.44)/1.5 = £4.13

Total cost / mmol = (4.13*788.27)/1000 = £3.26

[a]250g bottle from Sigma. [b]100g bottle from Sigma. [c]5g bottle from Fluorochem. Prices as of 12/05/2022.

DiKTa:

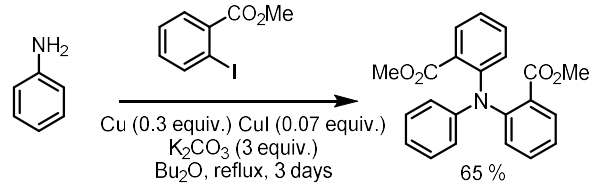

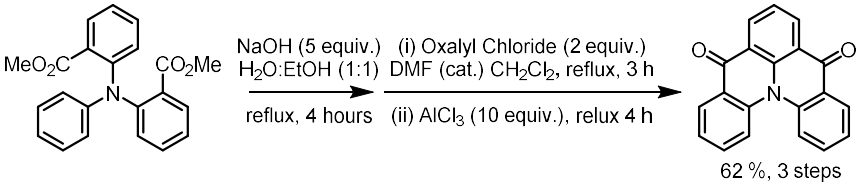

First step:

Chemical	Equivalents	Mass / g	Cost / £
Aniline	1	2.33	0.08[a]
Cu (powder)	0.3	0.48	0.07[b]
Cu(I)I	0.07	0.33	0.06[c]
K_2CO_3 (anhydrous)	3	10.4	0.31[d]
Bu_2O (anhydrous)	Solvent	19.3	2.53[e]
Methyl 2-iodobenzoate	3	19.7	3.94[f]
Diester	-	5.9	6.99

Total cost / g = (0.08+0.07+0.06+0.31+2.53+3.94)/5.9 = £1.18 / g

Total cost / mmol = (1.18*361.4)/1000 = £0.43 / mmol

[a]500g bottle from TCI Chemicals. [b]100g bottle from Alfa Aesar. [c]100g bottle from Fluorochem. [d]500g bottle from Alfa Aesar. [e]1L bottle from Sigma. [f]250g bottle from CarboSynth. Prices as of 12/05/2022.

Second Step:

Chemical	Equivalent	Mass / g	Cost / £
Diester	1	1.0	1.18[a]
NaOH	5	0.55	0.02[b]
Oxalyl Chloride	2	0.70	0.24[c]
Aluminium Chloride	10	3.69	0.18[d]
DiKTa	-	0.51	1.62

Total cost/g = (1.18+0.02+0.24+0.18)/0.51 = £3.18 / g

Total cost/mmol = (2.31*297.31)/1000 = £0.94 / mmol

[a]Calculated above. [b]500g bottle from Alfa Aesar. [c]100g bottle from TCI Chemicals. [d]500g bottle from TCI Chemicals. Prices as of 12/05/2022.

7.4 Experimental procedures and characterization for Chapter 4.

Azolium salts **1**,[204] **2**,[205] **3**,[205] **4**,[205] **5**,[204] **6**,[204] **7**,[206] **8**,[207] and **9**[208] used in this section were prepared in-house using standard literature methods. Azolium salt **10** was purchased from Sigma Aldrich and used without further purification.

General Procedure A – optimization

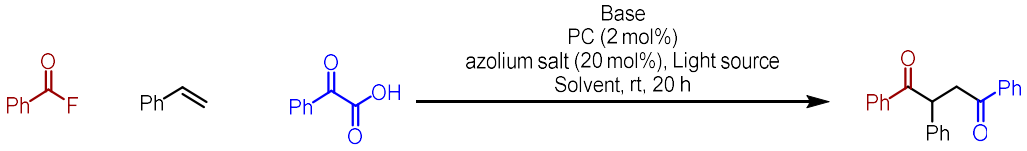

To an oven dried vial was added a base, a photocatalyst, phenylglyoxylic acid and an azolium salt. The vial was then evacuated and backfilled with nitrogen three times. Benzoyl fluoride and styrene were then added. In a separate oven dried Schlenk flask anhydrous solvent was sparged for 10 minutes and then added to the reaction vial and the vial was sealed further with parafilm. The reaction was then stirred under 427 nm irradiation using photoreactor set-up B at room temperature for 20 h. After the reactions were completed, the products were analysed by ^{1}H NMR spectroscopy with 1,3,5-trimethoxybenzene as an internal standard.

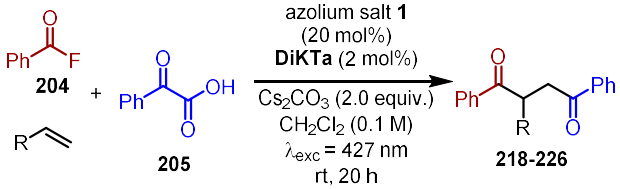

General Procedure B – variation of the alkene.

To an oven dried vial was added Cs_2CO_3 (65.2 mg, 0.20 mmol, 2.0 equiv.), **DiKTa** (0.6 mg, 2 µmol, 2.0 mol%), phenylglyoxylic acid (22.5 mg, 0.15 mmol, 1.5 equiv.) and azolium salt **1** (7.4 mg, 0.020 mmol, 20 mol%). The vial was then evacuated and backfilled with nitrogen three times. Benzoyl fluoride (43.5 µL, 0.40 mmol, 4.0 equiv.) and an alkene (0.10 mmol, 1.0 equiv.) were then injected. In a separate dry Schlenk flask anhydrous CH_2Cl_2 was sparged for 10 minutes and was then added to the reaction vial (1.0 mL) and the vial was sealed further with parafilm. The reaction was then stirred under 427 nm irradiation using photoreactor set-up B at room temperature for 20 h. The reaction was then

evaporated to dryness and THF (4 mL) and NaOH (2 mL, 2 M) were added. The resulting solution was stirred at 70 °C for 2 h. NaOH (5 mL, 2 M) was added, and the resulting mixture was extracted with CH_2Cl_2 (3 × 5 mL). The organic phases were combined and dried ($MgSO_4$) then concentrated *in vacuo*. Purification by silica chromatography EtOAc/Hexane afforded the desired products.

General Procedure C – variation of the alkene without hydrolysis step.

To an oven dried vial was added Cs_2CO_3 (65.2 mg, 0.20 mmol, 2.0 equiv.), **DiKTa** (0.6 mg, 2 µmol, 2.0 mol%), phenylglyoxylic acid (22.5 mg, 0.15 mmol, 1.5 equiv.) and azolium salt **1** (7.4 mg, 0.020 mmol, 20 mol%). The vial was then evacuated and backfilled with nitrogen three times. Benzoyl fluoride (43.5 µL, 0.40 mmol, 4.0 equiv.) and an alkene (0.10 mmol, 1.0 equiv.) were then injected. In a separate dry Schlenk flask anhydrous CH_2Cl_2 was sparged for 10 minutes and then 1.0 mL was added to the reaction vial and the vial was sealed further with parafilm. The reaction was then stirred under 427 nm irradiation using photoreactor set-up B at room temperature for 20 h. NaOH (5 mL, 2 M) was added, and the resulting mixture was extracted with CH_2Cl_2 (3 × 5 mL). The organic phases were combined and dried ($MgSO_4$) then concentrated *in vacuo*. Purification by silica chromatography EtOAc/Hexane afforded the desired products.

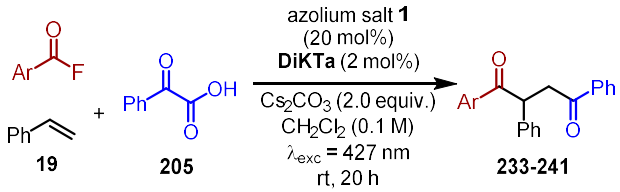

General Procedure D – variation of the aroyl fluoride.

To an oven dried vial was added Cs_2CO_3 (65.2 mg, 0.20 mmol, 2.0 equiv.), **DiKTa** (0.6 mg, 2 µmol, 2.0 mol%), phenylglyoxylic acid (22.5 mg, 0.15 mmol, 1.5 equiv.), azolium salt **1** (7.4 mg, 0.020 mmol, 20 mol%) and, if solid, aroyl fluoride (0.40 mmol, 4.0 equiv.). The vial was then evacuated and backfilled with nitrogen three times. Aroyl fluoride (0.40 mmol, 4.0 equiv.), if liquid, and styrene (11.5 µL, 0.10 mmol, 1.0 equiv.) were then injected. In a separate dry Schlenk flask anhydrous CH_2Cl_2 was sparged for 10 minutes and then 1.0 mL was added to the reaction vial and the vial was sealed further with parafilm. The reaction was then stirred under 427 nm irradiation using photoreactor set-up B at room

temperature for 20 h. NaOH (5 mL, 2 M) was added, and the resulting mixture was extracted with CH_2Cl_2 (3 × 5 mL). The organic phases were combined and dried ($MgSO_4$) then concentrated *in vacuo*. Purification by silica chromatography EtOAc/Hexane afforded the desired products.

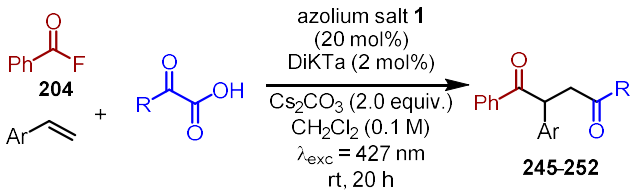

General Procedure E – variation of the α-keto acid.

To an oven dried vial was added Cs_2CO_3 (65.2 mg, 0.20 mmol, 2.0 equiv.), **DiKTa** (0.6 mg, 2 µmol, 2.0 mol%), α-keto acid (0.15 mmol, 1.5 equiv.), and azolium salt **1** (7.4 mg, 0.020 mmol, 20 mol%). The vial was then evacuated and backfilled with nitrogen three times. Benzoyl fluoride (43.5 µL, 0.40 mmol, 4.0 equiv.) and styrene (11.5 µL, 0.10 mmol, 1.0 equiv.) were then injected. In a separate dry Schlenk flask anhydrous CH_2Cl_2 was sparged for 10 minutes and then 1.0 mL was added to the reaction vial and the vial was sealed further with parafilm. The reaction was then stirred under 427 nm irradiation using photoreactor set-up B at room temperature for 20 h. NaOH (5 mL, 2 M) was added, and the resulting mixture was extracted with CH_2Cl_2 (3 × 5 mL). The organic phases were combined and dried ($MgSO_4$) then concentrated *in vacuo*. Purification by silica chromatography EtOAc/Hexane afforded the desired products.

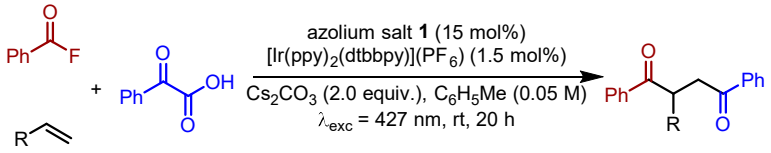

General Procedure F – [Ir(ppy)$_2$(dtbbpy)](PF$_6$) catalysed conditions for symmetrical 1,4-diones.[166]

To an oven dried vial was added Cs_2CO_3 (130 mg, 0.40 mmol, 2.0 equiv.), [Ir(ppy)$_2$(dtbbpy)](PF$_6$) (2.7 mg, 3 µmol, 1.5 mol%), phenylglyoxylic acid (60.0 mg, 0.40 mmol, 2.0 equiv.) and azolium salt **1** (11.1 mg, 0.030 mmol, 15 mol%). The vial was then evacuated and backfilled with nitrogen three times. Benzoyl fluoride (43.5 µL, 0.40 mmol, 2.0 equiv.), and an alkene (0.20 mmol, 1.0 equiv.) were then

injected. In a separate dry Schlenk flask anhydrous toluene was sparged for 10 minutes and then 4.0 mL was added to the reaction vial and the vial was sealed further with parafilm. The reaction was then stirred under 456 nm irradiation using photoreactor set-up B at room temperature for 20 h. NaOH (5 mL, 2 M) was added, and the resulting mixture was extracted with CH_2Cl_2 (3 × 5 mL). The organic phases were combined and dried ($MgSO_4$) then concentrated *in vacuo*. Purification by silica chromatography EtOAc/Hexane afforded the desired products.

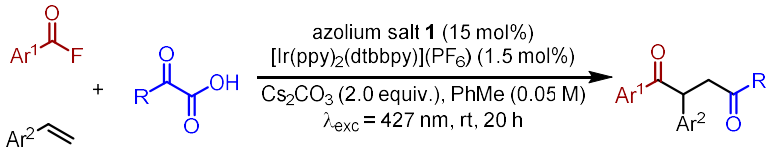

General Procedure G – [Ir(ppy)$_2$(dtbbpy)](PF$_6$) catalysed conditions for unsymmetrical 1,4-diones.[166]

To an oven dried vial was added Cs_2CO_3 (130 mg, 0.40 mmol, 2.0 equiv.), [Ir(ppy)$_2$(dtbbpy)](PF$_6$) (2.7 mg, 3 µmol, 1.5 mol%), α-keto acid (0.60 mmol, 3.0 equiv.), azolium salt **1** (11.1 mg, 0.030 mmol, 15 mol%) and, if solid, aroyl fluoride (0.60 mmol, 3.0 equiv.). The vial was then evacuated and backfilled with nitrogen three times. Aroyl fluoride (0.60 mmol, 3.0 equiv.), if liquid, and styrene (23 µL, 0.20 mmol, 1.0 equiv.) were then injected. In a separate dry Schlenk flask anhydrous toluene was sparged for 10 minutes and then 4.0 mL was added to the reaction vial and the vial was sealed further with parafilm. The reaction was then stirred under 456 nm irradiation using photoreactor set-up B at room temperature for 20 h. NaOH (5 mL, 2 M) was added, and the resulting mixture was extracted with CH_2Cl_2 (3 × 5 mL). The organic phases were combined and dried ($MgSO_4$) then concentrated *in vacuo*. Purification by silica chromatography EtOAc/Hexane afforded the desired products.

General Procedure H – Synthesis of Acyl Fluorides

Based on a procedure reported by Wang *et al.*[170] 18-crown-6 (198 mg, 0.75 mmol, 0.05 equiv.), potassium fluoride (8.71g, 150.0 mmol, 10.0 equiv.) and an acyl chloride (15.0 mmol, 1.0 equiv.) were added to an oven-dried Schlenk flask under nitrogen. Then THF (75 mL) was added, and the reaction was heated to 50 °C then stirred for 20 h. The reaction mixture was cooled to room temperature and

filtered. The residue was washed with THF, and the filtrate was concentrated *in vacuo*. Purification through bulb to bulb distillation afforded the desired acyl fluorides.

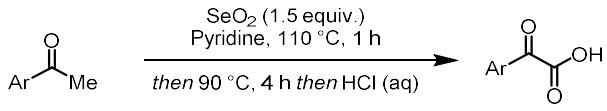

General Procedure I – synthesis of aryl α-ketoacids.

Based on a procedure reported by Wadhwa *et al*.[171] selenium dioxide (1.7 g, 15 mmol, 1.5 equiv.) and an acetophenone (10 mmol, 1.0 equiv.) were added to an oven-dried Schlenk flask which was then evacuated and back filled with nitrogen three times. Then pyridine (30 mL) was added, and the reaction mixture was heated to 110 °C and stirred for 1 h. Then the reaction mixture was allowed to cool to 90 °C and stirred for a further 4 h. After cooling to room temperature the reaction mixture was filtered through a pad of celite. The pH of the filtrate was then adjusted to 1 using dilute hydrochloric acid and extracted with EtOAc (2 × 30 mL). The organic layers were combined, washed with brine (20 mL), dried (Na_2SO_4) and concentrated *in vacuo*. Purification through silica column chromatography (EtOAc/Hexane) afforded the desired α-ketoacid products.

2-Phenyl-1,4-diphenylbutane-1,4-dione (182):

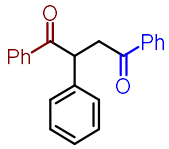

Synthesised using general procedure B to give 18.2 mg of **182** (58%) after silica column chromatography (3% EtOAc/Hexane).

Colourless solid. **Mp** 121-124 °C {Lit. Mp[209] 124-126 °C}. **^{1}H NMR (500 MHz, $CDCl_3$) δ (ppm):** 3.34 (1H, dd, *J* = 18.0 Hz, 3.6 Hz, CHC*H*^{A}H^{B}), 4.25 (1H, dd, *J* = 18.0 Hz, 10.1 Hz, CHCH^{A}*H*^{B}), 5.35 (1H, dd, *J* = 10.1 Hz, 3.7 Hz, C*H*CH^{A}H^{B}), 7.23 – 7.28 (1H, m, Ar*H*), 7.34 (2H, dd, *J* = 8.5 Hz, 6.8 Hz, Ar*H*), 7.37 – 7.55 (7H, m, Ar*H*), 7.56 – 7.61 (1H, m, Ar*H*), 7.98 – 8.04 (2H, m, Ar*H*), 8.05 – 8.09 (2H, m, Ar*H*); **^{13}C{^{1}H} NMR (126 MHz, $CDCl_3$) δ (ppm):** 43.9 (CH*C*H$_2$), 48.7 (*C*HCH$_2$), 127.4 (Ar*C*), 128.2 (Ar*C*), 128.3 (Ar*C*), 128.5 (Ar*C*), 128.6 (Ar*C*), 129.0 (Ar*C*), 129.2 (Ar*C*), 130.0 (Ar*C*), 132.9 (Ar*C*), 133.3 (Ar*C*), 136.4 (Ar*C*), 138.6 (Ar*C*), 198.1 (*C*=O), 198.9 (*C*=O). **HPLC:** chiralcel OD-H (97:3 hexane:IPA, flow rate 1.0 mL min^{-1}, 211 nm, 30°C) t_R (major): 14.0 min t_R (minor): 15.6 min, 53:47 er.

Data matches that previously reported.[210]

2-(4-Bromophenyl)-1,4-diphenylbutane-1,4-dione (218):

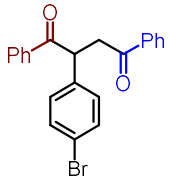

Synthesised using general procedure B to give 17.6 mg of **218** (45%) after silica column chromatography (3% EtOAc/Hexane).

Colourless solid. **Mp** 123-126 °C. **^{1}H NMR (500 MHz, $CDCl_3$) δ (ppm):** 3.30 (1H, dd, *J* = 18.0 Hz, 4.0 Hz, CHC*H*^{A}H^{B}), 4.16 (1H, dd, *J* = 18.0 Hz, 9.7 Hz, CHCH^{A}*H*^{B}), 5.30 (1H, dd, *J* = 9.7 Hz, 4.0 Hz, C*H*CH^{A}H^{B}), 7.22 – 7.26 (2H, m, Ar*H*), 7.38 – 7.48 (6H, m, Ar*H*), 7.49 – 7.54 (1H, m, Ar*H*), 7.54 – 7.59 (1H, m, Ar*H*), 7.95 – 8.04 (4H, m, Ar*H*).

^{13}C{^{1}H} NMR (126 MHz, $CDCl_3$) δ (ppm): 43.6 (CH*C*H$_2$), 48.1 (*C*HCH$_2$), 121.4 (Ar*C*), 128.2 (Ar*C*), 128.60 (Ar*C*), 128.62 (Ar*C*), 128.9 (Ar*C*), 130.0 (Ar*C*), 132.3 (Ar*C*), 133.1 (Ar*C*), 133.3 (Ar*C*), 136.3 (Ar*C*), 136.4 (Ar*C*), 137.7 (Ar*C*), 197.7 (*C*=O), 198.6 (*C*=O).

Data matches that previously reported.[164]

2-(4-Fluorophenyl)-1,4-diphenylbutane-1,4-dione (219):

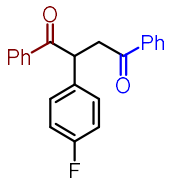

Synthesised using general procedure B to give 15.3 mg of **219** (46%) after silica column chromatography (3% EtOAc/Hexane).

Colourless solid. **Mp** 113-116 °C. **^{1}H NMR (500 MHz, $CDCl_3$) δ (ppm):** 3.31 (1H, dd, *J* = 18.0 Hz, 4.0 Hz, CHC*H*^{A}H^{B}), 4.17 (1H, dd, *J* = 18.0 Hz, 9.8 Hz, CHCH^{A}*H*^{B}), 5.32 (1H, dd, *J* = 9.8 Hz, 3.9 Hz, C*H*CH^{A}H^{B}), 6.97 – 7.04 (2H, m, Ar*H*), 7.31 – 7.36 (2H, m, Ar*H*), 7.39 – 7.48 (4H, m, Ar*H*), 7.49 – 7.54 (1H, m, Ar*H*), 7.94 – 8.06 (4H, m, Ar*H*); **^{19}F NMR (471 MHz, $CDCl_3$) δ (ppm):** -114.9; **^{13}C{^{1}H} NMR (126 MHz, $CDCl_3$) δ (ppm):** 43.8 (CH*C*H$_2$), 47.8 (*C*HCH$_2$), 116.1 (d, *J* = 21.5 Hz, Ar*C*), 128.2 (Ar*C*), 128.60 (Ar*C*), 128.64 (Ar*C*), 128.9 (Ar*C*), 129.8 (d, *J* = 8.1 Hz, Ar*C*), 133.1 (Ar*C*), 133.4 (Ar*C*), 134.3 (d, *J* = 3.1 Hz, Ar*C*),136.3 (Ar*C*), 136.4 (Ar*C*), 162.1 (d, *J* = 245.8 Hz, Ar*C*), 197.9 (*C*=O), 198.9 (*C*=O).

Data matches that previously reported.[164]

1,4-Diphenyl-2-(4-(trifluoromethyl)phenyl)butane-1,4-dione (220):

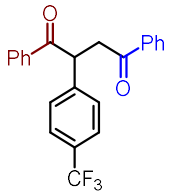

Synthesised using general procedure B to give 16.0 mg of **220** (42%) after silica column chromatography (3% EtOAc/Hexane).

Colourless oil. **^{1}H NMR (500 MHz, $CDCl_3$) δ (ppm):** 3.36 (1H, dd, *J* = 18.0 Hz, 4.0 Hz, CHC*H*^{A}H^{B}), 4.24 (1H, dd, *J* = 18.0 Hz, 9.8 Hz, CHCH^{A}*H*^{B}), 5.44 (1H, dd, *J* = 9.7 Hz, 4.0 Hz, C*H*CH^{A}H^{B}), 7.43 – 7.51 (4H, m, Ar*H*), 7.54 (3H, dd, *J* = 9.6 Hz, 7.8 Hz, Ar*H*), 7.57 – 7.62 (3H, m, Ar*H*), 7.99 – 8.03 (2H, m, Ar*H*), 8.03 – 8.07 (2H, m, Ar*H*); **^{19}F NMR (471 MHz, $CDCl_3$) δ (ppm):** -62.6; **^{13}C{^{1}H} NMR (126 MHz, $CDCl_3$) δ (ppm):** 43.7 (CH*C*H$_2$), 48.3 (*C*HCH$_2$), 123.9 (q, *J* = 272.4 Hz *C*F$_3$) 126.1 (q, *J* = 3.5 Hz, Ar*C*), 128.2 (Ar*C*), 128.66 (Ar*C*), 128.68 (Ar*C*), 128.71 (Ar*C*), 128.9 (Ar*C*), 129.7 (q, *J* = 32.7 Hz, Ar*C*) (Ar*C*), 133.3 (Ar*C*), 133.5 (Ar*C*), 136.1 (Ar*C*), 136.2 (Ar*C*), 142.7 (Ar*C*), 197.7 (*C*=O), 198.6 (*C*=O).

Data matches that previously reported.[210]

1,4-Diphenyl-2-(pyridin-2-yl)butane-1,4-dione (221):

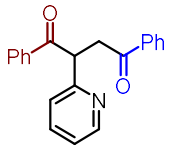

Synthesised using general procedure B to give 17.4 mg of **221** (55%) after silica column chromatography (30% EtOAc/Hexane).

Yellow oil. **^{1}H NMR (500 MHz, $CDCl_3$) δ (ppm):** 3.54 (1H, dd, *J* = 18.0 Hz, 4.1 Hz, CHC*H*^{A}H^{B}), 4.26 (1H, dd, *J* = 18.0 Hz, 9.6 Hz, CHCH^{A}*H*^{B}), 5.60 (1H, dd, *J* = 9.6 Hz, 4.1 Hz, C*H*CH^{A}H^{B}), 7.17 (1H, ddd, *J* = 7.6 Hz, 4.9 Hz, 1.1 Hz, Ar*H*), 7.38 (1H, d, *J* = 7.7 Hz, Ar*H*), 7.42 – 7.50 (4H, m, Ar*H*), 7.51 – 7.56 (1H, m, Ar*H*), 7.56 – 7.61 (1H, m, Ar*H*), 7.64 (1H, td, *J* = 7.7 Hz, 1.8 Hz, Ar*H*), 8.00 – 8.06 (2H, m, Ar*H*), 8.10 – 8.14 (2H, m, Ar*H*), 8,59 (1H, q, *J* = 1.7 Hz, Ar*H*); **^{13}C{^{1}H} NMR (126 MHz, $CDCl_3$) δ (ppm):** 42.2 (CH*C*H$_2$), 51.3 (*C*HCH$_2$), 122.2 (Ar*C*), 123.0 (Ar*C*), 128.2 (Ar*C*), 128.57 (Ar*C*), 128.58 (Ar*C*), 129.1 (Ar*C*), 133.0 (Ar*C*), 133.3 (Ar*C*), 136.4 (Ar*C*), 137.1 (Ar*C*), 150.0 (Ar*C*), 158.5 (Ar*C*), 197.8 (*C*=O), 198.0 (*C*=O).

Data matches that previously reported.[159]

1,4-Diphenyl-2-(p-tolyl)butane-1,4-dione (222):

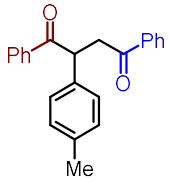

Synthesised using general procedure B to give 18.7 mg of **222** (57%) after silica column chromatography (3% EtOAc/Hexane).

Colourless oil. **^{1}H NMR (500 MHz, $CDCl_3$) δ (ppm):** 2.31 (3H, s, CH_3), 3.31 (1H, dd, *J* = 18.0 Hz, 3.7 Hz, CHCH^AH^B), 4.22 (1H, dd, *J* = 18.0 Hz, 10.0 Hz, CHCH^AH^B), 5.32 (1H, dd, *J* = 10.7 Hz, 3.7 Hz, CHCH^{A}H^B), 7.14 (2H, d, *J* = 7.8 Hz, Ar*H*), 7.25 – 7.28 (2H, m, Ar*H*), 7.40 – 7.54 (5H, m, Ar*H*), 7.56 – 7.60 (1H, m, Ar*H*), 7.99 – 8.02 (2H, m, Ar*H*), 8.04 – 8.07 (2H, m, Ar*H*); **^{13}C{^{1}H} NMR (126 MHz, $CDCl_3$) δ (ppm):** 21.1 (*C*H$_3$), 43.9 (CH*C*H$_2$), 48.3 (*C*HCH$_2$), 128.1 (Ar*C*), 128.2 (Ar*C*), 128.5 (Ar*C*), 128.6 (Ar*C*), 128.9 (Ar*C*), 129.9 (Ar*C*), 132.9 (Ar*C*), 133.2 (Ar*C*), 135.6 (Ar*C*), 136.5 (Ar*C*), 137.1 (Ar*C*), 198.2 (*C*=O), 199.0 (*C*=O).

Data matches that previously reported.[159]

2-(4-(Tert-butyl)phenyl)-1,4-diphenylbutane-1,4-dione (223):

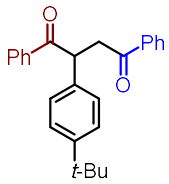

Synthesised using general procedure B to give 15.9 mg of **223** (43%) after silica column chromatography (3% EtOAc/Hexane).

Colourless solid. **Mp** 106-109 °C. **^{1}H NMR (500 MHz, $CDCl_3$) δ (ppm):** 1.30 (9H, s, C(CH_3)$_3$), 3.33 (1H, dd, *J* = 18.1 Hz, 3.6 Hz, CHCH^AH^B), 4.24 (1H, dd, *J* = 18.1 Hz, 10.2 Hz, CHCH^AH^B), 5.33 (1H, dd, *J* = 10.3 Hz, 3.6 Hz, CHCH^{A}H^B), 7.29 – 7.37 (4H, m, Ar*H*), 7.39 – 7.61 (6H, m, Ar*H*), 7.97 – 8.05 (2H, m, Ar*H*), 8.05 – 8.11 (2H, m, Ar*H*); **^{13}C{^{1}H} NMR (126 MHz, $CDCl_3$) δ (ppm):** 31.3 (*C*H$_3$), 34.5 (*C*(CH$_3$)$_3$) 44.0 (CH*C*H$_2$), 48.1 (*C*HCH$_2$), 126.1 (Ar*C*), 127.8 (Ar*C*), 128.2 (Ar*C*), 128.5 (Ar*C*), 128.6 (Ar*C*), 129.0 (Ar*C*), 132.8 (Ar*C*), 133.2 (Ar*C*), 135.4 (Ar*C*), 136.5 (Ar*C*), 136.6 (Ar*C*), 150.2 (Ar*C*) 198.2 (*C*=O), 199.0 (*C*=O).

Data matches that previously reported.[159]

2-(4-(Chloromethyl)phenyl)-1,4-diphenylbutane-1,4-dione (224):

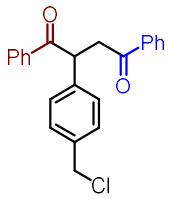

Synthesised using general procedure C to give 14.9 mg of **224** (41%) after silica column chromatography (3% EtOAc/Hexane).

Colourless solid. **Mp** 155-160 °C. **^{1}H NMR (500 MHz, $CDCl_3$) δ (ppm):** 3.33 (1H, dd, *J* = 18.1 Hz, 3.8 Hz, CHC*H*^{A}H^{B}), 4.23 (1H, dd, *J* = 18.0 Hz, 10.0 Hz, CHCH^{A}*H*^{B}), 4.55 (2H, s, CH_2Cl), 5.37 (1H, dd, *J* = 10.0 Hz, 3.8 Hz, C*H*CH^{A}H^{B}), 7.34 – 7.42 (4H, m, Ar*H*), 7.50 – 7.56 (1H, m, Ar*H*), 7.56 – 7.64 (1H, m, Ar*H*), 7.98 – 8.03 (2H, m, Ar*H*), 8.03 – 8.07 (2H, m, Ar*H*); **^{13}C{^{1}H} NMR (126 MHz, $CDCl_3$) δ (ppm):** 43.8 (CH*C*H_2), 45.8 (*C*H_2Cl), 48.3 (*C*HCH$_2$), 128.2 (Ar*C*), 128.60 (Ar*C*), 128.63 (Ar*C*), 128.9 (Ar*C*), 129.5 (Ar*C*), 133.1 (Ar*C*), 133.4 (Ar*C*), 136.3 (Ar*C*), 136.4 (Ar*C*), 136.6 (Ar*C*), 138.9 (Ar*C*), 197.9 (*C*=O), 198.7 (*C*=O).

Data matches that previously reported.[159]

1,4-Diphenyl-2-(o-tolyl)butane-1,4-dione (225):

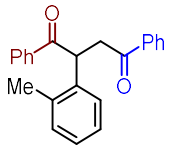

Synthesised using general procedure B to give 12.8 mg of **225** (39%) after silica column chromatography (3% EtOAc/Hexane).

Colourless oil. **^{1}H NMR (500 MHz, $CDCl_3$) δ (ppm):** 2.57 (3H, s), 3.12 (1H, dd, *J* = 18.0 Hz, 2.9 Hz, CHC*H*^{A}H^{B}), 4.18 (1H, dd, *J* = 18.0 Hz, 10.6 Hz, CHCH^{A}*H*^{B}), 5.49 (1H, dd, *J* = 10.5 Hz, 2.9 Hz, C*H*CH^{A}H^{B}), 7.12 (1H, d, *J* = 2.9 Hz, Ar*H*), 7.17 (1H, ddd, *J* = 7.5 Hz, 5,4 Hz, 3.4 Hz, Ar*H*), 7.27 (2H, d, *J* = 13.6 Hz, Ar*H*), 7.40 (2H, t, *J* = 7.7 Hz, Ar*H*), 7.49 (3H, dt, *J* = 9.2 Hz, 7.4 Hz, Ar*H*), 7.57-7.61 (1H, m, Ar*H*), 7.90 – 7.95 (2H, m, Ar*H*), 8.01 – 8.05 (2H, m, Ar*H*); **^{13}C{^{1}H} NMR (126 MHz, $CDCl_3$) δ (ppm):** 19.8 (*C*H$_3$), 42.5 (CH*C*H$_2$), 45.2 (*C*HCH$_2$), 126.9 (Ar*C*), 127.4 (Ar*C*), 127.5 (Ar*C*), 128.2 (Ar*C*), 128.5 (Ar*C*), 128.6 (Ar*C*), 128.7 (Ar*C*), 131.3 (Ar*C*), 132.8 (Ar*C*), 133.3 (Ar*C*), 135.1 (Ar*C*), 136.5 (Ar*C*), 136.6 (Ar*C*), 137.2 (Ar*C*), 198.2 (*C*=O), 199.5 (*C*=O).

Data matches that previously reported.[164]

2-(4-Methoxyphenyl)-1,4-diphenylbutane-1,4-dione (226):

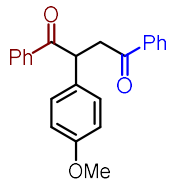

Synthesised using general procedure B to give 8.9 mg of **226** (26%) and general procedure F to give 40.0 mg of **15** (58%) after silica column chromatography (3% EtOAc/Hexane).

Colourless solid. **Mp** 134-137 °C {Lit. Mp[211] 138-139 °C}. **^{1}H NMR (500 MHz, $CDCl_3$) δ (ppm):** 3.29 (1H, dd, *J* = 18.0 Hz, 3.8 Hz, CHC*H*^{A}H^{B}), 3.76 (3H, s, OCH_3), 4.18 (1H, dd, *J* = 18.0 Hz, 10.0 Hz, CHCH^{A}*H*^{B}), 5.28 (1H, dd, *J* = 9.9 Hz, 3.8 Hz, C*H*CH^{A}H^{B}), 6.82 – 6.87 (2H, m, Ar*H*), 7.26 – 7.29 (2H, m, Ar*H*), 7.38 – 7.51 (5H, m, Ar*H*), 7.52 – 7.58 (1H, m, Ar*H*), 7.96 – 8.01 (2H, m, Ar*H*), 8.01 – 8.05 (2H, m, Ar*H*); **^{13}C{^{1}H} NMR (126 MHz, $CDCl_3$) δ (ppm):** 43.9 (CH*C*H$_2$), 47.8 (*C*HCH$_2$), 55.3 (O*C*H$_3$), 114.6 (Ar*C*), 128.2 (Ar*C*), 128.5 (Ar*C*), 128.6 (Ar*C*), 128.9 (Ar*C*), 129.3 (Ar*C*), 130.5 (Ar*C*), 132.9 (Ar*C*), 133.3 (Ar*C*), 136.48 (Ar*C*), 136.51 (Ar*C*), 158.8 (Ar*C*), 198.3 (*C*=O), 199.1 (*C*=O).

Data matches that previously reported.[164]

1-([1,1'-Biphenyl]-4-yl)-2,4-diphenylbutane-1,4-dione (233):

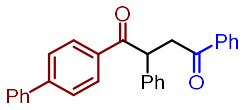

Synthesised using general procedure D to give 20.7 mg of **233** (53%) after silica column chromatography (3% EtOAc/Hexane).

Colourless solid. **Mp** 196-199 °C {Lit. Mp[212] 200 °C}. **^{1}H NMR (500 MHz, $CDCl_3$) δ (ppm):** 3.33 (1H, dd, *J* = 18.0 Hz, 3.7 Hz, CHC*H*^{A}H^{B}), 4.25 (1H, dd, *J* = 18.0 Hz, 10.1 Hz, CHCH^{A}*H*^{B}), 5.36 (1H, dd, *J* = 10.1 Hz, 3.6 Hz, C*H*CH^{A}H^{B}), 7.21 – 7.25 (1H, m, Ar*H*), 7.33 (2H, dd, *J* = 8.5 Hz, 6.8 Hz, Ar*H*), 7.37 – 7.42 (3H, m, Ar*H*), 7.42 – 7.49 (4H, m, Ar*H*), 7.54 – 7.61 (3H, m, Ar*H*), 7.61 – 7.65 (2H, m, Ar*H*), 7.97 – 8.02 (2H, m, Ar*H*), 8.09 – 8.14 (2H, m, Ar*H*); **^{13}C{^{1}H} NMR (126 MHz, $CDCl_3$) δ (ppm):** 43.9 (CH*C*H$_2$), 48.7 (*C*HCH$_2$), 122.6 (Ar*C*), 127.3 (Ar*C*), 127.4 (Ar*C*), 128.1 (Ar*C*), 128.2 (Ar*C*), 128.3 (Ar*C*), 128.6 (Ar*C*), 128.9 (Ar*C*), 129.3 (Ar*C*), 129.5 (Ar*C*), 133.3 (Ar*C*), 135.1 (Ar*C*), 136.5 (Ar*C*), 138.7 (Ar*C*), 140.0 (Ar*C*), 143.3 (Ar*C*), 145.6 (Ar*C*), 198.1 (*C*=O), 198.5 (*C*=O).

Data matches that previously reported.[157]

1-(Naphthalen-2-yl)-2,4-diphenylbutane-1,4-dione (234):

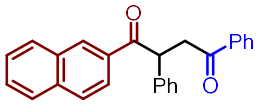

Synthesised using general procedure D to give 14.9 mg of **234** (41%) after silica column chromatography (3% EtOAc/Hexane).

Colourless oil. **^{1}H NMR (500 MHz, $CDCl_3$) δ (ppm):** 3.37 (1H, dd, *J* = 18.1 Hz, 3.7 Hz, CHC*H*^{A}H^{B}), 4.28 (1H, dd, *J* = 18.0 Hz, 10.0 Hz, CHCH^{A}*H*^{B}), 5.50 (1H, dd, *J* = 10.0 Hz, 3.7 Hz, C*H*CH^{A}H^{B}), 7.22 (1H, t, *J* = 7.7 Hz, Ar*H*), 7.32 (2H, t, *J* = 7.6 Hz, Ar*H*), 7.38 – 7.60 (7H, m, Ar*H*), 7.80 – 7.87 (2H, m, Ar*H*), 7.93 (1H, d, *J* = 8.0 Hz, Ar*H*) 7.99 – 8.05 (2H, m, Ar*H*), 8.07 (1H, dd, *J* = 8.7 Hz, 1.8 Hz, Ar*H*), 8.61 (1H, d, *J* = 1.7 Hz, Ar*H*); **^{13}C{^{1}H} NMR (126 MHz, $CDCl_3$) δ (ppm):** 43.9 (CH*C*H$_2$), 48.8 (*C*HCH$_2$), 124.7 (Ar*C*), 126.6 (Ar*C*), 127.4 (Ar*C*), 127.7 (Ar*C*), 128.2 (Ar*C*), 128.3 (Ar*C*), 128.36 (Ar*C*), 128.39 (Ar*C*), 128.6 (Ar*C*), 129.3 (Ar*C*), 129.7 (Ar*C*), 130.8 (Ar*C*), 132.5 (Ar*C*), 133.3 (Ar*C*), 133.8 (Ar*C*), 135.5 (Ar*C*), 136.5 (Ar*C*), 138.8 (Ar*C*), 198.2 (*C*=O), 198.9 (*C*=O).

Data matches that previously reported.[157]

1-(Naphthalen-1-yl)-2,4-diphenylbutane-1,4-dione (235):

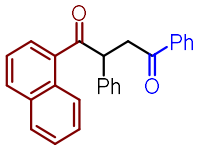

Synthesised using general procedure D to give 9.8 mg of **235** (27%) after silica column chromatography (3% EtOAc/Hexane).

Colourless solid. **Mp** 129-132 °C. **^{1}H NMR (500 MHz, $CDCl_3$) δ (ppm):** 3.38 (1H, dd, *J* = 18.0 Hz, 3.4 Hz, CHC*H*^{A}H^{B}), 4.40 (1H, dd, *J* = 18.0 Hz, 10.5 Hz, CHCH^{A}*H*^{B}), 5.35 (1H, dd, *J* = 10.5 Hz, 3.4 Hz, C*H*CH^{A}H^{B}), 7.19 – 7.25 (1H, m, Ar*H*), 7.31 (2H, d, *J* = 7.6 Hz, Ar*H*), 7.37 – 7.42 (2H, m, Ar*H*), 7.50 (5H, dddd, *J* = 9.4 Hz, 7.4 Hz, 3.2 Hz, 1.6 Hz, Ar*H*), 7.59 – 7.63 (1H, m, Ar*H*) 7.83 (1H, dd, *J* = 8.3 Hz, 1.6 Hz, Ar*H*), 7.95 (1H, d, *J* = 8.2 Hz, Ar*H*), 8.03 – 8.09 (2H, m, Ar*H*), 8.20 (1H, dd, *J* = 7.2 Hz, 1.2 Hz, Ar*H*), 8.36 (1H, dd, *J* =8.3 Hz, 1.6 Hz, Ar*H*); **^{13}C{^{1}H} NMR (126 MHz, $CDCl_3$) δ (ppm):** 43.5 (CH*C*H$_2$), 52.3 (*C*HCH$_2$), 124.4 (Ar*C*), 125.7 (Ar*C*), 126.2 (Ar*C*), 127.5 (Ar*C*), 127.6 (Ar*C*), 127.7 (Ar*C*), 128.19 (Ar*C*), 128.21 (Ar*C*), 128.3 (Ar*C*), 128.7 (Ar*C*), 129.1 (Ar*C*), 130.7 (Ar*C*), 132.3 (Ar*C*), 133.3 (Ar*C*), 133.8 (Ar*C*), 136.4 (Ar*C*), 136.6 (Ar*C*), 137.9 (Ar*C*), 198.3 (*C*=O), 202.4 (*C*=O).

HRMS (ESI) $C_{26}H_{21}O_2$ $[M+H]^+$ found 365.1548, theoretical 365.1536 (+ 3.3 ppm)

1-(4-Fluorophenyl)-2,4-diphenylbutane-1,4-dione (236):

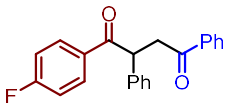

Synthesised using general procedure D to give 17.0 mg of **236** (51%) after silica column chromatography (3% EtOAc/Hexane).

Colourless oil. **^{1}H NMR (500 MHz, $CDCl_3$) δ (ppm):** 3.33 (1H, dd, *J* = 18.1 Hz, 3.5 Hz, CHC*H*^{A}H^{B}), 4.24 (1H, dd, *J* = 18.1 Hz, 10.2 Hz, CHCH^{A}*H*^{B}), 5.29 (1H, dd, *J* = 10.2 Hz, 3.5 Hz, C*H*CH^{A}H^{B}), 7.05 – 7.09 (2H, m, Ar*H*), 7.22 – 7.26 (1H, m, Ar*H*), 7.30 – 7.37 (4H, m, Ar*H*), 7.43 – 7.48 (2H, m, Ar*H*), 7.53 – 7.59 (1H, m, Ar*H*), 7.96 – 8.00 (2H, m, Ar*H*), 8.04 – 8.08 (2H, m, Ar*H*); **^{19}F NMR (471 MHz, $CDCl_3$) δ (ppm):** -105.4; **^{13}C{^{1}H} NMR (126 MHz, $CDCl_3$) δ (ppm):** 43.9 (CH*C*H$_2$), 48.7 (*C*HCH$_2$), 115.6 (d, *J* = 21.8 Hz, Ar*C*), 127.5 (Ar*C*), 128.2 (d, *J* = 2.6 Hz, Ar*C*), 128.6 (Ar*C*), 129.3 (Ar*C*), 131.6 (d, *J* = 9.2 Hz, Ar*C*), 133.4 (Ar*C*), 136.3 (Ar*C*), 138.4 (Ar*C*), 165.6 (d, *J* = 254.3 Hz, Ar*C*), 197.4 (*C*=O), 198.1 (*C*=O).

Data matches that previously reported.[157]

1-(4-Chlorophenyl)-2,4-diphenylbutane-1,4-dione (237):

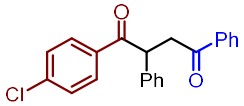

Synthesised using general procedure D to give 17.1 mg of **237** (49%) after silica column chromatography (3% EtOAc/Hexane).

Yellow oil. **^{1}H NMR (500 MHz, $CDCl_3$) δ (ppm):** 3.31 (1H, dd, *J* = 18.1 Hz, 3.6 Hz, CHC*H*^{A}H^{B}), 4.21 (1H, dd, *J* = 18.1 Hz, 10.2 Hz, CHCH^{A}*H*^{B}), 5.26 (1H, dd, *J* = 10.2 Hz, 3.6 Hz, C*H*CH^{A}H^{B}), 7.31 – 7.35 (4H, m, Ar*H*), 7.35 – 7.39 (2H, m, Ar*H*), 7.41 – 7.48 (3H, m, Ar*H*), 7.53 – 7.60 (2H, m, Ar*H*), 7.94 – 8.00 (4H, m, Ar*H*); **^{13}C{^{1}H} NMR (126 MHz, $CDCl_3$) δ (ppm):** 43.9 (CH*C*H$_2$), 48.8 (*C*HCH$_2$), 127.6 (Ar*C*), 128.2 (Ar*C*), 128.6 (Ar*C*), 128.9 (Ar*C*), 129.3 (Ar*C*), 130.4 (d, *J* = 9.2 Hz, Ar*C*), 133.4 (Ar*C*), 134.8 (Ar*C*), 136.3 (Ar*C*), 138.3 (Ar*C*), 139.3 (Ar*C*), 197.8 (*C*=O), 198.0 (*C*=O).

Data matches that previously reported.[213]

1-(4-Bromophenyl)-2,4-diphenylbutane-1,4-dione (238):

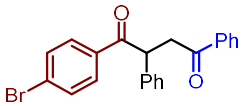

Synthesised using general procedure D to give 9.8 mg of **238** (25%) and general procedure G to give 30.7 mg of **21** (58%) after silica column chromatography (3% EtOAc/Hexane).

Colourless foam. **^{1}H NMR (500 MHz, $CDCl_3$) δ (ppm):** 3.31 (1H, dd, *J* = 18.1 Hz, 3.5 Hz, CHC*H*^{A}H^{B}), 4.21 (1H, dd, *J* = 18.1 Hz, 10.2 Hz, CHCH^{A}*H*^{B}), 5.24 (1H, dd, *J* = 10.2 Hz, 3.5 Hz, C*H*CH^{A}H^{B}), 7.24 (1H, dd, *J* = 5.9 Hz, 2.9 Hz, Ar*H*), 7.28 – 7.35 (4H, m, Ar*H*), 7.45 (2H, t, *J* = 7.7 Hz, Ar*H*), 7.55 (3H, dd, *J* = 8.5 Hz, 6.7 Hz Ar*H*), 7.86 – 7.92 (2H, m, Ar*H*), 7.94 – 8.02 (2H, m, Ar*H*); **^{13}C{^{1}H} NMR (126 MHz, $CDCl_3$) δ (ppm):** 43.9 (CH*C*H$_2$), 48.8 (*C*HCH$_2$), 127.6 (Ar*C*), 128.2 (Ar*C*), 128.6 (Ar*C*), 129.3 (Ar*C*), 130.5 (Ar*C*), 131.9 (Ar*C*), 133.4 (Ar*C*), 135.2 (Ar*C*), 136.3 (Ar*C*), 138.2 (Ar*C*), 139.3 (Ar*C*), 197.98 (*C*=O), 198.02 (*C*=O).

Data matches that previously reported.[214]

1-(4-Iodophenyl)-2,4-diphenylbutane-1,4-dione (239):

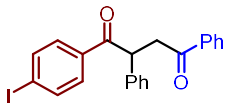

Synthesised using general procedure D to give 8.8 mg of **239** (20%) and general procedure G to give 44.0 mg of **22** (50%) after silica column chromatography (3% EtOAc/Hexane).

Colourless solid. **Mp** 107-109 °C **^{1}H NMR (500 MHz, $CDCl_3$) δ (ppm):** 3.33 (1H, dd, *J* = 18.1 Hz, 3.6 Hz, CHC*H*^{A}H^{B}), 4.23 (1H, dd, *J* = 18.1 Hz, 10.2 Hz, CHCH^{A}*H*^{B}), 5.26 (1H, dd, *J* = 10.2 Hz, 3.6 Hz, C*H*CH^{A}H^{B}), 7.24 – 7.30 (3H, m, Ar*H*), 7.34 (2H, d, *J* = 1.8 Hz, Ar*H*), 7.47 (2H, dd, *J* = 8.4 Hz, 7.1 Hz, Ar*H*), 7.55 – 7.63 (1H, m, Ar*H*), 7.71 – 7.82 (4H, m, Ar*H*) 7.96 – 8.03 (2H, m, Ar*H*); **^{13}C{^{1}H} NMR (126 MHz, $CDCl_3$) δ (ppm):** 43.9 (CH*C*H$_2$), 48.7 (*C*HCH$_2$), 101.0 (Ar*C*), 127.6 (Ar*C*), 128.2 (Ar*C*), 128.6 (Ar*C*), 129.3 (Ar*C*), 130.3 (Ar*C*), 133.4 (Ar*C*), 135.7 (Ar*C*), 136.3 (Ar*C*), 137.9 (Ar*C*), 197.8 (*C*=O), 198.0 (*C*=O).

HRMS (ESI) $C_{22}H_{18}IO_2$ [M+H]$^{+}$ found 441.0336, theoretical 441.0346 (– 2.3 ppm)

1-(4-Methoxyphenyl)-2,4-diphenylbutane-1,4-dione (240):

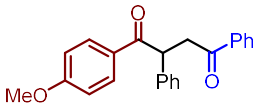

Synthesised using general procedure D to give 19.6 mg of **240** (57%) after silica column chromatography (3% EtOAc/Hexane).

Colourless oil. **^{1}H NMR (500 MHz, $CDCl_3$) δ (ppm):** 3.30 (1H, dd, *J* = 18.0 Hz, 3.8 Hz, CHC*H*^{A}H^{B}), 3.84 (3H, s, OC*H*$_3$), 4.23 (1H, dd, *J* = 18.0 Hz, 10.0 Hz, CHCH^{A}*H*^{B}), 5.32 (1H, dd, *J* = 10.0 Hz, 3.8 Hz, C*H*CH^{A}H^{B}), 6.87 – 6.93 (2H, m, Ar*H*), 7.21 – 7.28 (1H, m, Ar*H*), 7.33 (2H, ddd, *J* = 7.8 Hz, 6.7 Hz, 1.2 Hz, Ar*H*), 7.37 – 7.42 (2H, m, Ar*H*), 7.44 – 7.50 (2H, m, Ar*H*) 7.54 – 7.62 (1H, m, Ar*H*), 7.99 – 8.03 (2H, m, Ar*H*), 8.03 – 8.08 (2H, m, Ar*H*). **^{13}C{^{1}H} NMR (126 MHz, $CDCl_3$) δ (ppm):** 43.8 (CH*C*H$_2$), 48.4 (*C*HCH$_2$), 55.4 (OCH$_3$), 113.7 (Ar*C*), 127.3 (Ar*C*), 128.2 (Ar*C*), 128.6 (Ar*C*), 129.2 (Ar*C*), 129.4 (Ar*C*), 131.3 (Ar*C*), 133.2 (Ar*C*), 136.6 (Ar*C*), 139.2 (Ar*C*), 163.4 (Ar*C*), 197.3 (*C*=O), 198.2 (*C*=O).

Data matches that previously reported.[215]

1-(4-(Tert-butyl)phenyl)-2,4-diphenylbutane-1,4-dione (241):

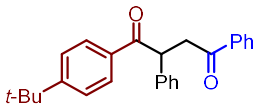

Synthesised using general procedure D to give 13.3 mg of **241** (36%) after silica column chromatography (3% EtOAc/Hexane).

Colourless solid. **Mp** 116-118 °C. **^{1}H NMR (500 MHz, $CDCl_3$) δ (ppm):** 1.30 (9H, s, C(C*H*$_3$)$_3$) 3.30 (1H, dd, *J* = 18.0 Hz, 3.7 Hz, CHC*H*^{A}H^B), 4.22 (1H, dd, *J* = 18.0 Hz, 10.1 Hz, CHCH^A*H*^{B}), 5.33 (1H, dd, *J* = 10.1 Hz, 3.7 Hz, C*H*CH^{A}H^B), 7.19 – 7.26 (1H, m, Ar*H*), 7.32 (2H, ddd, *J* = 7.8 Hz, 6.8 Hz, 1.2 Hz, Ar*H*), 7.36 – 7.47 (6H, m, Ar*H*), 7.52 – 7.58 (1H, m, Ar*H*), 7.95 – 8.01 (4H, m, Ar*H*); **^{13}C{^{1}H} NMR (126 MHz, $CDCl_3$) δ (ppm):** 31.1 (*C*H$_3$), 35.1 (*C*(CH$_3$)$_3$), 44.0 (CH*C*H$_2$), 48.5 (*C*HCH$_2$), 125.5 (Ar*C*), 127.3 (Ar*C*), 128.2 (Ar*C*), 128.3 (Ar*C*), 128.6 (Ar*C*), 128.9 (Ar*C*), 129.2 (Ar*C*), 133.3 (Ar*C*), 133.8 (Ar*C*), 136.5 (Ar*C*), 138.9 (Ar*C*), 156.6 (Ar*C*), 198.2 (*C*=O), 198.5 (*C*=O).

Data matches that previously reported.[157]

1,2-Diphenyl-4-(p-tolyl)butane-1,4-dione (245):

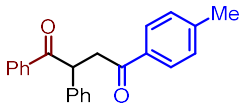

Synthesised using general procedure E to give 9.8 mg of **245** (30%) and general procedure G to give 32.8 mg of **25** (50%) after silica column chromatography (3% EtOAc/Hexane).

Colourless oil. **^{1}H NMR (500 MHz, $CDCl_3$) δ (ppm):** 2.40 (3H, s, C*H*$_3$) 3.29 (1H, dd, *J* = 18.0 Hz, 3.6 Hz, CHC*H*^{A}H^B), 4.19 (1H, dd, *J* = 18.0 Hz, 10.0 Hz, CHCH^A*H*^{B}), 5.32 (1H, dd, *J* = 10.1 Hz, 3.7 Hz, C*H*CH^{A}H^B), 7.21 – 7.26 (3H, m, Ar*H*), 7.28 – 7.34 (2H, m, Ar*H*), 7.34 – 7.43 (4H, m, Ar*H*), 7.46 – 7.52 (1H, m, Ar*H*), 7.86 – 7.90 (2H, m, Ar*H*), 8.02 – 8.05 (2H, m, Ar*H*); **^{13}C{^{1}H} NMR (126 MHz, $CDCl_3$) δ (ppm):** 21.7 (*C*H$_3$), 43.8 (CH*C*H$_2$), 48.7 (*C*HCH$_2$), 127.3 (Ar*C*), 128.27 (Ar*C*), 128.31 (Ar*C*), 128.5 (Ar*C*), 129.0 (Ar*C*), 129.2 (Ar*C*), 129.3 (Ar*C*), 132.9 (Ar*C*), 134.0 (Ar*C*), 136.5 (Ar*C*), 138.7 (Ar*C*), 144.1 (Ar*C*), 198.2 (*C*=O), 198.5 (*C*=O).

Data matches that previously reported.[216]

4-(4-Bromophenyl)-1,2-diphenylbutane-1,4-dione (246):

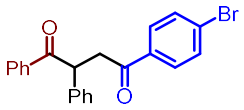

Synthesised using general procedure E to give 10.6 mg of **246** (27%) and general procedure G to give 42.5 mg of **26** (54%) after silica column chromatography (3% EtOAc/Hexane).

Colourless oil. **^{1}H NMR (500 MHz, $CDCl_3$) δ (ppm):** 3.24 (1H, dd, *J* = 18.0 Hz, 3.7 Hz, CHC*H*^{A}H^{B}), 4.16 (1H, dd, *J* = 18.0 Hz, 10.0 Hz, CHCH^{A}*H*^{B}), 5.31 (1H, dd, *J* = 10.0 Hz, 3.7 Hz, C*H*CH^{A}H^{B}), 7.21 – 7.26 (1H, m, Ar*H*), 7.28 – 7.37 (4H, m, Ar*H*), 7.38 – 7.42 (2H, m, Ar*H*), 7.46 – 7.51 (1H, m, Ar*H*), 7.57 – 7.61 (2H, m, Ar*H*), 7.82 – 7.86 (2H, m, Ar*H*), 8.00 – 8.03 (2H, m, Ar*H*); **^{13}C{^{1}H} NMR (126 MHz, $CDCl_3$) δ (ppm):** 43.8 (CH*C*H$_2$), 48.8 (*C*HCH$_2$), 127.5 (Ar*C*), 128.2 (Ar*C*), 128.6 (Ar*C*), 129.0 (Ar*C*), 129.3 (Ar*C*), 129.7 (Ar*C*), 131.9 (Ar*C*), 133.0 (Ar*C*), 135.2 (Ar*C*), 136.3 (Ar*C*), 138.5 (Ar*C*), 197.2 (*C*=O), 198.8 (*C*=O).

Data matches that previously reported.[216]

4-(4-Methoxyphenyl)-1,2-diphenylbutane-1,4-dione (247):

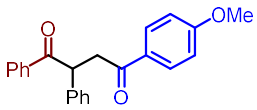

Synthesised using general procedure E to give 7.6 mg of **247** (22%) and general procedure G to give 30.3 mg of **27** (44%) after silica column chromatography (3% EtOAc/Hexane).

Colourless foam. **^{1}H NMR (500 MHz, $CDCl_3$) δ (ppm):** 3.27 (1H, dd, *J* = 17.8 Hz, 3.7 Hz, CHC*H*^{A}H^{B}), 3.86 (3H, s, OC*H*$_3$), 4.17 (1H, dd, *J* = 17.8 Hz, 10.1 Hz, CHCH^{A}*H*^{B}), 5.32 (1H, dd, *J* = 10.1 Hz, 3.7 Hz, C*H*CH^{A}H^{B}), 6.88 – 6.94 (2H, m, Ar*H*), 7.20 – 7.25 (1H, m, Ar*H*), 7.28 – 7.34 (2H, m, Ar*H*), 7.34 – 7.43 (4H, m, Ar*H*), 7.46 – 7.51 (1H, m, Ar*H*), 7.94 – 7.98 (2H, m, Ar*H*), 8.02 – 8.05 (2H, m, Ar*H*); **^{13}C{^{1}H} NMR (126 MHz, $CDCl_3$) δ (ppm):** 43.6 (CH*C*H$_2$), 48.7 (*C*HCH$_2$), 55.5 (OCH$_3$), 113.7 (Ar*C*), 127.3 (Ar*C*), 128.3 (Ar*C*), 128.5 (Ar*C*), 129.0 (Ar*C*), 129.2 (Ar*C*), 129.6 (Ar*C*), 130.5 (Ar*C*), 132.9 (Ar*C*), 136.5 (Ar*C*), 138.8 (Ar*C*), 163.6 (Ar*C*), 196.6 (*C*=O), 199.1 (*C*=O).

Data matches that previously reported.[217]

4-(4-Fluorophenyl)-1,2-diphenylbutane-1,4-dione (248):

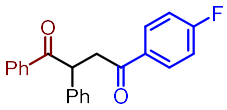

Synthesised using general procedure E to give 7.3 mg of **248** (22%) and general procedure G to give 47.2 mg of **28** (71%) after silica column chromatography (3% EtOAc/Hexane).

Colourless oil. **^{1}H NMR (500 MHz, $CDCl_3$) δ (ppm):** 3.26 (1H, dd, *J* = 17.9 Hz, 3.7 Hz, CHC*H*^{A}H^{B}), 4.18 (1H, dd, *J* = 17.9 Hz, 10.1 Hz, CHCH^{A}*H*^{B}), 5.31 (1H, dd, *J* = 10.1 Hz, 3.7 Hz, C*H*CH^{A}H^{B}), 7.12 (2H, t, *J* = 8.6 Hz, Ar*H*), 7.21 – 7.25 (1H, m, Ar*H*), 7.29 – 7.37 (4H, m, Ar*H*), 7.38 – 7.42 (2H, m, Ar*H*), 7.47 – 7.52 (1H, m, Ar*H*), 7.98 – 8.05 (4H, m, Ar*H*); **^{19}F NMR (471 MHz, $CDCl_3$) δ (ppm):** -104.9; **^{13}C{^{1}H} NMR (126 MHz, $CDCl_3$) δ (ppm):** 43.8 (CH*C*H$_2$), 48.8 (*C*HCH$_2$), 115.6 (d, *J* = 21.9 Hz, Ar*C*) 127.5 (Ar*C*), 128.2 (Ar*C*), 128.6 (Ar*C*), 129.0 (Ar*C*), 129.3 (Ar*C*), 130.8 (d, *J* = 9.4 Hz, Ar*C*), 133.0 (Ar*C*), 136.3 (Ar*C*), 138.5 (Ar*C*), 165.9 (d, *J* = 254.2 Hz, Ar*C*), 198.2 (*C*=O), 198.5 (*C*=O).

Data matches that previously reported.[217]

1,2-Diphenyl-4-(4-(trifluoromethyl)phenyl)butane-1,4-dione (249):

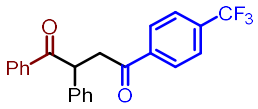

Synthesised using general procedure E to give 6.5 mg of **249** (17%) and general procedure G to give 22.2 mg of **29** (29%) after silica column chromatography (3% EtOAc/Hexane).

Yellow Oil. **^{1}H NMR (500 MHz, $CDCl_3$) δ (ppm):** 3.31 (1H, dd, *J* = 18.0 Hz, 3.7 Hz, CHC*H*^{A}H^{B}), 4.25 (1H, dd, *J* = 18.0 Hz, 10.1 Hz, CHCH^{A}*H*^{B}), 5.35 (1H, dd, *J* = 10.1 Hz, 3.6 Hz, C*H*CH^{A}H^{B}), 7.24 – 7.28 (1H, m, Ar*H*), 7.33 – 7.40 (4H, m, Ar*H*), 7.43 (2H, t, *J* = 7.7 Hz, Ar*H*), 7.50 – 7.55 (1H, m, Ar*H*), 7.73 – 7.78 (2H, m, Ar*H*), 8.03 – 8.07 (2H, m, Ar*H*), 8.10 – 8.14 (2H, m, Ar*H*); **^{19}F NMR (471 MHz, $CDCl_3$) δ (ppm):** -63.1; **^{13}C{^{1}H} NMR (126 MHz, $CDCl_3$) δ (ppm):** 44.1 (CH*C*H$_2$), 48.8 (*C*HCH$_2$), 123.5 (q, *J* = 272.4 Hz, *C*F$_3$), 125.7 (q, *J* = 3.9 Hz, Ar*C*), 127.6 (Ar*C*), 128.2 (Ar*C*), 128.5 (Ar*C*), 128.6 (Ar*C*), 129.0 (Ar*C*), 129.3 (Ar*C*), 133.1 (Ar*C*), 134.6 (q, *J* = 32.6 Hz, Ar*C*), 136.2 (Ar*C*), 138.3 (Ar*C*), 139.1.6 (Ar*C*), 197.3 (*C*=O), 198.7 (*C*=O).

Data matches that previously reported.[157]

1,2-Diphenylpentane-1,4-dione (250):

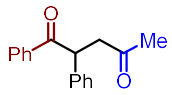

Synthesised using general procedure E to give 11.4 mg of **250** (45%) after silica column chromatography (10% EtOAc/Hexane).

Yellow oil. **^{1}H NMR (400 MHz, $CDCl_3$) δ (ppm):** 2.19 (3H, s, CH_3) 2.76 (1H, dd, *J* = 18.0 Hz, 4.0 Hz, CHC$H^{A}H^{B}$), 3.61 (1H, dd, *J* = 18.0 Hz, 10.1 Hz, CHC$H^{A}H^{B}$), 5.11 (1H, dd, *J* = 10.1 Hz, 4.0 Hz, CHC$H^{A}H^{B}$), 7.20 (1H, ddd, *J* = 8.1 Hz, 4.6 Hz, 2.4 Hz, Ar*H*), 7.26 – 7.31 (4H, m, Ar*H*), 7.37 (2H, dd, *J* = 8.3 Hz, 6.9 Hz, Ar*H*), 7.44 – 7.50 (1H, m, Ar*H*), 7.94 – 7.98 (2H, m, Ar*H*); **^{13}C{^{1}H} NMR (126 MHz, $CDCl_3$) δ (ppm):** 30.0 (*C*H_3), 48.1 (CH*C*H_2), 48.8 (*C*HCH_2), 127.3 (Ar*C*), 128.1 (Ar*C*), 128.4 (Ar*C*), 128.9 (Ar*C*), 129.2 (Ar*C*), 132.9 (Ar*C*), 138.6 (Ar*C*), 198.9 (*C*=O), 206.7 (*C*=O).

Data matches that previously reported.[218]

4-Cyclopentyl-1-phenyl-2-(pyridin-2-yl)butane-1,4-dione (251):

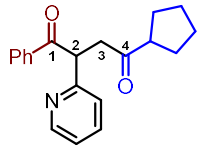

Synthesised using general procedure E to give 12.3 mg of **251** (40%) after silica column chromatography (20% EtOAc/Hexane).

Yellow oil. **Infra-Red (ν max, cm^{-1}):** 2955.0 (C-H), 2868.2 (C-H), 1707.0 (C=O), 1683.9 (C=O). **^{1}H NMR (400 MHz, $CDCl_3$) δ (ppm):** 1.51 – 1.89 (8H, m, CH_2CH_2CH_2CH_2), 2.87 – 3.01 (2H, m, CH_2CHCH_2 + C(3)H^AH^B), 3.66 (1H, dd, *J* = 17.9 Hz, 9.9 Hz, C(3)H^AH^B), 5.37 (1H, dd, *J* = 9.8 Hz, 4.2 Hz, C(2)*H*), 7.11 (1H, ddd, *J* = 7.6 Hz, 4.9 Hz, 1.2 Hz, Ar*H*), 7.23 – 7.26 (1H, m, Ar*H*), 7.35 – 7.41 (2H, m, Ar*H*), 7.45 – 7.50 (1H, m, Ar*H*), 7.58 (1H, td, *J* = 7.7 Hz, 1.8 Hz, Ar*H*), 8.00 – 8.05 (2H, m, Ar*H*); **^{13}C{^{1}H} NMR (126 MHz, $CDCl_3$) δ (ppm):** 26.0 ($CH_2CH_2CH_2CH_2$), 26.1 ($CH_2CH_2CH_2CH_2$), 28.8 ($CH_2CH_2CH_2CH_2$), 44.9 (*C*(3)), 51.1 (*C*(2)), 51.2 (CH_2CHCH_2), 122.1 (Ar*C*), 122.9 (Ar*C*), 128.5 (Ar*C*), 129.0 (Ar*C*), 133.0 (Ar*C*), 136.4 (Ar*C*), 137.1 (Ar*C*), 150.0 (Ar*C*), 158.5 (Ar*C*), 198.9 (*C*=O), 206.7 (*C*=O).

HRMS (ESI) $C_{20}H_{21}O_2NNa$ $[M+Na]^+$ found 330.1459, theoretical 330.1465 (– 1.8 ppm)

4,4-dimethyl-1,2-diphenylpentan-1-one (252):

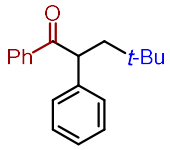

Synthesised using general procedure E to give 14.0 mg of **252** (53%) after silica column chromatography (3% EtOAc/Hexane).

Colourless solid. **^{1}H NMR (400 MHz, $CDCl_3$) δ (ppm):** 0.89 (9H, s, C(C*H*$_3$)$_3$), 1.56 – 1.61 (1H, m, C(3)*H*^{A}H^{B}) 2.63 (1H, dd, *J* = 14.0 Hz, 8.9 Hz, C(3)H^{A}C*H*^{B}), 4.73 (1H, dd, *J* = 8.9 Hz, 3.3 Hz, C(2)*H*), 7.15 – 7.20 (1H, m, Ar*H*), 7.24 – 7.29 (2H, m, Ar*H*), 7.30 – 7.35 (2H, m, Ar*H*), 7.39 – 7.45 (2H, m, Ar*H*), 7.48 – 7.53 (1H, m, Ar*H*), 7.98 – 8.03 (2H, m, Ar*H*); **^{13}C{^{1}H} NMR (126 MHz, $CDCl_3$) δ (ppm):** 29.8 (C(*C*H$_3$)$_3$, 31.2 (*C*(CH$_3$)), 47.6 (*C*(3)), 49.6 (*C*(2)), 126.8 (Ar*C*), 128.1 (Ar*C*), 128.6 (Ar*C*), 128.9 (Ar*C*), 129.5 (Ar*C*), 132.8 (Ar*C*), 137.0 (Ar*C*), 141.1 (Ar*C*), 200.0 (*C*=O).

Data matches that previously reported.[219]

[1,1'-Biphenyl]-4-carbonyl fluoride (266):

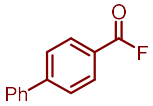

Synthesised using general procedure H.

Colourless solid. **^{1}H NMR (400 MHz, $CDCl_3$) δ (ppm):** 7.41 – 7.54 (3H, m, Ar*H*), 7.62 – 7.66 (2H, m, Ar*H*), 7.72 – 7.77 (2H, m, Ar*H*), 8.09 – 8.15 (2H, m, Ar*H*); **^{19}F NMR (376 MHz, $CDCl_3$) δ (ppm):** 18.1.

Data matches that previously reported.[220]

2-Naphthoyl fluoride (267):

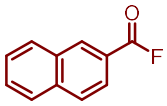

Synthesised using general procedure H.

Colourless solid. **^{1}H NMR (400 MHz, $CDCl_3$) δ (ppm):** 7.62 (1H, ddd, *J* = 8.1 Hz, 6.9 Hz, 1.3 Hz, Ar*H*), 7.69 (1H, ddd, *J* = 8.2 Hz, 6.9 Hz, 1.3 Hz, Ar*H*), 7.90 – 8.03 (4H, m, Ar*H*), 8.63 – 8.65 (1H, m, Ar*H*); **^{19}F NMR (376 MHz, $CDCl_3$) δ (ppm):** 18.1.

Data matches that previously reported.[220]

1-Naphthoyl fluoride (268):

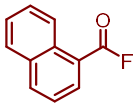

Synthesised using general procedure H.

Colourless solid. **^{1}H NMR (400 MHz, $CDCl_3$) δ (ppm):** 7.58 (1H, dd, *J* = 8.2 Hz, 7.4 Hz, Ar*H*), 7.69 (1H, ddd, *J* = 8.2 Hz, 6.9 Hz, 1.3 Hz, Ar*H*), 7.90 – 8.03 (4H, m, Ar*H*), 8.63 – 8.65 (1H, m, Ar*H*); **^{19}F NMR (376 MHz, $CDCl_3$) δ (ppm):** 29.9.

Data matches that previously reported.[220]

4-Chlorobenzoyl fluoride (269):

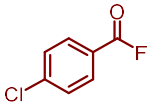

Synthesised using general procedure H.

Colourless solid. **^{1}H NMR (400 MHz, $CDCl_3$) δ (ppm):** 7.50 – 7.59 (2H, m, C(3)*H*), 7.97 – 8.06 (2H, m, C(2)*H*); **^{19}F NMR (376 MHz, $CDCl_3$) δ (ppm):** 29.9.

Data matches that previously reported.[220]

4-Bromobenzoyl fluoride (270):

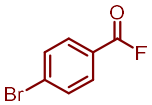

Synthesised using general procedure H.

Colourless solid. **^{1}H NMR (400 MHz, $CDCl_3$) δ (ppm):** 7.61 – 7.81 (2H, m, C(3)*H*), 7.81 – 8.00 (2H, m, C(2)*H*); **^{19}F NMR (376 MHz, $CDCl_3$) δ (ppm):** 18.4.

Data matches that previously reported.[221]

4-Iodobenzoyl fluoride (271):

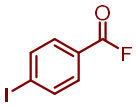

Synthesised using general procedure H.

Colourless solid. **^{1}H NMR (400 MHz, $CDCl_3$) δ (ppm):** 7.70 – 7.78 (2H, m, C(3)*H*), 7.87 – 7.95 (2H, m, C(2)*H*); **^{19}F NMR (376 MHz, $CDCl_3$) δ (ppm):** 18.4.

Data matches that previously reported.[220]

4-Methoxybenzoyl fluoride (272):

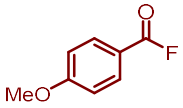

Synthesised using general procedure H.

Colourless oil. **^{1}H NMR (400 MHz, $CDCl_3$) δ (ppm):** 3.92 (3H, s, OCH_3), 6.95 – 7.09 (2H, m, C(3)*H*), 7.99 – 8.06 (2H, m, C(2)*H*); **^{19}F NMR (376 MHz, $CDCl_3$) δ (ppm):** 16.0.

Data matches that previously reported.[220]

4-(*tert*-butyl)benzoyl fluoride (273):

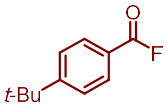

Synthesised using general procedure H.

Colourless solid. **^{1}H NMR (400 MHz, $CDCl_3$) δ (ppm):** 1.35 (9H, s, C(CH_3)$_3$), 7.54 (2H, dd, *J* = 8.6 Hz, 1.4 Hz, (C(3)*H*), 7.98 (2H, d, *J* = 8.5 Hz, C(2)*H*); **^{19}F NMR (376 MHz, $CDCl_3$) δ (ppm):** 17.7.

Data matches that previously reported.[222]

4-Cyanobenzoyl fluoride (274):

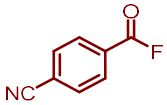

Synthesised using general procedure H.

Colourless solid. **^{1}H NMR (400 MHz, $CDCl_3$) δ (ppm):** 7.67 – 7.92 (2H, m, C(3)*H*), 8.17 (2H, d, *J* = 8.4 Hz, C(2)*H*); **^{19}F NMR (376 MHz, $CDCl_3$) δ (ppm):** 20.2.

Data matches that previously reported.[223]

Cyclohexanecarbonyl fluoride (275):

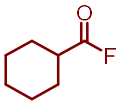

Synthesised using general procedure H.

Colourless oil. **^{1}H NMR (400 MHz, $CDCl_3$) δ (ppm):** 1.23 – 1.34 (3H, m, CH_2), 1.45 – 1.62 (2H, m, CH_2), 1.62 (1H, m, CH_2), 1.62 – 1.72 (1H, m, CH_2), 1.75 – 1.80 (2H, m, CH_2), 1.95 – 2.02 (2H, m, CH_2), 2.47 – 2.54 (1H, m, C*H*); **^{19}F NMR (376 MHz, $CDCl_3$) δ (ppm):** 36.7.

Data matches that previously reported.[220]

2-Furanoyl fluoride (276):

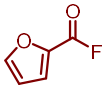

Synthesised using general procedure H.

Colourless oil. **^{1}H NMR (400 MHz, $CDCl_3$) δ (ppm):** 6.65 (1H, ddd, *J* = 3.6 Hz, 1.8 Hz, 0.8 Hz, C(4)*H*), 7.45 (1H, dd, *J* = 3.7 Hz, 0.8 Hz, C(3)*H*), 7.77 (1H, ddd, *J* = 2.5 Hz, 1.7 Hz, 0.8 Hz, C(4)*H*)

^{19}F NMR (376 MHz, $CDCl_3$) δ (ppm): 15.4.

Data matches that previously reported.[224]

2-Oxo-2-(p-tolyl)acetic acid (277):

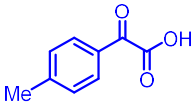

Synthesised according to general procedure I.

Colourless solid. **Mp** 97-99 °C {Lit.[225] 97-99 °C}. **^{1}H NMR (500 MHz, $CDCl_3$) δ (ppm):** 2.46 (3H, s, CH_3), 7.34 (2H, d, *J* = 8.1 Hz, ArC(3)*H*), 8.28 (2H, d, *J* = 8.0 Hz, ArC(2)*H*); **^{13}C{^{1}H} NMR (126 MHz, $CDCl_3$) δ (ppm):** 22.1 (*C*H_3), 129.2 (Ar*C*), 129.8 (Ar*C*), 131.7 (Ar*C*), 147.4 (Ar*C*), 161.3 (*C*(O)OH), 183.6 (*C*=O)).

Data matches that previously reported.[226]

2-(4-Bromophenyl)-2-oxoacetic acid (278):

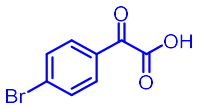

Synthesised according to general procedure I.

Colourless solid. **Mp** 97-99 °C {Lit. Mp[227] 100-102 °C}. **^{1}H NMR (500 MHz, $CDCl_3$) δ (ppm):** 7.66 – 7.70 (2H, m, ArC(3)*H*), 8.20 – 8.24 (2H, m, ArC(2)*H*); **^{13}C{^{1}H} NMR (126 MHz, $CDCl_3$) δ (ppm):** 130.5 (Ar*C*), 131.6 (Ar*C*), 132.4 (Ar*C*), 132.7 (Ar*C*), 161.1 (*C*(O)OH), 183.8 (*C*=O)).

Data matches that previously reported.[226]

2-(4-Methoxyphenyl)-2-oxoacetic acid (279):

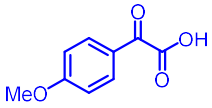

Synthesised according to general procedure I.

Colourless solid. **Mp** 74-76 °C {Lit. Mp[160] 79-81 °C}. **^{1}H NMR (500 MHz, $CDCl_3$) δ (ppm):** 3.91 (3H, s, OCH_3), 6.95 – 7.00 (2H, m, ArC(3)*H*), 8.33 – 8.39 (2H, m, ArC(2)*H*); **^{13}C{^{1}H} NMR (126 MHz, $CDCl_3$) δ (ppm):** 55.7 (OCH_3), 114.4 (Ar*C*), 124.9 (Ar*C*), 162.6 (*C*(O)OH), 165.6 (Ar*C*), 183.0 (*C*=O).

Data matches that previously reported.[226]

2-(4-Fluorophenyl)-2-oxoacetic acid (280):

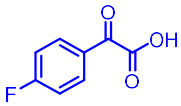

Synthesised according to general procedure I.

Colourless solid. **Mp** 95-97 °C {Lit. Mp[228] 95-96 °C}. **^{1}H NMR (500 MHz, $CDCl_3$) δ (ppm):** 7.14 – 7.25 (2H, m, ArC(3)*H*), 8.41 – 8.49 (2H, m, ArC(2)*H*); **^{19}F NMR (471 MHz, $CDCl_3$) δ (ppm):** -99.2; **^{13}C{^{1}H} NMR (126 MHz, $CDCl_3$) δ (ppm):** 116.5 (d, *J* = 22.3 Hz, Ar*C*), 128.2 (Ar*C*), 134.6 (d, *J* = 10.0 Hz, Ar*C*), 163.8 (d, *J* = 662.7 Hz, Ar*C*), 168.5 (*C*(O)OH), 182.4 (*C*=O).

Data matches that previously reported.[226]

2-oxo-2-(4-(trifluoromethyl)phenyl)acetic acid (281):

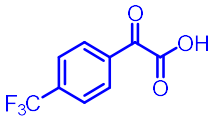

Synthesised according to general procedure I.

Colourless solid. **Mp** 56-59 °C {Lit. Mp[227] 53-55 °C}. **^{1}H NMR (400 MHz, $CDCl_3$) δ (ppm):** 7.81 (2H, d, *J* = 8.3 Hz, ArC(3)*H*), 8.42 (2H, d, *J* = 8.2 Hz, ArC(2)*H*), 8.90 (1H, s, O*H*); **^{13}C{^{1}H} NMR (126 MHz, $CDCl_3$) δ (ppm):** 123.2 (q, *J* = 273.0 Hz, *C*F_3), 126.0 (q, *J* = 3.7 Hz), 131.5 (Ar*C*), 134.4 (Ar*C*), 136.5 (q, *J* = 33.0 Hz), 161.8 (*C*(O)OH), 183.6 (*C*=O).

Data matches that previously reported.[229]

2-cyclopentyl-2-oxoacetic acid (282):

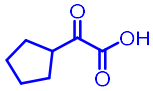

Diethyl oxalate (2.0 g, 13.7 mmol, 1.0 equiv.) and THF (30 mL) were added to an oven-dried schlenk flask under nitrogen and cooled to -78 °C. Then cyclopentyl magnesium chloride (8.2 mL, 2 M, 16.4 mmol, 1.2 equiv.) was added dropwise. The reaction mixture was then stirred for 1 h before being allowed to warm to room temperature. Then the reaction mixture was poured on to ice water and extracted with Et_2O (3 × 20 mL). The organic layers were combined, dried (Na_2SO_4) and concentrated *in vacuo*. The resulting crude material was then dissolved in EtOH (30 mL) and water (30 mL). Sodium hydroxide (1.1 g, 27.4 mmol, 2.0 equiv.) is added to the solution and the reaction mixture is stirred at room temperature for 24 h. Then the pH of the reaction is adjusted to 1 using dilute hydrochloric acid and extracted with EtOAc (3 × 30 mL). The organic layers were combined, dried (Na_2SO_4) and concentrated *in vacuo*. Purification through silica column chromatography (10% to 30% EtOAc/Hexane) afforded the desired product as a pale yellow oil (0.40 g, 21%).

^{1}H NMR (500 MHz, $CDCl_3$) δ (ppm): 1.65 – 1.75 (4H, m, CH_2), 1.77 – 1.88 (2H, m, CH_2), 1.95 – 2.05 (2H, m, CH_2), 3.69 (1H, tt, *J* = 9.0 Hz, 6.9 Hz); **^{13}C{^{1}H} NMR (126 MHz, $CDCl_3$) δ (ppm):** 26.2 (*C*H_2) 28.8 (*C*H_2), 45.6 (*C*H), 159.9 (*C*(O)OH), 197.7 (*C*=O).

Data matches that previously reported.[230]

7.5 Experimental procedures and characterization for Chapter 5.

General Method A - BCl_3 catalysed [2+2] cycloaddition

endo-2,4-Dibromodicyclo-pentadiene-8-oxane-1-one (31.8 mg, 0.1 mmol, 1.0 equiv.) was added to an oven dried vial. The vial was sealed and evacuated then back filled with nitrogen three times. In a separate Schlenk flask anhydrous CH_2Cl_2 was sparged with nitrogen for 10 minutes then added to the vial (1.9 mL). Then BCl_3 (0.1 mL, 1 M, 1.0 equiv.) was added. The reaction mixture was stirred under 370 nm irradiation at room temperature for 20 h using photoreactor set-up B. The reaction mixture was quenched with distilled water (5 mL) then extracted with DCM (3 × 5 mL). The organic phases were combined, dried with $MgSO_4$, filtered, and concentrated under vacuum to afford crude product.

General Method B – optimization of benzophenone catalysed [2+2] cycloaddition

256 or **257** (1.0 equiv.) and benzophenone were added to a Schlenk flask or vial and sealed. Solvent was added and the solution was sparged with nitrogen for 15 minutes. The flask or vial was then stirred under 370 or 390 nm irradiation at room temperature using photoreactor set-up B or C. The progress of the reaction was monitored by taking an aliquot and submitting it to ^{1}H NMR analysis and conversions were calculated using the same methods as Collin and Linclau.[184]

Theoretical Calculations

Calculations were performed with Gaussian16, Revision C.01,[231] employing either pure or hybrid levels of DFT using the 6-31G(d,p)[232] basis set with a variety of functionals; B3LYP, PBE0 and BLYP.[233–236] An ultrafine integration grid (99 radial shells with 590 angular points per shell) was used. Implicit solvation was used at both the optimisation and single point steps using the Polarizable Continuum Model (PCM),[237,238] employing parameters for DCM (ε = 8.93).[239–241] Corrections for dispersion were also included for optimisation and single point calculations using the Grimme DFT-D3 correction with Becke Johnson dampening.[242,243] Calculations were submitted and processed using an in-house developed software, *Silico*, which incorporates a number of publicly available software libraries, including: cclib[244] for parsing of result files and Open Babel[245]/Pybel[246] for file interconversion.

1,4–dioxaspiro[4.4]nonane (283):

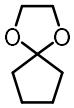

Based on a procedure reported by Collin *et al*.[184] DOWEX® 50WX8 200-400 cation exchange resin (0.60 g) was washed with MeOH and dired under vacuum then added to a round bottom flask with cyclopentanone (50.0 mL, 0.56 mol, 1.0 equiv.), ethylene glycol (40.0 mL, 0.72 mol, 1.3 equiv.) and anhydrous benzene (100 mL). The reaction mixture was then heated to reflux under a Dean-Stark apparatus and stirred for 30 h. After the reaction cooled to room temperature it was washed with 4% sodium hydroxide (2 × 50 mL) and brine (2 × 100 mL) then dired ($MgSO_4$). Purification through distillation afforded **283** as a colourless oil with some trace ethylene glycol and cyclopentanone impurities (41.5g, 52%).

^{1}H NMR (400 MHz, $CDCl_3$) δ (ppm): 1.71 – 1.65 (m, 4H, $CH_2CH_2CH_2CH_2$), 1.80 – 1.75 (m, 4H, $CH_2CH_2CH_2CH_2$), 3.90 (s, 4H, OCH_2CH_2O); **^{13}C{^{1}H} NMR (101 MHz, $CDCl_3$) δ (ppm):** 118.5 (*C*O), 64.2 (OCH_2CH_2O), 35.9 ($CH_2CH_2CH_2CH_2$), 23.6 ($CH_2CH_2CH_2CH_2$).

Data matches that previously reported.[184]

***endo*–2,4–dibromodicyclopentadiene–1,8–dione bisethylene ketal (254):**

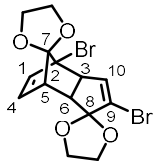

Based on a procedure reported by Collin *et al*.[184] **283** (20.0 g, 156 mmol, 1.0 equiv.) and anhydrous 1,4-dioxane (125 mL) were added to an oven-dried three-neck flask and sparged with nitrogen for 15 minutes then cooled to 0 °C. Bromine (28.1 mL, 0.55 mol, 3.5 equiv.) was added using a dropping funnel over 2 h, then the reaction mixture was stirred at room temperature for 20 h. A 4% sodium hydroxide trap was linked to the reaction to trap any HBr. Then a solution of sodium hydroxide (48.7 g, 1.2 mol, 7.8 equiv.) in methanol (250 mL) was added using a dropping funnel over 2 h and the reaction mixture was heated to reflux and stirred for 24 h. After the reaction cooled to room temperature it was poured onto rapidly stirring ice water (750 mL). The resulting precipitate was collected through vacuum filtration and washed with ice water (100 mL) then dried under vacuum to afford **254** as a beige solid (37.5 g, 59%).

Mp: 164-165 °C {Lit:[247] 174-176 °C). **^{1}H NMR (400 MHz, $CDCl_3$) δ (ppm):** 2.72 (1H, td, *J* = 4.7, 0.7 Hz, C(6)*H*), 3.08 (1H, dd, *J* = 7.4, 4.7 Hz, C(6)*H*), 3.50 (1H, dd, *J* = 7.4, 2.5 Hz, C(3)*H*), 4.04 – 3.87 (4H, m, OCH_2CH_2O), 4.26 – 4.11 (4H, m, OCH_2CH_2O), 5.84 (1H, dd, *J* = 6.4, 1.3 Hz, C(1)*H*), 6.07 (1H, d, *J* = 2.5 Hz, C(10)*H*), 6.19 (1H, dd, *J* = 6.4, 3.6 Hz, C(4)*H*); **^{13}C NMR (101 MHz, $CDCl_3$) δ (ppm):** 47.3 (*C*(5)), 49.6 (*C*(6)), 55.8 (*C*(3)), 65.3 (OCH_2*C*H_2O), 65.4 (OCH_2*C*H_2O), 66.3 (O*C*H_2CH_2O), 66.5 (O*C*H_2CH_2O), 67.8 (*C*(2)), 115.7(*C*(2)), 126.1 (*C*(7)), 128.1 (*C*(8)), 132.6 (*C*(4)), 133.1 (*C*(1)), 134.6 (*C*(10)).

GCMS $C_{14}H_{14}Br_2O_4$ [M]$^+$ found: 406.0, theoretical: 406.1, retention time = 8.9 min.

Data matches that previously reported.[184]

(3a'R,4'S,7'S,7a'S)-2',4'-dibromo-3a',4',7',7a'-tetrahydro-1'H-spiro[[1,3]dioxolane-2,8'-[4,7]methanoinden]-1'-one (257):

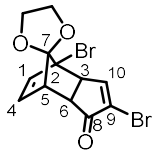

Based on a procedure reported by Chapman *et al*.[182] **254** (300 mg, 0.74 mmol, 1.0 equiv.) and THF (3 mL) were added to a round bottom flask. Hydrochloric acid (0.30 mL, conc., 4.9 equiv.) was added dropwise and the reaction was stirred at room temperature for 18 h. The reaction mixture was then poured onto a 10% solution of $NaHCO_3$ (20 mL) and left at room temperature for 1 h. The resulting precipitate was collected through vacuum filtration and washed with water then dried under vacuum. Purification through recrystallization (toluene) afforded **257** as a beige solid (186 mg, 69%)

Mp: 172-174 °C {Lit.[182] 171-172 °C}. **^{1}H NMR (400 MHz, $CDCl_3$) δ (ppm):** 3.05 – 3.11 (1H, m, C(6)*H*), 3.20 (1H, t, *J* = 5.4 Hz, C(5)*H*), 3.63 – 3.67 (1H, m, C(3)*H*), 3.93 – 4.00 (1H, m, OCH_2CH_2O), 4.02 – 4.09 (1H, m, OCH_2CH_2O), 4.15 – 4.29 (2H, m, OCH_2CH_2O), 5.93 (1H, dd, *J* 6.5, 1.4, C(1)*H*), 6.01 (1H, dd, *J* 6.5, 3.6, C(4)*H*), 7.63 (1H, dd, *J* 2.9, 0.7, C(10)*H*).

Data matches that previously reported.[182]

***endo*-2,4-dibromodicyclo-pentadiene-1,8-dione (256):**

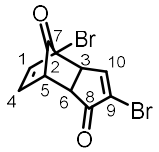

Based on a procedure reported by Collin *et al*.[184] H_2SO_4 (113 mL, 2.1 mol, excess) was added to a round bottom flask and cooled to 0 °C. Then **254** (37.5 g, 92.8 mmol, 1.0 equiv.) was added portionwise and the reaction mixture was stirred at room temperature for 30 h. The reaction mixture was then poured onto rapidly stirring ice water (300 mL). The resulting beige precipitate was collected through vacuum filtration and washed with ice water (100 mL) and dried under vacuum. Purification through recrystallization (50% EtOAc/Hexane) afforded the desired product as a colourless solid (15.0 g, 51%) **Mp:** 154-155 °C {Lit.[182] 154-155 °C}. **^{1}H NMR (400 MHz, $CDCl_3$) δ (ppm):** 3.20 (1H, dd, *J* = 6.4, 5.0 Hz, C(6)*H*), 3.52 (1H, dd, J = 6.9, 3.0 Hz, C(3)*H*), 3.59 (1H, ddd, *J* = 5.2, 3.9, 0.6 Hz, C(5)*H*), 6.25 (1H, dt, J= 6.9, 0.8 Hz, C(1)*H*), 6.36 (1H, dd, *J* = 6.9, 3.9 Hz, C(4)*H*), 7.67 (1H, d, *J* = 3.1 Hz, C(10)*H*); **^{13}C NMR (101 MHz, $CDCl_3$) δ (ppm):** 44.1 (*C*(6)), 47.3 (*C*(5)), 49.0 (*C*(3)), 60.4 (*C*(9)), 129.9 (*C*(9)), 133.9 (*C*(4)), 134.2 (*C*(1)), 156.5 (*C*(10)), 192.5 (*C*(7)), 197.1 (*C*(8)).

Data matches that previously reported.[184]

Dimethyl 1,4-cubanedicarboxylate (253):

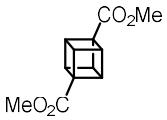

256 (328 mg, 1.0 mmol, 1 equiv.) and benzophenone (91.0 mg, 0.5 mmol, 0.5 equiv.) were added to a Schlenk flask. The flask was sealed with a suba-seal and MeCN (10 mL) was added, and the solution was sparged with nitrogen for 15 minutes. The reaction was stirred under 390 nm irradiation at room temperature using photoreactor set-up C for 24 hours then concentrated *in vacuo*. The crude product was used without further purification.

The crude materials of six runs were combined and suspended in water (10 mL). NaOH solution (10 mL, 26% w/v solution) was added to the brown suspension and the reaction was refluxed vigorously for 16 h. After the reaction cooled to room temperature the pH was adjusted to 1 using conc. hydrochloric acid. The solution was filtered and washed with ice-cold water. In our hands, the 1,4-cubanedicarboxylic acid did not precipitate out and filtration simply removed benzophenone. The filtrate was then concentrated *in vacuo* to yield a dark brown solid. This material was then suspended in methanol and filtered to remove some of the salts. This filtrate was then concentrated *in vacuo* and thoroughly dried to yield a brown solid which was used without further purification.

Crude 1,4-cubanedicarboxylic acid (ca. 6.0 mmol) was dissolved in methanol (30 mL) and conc. hydrochloric acid (0.89 mL, 10.8 mmol, 1.8 equiv.) was added to the reaction mixture. The reaction was then refluxed for 16 h under a nitrogen atmosphere. After the reaction cooled to room temperature the reaction was concentrated *in vacuo* to obtain a brown solid, which was then dissolved in CH_2Cl_2 (30 mL). Water (30 mL) was added, and the aqueous phase was extracted with DCM (3 × 30 mL). The organic phases were combined, washed with brine (30 mL), dried (Na_2SO_4), and concentrated *in vacuo* to afford the crude product. Purification through silica column chromatography (20% EtOAc/Hexane) afforded **253** as a colourless solid 0.27 g (20%). **Mp**: 160-164 °C {Lit:[184] 164-165 °C}. **^{1}H NMR (400 MHz, $CDCl_3$) δ (ppm):** 3.71 (s, 6H, OC*H*$_3$), 4.23 (s, 6H, C*H*); **^{13}C{^{1}H} NMR (126 MHz, $CDCl_3$) δ (ppm):** 47.1 (*C*H), 51.7 (O*C*H$_3$), 55.8 (*C*COOCH$_3$), 172.0 (*C*=O).

Data matches that previously reported.[184]

4-(methoxycarbonyl)cubane-1-carboxylic acid (262):

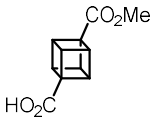

Based on a procedure reported by Eaton *et al*.[188] **253** (0.25 g, 1.14 mmol, 1.0 equiv.) and THF (10 mL) were added to a round bottom flask. NaOH (2.3 M, 0.5 mL, 1.0 equiv.) in MeOH was added dropwise and the reaction was stirred at room temperature for 24 h. Then the reaction was concentrated *in vacuo* and suspended in water. Extraction with CH_2Cl_2 (3 × 10 mL) yielded unreacted **253** (0.11 g, 44%). The aqueous phase was acidified with 2 M HCl to a pH of 1 and extracted with CH_2Cl_2 (3 × 10 mL). The organic layers were combined, washed with brine (1 × 10 mL), dried (Na_2SO_4) and concentrated *in vacuo* to afford **262** as a colourless solid (0.12 g, 50%)

Mp: 180-182 °C {Lit:[188] 182-183 °C}. **^{1}H NMR (400 MHz, DMSO) δ (ppm):** 3.62 (s, 3H, OC*H*$_3$), 4.16 – 4.12 (m, 6H, C*H*), 12.41 (s, 1H, COO*H*); **^{13}C{^{1}H} NMR (126 MHz, DMSO) δ (ppm):** 46.55 (*C*H), 46.58 (*C*H), 51.8 (O*C*H$_3$), 55.5 (*C*COO), 56.0 (*C*COO), 172.2 (*C*=O), 172.7 (*C*=O).

Data matches that previously reported.[188]

8 References

1 G. Ciamician, *Science*, 1912, **36**, 385–394.
2 N. Hoffmann, *Chem. Rev.*, 2008, **108**, 1052–1103.
3 S. E. Braslavsky, *Pure Appl. Chem.*, 2007, **79**, 293–465.
4 D. M. Hedstrand, W. H. Kruizinga and R. M. Kellogg, *Tetrahedron Lett.*, 1978, **19**, 1255–1258.
5 Benjamin Cummings, *Modern Molecular Photochemistry*.
6 S. Majumdar, H. S. Majumdar, R. Österbacka and E. McCarthy, in *Reference Module in Materials Science and Materials Engineering*, Elsevier, 2016.
7 D. Rehm and A. Weller, *Isr. J. Chem.*, 1970, **8**, 259–271.
8 C. R. Bock, J. A. Connor, A. R. Gutierrez, T. J. Meyer, D. G. Whitten, B. P. Sullivan and J. K. Nagle, *J. Am. Chem. Soc.*, 1979, **101**, 4815–4824.
9 W. E. Jr. Jones and M. A. Fox, *J. Phys. Chem.*, 1994, **98**, 5095–5099.
10 J. Luo, B. Hu, W. Wu, M. Hu and T. L. Liu, *Angew. Chem. Int. Ed.*, 2021, **60**, 6107–6116.
11 F. Strieth-Kalthoff, M. J. James, M. Teders, L. Pitzer and F. Glorius, *Chem. Soc. Rev.*, 2018, **47**, 7190–7202.
12 R. M. Clegg, in *Fret and Flim Techniques*, Elsevier, 2009, vol. 33, pp. 1–57.
13 K. Singh, S. J. Staig and J. D. Weaver, *J. Am. Chem. Soc.*, 2014, **136**, 5275–5278.
14 J. B. Metternich, S. Sagebiel, A. Lückener, S. Lamping, B. J. Ravoo and R. Gilmour, *Chem. Eur. J.*, 2018, **24**, 4228–4233.
15 A. Sinicropi, F. Barbosa, R. Basosi, B. Giese and M. Olivucci, *Angew. Chem. Int. Ed.*, 2005, **44**, 2390–2393.
16 P. Jia, Y. Hu, Z. Zeng, Y. Wang, B. Song, Y. Jiang, H. Sun, M. Wang, W. Qiu and L. Xu, *Chin. Chem. Lett.*, 2023, **34**, 107511.
17 M. A. Cismesia and T. P. Yoon, *Chem. Sci.*, 2015, **6**, 5426–5434.
18 C. Stephenson, T. Yoon and D. W. C. MacMillan, *Visible Light Photocatalysis in Organic Chemistry*, Wiley-VCH Verlag GmbH & Co. KGaA, Weinheim, Germany, 2018.
19 A. Juris, V. Balzani, F. Barigelletti, S. Campagna, P. Belser and A. von Zelewsky, *Coord. Chem. Rev.*, 1988, **84**, 85–277.
20 L. Flamigni, A. Barbieri, C. Sabatini, B. Ventura and F. Barigelletti, in *Photochemistry and Photophysics of Coordination Compounds II*, eds. V. Balzani and S. Campagna, Springer Berlin Heidelberg, Berlin, Heidelberg, 2007, pp. 143–203.
21 M. S. Lowry, J. I. Goldsmith, J. D. Slinker, R. Rohl, R. A. Pascal, G. G. Malliaras and S. Bernhard, *Chem. Mater.*, 2005, **17**, 5712–5719.
22 M. S. Lowry, W. R. Hudson, R. A. Pascal and S. Bernhard, *J. Am. Chem. Soc.*, 2004, **126**, 14129–14135.
23 N. A. Romero and D. A. Nicewicz, *Chem. Rev.*, 2016, **116**, 10075–10166.
24 T. Shen, Z.-G. Zhao, Q. Yu and H.-J. Xu, *J. Photochem. Photobiol. Chem.*, 1989, **47**, 203–212.
25 J. Widengren, U. Mets and R. Rigler, *J. Phys. Chem.*, 1995, **99**, 13368–13379.
26 X. Zhang and T. Rovis, *J. Am. Chem. Soc.*, 2021, **143**, 21211–21217.
27 U. Megerle, M. Wenninger, R.-J. Kutta, R. Lechner, B. König, B. Dick and E. Riedle, *Phys Chem Chem Phys*, 2011, **13**, 8869–8880.
28 J. W. Verhoeven, *J. Photochem. Photobiol. C Photochem. Rev.*, 2006, **7**, 40–60.
29 C. A. Parker and C. G. Hatchard, *Trans Faraday Soc*, 1961, **57**, 1894–1904.
30 H. Uoyama, K. Goushi, K. Shizu, H. Nomura and C. Adachi, *Nature*, 2012, **492**, 234–238.
31 M. A. Bryden and E. Zysman-Colman, *Chem. Soc. Rev.*, 2021, **50**, 7587–7680.
32 F. B. Dias, T. J. Penfold and A. P. Monkman, *Methods Appl. Fluoresc.*, 2017, **5**, 012001.
33 Y. Tao, K. Yuan, T. Chen, P. Xu, H. Li, R. Chen, C. Zheng, L. Zhang and W. Huang, *Adv. Mater.*, 2014, **26**, 7931–7958.
34 Z. Yang, Z. Mao, Z. Xie, Y. Zhang, S. Liu, J. Zhao, J. Xu, Z. Chi and M. P. Aldred, *Chem. Soc. Rev.*, 2017, **46**, 915–1016.

35 S. Madayanad Suresh, D. Hall, D. Beljonne, Y. Olivier and E. Zysman-Colman, *Adv. Funct. Mater.*, 2020, **30**, 1908677.
36 D. Hall, P. Rajamalli, E. Duda, S. M. Suresh, F. Rodella, S. Bagnich, C. L. Carpenter-Warren, D. B. Cordes, A. M. Z. Slawin, P. Strohriegl, D. Beljonne, A. Köhler, Y. Olivier and E. Zysman-Colman, *Adv. Opt. Mater.*, 2021, **9**, 2100846.
37 D. Hall, S. M. Suresh, P. L. dos Santos, E. Duda, S. Bagnich, A. Pershin, P. Rajamalli, D. B. Cordes, A. M. Z. Slawin, D. Beljonne, A. Köhler, I. D. W. Samuel, Y. Olivier and E. Zysman-Colman, *Adv. Opt. Mater.*, 2020, **8**, 1901627.
38 H. Hirai, K. Nakajima, S. Nakatsuka, K. Shiren, J. Ni, S. Nomura, T. Ikuta and T. Hatakeyama, *Angew. Chem. Int. Ed.*, 2015, **54**, 13581–13585.
39 T. Hatakeyama, K. Shiren, K. Nakajima, S. Nomura, S. Nakatsuka, K. Kinoshita, J. Ni, Y. Ono and T. Ikuta, *Adv. Mater.*, 2016, **28**, 2777–2781.
40 Y. Yuan, X. Tang, X.-Y. Du, Y. Hu, Y.-J. Yu, Z.-Q. Jiang, L.-S. Liao and S.-T. Lee, *Adv. Opt. Mater.*, 2019, **7**, 1801536.
41 J. E. Field and D. Venkataraman, *Chem. Mater.*, 2002, **14**, 962–964.
42 D. Hall, K. Stavrou, E. Duda, A. Danos, S. Bagnich, S. Warriner, A. M. Z. Slawin, D. Beljonne, A. Köhler, A. Monkman, Y. Olivier and E. Zysman-Colman, *Mater Horiz*, 2022, **9**, 1068–1080.
43 J. Luo and J. Zhang, *ACS Catal.*, 2016, **6**, 873–877.
44 E. Speckmeier, T. G. Fischer and K. Zeitler, *J. Am. Chem. Soc.*, 2018, **140**, 15353–15365.
45 J. Lu, B. Pattengale, Q. Liu, S. Yang, W. Shi, S. Li, J. Huang and J. Zhang, *J. Am. Chem. Soc.*, 2018, **140**, 13719–13725.
46 M. A. Bryden, F. Millward, T. Matulaitis, D. Chen, M. Villa, A. Fermi, S. Cetin, P. Ceroni and E. Zysman-Colman, *J. Org. Chem.*, DOI:10.1021/acs.joc.2c01137.
47 M. Bouzrati-Zerelli, N. Guillaume, F. Goubard, T.-T. Bui, S. Villotte, C. Dietlin, F. Morlet-Savary, D. Gigmes, J. P. Fouassier, F. Dumur and J. Lalevée, *New J Chem*, 2018, **42**, 8261–8270.
48 E. R. Sauvé, D. M. Mayder, S. Kamal, M. S. Oderinde and Z. M. Hudson, *Chem. Sci.*, 2022, **13**, 2296–2302.
49 P. Muller, *Pure Appl. Chem.*, 1994, **66**, 1077–1184.
50 S. E. Denmark and G. L. Beutner, *Angew. Chem. Int. Ed.*, 2008, **47**, 1560–1638.
51 J. B. Brazier and N. C. O. Tomkinson, in *Asymmetric Organocatalysis*, ed. B. List, Springer Berlin Heidelberg, Berlin, Heidelberg, 2009, pp. 281–347.
52 H. Guo, Y. C. Fan, Z. Sun, Y. Wu and O. Kwon, *Chem. Rev.*, 2018, **118**, 10049–10293.
53 C. McLaughlin and A. D. Smith, *Chem. Eur. J.*, 2021, **27**, 1533–1555.
54 J. Bitai, M. T. Westwood and A. D. Smith, *Org. Biomol. Chem.*, 2021, **19**, 2366–2384.
55 M. N. Hopkinson and F. Glorius, in *N-Heterocyclic Carbenes in Organocatalysis*, John Wiley & Sons, Ltd, 2018, pp. 1–35.
56 V. B. Birman and X. Li, *Org. Lett.*, 2006, **8**, 1351–1354.
57 C. I. Sheppard, J. L. Taylor and S. L. Wiskur, *Org. Lett.*, 2011, **13**, 3794–3797.
58 S. Pandiancherri, S. J. Ryan and D. W. Lupton, *Org. Biomol. Chem.*, 2012, **10**, 7903–7911.
59 E. R. T. Robinson, C. Fallan, C. Simal, A. M. Z. Slawin and A. D. Smith, *Chem. Sci.*, 2013, **4**, 2193–2200.
60 M. E. Abbasov, B. M. Hudson, D. J. Tantillo and D. Romo, *J. Am. Chem. Soc.*, 2014, **136**, 4492–4495.
61 A. Matviitsuk, M. D. Greenhalgh, D.-J. B. Antúnez, A. M. Z. Slawin and A. D. Smith, *Angew. Chem. Int. Ed.*, 2017, **56**, 12282–12287.
62 C. Shu, H. Liu, A. M. Z. Slawin, C. Carpenter-Warren and A. D. Smith, *Chem. Sci.*, 2020, **11**, 241–247.
63 G. P. Moss, P. A. S. Smith and D. Tavernier, *Pure Appl. Chem.*, 1995, **67**, 1307–1375.
64 J. Clayden, N. Greeves and S. G. Warren, *Organic chemistry.*, Oxford University Press, Oxford, 2nd ed. / Jonathan Clayden, Nick Greeves, Stuart Warren., 2012.
65 A. J. I. Arduengo, R. L. Harlow and M. Kline, *J. Am. Chem. Soc.*, 1991, **113**, 361–363.
66 E. Peris, *Chem. Rev.*, 2018, **118**, 9988–10031.
67 T. B. Fitzpatrick and L. M. Chapman, *J. Biol. Chem.*, 2020, **295**, 12002–12013.

68 T. Ukai, R. Tanaka and T. A. Dokawa, *J Pharm Soc Jpn*, 1943, **63**, 296–300.
69 R. Breslow, *J. Am. Chem. Soc.*, 1958, **80**, 3719–3726.
70 K. L. Skubi, T. R. Blum and T. P. Yoon, *Chem. Rev.*, 2016, **116**, 10035–10074.
71 C. Prentice, J. Morrisson, A. D. Smith and E. Zysman-Colman, *Beilstein J Org Chem*, 2020, 79.
72 Q. Liu and X.-Y. Chen, *Org Chem Front*, 2020, **7**, 2082–2087.
73 D. A. DiRocco and T. Rovis, *J. Am. Chem. Soc.*, 2012, **134**, 8094–8097.
74 L. Dai, Z.-H. Xia, Y.-Y. Gao, Z.-H. Gao and S. Ye, *Angew. Chem. Int. Ed.*, 2019, **58**, 18124–18130.
75 A. V. Bay, K. P. Fitzpatrick, R. C. Betori and K. A. Scheidt, *Angew. Chem. Int. Ed.*, 2020, **59**, 9143–9148.
76 K. Liu, M. Schwenzer and A. Studer, *ACS Catal.*, 2022, **12**, 11984–11999.
77 Q. Meng, N. Döben and A. Studer, *Angew. Chem. Int. Ed.*, 2020, **59**, 19956–19960.
78 S.-C. Ren, W.-X. Lv, X. Yang, J.-L. Yan, J. Xu, F.-X. Wang, L. Hao, H. Chai, Z. Jin and Y. R. Chi, *ACS Catal.*, 2021, **11**, 2925–2934.
79 S. Jin, X. Sui, G. C. Haug, V. D. Nguyen, H. T. Dang, H. D. Arman and O. V. Larionov, *ACS Catal.*, 2022, **12**, 285–294.
80 G. E. M. Crisenza, D. Mazzarella and P. Melchiorre, *J. Am. Chem. Soc.*, 2020, **142**, 5461–5476.
81 T. Rigotti, A. Casado-Sánchez, S. Cabrera, R. Pérez-Ruiz, M. Liras, V. A. de la Peña O'Shea and J. Alemán, *ACS Catal.*, 2018, **8**, 5928–5940.
82 X. Huang and E. Meggers, *Acc. Chem. Res.*, 2019, **52**, 833–847.
83 R. Alonso and T. Bach, *Angew. Chem. Int. Ed.*, 2014, **53**, 4368–4371.
84 K. L. Skubi, J. B. Kidd, H. Jung, I. A. Guzei, M.-H. Baik and T. P. Yoon, *J. Am. Chem. Soc.*, 2017, **139**, 17186–17192.
85 H. Huo, K. Harms and E. Meggers, *J. Am. Chem. Soc.*, 2016, **138**, 6936–6939.
86 L. Ruiz Espelt, I. S. McPherson, E. M. Wiensch and T. P. Yoon, *J. Am. Chem. Soc.*, 2015, **137**, 2452–2455.
87 R. M. Neyyappadath, R. Chisholm, M. D. Greenhalgh, C. Rodríguez-Escrich, M. A. Pericàs, G. Hähner and A. D. Smith, *ACS Catal.*, 2018, **8**, 1067–1075.
88 R. A. Al-Balushi, A. Haque, M. Jayapal, M. K. Al-Suti, J. Husband, M. S. Khan, O. F. Koentjoro, K. C. Molloy, J. M. Skelton and P. R. Raithby, *Inorg. Chem.*, 2016, **55**, 6465–6480.
89 D. Chen, Y. Kusakabe, Y. Ren, D. Sun, P. Rajamalli, Y. Wada, K. Suzuki, H. Kaji and E. Zysman-Colman, *J. Org. Chem.*, 2021, **86**, 11531–11544.
90 R. Ishimatsu, S. Matsunami, T. Kasahara, J. Mizuno, T. Edura, C. Adachi, K. Nakano and T. Imato, *Angew. Chem. Int. Ed.*, 2014, **53**, 6993–6996.
91 N. G. Connelly and W. E. Geiger, *Chem. Rev.*, 1996, **96**, 877–910.
92 K. A. King, P. J. Spellane and R. J. Watts, *J. Am. Chem. Soc.*, 1985, **107**, 1431–1432.
93 A. G. Condie, J. C. González-Gómez and C. R. J. Stephenson, *J. Am. Chem. Soc.*, 2010, **132**, 1464–1465.
94 C. McLaughlin, A. M. Z. Slawin and A. D. Smith, *Angew. Chem. Int. Ed.*, 2019, **58**, 15111–15119.
95 R. del Río-Rodríguez, M. T. Westwood, M. Sicignano, M. Juhl, J. A. Fernández-Salas, J. Alemán and A. D. Smith, *Chem. Commun.*, 2022, **58**, 7277–7280.
96 W. C. Hartley, F. Schiel, E. Ermini and P. Melchiorre, *Angew. Chem. Int. Ed.*, 2022, **61**, e202204735.
97 C. K. Prier, D. A. Rankic and D. W. C. MacMillan, *Chem. Rev.*, 2013, **113**, 5322–5363.
98 B. M. Hockin, C. Li, N. Robertson and E. Zysman-Colman, *Catal Sci Technol*, 2019, **9**, 889–915.
99 S. Fukuzumi and K. Ohkubo, *Org. Biomol. Chem.*, 2014, **12**, 6059–6071.
100 V. Srivastava and P. P. Singh, *RSC Adv.*, 2017, **7**, 31377–31392.
101 A. Joshi-Pangu, F. Lévesque, H. G. Roth, S. F. Oliver, L.-C. Campeau, D. Nicewicz and D. A. DiRocco, *J. Org. Chem.*, 2016, **81**, 7244–7249.
102 T.-Y. Shang, L.-H. Lu, Z. Cao, Y. Liu, W.-M. He and B. Yu, *Chem. Commun.*, 2019, **55**, 5408–5419.
103 M. A. Bryden and E. Zysman-Colman, *Chem. Soc. Rev.*, 2021.
104 A. Tlili and S. Lakhdar, *Angew. Chem. Int. Ed.*, 2021, **60**, 19526–19549.
105 S. Grotjahn and B. König, *Org. Lett.*, 2021, **23**, 3146–3150.

106 Z. Zuo and D. W. C. MacMillan, *J. Am. Chem. Soc.*, 2014, **136**, 5257–5260.
107 J. D. Griffin, M. A. Zeller and D. A. Nicewicz, *J. Am. Chem. Soc.*, 2015, **137**, 11340–11348.
108 C. J. O'Brien, D. G. Droege, A. Y. Jiu, S. S. Gandhi, N. A. Paras, S. H. Olson and J. Conrad, *J. Org. Chem.*, 2018, **83**, 8926–8935.
109 C.-J. Wallentin, J. D. Nguyen, P. Finkbeiner and C. R. J. Stephenson, *J. Am. Chem. Soc.*, 2012, **134**, 8875–8884.
110 M. Pirtsch, S. Paria, T. Matsuno, H. Isobe and O. Reiser, *Chem. Eur. J.*, 2012, **18**, 7336–7340.
111 M. L. Czyz, G. K. Weragoda, T. H. Horngren, T. U. Connell, D. Gomez, R. A. J. O'Hair and A. Polyzos, *Chem. Sci.*, 2020, **11**, 2455–2463.
112 D. D. Tanner and H. K. Singh, *J. Org. Chem.*, 1986, **51**, 5182–5186.
113 A. Bahamonde and P. Melchiorre, *J. Am. Chem. Soc.*, 2016, **138**, 8019–8030.
114 L. Wang, I. Rörich, C. Ramanan, P. W. M. Blom, W. Huang, R. Li and K. A. I. Zhang, *Catal Sci Technol*, 2018, **8**, 3539–3547.
115 W. G. Herkstroeter and D. S. McClure, *J. Am. Chem. Soc.*, 1968, **90**, 4522–4527.
116 F. Strieth-Kalthoff and F. Glorius, *Chem*, 2020, **6**, 1888–1903.
117 J. Twilton, C. (Chip) Le, P. Zhang, M. H. Shaw, R. W. Evans and D. W. C. MacMillan, *Nat. Rev. Chem.*, 2017, **1**, 0052.
118 Z.-H. Qi and J. Ma, *ACS Catal.*, 2018, **8**, 1456–1463.
119 T. Constantin, M. Zanini, A. Regni, N. S. Sheikh, F. Juliá and D. Leonori, *Science*, 2020, **367**, 1021–1026.
120 C. Cassani, G. Bergonzini and C.-J. Wallentin, *Org. Lett.*, 2014, **16**, 4228–4231.
121 S. P. Pitre, C. D. McTiernan, H. Ismaili and J. C. Scaiano, *J. Am. Chem. Soc.*, 2013, **135**, 13286–13289.
122 Y. Ji, D. A. DiRocco, C. M. Hong, M. K. Wismer and M. Reibarkh, *Org. Lett.*, 2018, **20**, 2156–2159.
123 K. Donabauer, M. Maity, A. L. Berger, G. S. Huff, S. Crespi and B. König, *Chem. Sci.*, 2019, **10**, 5162–5166.
124 M. Cherevatskaya and B. König, *Russ. Chem. Rev.*, 2014, **83**, 183.
125 M. Umar and H. A. Aziz, in *Organic Pollutants*, ed. M. N. Rashed, IntechOpen, Rijeka, 2013.
126 K. Maeda and K. Domen, *J. Phys. Chem. Lett.*, 2010, **1**, 2655–2661.
127 R. Pachaiappan, S. Rajendran, P. S. Kumar, D.-V. N. Vo and T. K. A. Hoang, *Chem. Eng. Res. Des.*, 2022, **177**, 304–320.
128 K. Feng, R.-Y. Zhang, L.-Z. Wu, B. Tu, M.-L. Peng, L.-P. Zhang, D. Zhao and C.-H. Tung, *J. Am. Chem. Soc.*, 2006, **128**, 14685–14690.
129 D. González-Muñoz, A. Casado-Sánchez, I. del Hierro, S. Gómez-Ruiz, S. Cabrera and J. Alemán, *J. Catal.*, 2019, **373**, 374–383.
130 X. Yu and C. T. Williams, *Catal Sci Technol*, 2022, **12**, 5765–5794.
131 D. Sun, S. M. Suresh, D. Hall, M. Zhang, C. Si, D. B. Cordes, A. M. Z. Slawin, Y. Olivier, X. Zhang and E. Zysman-Colman, *Mater Chem Front*, 2020, **4**, 2018–2022.
132 J. Dong, X. Pan, J. Wang, P. Su, L. Zhang, F. Wei and J. Zhang, *Eur. J. Med. Chem.*, 2015, **101**, 780–789.
133 N. Kühl, M. M. Leuthold, M. A. M. Behnam and C. D. Klein, *J. Med. Chem.*, 2021, **64**, 4567–4587.
134 T. Kitanosono, K. Masuda, P. Xu and S. Kobayashi, *Chem. Rev.*, 2018, **118**, 679–746.
135 S. Barata-Vallejo, D. E. Yerien and A. Postigo, *ACS Sustain. Chem. Eng.*, 2021, **9**, 10016–10047.
136 K. Sun, Q.-Y. Lv, X.-L. Chen, L.-B. Qu and B. Yu, *Green Chem.*, 2021, **23**, 232–248.
137 D. Xia, T. Miao, P. Li and L. Wang, *Chem. – Asian J.*, 2015, **10**, 1919–1925.
138 L. Zou, P. Li, B. Wang and L. Wang, *Green Chem.*, 2019, **21**, 3362–3369.
139 P. Natarajan, D. Chuskit, and Priya, *Green Chem.*, 2019, **21**, 4406–4411.
140 M. Bu, G. Lu, J. Jiang and C. Cai, *Catal Sci Technol*, 2018, **8**, 3728–3732.
141 M.-S. Bertrams and C. Kerzig, *Chem. Commun.*, 2021, **57**, 6752–6755.
142 C. Kerzig, X. Guo and O. S. Wenger, *J. Am. Chem. Soc.*, 2019, **141**, 2122–2127.
143 Q. Ye, S. Chen, D. Zhu, X. Lu and Q. Lu, *J Mater Chem B*, 2015, **3**, 3091–3097.

144 R. Naumann and M. Goez, *Green Chem.*, 2019, **21**, 4470–4474.
145 C. P. Andrieux and J. Pinson, *J. Am. Chem. Soc.*, 2003, **125**, 14801–14806.
146 D. Xue, Z.-H. Jia, C.-J. Zhao, Y.-Y. Zhang, C. Wang and J. Xiao, *Chem. Eur. J.*, 2014, **20**, 2960–2965.
147 J. Xu, M. Arkin, Y. Peng, W. Xu, H. Yu, X. Lin and Q. Wu, *Green Chem.*, 2019, **21**, 1907–1911.
148 M. M. Heravi, V. Zadsirjan, K. Kafshdarzadeh and Z. Amiri, *Asian J. Org. Chem.*, 2020, **9**, 1999–2034.
149 W. H. García-Santos, J. B. Mateus-Ruiz and A. Cordero-Vargas, *Org. Lett.*, 2019, **21**, 4092–4096.
150 W. Li, W. Wu, J. Yang, X. Liang and J. Ye, *Synthesis*, 2011, **2011**, 1085–1091.
151 A. Deepthi, B. P. Babu and A. L. Balachandran, *Org. Prep. Proced. Int.*, 2019, **51**, 409–442.
152 G. Minetto, L. F. Raveglia, A. Sega and M. Taddei, *Eur. J. Org. Chem.*, 2005, **2005**, 5277–5288.
153 G. E. Veitch, K. L. Bridgwood, K. Rands-Trevor and S. V. Ley, *Synlett*, 2008, **2008**, 2597–2600.
154 Q. Xia, X. Li, X. Fu, Y. Zhou, Y. Peng, J. Wang and G. Song, *J. Org. Chem.*, 2021, **86**, 9914–9923.
155 J. Yang, F. Mei, S. Fu and Y. Gu, *Green Chem.*, 2018, **20**, 1367–1374.
156 D. Wang and L. Ackermann, *Chem. Sci.*, 2022, **13**, 7256–7263.
157 S. Jin, X. Sui, G. C. Haug, V. D. Nguyen, H. T. Dang, H. D. Arman and O. V. Larionov, *ACS Catal.*, 2022, **12**, 285–294.
158 Q.-Z. Li, Y.-Q. Liu, X.-X. Kou, W.-L. Zou, P. Xiang, J.-D. Xing, T. Qi, X. Zhang and J.-L. Li, *Angew. Chem. Int. Ed.*, 2022, anie.202207824.
159 Y. Cheng, J. Yu, T. Lei, H. Hou, B. Chen, C. Tung and L. Wu, *Angew. Chem.*, 2021, **133**, 27026–27032.
160 T. Morack, C. Mück-Lichtenfeld and R. Gilmour, *Angew. Chem. Int. Ed.*, 2019, **58**, 1208–1212.
161 M. Zhang, J. Xi, R. Ruzi, N. Li, Z. Wu, W. Li and C. Zhu, *J. Org. Chem.*, 2017, **82**, 9305–9311.
162 R. C. Betori, C. M. May and K. A. Scheidt, *Angew. Chem. Int. Ed.*, 2019, **58**, 16490–16494.
163 L. Wang, R. Ma, J. Sun, G. Zheng and Q. Zhang, *Chem. Sci.*, 2022, **13**, 3169–3175.
164 S. Li, H. Shu, S. Wang, W. Yang, F. Tang, X.-X. Li, S. Fan and Y.-S. Feng, *Org. Lett.*, 2022, **24**, 5710–5714.
165 C. Prentice, J. Morrison, A. D. Smith and E. Zysman-Colman, *Chem. Eur. J.*, 2023, **29**, e202202998.
166 L. Wang, J. Sun, J. Xia, M. Li, L. Zhang, R. Ma, G. Zheng and Q. Zhang, *Sci. China Chem.*, 2022, **65**, 1938–1944.
167 M. He, J. R. Struble and J. W. Bode, *J. Am. Chem. Soc.*, 2006, **128**, 8418–8420.
168 E. G. Delany, C.-L. Fagan, S. Gundala, K. Zeitler and S. J. Connon, *Chem. Commun.*, 2013, **49**, 6513–6515.
169 E. Voutyritsa and C. G. Kokotos, *Angew. Chem. Int. Ed.*, 2020, **59**, 1735–1741.
170 Z. Wang, X. Wang and Y. Nishihara, *Chem. Commun.*, 2018, **54**, 13969–13972.
171 K. Wadhwa, C. Yang, P. R. West, K. C. Deming, S. R. Chemburkar and R. E. Reddy, *Synth. Commun.*, 2008, **38**, 4434–4444.
172 J. F. Thorpe and R. M. Beesley, *Proc Chem Soc Lond.*, 1913, **29**, 343–365.
173 P. E. Eaton, *Angew. Chem. Int. Ed. Engl.*, 1992, **31**, 1421–1436.
174 B. A. Chalmers, H. Xing, S. Houston, C. Clark, S. Ghassabian, A. Kuo, B. Cao, A. Reitsma, C.-E. P. Murray, J. E. Stok, G. M. Boyle, C. J. Pierce, S. W. Littler, D. A. Winkler, P. V. Bernhardt, C. Pasay, J. J. De Voss, J. McCarthy, P. G. Parsons, G. H. Walter, M. T. Smith, H. M. Cooper, S. K. Nilsson, J. Tsanaktsidis, G. P. Savage and C. M. Williams, *Angew. Chem. Int. Ed.*, 2016, **55**, 3580–3585.
175 T. Yildirim, P. M. Gehring, D. A. Neumann, P. E. Eaton and T. Emrick, *Carbon*, 1998, **36**, 809–815.
176 E. G. Cox, *Rev Mod Phys*, 1958, **30**, 159–162.
177 F. Lovering, J. Bikker and C. Humblet, *J. Med. Chem.*, 2009, **52**, 6752–6756.
178 H. Takebe and S. Matsubara, *Eur. J. Org. Chem.*, 2022, e202200567.
179 P. E. Eaton, M.-X. Zhang, R. Gilardi, N. Gelber, S. Iyer and R. Surapaneni, *Propellants Explos. Pyrotech.*, 2002, **27**, 1–6.
180 P. E. Eaton, K. Pramod, T. Emrick and R. Gilardi, *J. Am. Chem. Soc.*, 1999, **121**, 4111–4123.
181 P. E. Eaton and T. W. Cole, *J. Am. Chem. Soc.*, 1964, **86**, 962–964.
182 N. B. Chapman, J. M. Key and K. J. Toyne, *J. Org. Chem.*, 1970, **35**, 3860–3867.
183 M. Bliese and J. Tsanaktsidis, *Aust. J. Chem.*, 1997, **50**, 189–192.

184 D. E. Collin, E. H. Jackman, N. Jouandon, W. Sun, M. E. Light, D. C. Harrowven and B. Linclau, *Synthesis*, 2021, **53**, 1307–1314.
185 R. Brimioulle and T. Bach, *Science*, 2013, **342**, 840–843.
186 E. Y. Y. Lam, Donald. Valentine and G. S. Hammond, *J. Am. Chem. Soc.*, 1967, **89**, 3482–3487.
187 F. Bayrakçeken, *Spectrochim. Acta. A. Mol. Biomol. Spectrosc.*, 2008, **71**, 603–608.
188 P. E. N. Eaton Nereo; Tsanaktsidis, John; Upadhyaya, Subhash P., *Synthesis*, 2000, **1995**, 501–502.
189 F. Toriyama, J. Cornella, L. Wimmer, T.-G. Chen, D. D. Dixon, G. Creech and P. S. Baran, *J. Am. Chem. Soc.*, 2016, **138**, 11132–11135.
190 E. B. McLean, D. T. Mooney, D. J. Burns and A.-L. Lee, *Org. Lett.*, 2022, **24**, 686–691.
191 M. P. Wiesenfeldt, J. A. Rossi-Ashton, I. B. Perry, J. Diesel, O. L. Garry, F. Bartels, S. C. Coote, X. Ma, C. S. Yeung, D. J. Bennett and D. W. C. MacMillan, *Nature*, , DOI:10.1038/s41586-023-06021-8.
192 Y. Toya, M. Takagi, H. Nakata, N. Suzuki, M. Isobe and T. Goto, *Bull. Chem. Soc. Jpn.*, 1992, **65**, 392–395.
193 D. S. B. Daniels, S. R. Smith, T. Lebl, P. Shapland and A. D. Smith, *Synthesis*, 2014, **47**, 34–41.
194 Y.-S. Ye, W.-C. Shen, C.-Y. Tseng, J. Rick, Y.-J. Huang, F.-C. Chang and B.-J. Hwang, *Chem. Commun.*, 2011, **47**, 10656–10658.
195 Y. Wang, S. Li, X. Wang, Y. Yao, L. Feng and C. Ma, *RSC Adv.*, 2022, **12**, 5919–5927.
196 L. De Luca, G. Giacomelli, S. Masala and A. Porcheddu, *J. Org. Chem.*, 2003, **68**, 4999–5001.
197 B. Abadie, D. Jardel, G. Pozzi, P. Toullec and J.-M. Vincent, *Chem. Eur. J.*, 2019, **25**, 16120–16127.
198 D. Xue, Z.-H. Jia, C.-J. Zhao, Y.-Y. Zhang, C. Wang and J. Xiao, *Chem. Eur. J.*, 2014, **20**, 2960–2965.
199 F. Echalier, O. Constant and J. Bolte, *J. Org. Chem.*, 1993, **58**, 2747–2750.
200 R. Beniazza, L. Remisse, D. Jardel, D. Lastécouères and J.-M. Vincent, *Chem. Commun.*, 2018, **54**, 7451–7454.
201 N. Kaplaneris, A. Bisticha, G. N. Papadopoulos, D. Limnios and C. G. Kokotos, *Green Chem.*, 2017, **19**, 4451–4456.
202 H. R. Snyder, A. J. Reedy and Wm. J. Lennarz, *J. Am. Chem. Soc.*, 1958, **80**, 835–838.
203 L.-E. Carloni, S. Mohnani and D. Bonifazi, *Eur. J. Org. Chem.*, 2019, **2019**, 7322–7334.
204 S. Kobayashi, T. Kinoshita, H. Uehara, T. Sudo and I. Ryu, *Org. Lett.*, 2009, **11**, 3934–3937.
205 K. B. Ling and A. D. Smith, *Chem. Commun.*, 2011, **47**, 373–375.
206 T. Klein and G. Kickelbick, *Dalton Trans*, 2020, **49**, 9820–9834.
207 D. Li, Q. Tian, X. Wang, Q. Wang, Y. Wang, S. Liao, P. Xu, X. Huang and J. Yuan, *Synth. Commun.*, 2021, **51**, 2041–2052.
208 S. B. Garber, J. S. Kingsbury, B. L. Gray and A. H. Hoveyda, *J. Am. Chem. Soc.*, 2000, **122**, 8168–8179.
209 F. Yu, R. Zhang, C. Xie and S. Yu, *Tetrahedron*, 2010, **66**, 9145–9150.
210 X. Zhao, B. Li and W. Xia, *Org. Lett.*, 2020, **22**, 1056–1061.
211 M. Nagarajan and H. Shechter, *J. Org. Chem.*, 1984, **49**, 62–74.
212 C. R. Bauer and R. E. Lutz, *J. Am. Chem. Soc.*, 1953, **75**, 5997–6002.
213 A. E. Mattson, A. R. Bharadwaj and K. A. Scheidt, *J. Am. Chem. Soc.*, 2004, **126**, 2314–2315.
214 M. Rezazadeh Khalkhali, M. M. D. Wilde and M. Gravel, *Org. Lett.*, 2021, **23**, 155–159.
215 M. M. D. Wilde and M. Gravel, *Angew. Chem. Int. Ed.*, 2013, **52**, 12651–12654.
216 C. Pan, Q. Ni, Y. Fu and J.-T. Yu, *J. Org. Chem.*, 2017, **82**, 7683–7688.
217 Y. Li, Y. Leng, S. Wang, Y. Gao, H. Lv, J. Chang, Y. Wu and Y. Wu, *Appl. Organomet. Chem.*, 2018, **32**, e4407.
218 M.-Y. Chang and Y.-C. Cheng, *Synlett*, 2016, **27**, 1931–1935.
219 N. Döben, J. Reimler and A. Studer, *Adv. Synth. Catal.*, 2022, **364**, 3348–3353.
220 M. Tryniszewski and M. Barbasiewicz, *Synthesis*, 2021, **54**, 1446–1460.
221 S. B. Munoz, H. Dang, X. Ispizua-Rodriguez, T. Mathew and G. K. S. Prakash, *Org. Lett.*, 2019, **21**, 1659–1663.
222 H.-X. Song, Z.-Y. Tian, J.-C. Xiao and C.-P. Zhang, *Chem. Eur. J.*, 2020, **26**, 16261–16265.

223 F.-W. Wu, Y.-J. Mao, J. Pu, H.-L. Li, P. Ye, Z.-Y. Xu, S.-J. Lou and D.-Q. Xu, *Org. Biomol. Chem.*, 2022, **20**, 4091–4095.
224 M. Aliyu Idris, K. H. Song and S. Lee, *Adv. Synth. Catal.*, 2022, **364**, 2449–2453.
225 J. B. Nagwekar and J. W. Cheon, *J. Pharm. Sci.*, 1981, **70**, 295–298.
226 S. Rajput, R. Kaur and N. Jain, *Org. Biomol. Chem.*, 2022, **20**, 1453–1461.
227 K. Furukawa, H. Inada, M. Shibuya and Y. Yamamoto, *Org. Lett.*, 2016, **18**, 4230–4233.
228 H. Guo, J. Li, D. Liu and W. Zhang, *Adv. Synth. Catal.*, 2017, **359**, 3665–3673.
229 K. Merkens, F. J. Aguilar Troyano, J. Djossou and A. Gómez-Suárez, *Adv. Synth. Catal.*, 2020, **362**, 2354–2359.
230 R. Marín-Valls, K. Hernández, M. Bolte, T. Parella, J. Joglar, J. Bujons and P. Clapés, *J. Am. Chem. Soc.*, 2020, **142**, 19754–19762.
231 M. J. Frisch, G. W. Trucks, H. B. Schlegel, G. E. Scuseria, M. A. Robb, J. R. Cheeseman, G. Scalmani, V. Barone, G. A. Petersson, H. Nakatsuji, X. Li, M. Caricato, A. V. Marenich, J. Bloino, B. G. Janesko, R. Gomperts, B. Mennucci, H. P. Hratchian, J. V. Ortiz, A. F. Izmaylov, J. L. Sonnenberg, D. Williams-Young, F. Ding, F. Lipparini, F. Egidi, J. Goings, B. Peng, A. Petrone, T. Henderson, D. Ranasinghe, V. G. Zakrzewski, J. Gao, N. Rega, G. Zheng, W. Liang, M. Hada, M. Ehara, K. Toyota, R. Fukuda, J. Hasegawa, M. Ishida, T. Nakajima, Y. Honda, O. Kitao, H. Nakai, T. Vreven, K. Throssell, J. A. Montgomery, Jr., J. E. Peralta, F. Ogliaro, M. J. Bearpark, J. J. Heyd, E. N. Brothers, K. N. Kudin, V. N. Staroverov, T. A. Keith, R. Kobayashi, J. Normand, K. Raghavachari, A. P. Rendell, J. C. Burant, S. S. Iyengar, J. Tomasi, M. Cossi, J. M. Millam, M. Klene, C. Adamo, R. Cammi, J. W. Ochterski, R. L. Martin, K. Morokuma, O. Farkas, J. B. Foresman, and D. J. Fox, Gaussian, Inc., Wallingford CT, Gaussian 16 Rev. C.01 2016.
232 G. A. Petersson and M. A. Al-Laham, *J. Chem. Phys.*, 1991, **94**, 6081–6090.
233 C. Adamo and V. Barone, *J. Chem. Phys.*, 1999, **110**, 6158–6170.
234 A. D. Becke, *Phys Rev A*, 1988, **38**, 3098–3100.
235 C. Lee, W. Yang and R. G. Parr, *Phys Rev B*, 1988, **37**, 785–789.
236 B. Miehlich, A. Savin, H. Stoll and H. Preuss, *Chem. Phys. Lett.*, 1989, **157**, 200–206.
237 S. Miertuš, E. Scrocco and J. Tomasi, *Chem. Phys.*, 1981, **55**, 117–129.
238 J. L. Pascual-ahuir, E. Silla and I. Tuñon, *J. Comput. Chem.*, 1994, **15**, 1127–1138.
239 J. Tomasi, B. Mennucci and R. Cammi, *Chem. Rev.*, 2005, **105**, 2999–3094.
240 J. Tomasi, B. Mennucci and E. Cancès, *J. Mol. Struct. THEOCHEM*, 1999, **464**, 211–226.
241 B. Mennucci and J. Tomasi, *J. Chem. Phys.*, 1997, **106**, 5151–5158.
242 S. Grimme, S. Ehrlich and L. Goerigk, *J. Comput. Chem.*, 2011, **32**, 1456–1465.
243 S. Grimme, J. Antony, S. Ehrlich and H. Krieg, *J. Chem. Phys.*, 2010, **132**, 154104.
244 N. M. O'boyle, A. L. Tenderholt and K. M. Langner, *J. Comput. Chem.*, 2008, **29**, 839–845.
245 N. M. O'Boyle, M. Banck, C. A. James, C. Morley, T. Vandermeersch and G. R. Hutchison, *J. Cheminformatics*, 2011, **3**, 33.
246 N. M. O'Boyle, C. Morley and G. R. Hutchison, *Chem. Cent. J.*, 2008, **2**, 5.
247 M. L. Ingalsbe, J. D. St. Denis, J. L. Gleason, G. P. Savage and R. Priefer, *Synthesis*, 2009, **2010**, 98–102.